Bangor University

DOCTOR OF PHILOSOPHY

A.C. electrokinetic bioassays development of electrorotation assay for analytes in water.

Goater, Andrew David

Award date:
1999

Awarding institution:
Bangor University

[Link to publication](#)

A THESIS SUBMITTED TO THE UNIVERSITY OF WALES

IN CANDIDATURE FOR THE DEGREE OF

DOCTOR OF PHILOSOPHY

A.C. ELECTROKINETIC BIOASSAYS.

DEVELOPMENT OF ELECTROROTATION ASSAY FOR

ANALYTES IN WATER.

BY

Andrew David Goater

B.Sc. Applied Animal Biology
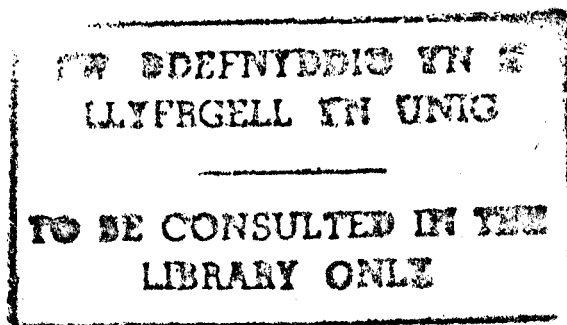
School of Electronic Engineering Science and Computer Systems

University of Wales, Bangor, Gwynedd. U.K.

Date 5ⁿ May. 1999

To my Mother
and in memory
of my Father

ACKNOWLEDGEMENTS

SUMMARY

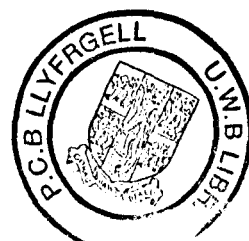The work described is primarily concerned with the understanding of the induced AC electrokinetic properties of the transmissive stages of two genera of waterborne protozoan pathogens, namely *Cryptosporidium* and *Giardia*. The assessment of viability through the use of electrorotation (ROT) has been investigated in comparison with conventional techniques. The optimum conditions for determining *C. parvum* viability using ROT are described and discussed.

Two *Giardia* and three *Cryptosporidium* species were investigated, as were a total of ten *Cryptosporidium parvum* isolates. With all species investigated a good correlation was found between the ROT response of clean particles and conventional vital dye techniques. Adherent bacteria on the particles surface have been identified as a major problem for subsequent ROT analysis. This is the first description of the effect of adherent bacteria on the dielectric response of biological particles.

A novel single layer electrode array was designed and successfully tested to overcome the problems of low particle concentration, interfering debris and particle position in the electrorotational electrodes. The device was shown to selectively concentrate particles into a central region whereupon their physiological state was then assessed through their ROT response. Modification of the device enabled the isolation of one or more particles onto a membrane, providing a suitable collection method for low particle number handling.

The clearest demonstration to date of the effect of membrane integrity on the ROT response is described from spectra obtained for an oocyst before and after excystation *in vitro*. Storage time effects for oocysts of *C. baileyi* are also described as are isolate differences for *C. parvum* oocysts which are apparent in the low frequency region of the spectra. The implications of these results to the water industry and potential diagnostic applications of electrorotation are discussed.

CONTENTS

FIGURES

TABLES

Giardia duodenalis cysts purified from a
semi-formed human stool.

Viable cyst with adherent bacterium.

Intact cyst (left) and emerging trophozoite
(right).

Non-viable cyst with contracted cytoplasm
(left) and viable intact cyst (right).
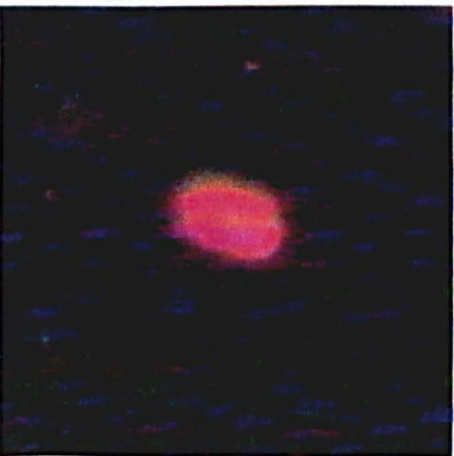
Non-viable cyst fluorescing after
incubation with propidium iodide.
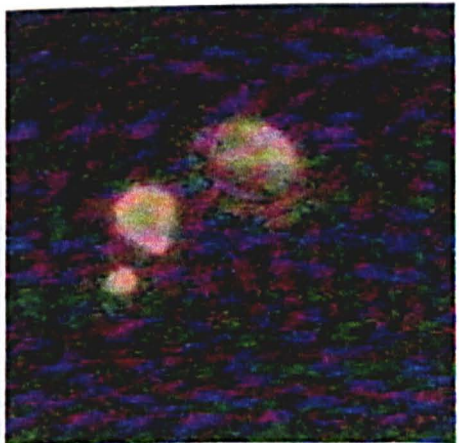
Cyst stained with fluorecein diacetate (object to
right) and pieces of debris brightly stained on left).

Plate 1. Images obtained during experiments of *Giardia duodenalis* using phase contrast microscopy.

Viable *Giardia muris* cysts.
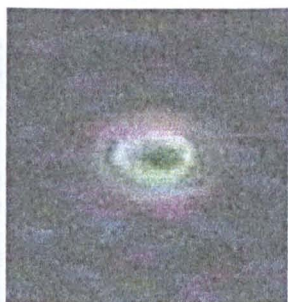
Nonviable *Giardia muris* cyst.
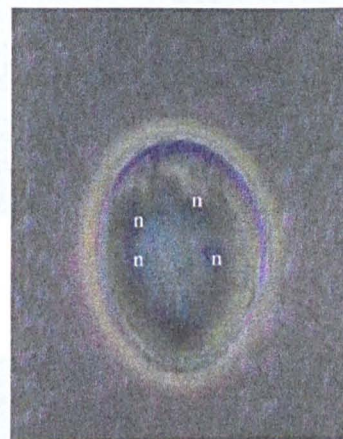
Viable cyst under higher magnification, with four nuclei (n) highlighted.

Plate 2. Images obtained during experiments of *Giardia muris* using phase contrast microscopy.

In vitro excystation event of *C. parvum* oocyst. Separation of frames 0.2 s.

Plate 3. Excystation of *C. parvum* oocyst.

Viable *C. parvum* oocyst.
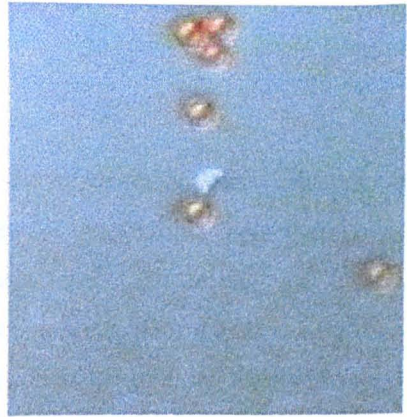
(a)
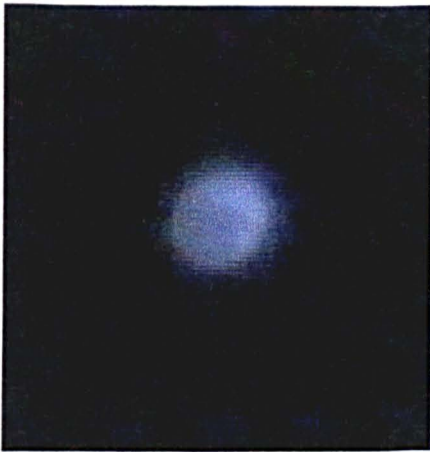
As above with DAPI highlighting four nuclei of sporozoites.

(b)
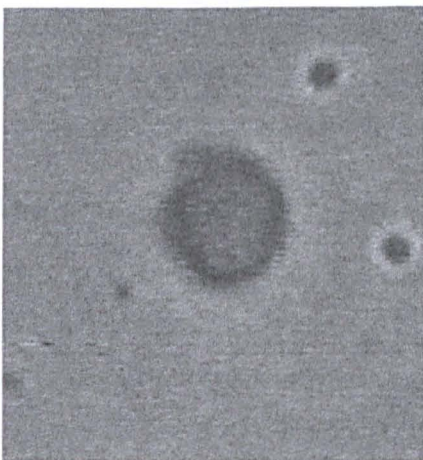
Oocyst ghost.

C. parvum oocyst attached to a Dynal bead via antibodies, rotating sequence (a-c) of separation 0.5 s viewed under Nomarski DIC optics. Note that the oocyst rotates around the denser iron cored bead.

Plate 4. Images obtained during experiments of *C. parvum*.

Chapter 1

Introduction.

1.1 Introduction

Safe and efficient treatment of drinking water has been one of the major public health advances of the twentieth century. People in developed countries generally take for granted that their water is safe to drink, a luxury the majority of the world's population does not have. The leading cause of infant mortality in the developing world is infectious diarrhoea, and the prevelence of diarrhoeal pathogens is largely influenced by the quality and quantity of clean water available for drinking and washing. Until recently, modern water treatment had all but eliminated these concerns in developed nations. Over the past two decades, however, the safety of our water supply has been threatened by the emergence of *Giardia lamblia* and more recently *Cryptosporidium parvum*, both protozoal pathogens of man.

In 1993, an estimated 403 000 people in Milwaukee, Wisconsin, developed an acute diarrhoeal illness as a result of contamination of the public water supply with *C. parvum* oocysts. This outbreak was unique in two ways. First, it was by far the largest waterborne outbreak ever reported in the United States. Second, the treated water responsible for the outbreak met all the federal water quality standards of the time. In this outbreak, the median duration of diarrhoea was nine days, with a median weight loss of 4.53kg (10 lb.), and 4400 people were hospitalised as a result of their illness. Among 82 HIV-infected patients who developed cryptosporidiosis, only 34 were still alive at one year (Steiner *et al.* 1997).

There is a clear need for better protection of the public water supply against *C. parvum*. Among the recommendations given by a Centres for Disease Control task force in September 1994, was the requirement for improvement of current techniques for identification of *C. parvum* oocysts in the water with regard to their specificity and sensitivity for detecting infectious oocysts as well as their cost and labour requirements (Steiner, *et al.* 1997).

1.2 The Electrorotation Assay

The term electrorotation (ROT) was first used to describe the motion of particles in rotating electric fields by Arnold and Zimmermann (1982) and Mischel, Voss and Pohl (1982). ROT has been reviewed in several journal articles (Arnold and Zimmermann, 1988; Pethig, 1991a; Schnelle, Glaser & Fuhr 1997) and has been described in texts (Jones, 1995; Pethig 1991b; Pethig, 1994). The ROT force on a particle depends on the dielectric properties of the particle and the suspending medium and as a result the fundamentals are based on dielectric theory and electromagnetism (a brief overview is given in chapter 2 of this thesis). A dielectric is defined as a material in which both electrical conduction losses and charge storage (polarisation) occurs when it is exposed to an electric field.

In brief, the magnitude and direction of the ROT force on a particle suspended in a dielectric medium depends on a number of factors including, the particle permittivity and conductivity, the medium permittivity and conductivity as well as the field strength and frequency. The fact that the ROT force is dependent on such a variety of parameters makes electrorotation a powerful tool for particle, especially biological particle, characterisation.

1.3 Overview of research in Electrorotation

A great deal of work has been carried out to elucidate the nature of the ROT force, in connection with dielectrophoresis (Wang, Pethig & Jones 1992; Wang *et al.* 1993) and travelling wave dielectrophoresis (Huang, *et al.* 1993; Wang *et al.* 1994). Specifically designed ROT electrodes have been used to characterise the dielectric properties of cells, starting with Arnold & Zimmermann's work on isolated plant cells (1982). Further work has been carried out on prokaryotic (Hodgson & Pethig, 1998) as well as other eukaryotic cells, including the indirect examination of protozoal particles through *Plasmodium falciparum* infected erythrocytes (Gascoyne *et al.* 1997a) as well as direct examination of fungal cells (Asami & Yonezawa, 1996) algae (Gimsa *et al.* 1991) an invertebrate cell line (Freitag *et al.* 1989) as well as mammalian cell lines (Gascoyne 1997b) lymphocytes (Ziervogel *et al.* 1986) and platelets (Egger & Donath 1995). Acellular particles have also been investigated, as with *Plasmodium falciparum*, virus particles have been studied indirectly through their interactions with erythrocytes. ROT data from non-biological particles such as artificial liposomes (Chan *et al.* 1997) have been of use in verifying the theoretical nature of the ROT force, as these are simple membraned cellular particles. Latex micro-particles have similarly been of use in probing the effects of surface groups and charges on the ROT spectra (Arnold, Schwan & Zimmermann, 1987; Meier, 1997).

As an investigative tool, ROT has several advantages. Firstly, it is non-invasive, allowing it to become part of a series of simultaneous investigations. Secondly, it functions at the single organism level, which can be extremely important when accurate viability information for low numbers of organisms is required, as is the case for parasitic particles with low (~10 - 30) infectious doses.

The information gained from such studies includes particle characterisation, detection of membrane events from either induced (e.g. chemicals such as Ag^+ or ionophores) or natural events (through parasitic invasion). Finally, particle viability information can be obtained (Gundel, Wicher & Matthies 1989; Zhou *et al.* 1995; Hodgson *et al.*, 1998). The use of ROT for particle characterisation and for determining viability are explored in this thesis, using the waterborne protozoans of the genera *Giardia* and *Cryptosporidium*.

1.4 Thesis outline

Chapter Two contains a review of, and the general theory of the dielectric techniques used in this thesis. It is written with the parasitologist in mind, as is the majority of this thesis. Chapter Three and Four review the biology of the organisms investigated, highlighting the problems with the current viability and detection methods. Chapter Four also presents the results from ROT studies of the *Giardia* work. Chapter Five describes the ROT results from *C. parvum* as a function of suspending medium conductivity

and viability for comparison with a fluorogenic vital dye assay as well as highlighting complications due to bacterial adhesion to the oocysts. Chapter Six describes travelling wave dielectrophoresis (TWD) of *C. parvum* which led to the design of a combined TWD and ROT device described in the subsequent chapter. Finally in Chapters Eight and Nine ROT studies of oocysts from species not infective to humans and ten *C. parvum* isolates of both human and non-human origin are described.

1.5 References

Arnold, W.M. & Zimmermann, U. (1982) Rotating-field-induced rotation and measurement of the membrane capacitance of single mesophyll cells of *Avena sativa. Zeitschrift fur Naturforsch.* 37c: 908-915.

Arnold, W.M., Schwan, H.P. & Zimmermann, U. (1987) Surface conductance and other properties of latex particles measured by electrorotation. *Journal of Physical Chemistry.* 91: 5093-5098.

Arnold, W.M. & Zimmermann, U. (1988) Electrorotation : development of a technique for dielectric measurements on individual cells and particles. *Journal of Electrostatics* 21: 151-191.

Asami, K. & Yonezawa, T. (1996) Dielectric behaviour of wild-type yeast and vacuole deficient mutant over a frequency range of 10kHz to 10GHz. *Biophysical Journal* 71: 2192-2200.

Chan, K.L., Gascoyne, P.R.C., Becker, F.F. & Pethig, R. (1997) Electrorotation of liposomes: verification of dielectric multi-shell model for cells. *Biochimica et Biophysica Acta-Lipids and Lipid metabolism.* 1349: 182-196.

Egger, M. & Donath, E. (1995) Electrorotation measurements of diamide-induced platelet activation changes. *Biophysical Journal.* 68: 364-372.

Freitag, R., Schügerl, K., Arnold, W.M. & Zimmermann, U. (1989) The effect of osmotic and mechanical stress and enzymatic digestion on the electrorotation of insect cells (*Spodoptera frugiperda*). *Journal of Biotechnology.* 11: 325-336.

Gascoyne, P., Pethig, R., Satayavivid, J., Becker, F.F. & Ruchirawat, M. (1997a) Dielectrophoretic detection of changes in erythrocyte membranes following malarial infection. *Biochimica et Biophysica Acta-Biomembranes.* 1323: 240-252.

Gascoyne, P.R.C., Wang, X-B., Huang, Y. & Becker, F.F. (1997b) Dielectrophoretic separation of cancer cells from blood. *IEEE Transactions on Industry Applications.* 33: 670-678.

Gimsa, J., Pritzen, C & Donath, E. (1989) Characterisation of virus-red-cell interaction by electrorotation. *Studia Biophysica.* 130: 123-131.

Gimsa, J., Marszlatek, P., Loewe, U. & Tsong, T.Y. (1991) Dielectrophoresis and electrorotation of *Neurospora* slime and murine myeloma cells. *Biophysical Journal* 60: 749-760.

Gundel, J., Wicher, D., & Matthies, H. (1989) Electrorotation as a Viability Test for Isolated Single Animal-Cells. *Studia Biophysica.* 133: 5-18.

Hodgson, C.E. & Pethig, R. (1998) Determination of the Viability of *Escherichia coli* at the single organism level by electrorotation. *Clinical Chemistry.* 44: 2049-2051.

Huang, Y., Wang, X-B, Tame, J. & Pethig, R. (1993) Electrokinetic behaviour of colloidal particles in travelling electric fields: Studies using yeast cells. *Journal of Physics D-Applied Physics.* 26: 1528-1535.

Jones, T.B. (1995) *Electromechanics of Particles.* Cambridge University Press, Cambridge. p 212.

Steiner, TS, Theilman, N.M. & Geurrant, R.L (1997) Protozoal agents: What are the dangers for the public water supply? *Annual Review of Medicine.* 48: 329-340.

Meier, H. (1997) Electrorotation of colloidal particles and cells depends on surface charge. *Biophysical Journal.* 73: 1617-1626.

Mischel, M., Voss, A. & Pohl, H.A. (1982) Cellular spin resonance in rotating electric fields. *Journal of Biological Physics.* 10: 223-226.

Pethig, R. (1991a) Biological electrostatics - Dielectrophoresis and Electrorotation. *Institute of Physics Conference Series.* 118: 13-26.

Pethig, R. (1991b) Application of AC electrical fields to the manipulation and characterisation of cells. *In: Automation in Biotechnology.* (Ed. I., Karube), pp. 159-185. Elsevier, Amsterdam.

Pethig, R. (1994) *Dielectric and A.C. Electrodynamic properties of cells.* In: *Bioelectrodynamics and biocommunication.* (Eds. M.W. Ho, F-A. Popp & U. Warnke) Ch. 9, pp. 229-249.

Schnelle, T, Glasser, H. & Fuhr, G. (1997) Opto-electronic technique for automatic detection of electrorotational spectra of single cells. *Cellular Engineering.* 2: 33-41.

Wang, X-B, Pethig, R. & Jones, T.B. (1992) Relationship of dielectrophoretic and electrorotational behaviour exhibited by polarised particles. *Journal of Physics D-Applied Physics.* 25: 905-912.

Wang, X-B., Huang, Y., Holzel, R., Burt, J.P.H. & Pethig, R. (1993) Theoretical and experimental investigations of the interdependence of the dielectric , dielectrophoretic and electrorotational behaviour of colloidal particles. *Journal of Physics D-Applied Physics.* 26: 312-322.

Wang, X-B., Huang, Y., Becker, F.F. & Gascoyne P.R.C. (1994) A unified theory of dielectrophoresis and travelling wave dielectrophoresis. *Journal of Physics D-Applied Physics.* 27: 1571-1574.

Zhou, X.F., Markx, G.H., Pethig, R. & Eastwood, I.M. (1995) Differentiation of viable and nonviable bacterial biofilms using electrorotation. *Biochimica et Biophysica Acta-General Subjects.* 1245: 85-93.

Ziervogel, H., Glaser, R., Schadow, D. & Heymann, S. (1986) Electrorotation of lymphocytes, the influence of membrane events and nucleus. *Bioscience reports.* 6: 973-982.

Chapter 2

Electrorotation and Dielectrophoresis.

2.1 Summary

Using microelectrode structures, various forms of electric fields, such as non-uniform, rotating and travelling wave, can be imposed on particles of sizes ranging from proteins and viruses to micro-organisms and cells. Each type of particle responds to the forces exerted on them in a unique way, allowing for their controlled and selective manipulation as well as their characterisation. Moreover, particles of the same type but of different viability can be distinguished in a simple, reliable manner. This Chapter outlines the principles that govern the way in which bioparticles respond to these various field types, and how they can be exploited. Examples of current and potential biotechnological and biomedical applications are given, along with a critical comparison of current techniques.

2.2 Introduction

The induced motion or orientation of bio-particles in electrical fields has been observed for over 100 years (e.g. Lortet, 1896). Until comparatively recently, only particle motion or *phoresis*, induced by DC electric fields was studied. From the generic idea of electrophoresis, a whole new branch of novel electrokinetic manipulation methods of bioparticles has arisen, simply by taking advantage of another dimension, the particle response to the frequency of the field. In this Chapter the AC field bio-particle kinetic techniques of relevance to the rest of the thesis are described and reviewed.

2.3 Innate Electrical Properties of Particles.

In order to understand the interactions of a particle with an electric field one must first consider the innate electrical properties of that particle. A generalised bioparticle suspended in an aqueous solution (weak electrolyte) is represented in Figure 2.1 with the relative distribution of innate charges, both bound and free. Many of the molecules that make up biological particles possess ionisable surface chemical groups such as COOH or NH_2. The ionisable head groups of lipids in the plasma membrane are one such example and because of these the particle possesses a net surface charge. An electrostatic potential due to these charges will be present around the particle, the effect of which decreases to that of the bulk medium with increasing distance from the particle (Pethig, 1979). Ions of opposite charge, counter-ions, to those on the surface will be attracted towards the particle by this electrostatic potential. Together, the bound surface charges and the surrounding counter-ion atmosphere, shown as the cation dense region in Figure 2.1, form what is termed an electrical double layer.
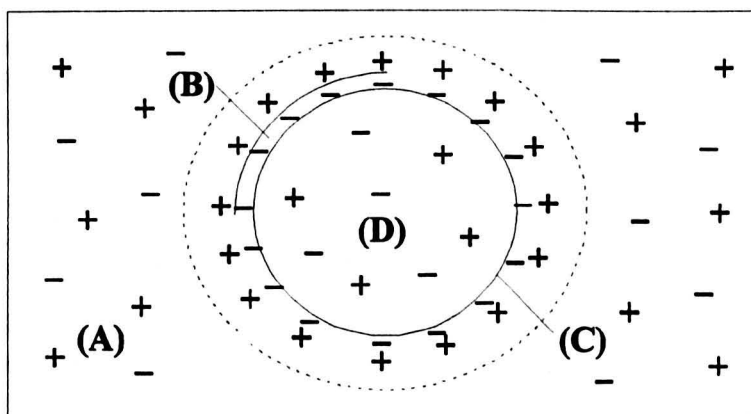
Figure 2.1 The relative distribution of charge for a suspended particle.
A simplified cell (solid circle) suspended in an aqueous medium at neutral pH showing the relative distributions of charge, both free and bound. Approximate conductivity (σ = S m^{-1}) and relative permittivity (ε_r, where air =1) of the bulk solution (A) σ = 10^{-4} ε_r = 80, cell wall (where present) (B) σ = 10^{-2} ε_r = 60, membrane (C) σ = 10^{-7} ε_r = 9, and interior (D) σ = 10^{-1} ε_r = 70 for a typical viable cell.

2.4   Application of a DC Field to Particles.

On the application of a DC electric field across the bioparticle, all the charges, bound and free, in the system will be attracted to the electrode of opposite polarity, see Figure 2.2. For a solution close to neutral pH only relatively small concentrations of H^+ and OH^- will be present, ions such as Na^+ and Cl^- will carry the bulk of the current. Those ions associated with the electrical double layer will respond to the field forming an asymmetric distribution around the particle (Hartley, 1935), the new equilibrium of which is established by the magnitude of the electric field and the opposing ionic concentration diffusion gradient, which tends to restore the random, symmetrical distribution (Bone & Zaba, 1992). Any motion of the particle towards the electrodes in a dc field is due to the net surface charge. Human erythrocytes, for example, in a standard saline solution under the influence of a DC field of 1 V cm^{-1} migrate towards the anode at around 1 μm s^{-1}. Particle separation is therefore possible due to differences in their mobility in an electric field, which may be due to their size, mass or charge. Reuss (1809) was first to use this technique (on clay particles) which, one hundred years later Michaelis (1909) termed electrophoresis. Later, Coulter (1920) extensively investigated cell surface properties.

Whereas bound charges and polar molecules in the system may orientate in the field, free charge carriers (e.g. ions) will migrate towards the electrodes, that is unless they encounter a material with different electrical properties. Ions encountering the plasma membrane, will be prevented from free motion towards the electrodes by this membrane if it is intact. The membranes of viable cells are only semi-(selectively) permeable to ions and non-lipid soluble molecules (i.e. are relatively non-conducting). The conductivity of the cell membrane tends to be around 10^{-7} S m^{-1}, some 10^7 times less conductive than that of the interior which can be as high as 1 S m^{-1}. For particles the size of erythrocytes, then within about a

microsecond after the application of an electric field, the ions will have fully built up at the particle boundary forming an aggregation of interfacial charges. The first description of interfacial charges in heterogeneous materials was given by Maxwell (1891) for DC fields, the theory of which was later elaborated by Wagner (1914) who extended the theory to include AC fields.

Importantly these induced charges are not uniformly distributed over the bioparticle surface, forming predominantly on the sides of the particle facing the electrodes. These charges and the distorted electrical double layer lend to the particle the properties of an electrical dipole moment, m. This dipole moment is in the order of 2.5×10^5 debye units* (D) for a cell of 5μm diameter, (c.f. 1.84 debye for a water molecule); the cellular dipole moment is therefore described as macroscopic, although the magnitude of the induced charge is still only a fraction, around 0.1%, of the net surface charge carried by cells and micro-organisms (Pethig, 1991).
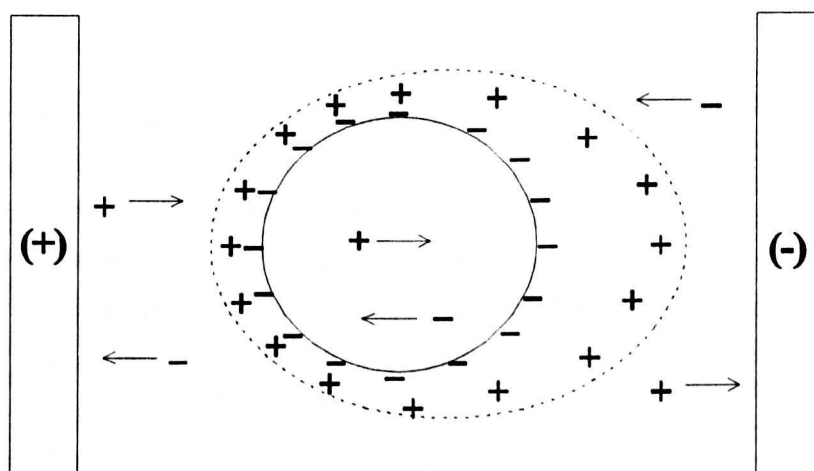
Figure 2.2 Application of a DC electric field to a suspended particle.
On the application of a DC electric field to a cell in aqueous solution, charges will experience a force towards the oppositely charged electrode. Ions in the bulk solution are free to migrate to the electrodes, whereas charges associated with the *electrical double layer* are restricted and show a distortion or polarisation.

2.5   Application of an AC Field to Particles.

If we now consider the application of an alternating field to a particle, we see that various phenomena occur over different frequency ranges of applied field. Starting close to the DC condition, with a field that reverses direction a few times a second, the particle motion is dominated by electrophoretic forces. The particle may follow reversals of the field electrophoretically for frequencies up to a few hundred Hz, where reversals of the field take less than a few milliseconds. Because of the particle's inertia, this electrophoretic motion becomes vanishingly small for frequencies above around 1 kHz.

Other mechanisms can respond to field reversals of much higher frequencies such as the dynamic behaviour of the electrical double layer distortion or polarisation around cells. This can follow changes in

---

Debye = A unit of electric dipole moment equal to 3.335 64 x 10^{-30} coulomb metre.

field direction that take as little as a few microseconds. Any faster than this (i.e. frequencies >50kHz) then the counter-ion cloud around cells does not have time to distort. Like the fall off in the electrophoretic motion with increasing field frequency, the decrease in response of the double layer to the changing field occurs gradually over a range of frequencies. This is termed a dielectric dispersion.

Interfacial polarisations are even more responsive to changing field directions and for sub-cellular sized particles can take as little as tens of nanoseconds to respond to a reversal in field direction, they can therefore exert their influence up to frequencies of 50MHz and beyond. This is still nowhere near as responsive as small polar molecules such as water to alternating fields. A measure of the ability of molecules in a material to align in an electric field is given by the relative permittivity of that material, which for bulk water molecules at 20°C in an alternating field less than 500MHz has a value of 80. At frequencies above 100 GHz the relative permittivity of water falls to that typical of non-polar molecules, around 4.5. A similar fall in permittivity is seen above about 50kHz on the freezing of water, because the molecules of the liquid become restricted in a solid lattice and can no longer rotate so freely to align with the field.

On cell death, membrane integrity is lost, it becomes permeable to ions and its conductivity increases by a factor of about 10^4 with the cell contents freely exchanging material with the external medium. This transition in the properties of the membrane shows up as a large change in the polarisability of the cell in an electric field. Other causes for particles having different polarisabilities include differences in their morphologies or structural architecture, which may be associated with the cells belonging to different species, different stages of differentiation or physiological state. Two such particles that differ in polarisability, are shown in Figure 2.3 subjected to an alternating homogenous field created between two parallel electrodes. The direction of the dipole moment formed by the interfacial charges is shown to depend on the relative polarisabilities of the particle compared with the medium.
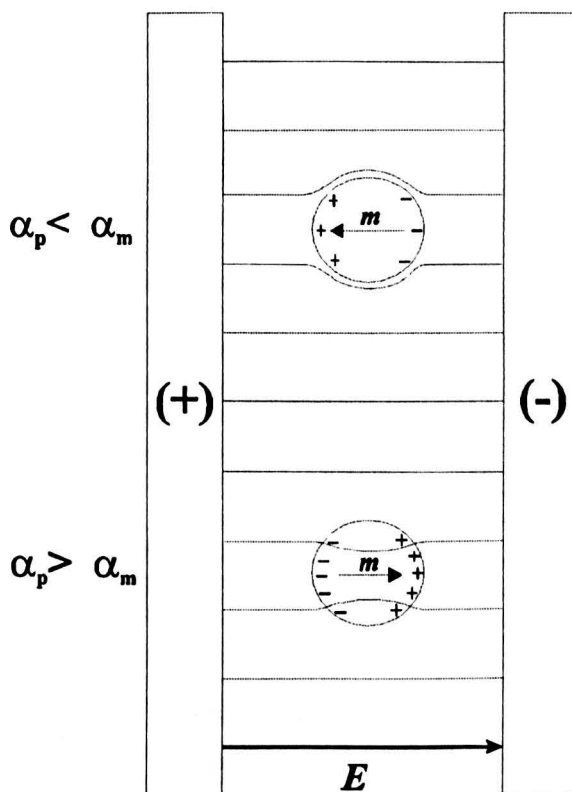
Figure 2.3 The polarisation of particles in an AC electric field.
Two particles of different polarisability are shown in a uniform AC electric field created between parallel electrodes. The alignment of the induced dipole moment m in the particle by the field E depends on whether the polarisability (α) of the particle is greater or less than that of the suspending medium. AC homogenous fields impart no motion on electrically neutral particles, due to the symmetry of forces on the sides of the particles.

2.6 Particle Motion in AC Inhomogeneous Electric Fields, Dielectrophoresis.

Homogenous AC electric fields do not induce motions in electrically neutral particles, due to equal forces acting on both sides of the polarised particle. If the particle carries a net charge, it will oscillate back and forth as a result of electrophoresis. As the frequency increases these translational oscillations become vanishingly small. Net translational motion is possible, however, if instead the field is inhomogeneous (see Figure 2.4). To distinguish this force from electrophoresis, Pohl adopted the term dielectrophoresis (DEP) (Pohl, 1951) from the term *dielectric* which is used to describe liquid and solid materials of low conductivity. For example, an intact membrane is a dielectric material characterised by having a conductivity 10^{16} times smaller than copper and a dielectric permittivity 3 times that of air. Examples of some particles investigated with DEP are given in Table 2.1.

(A) Negative DEP

$$\alpha_+ < \alpha_-$$

(B) Positive DEP

$$\alpha_+ > \alpha_-$$
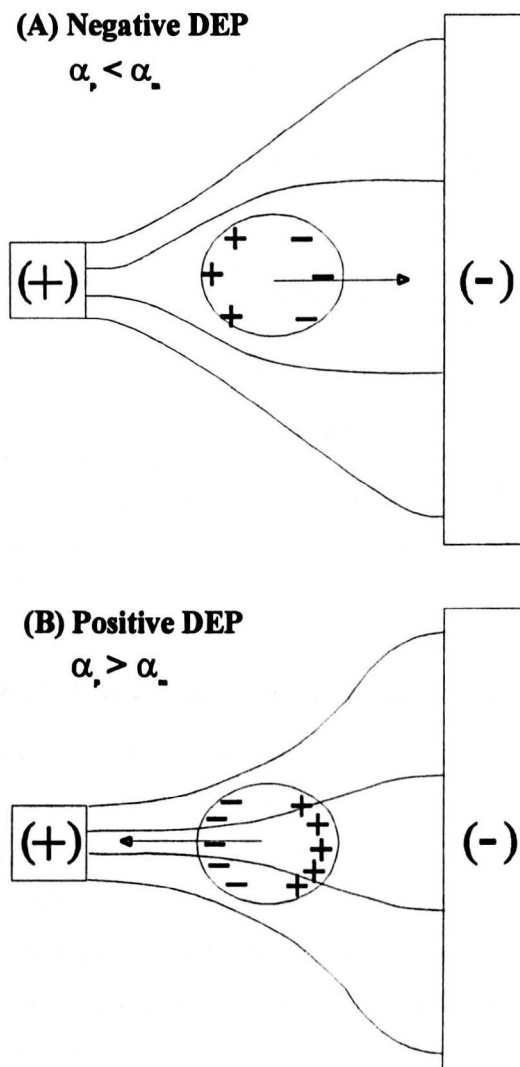
Figure 2.4 Polarisation of particles in non-uniform AC electric fields.
Two particles of different polarisability in a non-uniform (inhomogeneous) electric field. Particle (A) is less polarisable than the surrounding medium and so is directed (indicated by the arrow) away from the strong field region, whereas particle (B) of greater polarisability than the medium is attracted towards the strong field at the pin electrode. These effects occur whether or not the field is DC or AC.

PARTICLE TYPE		EXAMPLES
ACELLULAR	Virus	Trapping of single virion *Herpes simplex* type 1 (Hughes & Morgan, 1998)
PROKARYOTES	Bacteria	Characterisation and separation of bacteria (Markx *et al.*, 1994a, 1996)
EUKARYOTES	Protozoa	Differentiation between normal and *Plasmodium falciparum* infected erythrocytes (Gascoyne *et al.*, 1997b).
	Yeast	Batch separation of viable and non-viable (heat treated) *Saccharomyces cerevisiae.* (Markx *et al.*, 1994b).
	Plant cells	Batch separation of plant cells from mixture containing yeast and bacteria. (Markx & Pethig, 1995).
Mammalian cells	Cell lines	MDA231 human breast cancer cell separation from erythrocytes and T-lymphocytes (Gascoyne *et al.*, 1997a)
	Lymphocyte	Removal and collection of human leukaemia cells from blood (Becker *et al.* 1994).
OTHER PARTICLES	Proteins	Collection of proteins, e.g. avidin 68kDa and ribonuclease A 13.7kDa. (Washizu *et al.*, 1994).
	DNA	Separation of different sizes of DNA (9 - 48kb) using positive DEP with FFF (Washizu *et al.*, 1994).
	Liposomes	Alignment of cell size liposomes for subsequent electrofusion (Stoicheva & Hui, 1994).
	Artificial Nanoparticles	Separation of latex beads of diameter 93nm, with differing surface charge (Green & Morgan, 1997).

Table 2.1 Examples of particle types investigated by non-uniform AC electric fields (DEP).

2.7   Changing the DEP Force with the Medium Conductivity.

It was illustrated in Figure 2.4 that the polarity of the force exerted on the particle depends on the polarity of the induced dipole moment, which in turn is determined by the relative polarisability of the particle and the medium. As a consequence by altering the polarisability of the medium one can control the direction of motion of a particle. This principle can be exploited to gain particle separations by choosing a suspending medium with an intermediate polarisability, that is between the polarisabilities of two particles in the mixture, so that each particle type will be under the influence of a DEP force of different polarity. Selective manipulation using DEP force has been used to enable separations of various interspecific mixtures such as between some Gram +ve and Gram -ve bacteria (Markx *et al.*, 1994a), as well as the intraspecific separation of live and dead cells (Markx, Talary & Pethig, 1994b) or cancerous from normal cells (Becker *et al.*, 1994; Gascoyne *et al.*, 1997a). Differences between normal and parasitised cells within a population, for example erythrocytes parasitised with *Plasmodium falciparum* have also been observed (Gascoyne *et al.*, 1997b), and so separation of these two by DEP should also be possible. Examples of separations already demonstrated are listed in Table 2.2, along with the appropriate medium polarisabilities (conductivity) and field frequency. The DEP force imparted on a particle by an electrical field is also proportional to a number of other factors; the particle size (Pohl, 1978; Pethig, 1979) shape (Pethig, 1991) and the magnitude and degree of non-uniformity of the applied electric field.

CELL MIXTURE		CONDUCTIVITY (mS m⁻¹)	FREQUENCY (kHz)	RELEASED CELL
Escherichia coli (Gram -ve)	*Micrococcus luteus* (Gram +ve)	55	100	*E. coli*
Erythrocyte	*M. luteus*	10	10	Erythrocyte
Viable yeast	Nonviable yeast	1	10 MHz	Non-viable
Leukaemia cells	Blood cells	10	80	Blood cells
Human peripheral blood	Breast cancer cells	10	80	Erythrocyte
Peripheral blood stem-cell harvest samples		1	5	CD34+subpopulation

Table 2.2   Values of suspending medium conductivity and voltage frequency used to dielectrophoretically separate cell mixtures (adapted from Pethig, 1996).

The electrode geometry is very important in maximising the forces on the particles. For example, small and sharply pointed electrodes create strong field gradients, and therefore large DEP forces. Fabricated using standard photolithographic techniques, they typically take the form of thin 0.1 μm layers of gold on chromium, evaporated on glass (microscope slide size) substrates. One design, the interdigitated castellated electrodes Figure 2.5, through their geometry provide an efficient means of repeating regions of high and low field gradient, which, when fabricated over large areas, provide the means of large scale separations of particles. Although the cross-sectional area of these electrodes is small, the volume of liquid they energise is by comparison very large, and so the heat produced by electrical current dissipation is minimal. This means that large electric field gradients can be applied without the generation of thermal effects giving rise to cell damage or disruptive fluid convection flow.

Separation of particles under positive and negative DEP can be achieved either by gravity or fluid flow over the electrodes, which selectively removes the less immobilised particles under the influence of negative DEP and enables their subsequent collection. Those cells still held, under positive DEP, can be released by turning off the field and collected in a similar manner. Separation chambers based on this mechanism are usually composed of two electrode arrays sandwiching a thin layer of fluid. Thin chambers are used because the DEP force decays with distance in a near exponential manner, and an effective DEP force is considered to extend no further than 300 μm from the plane of the micro-electrode. Despite this possible limitation, separations of more than 10^7 cells per batch or at least 2.5×10^5 cells per minute are possible (Markx & Pethig 1995).
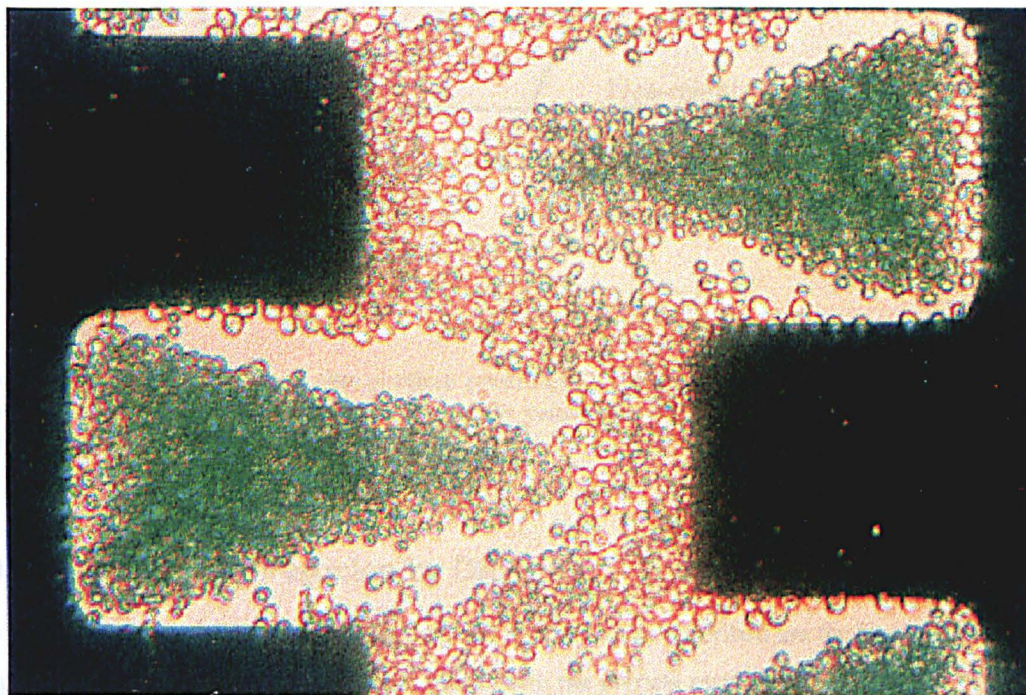
Figure 2.5 Separation of viable and non-viable cells by DEP.
By applying a 4 MHz signal to a cell suspension on castellated interdigitated electrodes, healthy and non-viable cells can be separated. Non-viable cells stained by a dye, experience a negative force and collect into loosely held triangular formations. The unstained viable cells, experience a positive dielectrophoretic force and collect in chains between opposite castellations (Pethig *et al.* 1992).

2.8   Controlling the DEP Force with Field Frequency.

The polarisability of a particle changes as a function of the frequency of the applied field. A single particle may therefore exhibit both positive and negative dielectrophoresis as its polarisability changes over a frequency range, for a constant medium conductivity. A typical DEP frequency spectrum with such a transition is shown for a live yeast cell in Figure 2.6. Also represented is the DEP spectra for a dead yeast cell, which only experiences a change in the polarity of DEP force for frequencies greater than a few MHz.
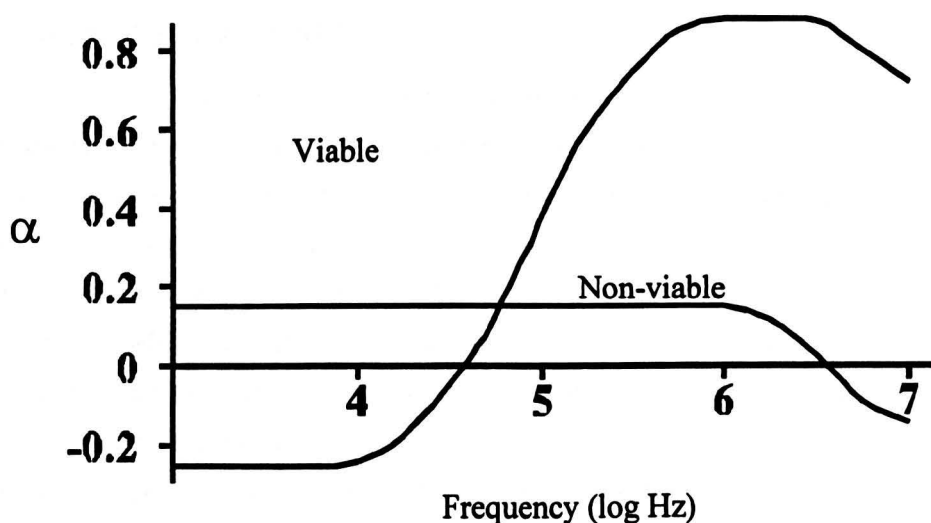
Figure 2.6 The variation of the particle polarisability α as a function of the frequency of the applied electric field for viable and nonviable yeast cells in a suspending medium of 8 mS m^{-1}. (Adapted from Talary *et al.*, 1996).

2.9 Levitation of Particles by DEP.

The attractive or repulsive forces on the particles by DEP so far described are for interactions where both the particle and electrode are in the same plane, with the particle resting on the substrate. Contact with the electrode induced by positive DEP may impinge on subsequent removal of the particle (e.g. by fluid flow or gravitational forces). The DEP force can, however, be applied to particles to make them levitate above the substrate, either from the result of an attractive high field region presented above the particle in the form of an electrode probe (Kaler & Jones, 1990) or by the repelling action of interdigitated electrodes on the plane of the glass, where the particle can be confined in a stable position above the electrodes (Markx, Rousselet & Pethig 1997). Particle levitation can be combined with other techniques, for example field flow fractionation (FFF), whereby particles levitated to different heights (up to 100μm and above) are exposed to different rates of fluid flow (Markx *et al.*, 1997; Gascoyne *et al.*, 1997a). Negative DEP forces can also be exerted from both above and below the particle to trap single particles in a '3D field cage', as was demonstrated for artificial particles (Schnelle *et al.*, 1993; Hughes & Morgan 1998) and for viral particles (Hughes *et al.* 1998).

Another application for DEP is the manipulation of cells prior to electrofusion. Attractive interactions between the induced dipoles of adjacent cells can result in the formation of chains of cells (pearl chains) of variable length. Close cell contact, followed by a high field strength DC pulse(s) of kV/cm and ms duration can lead to cell fusion of two to several thousand cells, so that giant cells can be formed as well as hybrid cells with two nuclei (Nuemann, Sowers & Jordan 1989).

2.10   Are Cells Damaged?

To induce cell fusion, or indeed electrical breakdown of the cell membrane, a field strength of at least ten times more than is typically used in DEP separations is required. Hybrid cells from electrofusion are viable, which suggests that cells having undergone exposure to normal DEP forces are not damaged. Further evidence was given for dielectrophoretically separated erythrocytes which excluded trypan blue (Becker *et al.*, 1994) and for yeast cells (Markx *et al.*, 1994b) and CD34+ cells (Stephens *et al.*, 1996) which were successfully cultured following exposure to DEP separation. Damage by the fluid flow has also been considered, the maximum shear stress exerted on the cell is around 3 dyn/cm^2 (Pethig, 1996). Erythrocytes have been reported to be able to withstand a shear stress 500 times this value (Leverett *et al.*, 1972), and T-lymphocytes over 50 times (Chittur, McIntire & Rich,1988) therefore almost insignificant levels of shear stress are experienced by these cells in DEP chambers. The conductivity of suspending medium used is normally much below that of a normal physiological medium, however, as long as the osmolarity is of the right value, osmotically sensitive cells can be investigated. This is achieved by additives such as sucrose at 280mM, which has little effect on the conductivity. An alternative approach has been that of Fuhr *et al.* (1994) who, using sub-micron electrodes which minimise heating effects, have been able to use normal physiological strength media.

2.11   DEP: Concluding Remarks

The method is non-invasive and does not require the use of antibodies or cell surface antigens or other labelling, although in some applications the use of specific markers or dielectric labels may be an advantage (Burt *et al.*, 1996). DEP can be employed at either the single-cell or multicell (more than 10^4 cells sec^{-1}) level, and it has already been demonstrated for a variety of applications, notably: the purification of cell cultures by DEP separation of non-viable or contaminating species, the isolation or enrichment of cell sub-populations, also the rapid isolation of toxic micro-organisms in water and food. Separation of microorganisms from faeces is seen as a potential for this technique, for example the isolation of trophozoites of *Entamoeba* from dysenteric stools prior to culture. Cell orientation, used prior to electroporation, can induce cellular contact between cells of the same or of different types, aiding electrofusion. Finally, manipulation of sub-micrometre particles such as single virions of the *Herpes Simplex* Virus (type-1) both in enveloped and in capsid form, gives an indication of the potential for sub-micron applications, such as studying single virion-bacterium interactions or virus harvesting. Rapid bioplymer (DNA or protein) fractionation has also been described in a method termed DEP chromatography (Washizu *et al.*, 1994).

2.12 Particles Subjected To Rotating Fields

Whereas conventional DEP utilises stationary fields, two closely related techniques utilise moving fields, more specifically either of rotating or travelling wave form. The investigation of particle motion in these moving fields has led to the development of some slightly different applications.

The generation of rotating electric fields was considered over 100 years ago, for example Meyer (1877) (quoted in Heydweiler 1897) described how to make a simple rotating electric field by the circular motion of an electrostatically charged rod. Using this method he induced antifield motion of a solar radiometer. Electrical generation of rotating fields are more suitable for scientific or technical purposes, examples of which were described by Arno (1892) and later improved by v. Lang (1906), for greater detail see the review by Arnold & Zimmermann, 1988).

Some important historical work concerning the rotation of objects in electric fields are listed below:

- **Hertz (1881)** stated that a rotating body exposed to a steady electric field would experience a retarding torque (electromagnetic braking),
- **Heydweiler (1897)** predicted that a rotating field would produce torque in a body,
- **v. Lang (1906)** demonstrated that the direction of rotation of an insulating dielectric cylinder in a rotating electric field could be either antifield or cofield, depending on the conductivity of the suspending liquid,
- **Lampa (1906)** following v. Lang's observations, wrote a detailed theory on how rotating electric field measurements could be interpreted,
- **Teixeira-Pinto *et al.* (1960)** observed rotation of suspended biological cells in linear electric fields,
- **Pohl (1978)** stated that non-uniform (inhomogeneous) fields can sometimes induce cellular spin,
- **Arnold & Zimmermann (1982)** demonstrated the rotation of a single biological particle in a rotating electric field.

The reliable method described by Arnold and Zimmermann (also by Mischel *et al.*, 1982) of inducing cellular spin by subjecting the cell to a uniform (homogeneous) rotating electrical field has been termed termed electrorotation (ROT). The basic format of the apparatus that may be used for studies of cell ROT study is shown in figure 2.7.
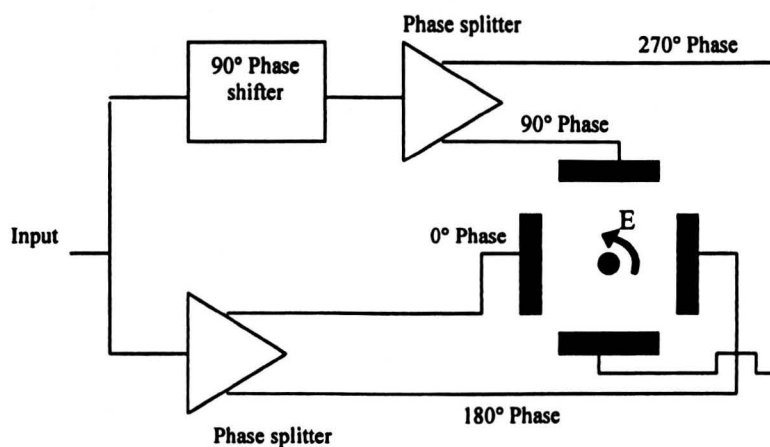
Figure 2.7 Schematic of apparatus used to produce a rotating electric field.

In this arrangement the test cell experiences sinusoidally varying fields produced by four electrodes that are driven with equal potential having four phases 90° apart. For two orthogonal linear field vectors of the form,

$$E_x = E_o \cos \omega t \tag{2.1}$$

and

$$E_y = E_o \cos(\omega t - 90°) = E_o \sin \omega t \tag{2.2}$$

then the amplitude of the field E resulting from their superposition at a given instant in time is given by

$$|E|^2 = |E_o|^2(\cos^2 \omega t + \sin^2 \omega t) \tag{2.3}$$
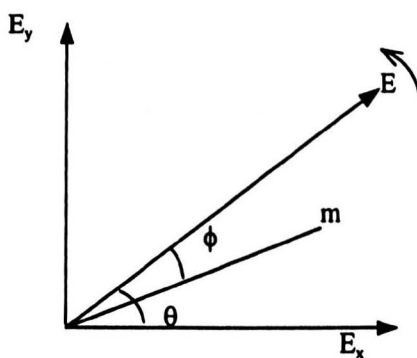
Figure 2.8 Superposition of two orthogonal linear field vectors to produce resultant field E at any instant and time. The dipole moment _m_ induced in the particle lags E by the angle ϕ.

giving $E = E_o$ at any instant in time. The angle θ in figure 2.8 is given by

$$\tan \theta = \frac{|E_o| \sin \omega t}{|E_o| \cos \omega t} = \tan \omega t \tag{2.4}$$

so that $\theta = \omega t$. The resultant field E thus rotates with angular frequency ω, the same as the applied sinusoidally varying fields. This rotating electric field can be produced, as shown in Figure 2.7, by four electrodes with 90° phase shifts, or by n electrodes phase shifted 360°/n apart.

Creation of the dipole moment in a particle by the field takes a characteristic time to reach its maximum value, equally when the field changes direction the dipole will respond and decay at a rate determined in part by the passive electric properties of the particle and suspending medium that appertain to the frequency of the applied voltage. Torque resulting in cellular spin is induced by the interaction between the rotating electric field and the remnant dipole. The torque T is therefore given by,

$$T = m \times E_o = mE_o \sin \phi \tag{2.5}$$

where ϕ (as shown in Figure 2.8) is the angle between the dipole moment and resultant field. This reveals an interesting fact, that for certain angles (360 > ϕ >180) the torque will be in the opposite direction to that of the field. This antifield rotation is shown in Figure 2.9. For a more mathematical approach see the review of Sauer and Schlögel (1985).

For a given particle, there is a unique rotation rate for each frequency of applied voltage. This variation in rotation rate is shown in Figure 2.10 for a viable and nonviable oocyst of *Cryptosporidium parvum* suspended in a $5\mu Scm^{-1}$ solution, whose viability had been confirmed using the fluorogenic vital dye technique of Campbell, Robertson & Smith (1992). Although the field may be rotating at rates greater than 10^7 s^{-1}, the induced particle rotation rate, which is dependent on the square of the field strength, remains measurable by the human eye. Depending on the frequency, typical rotation rates observed are between -3 and +1.5 rotations per second for a viable *C. parvum* oocyst subjected to a rotating field of around 10 kV m^{-1}, with negative rotation rates indicating antifield rotation of the particle. There is a frequency (around 800kHz for this conductivity) in the ROT spectra of Figure 2.10 where the viable and non-viable oocysts rotate in opposite directions, providing a convenient, single frequency, viability check on individual oocysts.
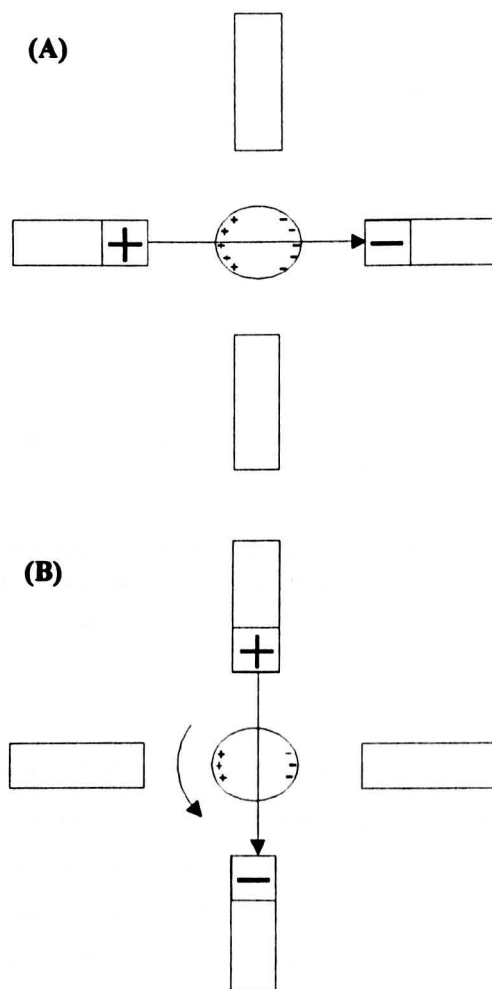
Figure 2.9 Generation of particle torque in a ROT chamber.
A particle in the ROT chamber. In a stationary field (A) the induced dipole moment for a particle that is less polarisable than the medium is directed against the field. On turning the field in a clockwise direction (B), the field interacts with the decaying charges to produce a torque and spin of the particle that opposes the direction of the moving field, termed *anti-field electrorotation*. Conversely for a particle that is more polarisable than the surrounding medium the torque induced results in a spin in the same direction as the field or *co-field rotation* (not shown) (from Huang *et al.*, 1993).
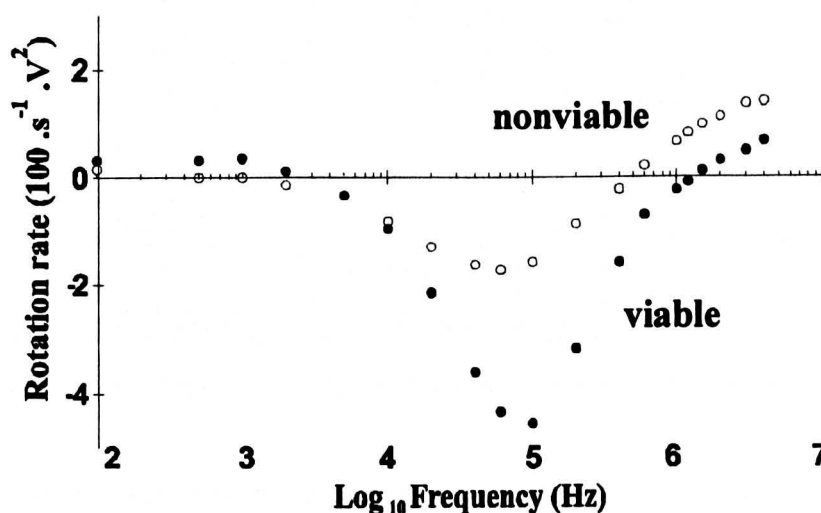
Figure 2.10 ROT spectra of live and dead *Cryptosporidium parvum* oocysts.
Viability was confirmed with the fluorogenic dyes 4',6-diamidino-2-phenylindole (DAPI) and propidium iodide (PI) according to Campbell *et al.* (1992).

Oocysts for observation in a ROT chamber, (which can be manufactured on a reusable glass slide or as a cheap 'use once - throw away' device) only require a few washes followed by resuspension in a known conductivity medium. Fluorogenic dyes in contrast, such as the fluorogenic vital dye assay (Campbell *et al.*, 1992) and the fluorogen exclusion test (Belosevich *et al.*, 1997) have several disadvantages: apart from expense, there is often a requirement for an incubation stage, specialist storage and handling, as well as a fluorescent microscope in a dark room. PI for example causes a list of acute toxicological effects, is carcinogenic, and requires refrigeration. ROT observation of a sample using a normal microscope can require less than 15 minutes preparation, which is also faster than a reverse transcription polymerase chain reaction (RT-PCR) test, which amplifies a sequence of mRNA from a *C. parvum* heat shock protein (Stinear *et al.*, 1996) that can determine the viability of individual oocysts. Although the particle suspension requires sufficient purification to avoid particle-debris interactions, ROT has found many applications, both with biological and synthetic particles (see Table 2.3).

PARTICLE TYPE		EXAMPLES
ACELLULAR	Virus	Virus erythrocyte interaction (Gimsa, Pritzen & Donath, 1989)
PROKARYOTES	Bacteria	Investigation of the flagellar motor torque of *E. coli* (Berry & Berg, 1996) Biocide treatment of bacterial biofilms (Zhou *et al.*, 1996)
EUKARYOTES Mammalian cells	Protozoa	*Plasmodium falciparum* infected erythrocytes (Gascoyne *et al.*, 1997) *Cryptosporidium spp.* oocysts (Goater, Burt & Pethig, 1997)
	Yeast	*Saccharomyces cerevisiae* comparison of wild type and vacuole deficient mutant (Asami & Yonezawa, 1996)
	Algae	*Neurospora* slime (Gimsa *et al.*, 1991)
	Plant cells	Barley Mesophyll protoplasts (Arnold & Zimmermann, 1982)
	Insect cell line	Effect of osmotic and mechanical stresses and enzymatic digestion on IPLB-Sf cell line of the Fall Armyworm (*Spodoptera frugiperda*, Lepidoptera) (Freitag *et al.*, 1989)
	Cell lines	MDA-231 human breast cancer cells (Gascoyne *et al.*, 1997a)
	Lymphocyte	Influence of membrane events and nucleus (Ziervogel *et al.*, 1986)
	Erythrocyte	Erythrocytes parasitised by *Plasmodium falciparum* (Gascoyne *et al.*, 1997)
	Platelet	Influence of activators (Egger & Donath, 1995)
OTHER PARTICLES	Liposomes	Liposomes with 1 to 11 bilayers (Chan *et al.*, 1997)
	Latex bead	Effect of surface conductance (Arnold, Schwan & Zimmermann, 1987)

Table 2.3 Examples of particle types investigated by rotating electric fields (ROT).

ROT demonstrates several features, the most important of which is the real-time assessment of viability of individual cells, which for *Cryptosporidium parvum* oocysts (Goater, Burt & Pethig, 1997) has been shown to correlate closely with the fluorogenic vital dye technique of Campbell *et al.* (1992). As well as the rapid (a few seconds per cell) straightforward assessment of the viability of individual cells, the viability of larger numbers of cells (e.g. 30 cells in a field of view at a magnification of 400) can also be assessed simultaneously. To assist the analyst, automatic measurement of the rotation rate or for a full spectrum is also possible (Schnelle, Glasser & Fuhr, 1997; Zhou, Burt & Pethig, 1998). A full frequency ROT spectrum, which can be thought of as a 'fingerprint' for heterogenous particles like oocysts, provides information not only about the viability of the particle, but also the conductivity and permittivity of the various 'compartments' within its structure (Chan *et al.*,1997). After ROT analysis, as with DEP, the particle remains intact and unchanged, and because ROT is a non-invasive method the particle can be subjected to further holistic or destructive analytical methods.

A variety of particle types, including the transmissive stages of parasites can be investigated by this technique. Indeed, whereas there is often the need to develop viability stains, molecular methods or excystation protocols for determining the viability of newly investigated cell types, ROT probes a common difference between all dead and viable cells, namely membrane integrity. Potential applications also include distinguishing between sub-types or strains of particles, whose surface or membrane properties differ, for example distinguishing between the cysts of the non-invasive *Entamoeba dispar* from the potentially invasive *E. histolytica* in which specific transmembrane proteins have recently been identified (Walderich *et al.*, 1998).

2.13 Particles Subjected to Travelling Wave Electric Fields

Like ROT, a third dielectric technique also uses moving fields, instead of rotating they are in the form of linear travelling waves, made simply by applying AC voltages in phase sequence to a linear array of electrodes. At low frequencies (< 100 Hz) translational motion is induced in the particles by largely electrophoretic forces, associated with surface charge characteristics. Early studies took this low frequency approach (e.g. Masuda, Washizu & Iwadare 1987). However, a problem encountered in these initial studies were erroneous particle trajectories and motion caused by the convection of suspending fluid.

Later, studies using higher frequencies (e.g. Fuhr *et al.*, 1991) at which DEP forces have the strongest effect on the motions of particles, were described, see Table 2.4 for a summary. Unlike DEP, the motion of particles in travelling waves or travelling wave dielectrophoresis (TWD) is achieved in a stationary supporting fluid : without the need for fluid flow there is no dilution of particle density. Indeed, the concentration of particles without the use of a centrifuge may be important for certain delicate particles which may be distorted or damaged. Centrifugation also incurs a loss of particles through adhesion to the centrifuge tube.

	PARTICLE TYPE	EXAMPLES
EUKARYOTES	Protozoa	*Cryptosporidium parvum* oocysts (Goater *et al.*, 1997)
	Yeast	*Saccharomyces cerevisiae* (Huang *et al.*, 1993)
	Plant cells	Membrane covered pine polls (Hagedorn *et al.*, 1992)
Mammalian cells	Blood cells	Erythrocytes (Masuda, Washizu & Kawabata, 1988) Separation of components of whole blood (Morgan *et al.*, 1997a)
OTHER PARTICLES	Artificial spheres	Cellulose spheres (Hagedorn *et al.*, 1992)

Table 2.4 Examples of particle types investigated by travelling wave electric fields (TWD).

Selective retention or transportation of subpopulations from a suspension is one application of TWD. Talary *et al.* (1996) demonstrated the separation of yeast cells using TWD, both by retaining viable cells at 5MHz and moving non-viable cells, and at a higher conductivity by moving viable cells while retaining non-viables. It was shown that for successful translational motion of particles by TWD, the particle must be under conditions of negative DEP (or negligible positive DEP) and at a frequency where ROT of the particle would be expected. The sense and magnitude of rotation expected indicates the direction and magnitude of the TWD force on the particle in the travelling wave. Electrode geometries were found to influence the TWD force, the optimum electrode gap was found to be similar to the effective particle size. The particles can be made to move over lines of electrodes (of the appropriate geometry, spacing width and voltage) as in the case of Fuhr *et al.* (1991) or for more convenient viewing, in the gap between the tips of many rows of electrodes (Huang *et al.*, 1993; Talary *et al.*, 1996) as shown in Figure 2.11. Transparent electrodes manufactured from ITO (indium titanium oxide) are also an option. Particles travelling over lines of electrodes do so a small distance from the surface. In this contact free manner, particle adesion to the substrate is avoided, which may be important for 'sticky' particles such as undecorticated *Ascaris* spp. ova (Dalton, personal communication).
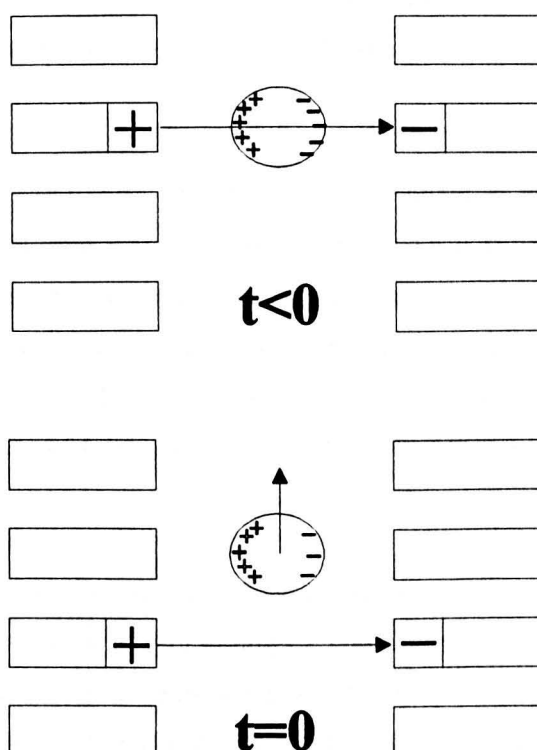
Figure 2.11 Travelling-wave dielectrophoresis (TWD) for a particle less polarisable than the medium ($\alpha_p < \alpha_m$).

In the instant before voltage switching between electrodes occurs (t < 0) the dipole moment induced is opposed to the direction of the field. On switching the electrode voltages (t = 0) the interaction between the remnant dipole and the field induces a translational force in the particle in the opposite direction to the travelling field, termed counter-field TWD.

Unless spiral electrode geometries are utilised, whose area can be increased *ad infinitum* by adding further helical turns, there are limits to the size of planar monolayer electrode arrays as there are spatial limitations for the connections to the individually addressed electrodes. Multilayer electrode fabrications only require four connections (for quadrature phases) to energise one or more TWD arrays of any length. Recently, multilayer TWD devices have been constructed and tested for their bioparticle manipulation and separation characteristics (*e.g.* Talary *et al.*, 1996; Morgan *et al.*, 1997). Theoretically, multilayer TWD devices can be built up (like a model railway track) so that particles may by taken to many investigative units such as ROT chambers, in a single integrated device. Separation, manipulation and characterisation of a particle in a single device, a sort of 'laboratory-on-a-chip device' has been proposed (see Ward, 1997 for a general review) and is under development.

A monolayer device has already been designed and constructed that combines TWD with ROT. This spiral electrode device was demonstrated for concentrating and testing the viability of cells (Goater *et al.* 1997). A travelling wave produced perpendicular to the spiral electrodes, directs and concentrates particles into the central region of the microelectrode structure, essentially a ROT chamber, where they

are then subjected to a rotating electric field. The viability of a cell is then obtained by observation of the sense of induced rotation at a single frequency. One application has been for the concentration and viability determination of the water-borne transmissive stage of *C. parvum* (Goater *et al*, 1997). A forecast of the potential of this particular device is its ability to handle particle concentrations of 10 ml^{-1} and less.

Although there is a current trend towards the miniaturisation of electrokinetic devices, along with investigations into submicron sized particles, it should be possible to investigate larger particles. Electrode geometries can be modified to suit particles up to 100µm in size or larger. Detection and viability determination of parasitic nematode ova, from urban sludge that is reused in agriculture, is one possibility. Presently, culture based viability techniques take more than one week (Gaspard, Wiart & Schwartzbrod 1996) but rapid determination of viability (<15 mins) can be predicted if this analysis is made using ROT.

Detection of environmental contaminates in food and water are of increasing public concern. Also, rapid automatic detection and enumeration of pathogenic micro-organisms such as those from patient samples; blood, urine and faeces, could improve diagnosis. Methods for the early determination of causative microbes are very limited. Conventional microbiological methods are slow, largely because incubations in cultural stages are required to generate detectable concentrations of cells, taking days. The rapid concentration, separation and identification of microbes (and their viability) already present in samples would avoid testing delays due to slow bacterial growth phases. The novel dielectric methods of DEP, ROT and TWD may offer a solution.

Table 2.5 summarises some potential applications of the described techniques, which either alone, in combination or in conjunction with conventional methods may assist in the fields of parasitological research, diagnostics and in disease treatment. Whereas some have already been demonstrated on bench-scale experiments, for the majority of these predictions to be realised as robust field techniques, further data must be collected on the electrokinetic responses of a wider range of bio-particles. These include non-target particles such as plant spores and non-pathogenic protozoan cysts, so the specificity of the tests can be optimised. Particles from different sources must also be investigated, for example there are subtle differences between preserved and fresh whole blood including lower cholesterol levels and a decrease in the level of phosphorylation of membrane proteins in the preserved erythrocytes, both of which may alter the electrokinetic response.

	APPROACH	COMMENTS
RESEARCH	Selective concentration, separation and manipulation of particles up to 100µm and above	General research tool
	Removal of contaminating bacteria from *in vitro* cultures of parasites	Leaving the culture unaffected, unlike chemical methods
	Real time detection of cell physiological state during interactions with chemicals, toxins or parasites	E.g. effect of antimalarial agents on the permeation pathway, or for studying merozoite inhibition
	Monitor parasite induced membrane alterations	Membrane architecture changes or ion channel activity
	Determination of viability in infectious doses which may be combined with testing of disinfection/drug sensitivity	*Cryptosporidium/ Giardia* (oo)cysts
	Isolation of individual parasite from sample for subsequent cloning/ molecular analysis	General research tool
DIAGNOSTIC	Specific identification and viability test for bio-particles from samples including; blood, urine, sputum, faeces, cerebrospinal fluid for deciding appropriate treatment, source of environmental contamination or risk assessment of water	Protozoans and ova of helminths
	Differentiate closely related species or sub-species	E.g. distinguishing between the morphologically similar cysts of *E. histolytica* (enteroinvasive form) from *E. dispar* (non-pathogenic)
	Manipulation of single bio-particles to specific antibody test sites or to combine with coated microbeads	Laboratory-on-a-chip applications
	Monitor antibody coating of microbeads, fractionate using DEP	Quality assurance, improve consistency of diagnostic assays such as agglutination and immunomagnetisable separation
TREATMENT	Removal of parasites/parasitised cells from body fluids e.g. blood / CSF for transfusion	Removal of *Plasmodium* stages including infected erythrocytes or trypanomastigotes

Table 2.5 Summary of potential applications in parasitology.

For these technologies to proceed and compete with current techniques they must be more specific, sensitive, reliable, rapid or more competitively priced. One simple way of achieving many of these requirements is to make the tests fully automated by integrating them onto a single disposable device. Following the introduction of microelectrodes into this field of study (Price, Burt & Pethig 1988, Masuda, Washizu & Nanba 1989; Fuhr *et al.,* 1991), using photolithography and associated semiconductor micro-fabrication technologies, and more recently the development of multilayer fabrication techniques, dielectrophoresis, electrorotation and travelling wave have all developed into techniques that can be incorporated onto a single 'bioprocessor-chip' device (Pethig *et al.,* 1998). The potential for incorporating all three techniques described, into one device, are outlined further by Talary, Burt & Pethig (1999).

2.14 References

Arno, R. (1892) Campo elettrico rotanto per mexxo di differenze di potenziali alternative. *Atti Accad. Naz. Lincei Rend.* **1**: 139-142.

Arnold, W.M. & Zimmermann, U. (1982) Rotating-field-induced rotation and measurement of the membrane capacitance of single mesophyll cells of *Avena sativa. Zeitschrift fur Naturforschung C* **37**: 908-915.

Arnold, W.M., Schwan, H.P. & Zimmermann, U. (1987) Surface conductance and other properties of latex particles measured by electrorotation. *Journal of Physical Chemistry.* **91**: 5093-5098.

Arnold, W.M. & Zimmermann, U. (1988). Electro-rotation: Development of a technique for dielectric measurements on individual cells and particles. *Journal of Electrostatics.* **21**: 151-191.

Asami, K. & Yonezawa, T. (1996) Dielectric behaviour of wild-type yeast and vacuole deficient mutant over a frequency range of 10kHz to 10GHz. *Biophysical Journal* **71**: 2192-2200.

Becker, F.F., Wang, X-B., Huang, Y., Pethig, R., Vykoukal, J. & Gascoyne, P.R.C. (1994) The removal of human leukaemia-cells from blood using interdigitated microelectrodes. *Journal of Physics D: Applied Physics* **27**: 2659-2662.

Belosevich, M., Guy, R.A., Taghi-Kilani, R., Neumann, N.F., Gyurek, L.L., Liyanage, L.R.J., Millard, P.J. & Finch, G.R. (1997) Nucleic acid stains as indicators of *Cryptosporidium parvum* oocyst viability. *International Journal For Parasitology.* **27**: 787-798.

Berry, R.M. & Berg, H.C. (1996) Torque generated by the bacterial flagellar motor close to stall. *Biophysical Journal.* **71**: 3501-3510.

Bone, S. & Zaba, B. (1992) *Bioelectronics.* John Wiley & Sons, Chichester, New York.

Burt, J.P.H., Chan, K.L., Dawson, P., Parton, A. & Pethig, R. (1996) Assays for microbial contamination and DNA analysis on electrorotation. *Annales de Biologie Clinique.* **54**: 253-257.

Campbell, A.T., Robertson, L.J. & Smith, H.V. (1992) Viability of *Cryptosporidium parvum* oocysts: correlation of *in vitro* excystation with inclusion or exclusion of fluorogenic vital dyes. *Applied and Environmental Microbiology.* **58**: 3488-3493.

Chan, K.L., Gascoyne, P.R.C., Becker, F.F. & Pethig, R. (1997) Electrorotation of liposomes: verification of dielectric multi-shell model for cells. *Biochimica et Biophysica Acta-Lipids and Lipid metabolism.* **1349**: 182-196.

Chittur, K.K., McIntire, L.V. & Rich, R.R. (1988) Shear stress effects on human T cell function. *Biotechnology Progress.* **4**: 89-93.

Coulter, C.B. (1920) The isolelectric point of red blood cells and its relation to agglutination. *Journal of General Physiology.* **3**: 309-406.

Egger, M. & Donath, E. (1995) Electrorotation measurements of diamide-induced platelet activation changes. *Biophysical Journal.* **68**: 364-372.

Freitag, R., Schügerl, K., Arnold, W.M. & Zimmermann, U. (1989) The effect of osmotic and mechanical stress and enzymatic digestion on the electrorotation of insect cells (*Spodoptera frugiperda*). *Journal of Biotechnology.* **11**: 325-336.

Fuhr, G., Hagedorn, R., Müller, T., Benecke, W., Wagner, B. & Gimsa, J. (1991) Asynchronous travelling-wave induced linear motion of living cells. *Studia Biophysica.* **140**: 79-102.

Fuhr, G., Glasser, H., Müller, T., & Schnelle, T. (1994) Cell manipulation and cultivation under AC electric field influence in highly conductive culture media. *Biophysica Biochimica Acta - General Subjects.* **1201**: 353-360.

Gascoyne, P.R.C., Wang, X-B., Huang, Y. & Becker, F.F. (1997a) Dielectrophoretic separation of cancer cells from blood. *IEEE Transactions on Industry Applications.* 33: 670-678.

Gascoyne, P., Pethig, R., Satayavivid, J., Becker, F.F. & Ruchirawat, M. (1997b) Dielectrophoretic detection of changes in erythrocyte membranes following malarial infection. *Biochimica et Biophysica Acta-Biomembranes.* 1323: 240-252.

Gaspard, P., Wiart, J. & Schwartzbrod, J. (1996) A method for assessing the viability of nematode eggs in sludge. *Environmental technology.* 17: 415-420.

Gimsa, J., Pritzen, C & Donath, E. (1989) Characterisation of virus-red-cell interaction by electrorotation. *Studia Biophysica.* 130: 123-131.

Gimsa, J., Marszlatek, P., Loewe, U. & Tsong, T.Y. (1991) Dielectrophoresis and electrorotation of *Neurospora* slime and murine myeloma cells. *Biophysical Journal* 60: 749-760.

Goater, A.D., Burt, J.P.H. & Pethig, R. (1997) A combined electrorotation and travelling wave device: applied to the concentration and viability of *Cryptosporidium. Journal of Physics D-Applied Physics.* 33: L65-L70.

Green, N.G. & Morgan, H. (1997) Dielectrophoresis of nano-particles. *Journal of Physics D-Applied Physics.* 30: L41-L44.

Hagedorn, R., Fuhr, G., Müller, T. & Gimsa, J. (1992) Travelling-wave dielectrophoresis of microparticles. *Electrophoresis.* 13: 49-54.

Hartley, G.S. (1935) The application of the Debye-Huckel theory to colloidal electrolytes. *Transactions of the Faraday Society.* 31: 31-50.

Hertz, H. (1881) Uber die vertheilung der electricitat auf der oberflache bewegter leiter. *Wied. Ann.* 13:266-275.

Heydweiler, A. (1897) Ueber Rotationen im constanten electrishen Felde. *Verh. Dtsch. Phys. Ges.* 16: 32-36.

Huang, Y., Wang, X-B, Tame, J. & Pethig, R. (1993) Electrokinetic behaviour of colloidal particles in travelling electric fields: Studies using yeast cells. *Journal of Physics D-Applied Physics.* 26: 1528-1535.

Hughes, M.P. & Morgan, H. (1998) Dielectrophoretic trapping of single sub-micrometre scale bioparticles. *Journal of Physics D-Applied Physics.* 31: 2205-2210.

Kaler, K.V.I.S. & Jones, T.B. (1990) Dielectrophoretic spectra of single cells determined by feedback-controlled levitation. *Biophysical Journal.* 57: 173-182.

Lampa, A. (1906) Ueber rotationen im elektrostatischen drehfelde. *Wien, Ber.* 2a 115: 1659-1690.

Lang, V.V. (1906) Vershuche im elektrostatishcen drehfelde *Wien, Ber.* 115: 211-222.

Leverett, L.B., Hellums, L.D., Alfrey, C.P. & Lynch, E.C. (1972) Red blood cell damage by shear stress. *Biophysics Journal.* 12: 257-273.

Lortet, M. (1896) Influence des courants induits sur l'orientation des bacteries vivantes. *Comptes Rendus de L'Academie des Sciences.* 122: 892-894.

Markx, G.H., Huang,Y., Zhou, X-F. & Pethig, R. (1994a) Dielectrophoretic characterisation and separation of micro-organisms. *Microbiology* 140: 585-591.

Markx, G.H., Talary, M.S. & Pethig, R. (1994b) Separation of viable and non-viable yeast using dielectrophoresis. *Journal of Biotechnology.* 32: 29-37.

Markx, G.H. & Pethig, R. (1995) Dielectrophoretic separation of cells - continuous separation. *Biotechnology and Bioengineering.* **45:** 337-343.

Markx, G.H., Dyda, P.A. & Pethig, R. (1996) Dielectrophoretic separation of bacteria using a conductivity gradient. *Journal of Biotechnology.* **34:** 175-180.

Markx, G.H., Rousselet, J. & Pethig, R. (1997) DEP-FFF: Field-flow fractionation using non-uniform electric fields. *Journal of Liquid Chromatography and Related Techniques.* **20:** 2857-2872.

Masuda, S., Washizu, M. & Iwadare, M. (1987) Separation of small particles suspended in liquid by non-uniform travelling fields. *IEEE Transactions on Industry Applications.* **23:** 474-480.
Masuda, S., Washizu, M. & Kawabata, I. (1988) Movement of blood cells in liquid by nonuniform travelling field. *IEEE Transactions on Industry Applications.* **24:** 217-222.

Masuda, S., Washizu, M. & Nanba, T. (1989) Novel method of cell fusion in field constriction area in fluid integrated circuit. *IEEE Transactions on Industry Applications.* **25:** 732-737.

Maxwell, J.C. (1891) *A treatise on electricity and magnetism.* 3rd edn. Clarendon Press, Oxford.

Michaelis, L. (1909) Elektrische Uberfuhrung von fermenten. *Biochemische Zeitschrift.* **16:** 81.

Mischel, M., Voss, A. & Pohl, H.A. (1982) Cellular spin resonance in rotating electric fields. *Journal of Biological Physics.* **10:** 223-226.

Morgan, H., Green, N.G., Hughes, M.P., Monaghan, W. & Tan, T.C. (1997) Large-area travelling-wave dielectrophoresis particle separator. *Journal of Micromechanics and Microengineering.* **7:** 65-70.

Neumann, E., Sowers, A.E. & Jordan, C.A. eds. (1989) *Electroporation and Electrofusion in cell biology.* Plenum Press, New York.

Pethig, R. (1979) *Dielectric and electronic properties of biological materials.* John Wiley & Sons. Chichester, UK.

Pethig, R. (1991) Application of AC electrical fields to the manipulation and characterisation of cells. In: *Automation in biotechnology.* (ed. *Karube, I.*), pp. 159-185. Elesevier, Amsterdam.

Pethig, R., Huang, Y., Wang, X-B. & Burt, J.P.H., (1992) Positive and negative dielectrophoretic collection of colloidal particles using interdigitated castellated microelectrodes. *Journal of Physics D: Applied Physics.* **25:** 881-888.

Pethig, R. (1996) Dielectrophoresis: Using inhomogeneous AC electrical fields to separate and manipulate cells. *Critical reviews in biotechnology.* **16:** 331-348.

Pethig, R. Burt, J.P.H., Parton, A., Rizvi, N., Talary, M.S. & Tame, J.A. (1998) Development of biofactory on a chip using Excimer laser micromachining. *Journal of Micromechanics and Microengineering.* **8:** 57-63.

Pohl, H.A. (1951) The motion and precipitation of suspensions in divergent electric fields. *Journal of Applied Physics.* **22:** 869-871.

Pohl, H.A. (1978) *Dielectrophoresis.* Cambridge University Press, Cambridge.

Price, J. A. R., Burt, J.P.H. & Pethig, R. (1988) Applications of a new optical technique for measuring the dielectrophoretic behaviour of micro-organisms. *Biochimica et Biophysica Acta.* **964:** 221-230.

Ruess, F.F. (1809) *Memoires de la Societe Imperiales de Naturalis tes de Moskou* **2:** 327-336.

Sauer, F.A. & Schlögel, R.W. (1985) Interactions between electromagnetic fields and cells. (Eds. Chiabera, A., Nicolini, C. & Schwan, H.P.). pp. 203-251. New York, Plenum.

Schnelle, T., Hagedorn, R., Fuhr, G. Fiedler, S. & Müller, T. (1993) 3-Dimensional electric-field traps for manipulation of cells: calculation and experimental verification. *Biochimica et Biophysica Acta.* **1157**: 127-140.

Schnelle, T., Glasser, H. & Fuhr, G. (1997) Opto-electronic technique for automatic detection of electrorotational spectra of single cells. *Cellular Engineering.* **2**: 33-41.

Stephens, M., Talary, M.S., Pethig, R., Burnett, A.K. & Mills, K.I. (1996) The dielectrophoresis enrichment of CD34(+) cells from peripheral-blood stem-cell harvests. *Bone marrow transplantation.* **18**: 777-782.

Stinear, T., Matusan, A., Himes, K. & Sandery, M. (1996) Detection of a single viable *Cryptosporidium parvum* oocyst in environmental water concentrates by reverse transcription PCR. *Applied and Environmental Microbiology.* **62**: 3385-3390.

Stoicheva, N.G. & Hui, S.W. (1994) Electrofusion of cell-size liposomes. *Biochimica et Biophysica Acta-Biomembranes.* **1195**: 31-38.

Talary, M.S., Mills, K.I., Hoy, T., Burnett, A.K. & Pethig, R. (1995) Dielectrophoretic separation and enrichment of CD34+ cell subpopulation from bone marrow and peripheral-blood stem cells. *Medical and Biological Engineering & Computing.* **33**: 235-237.

Talary, M.S., Burt, J. P. H., Tame, J.A. & Pethig, R. (1996) Electromanipulation and separation of cells using travelling electric fields. *Journal of Physics D-Applied Physics.* **29**: 2198-2203.

Talary, M.S., Burt, J.P.H. & Pethig, R. (1999) *Parasitology Supplement (in press).*

Teixeira-Pinto, A.A., Nejelski, L.L., Cutler, J.L. & Heller, J.H. (1960) the behaviour of unicellular organisms in an electromagnetic field. Experimental Cell Research. **20**: 548-564.

Wagner, K.W. (1914) Erklarung der dielektrischen nachwirkungsvorgange auf grund maxwellsher vorstellungen. *Archiv fur Elektrokinetik (Berlin).* **2**: 371-387.

Wang, X-B., Huang, Y., Burt, J.P.H., Markx, G.H. & Pethig, R. (1993) Selective dielectrophoretic confinement of bioparticles in potential energy wells. *Journal of Physics D-Applied Physics.* **26**: 1278-1285.

Ward, M. (1997) Devilish tricks with tiny chips. *New Scientist.* **153**:, No. 2071, 22-26.

Washizu, M., Suzuki, S., Kurosawa, O., Nishizaka, T. & Shinohara, T. (1994) Molecular dielectrophoresis of biopolymers. *IEEE Transactions on Industry Applications.* **30**: 835-843.

Zhou, X-F., Markx, G.H., Pethig, R. & Eastwood, I.M. (1995) Differentiation of viable and nonviable bacterial biofilms using electrorotation. *Biochimica et Biophysica Acta-General subjects.* **1245**: 85-93.

Zhou, X-F., Markx, G.H. & Pethig, R. (1996) Effect of biocide concentration on electrorotation spectra of yeast cells. *Biochimica Biophysica Acta- Biomembranes.* **1281**: 60-64.

Zhou, X-F., Burt, J.P.H. & Pethig, R. (1998) Automatic cell electrorotation measurements: Applied to studies of the biological effects of low-frequency magnetic fields and of heat shock. *Physics in Medicine and Biology.* **43**: 1075-1090.

Ziervogel, H., Glaser, R., Schadow, D. & Heymann, S. (1986) Electrorotation of lymphocytes, the influence of membrane events and nucleus. *Bioscience reports.* **6**: 973-982.

Chapter 3

Cryptosporidium species

3.1   Introduction to *Cryptosporidium* species

Infection with the protozoan *Cryptosporidium parvum* is one of the most common non-viral causes of human diarrhoea.   The genus was first proposed in 1910 with *C. muris,* from the gastric glands of laboratory mice, as the type species (Tyzzer, 1910).   Although *C. parvum* was described shortly after, in 1912, it was not until 1955 when *Cryptosporidium* spp. were recognised as a potential cause of diarrhoea (Slavin, 1955) and then not until 1976 before *C. parvum* was described as causing enteric disease in humans (Nime *et al.* 1976; Meisel *et al.* 1976).

Six years passed from the first human case descriptions until the first outbreak was recorded. Immunodeficient patients featured strongly in the first cases described, the Centres for Disease Control and Prevention (CDC, 1982) described 21 cases of cryptosporidiosis in acquired immune deficiency syndrome (AIDS) patients in the USA, occurring over a 3 year period.   *Cryptosporidium* remains the most commonly detected enteropathogen affecting AIDS patients.   Over the following 10 years, at least 12 well documented water-borne outbreaks occurred in the USA and UK (Lisle & Rose, 1995).   Then, in 1993, the largest outbreak of water-borne disease in recorded history occurred in Milwaukee, Wisconsin, affecting over 400 000 individuals (MacKenzie *et al.,* 1994).

From the period 1993 to 1996, there were at least 23 reported waterborne outbreaks of cryptosporidiosis in the UK and North America (where surveillance and epidemiology for this parasite has been reasonably comprehensive) (Fricker & Crabb, 1998).   The largest of these waterborne outbreaks occurred in Devon, UK, with at least 500 confirmed cases.   The fact that outbreaks continue to occur with such size and frequency following the Milwaukee incident indicates that there are considerable difficulties in the control of this parasite.

This chapter introduces the organism responsible for cryptosporidiosis, its biology (with particular attention to the structure of the oocyst) and reviews the problems associated with its detection and control.

3.1.1 Cryptosporidiosis : The disease

In immunocompetent people, the clinical signs of cryptosporidiosis include a 'flu-like' illness, diarrhoea, malaise, abdominal pain, anorexia, nausea, flatulence, malabsorption, vomiting, mild fever and weight loss (Fayer & Ungar, 1986).   Not all these signs are presented in every case, indeed some *Cryptosporidium* infections appear to be asymptomatic. High rates of asymptomatic infection may

probably reflect hyperendemicity and recurrent re-infection in immune subjects as in some developing countries. It must be noted that because an individual appears to be asymptomatic when sampled does not mean that they were so when they acquired their primary infection. Asymptomatic infection may help the parasite as it can persist in these individuals without incurring measures to be taken against it that may break its lifecycle, such as improved hygienic and sanitary practices.

Variation in the observed illness may be due to factors such as immune status, infecting dose, host age, and variations in the virulence of the organism. These factors also affect oocyst excretion patterns. Stools are characteristically described as loose-to-watery, malodorous, light coloured and containing mucus. In some immunocompromised individuals, such as those with AIDS, cryptosporidiosis can be a life-threatening condition causing profuse intractable diarrhoea with severe dehydration, malabsorption and wasting, with spread to other organs (Crawford & Vermund, 1988).

In most individuals *Cryptosporidium* infections are self-limiting. Symptoms commence on average 3 to 6 days post-infection, the duration of oocyst excretion generally occurs from less than 3 to 30 days (mean: 12 days). However, oocyst shedding can be intermittent and can continue for up to 50 days after the cessation of symptoms. Unlike other causative agents of diarrhoea such as rotavirus (mean duration of diarrhoea 5.9 days) and enterotoxigenic *E. coli*, it does not cause a rapid dehydration but the diarrhoea persists for a longer time (mean: 13 days for immunocompetent adults of the Milwaukee incident) and thereby produces malnutrition and further immunocompromise.

Unlike other protozoan intestinal diseases, such as giardiasis, which can be treated, there is presently no effective specific drug therapy for cryptosporidiosis. Treatment is limited to alleviating the symptoms; in cases where severe dehydration occurs, oral or intravenous rehydration therapy can be offered.

3.2   Biology of *Cryptosporidium*

3.2.1 Taxonomy

Cryptosporidium parvum is a coccidian protozoan of the phylum Apicomplexa, which includes other human pathogens such as *Plasmodium* and *Toxoplasma*. More specifically *Cryptosporidium* has been classified as follows:

Kingdom	Protozoa (Goldfuss, 1818)	predominantly unicellular,
Phylum	Apicomplexa (Levine, 1970)	possessing apical complex,
Class	Sporozoasida	asexual and sexual cycles, with oocyst formation,
Sub-class	Coccidiasina	life cycle with merogony, gametogony and sporogony,
Order	Eucoccidiorida (Leger & Duboscq, 1910)	
Suborder	Eimerioina	independent microgamy and macrogamy,
Family	Cryptosporidiidae (Levine, 1985)	four naked sporozoites without sporocyst,
Genus	*Cryptosporidium* (Tyzzer, 1907)	

Other than *C. parvum,* which infects a range of mammals, morphological and cross-infection studies indicate that there at least three other recognised species of *Cryptosporidium* (*C. muris* also infecting mammals, *C. baileyi* and *C. meleagridis* that infect birds). Species have also been reported that infect reptiles (*C. serpentis*) and fish (*C. nasorum*).

Differences have been also been found between material of the same species but from different hosts. Techniques used to differentiate isolates or species are listed below:

- 2D electrophoretic patterns from sporozoites

- isozyme typing

- Restriction Fragment Length Polymorphism (RFLP) analysis

- DNA sequencing

- immunoblotting with monoclonal antibodies (mAbs) or polyclonal antiserum

- immuno-surface labelling of oocysts

- incorporation of vital dyes

Using a PCR-RFLP analysis method targeting a fragment of the gene encoding for the *Cryptosporidium* oocyst wall protein, a method was developed that was able to distinguish oocysts of *C. wrairi* (derived from Guinea pigs) from *C. parvum* and to identify two groups of *C. parvum* isolates differentially associated with animal and human infections (Spano *et al.*1997).

3.2.2 Life cycle and Transmission

A coccidian of vertebrates, *Cryptosporidium* completes its lifecycle within the gastrointestinal tract of a single host. A simple schematic diagram of this lifecycle is presented in Figure 3.1. The prepatent period of this lifecycle (shortest time from ingestion of infective oocysts to complete the endogenous life cycle and excrete newly developed oocysts) has been determined as between 4 and 22 days for humans (Du Pont *et al.* 1995). In the same study using healthy volunteers, the patent period (duration of oocyst excretion) was found to range from 1 to 20 days.
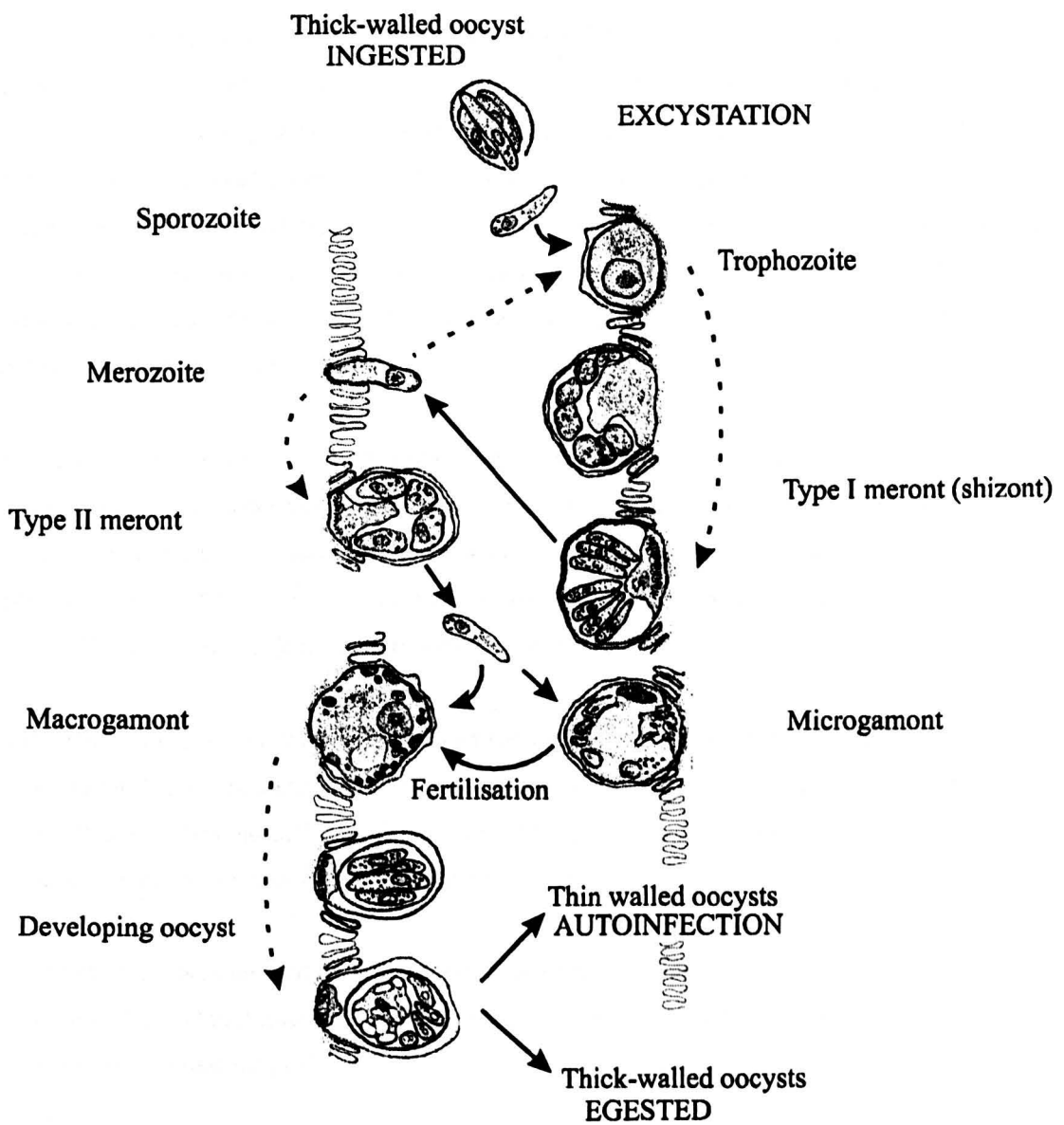
Figure 3.1 Life cycle of *Cryptosporidium parvum.*
Solid arrows indicate stages released into the lumen before reinfecting the epithelia. Development of stages is indicated by broken arrows. (Adapted from Fayer, Speer & Dubey, 1997).

Cryptosporidium infections occur world-wide, frequently in developed industrialised nations such as North America and the UK. Similar data are not generally available for other developed countries, but this probably represents under-detection and under-reporting.

Infection with *Cryptosporidium* may be transmitted either directly (person-to-person), from animals, and from contamination of the environment, especially water. Person-to-person transmission has been documented between family/household members, sexual partners, health workers and their patients, and children in day-care centres and other institutions. Zoonotic (animal-to-person) transmission from laboratory animals, household pets and domestic livestock have all been implicated, as have, feral and wild mammals which are known to excrete oocysts of *C. parvum*. Importantly, evidence implying waterborne bovine oocysts as a source of infection and disease in consumers of potable water has been forthcoming (Smith *et al.* 1989).

Transmission is by the environmentally robust oocyst, which following ingestion of a sufficient number by a suitable host and under favourable cues, excyst. The infective dose is very low. DuPont *et al.* (1994) determined that 30 oocysts could cause infection in man, with an infective dose that infected 50% of individuals (ID_{50}) of 132. 10 oocysts can cause infection in juvenile non-primates (Miller, Brondson & Morton 1990), 5 can cause infection in gnotobiotic lambs (Blewett *et al.*, 1993).

On excystation, each oocyst releases four naked sporozoites into the gut lumen (stomach for *C. muris*). Possible cues for excystation include, the increased temperature, the acid environment of the stomach and the more alkaline conditions in the small intestine. Bile salts and trypsin have also been shown to induce excystation *in vitro* (Robertson, Campbell & Smith, 1993).

In the gut lumen, sporozoites adhere to the surfaces of epithelial cells until microvilli surround it, making it intracellular but extracytoplasmic. Within this unique structure, termed the parasitophorous vesicle, they initiate asexual development.

Asexual multiplication called merogony or shizogony results when the trophozoite nucleus divides. *C. baileyi* has three types of schizonts, whereas *C. parvum* has two types. For *C. parvum* type I schizonts develop six or eight nuclei, and each is incorporated into a merozoite. After maturation and release, each merozoite infects another host cell to become either another type I, or a type II schizont which subsequently produces four merozoites.

On infection of another host enterocyte, merozoites from the type II schizont differentiate into either a microgamont (male), or a macrogamont (female) which initiate the sexual cycle. The microgamont becomes multinucleate (~16) (Current & Reese 1986) and each nucleus is incorporated into a microgamete (sperm equivalent) which, on release, may fertilise a macrogamont with its single nucleus (ovum equivalent).

Fertilised macrogamonts (zygotes) develop into one of two types of oocysts, thin or thick walled types, both of which sporulate *in situ* and contain sporozoites. The thin walled type, is thought to release its sporozoites into the gut which autoinfect the host. Sporozoites from these easily excyst as the oocyst is only limited by a single unit membrane. Interestingly, there is only one other coccidian genus, *Caryospora*, whose oocysts sporulate *in situ* and autoinfect the host. The presence of thin-walled, auto infective oocysts and recycling of type I meronts may explain why a small oral inoculum can produce an overwhelming infection in a suitable host and why immune deficient persons can have persistent, life-threatening cryptosporidiosis in the absence of repeated oral exposure to thick-walled oocysts. Autoinfection can be thought of as a 'bet-hedging' strategy, as maintaining the lifecycle in the host presumably gains the parasite the advantage of releasing oocysts over a greater time span and therefore more likely into a favourable environment.

The thick walled oocyst, in contrast, is environmentally resistant and survives egestion from the host with the faeces. Enormous numbers of infective oocysts are egested in the faeces, during a typical symptomatic infection 10^{10} oocysts are released. This vast number, resulting from many multiplication stages, along with the low infective dose; the requirement of only a single host and the apparent lack of or reduced host specificity increases the potential for environmental spread and contamination.

3.2.3 The oocyst

Egested oocysts, as outlined in the lifecycle, Figure 3.1, are the infective stage of the parasite. The demonstration of intact oocysts in faecal samples or concentrates by microscopy forms the usual method for the laboratory diagnosis of infection. To aid identification a number of staining methods are commonly used, for example the modified Ziehl-Neelsen stain or auramine-phenol (Casemore, 1991) which are generally reliable but of low sensitivity (Weber *et al.* 1991).

Some techniques have been shown to detect parasite products, rather the intact oocysts, often with the advantage of greater sensitivity. Immunoassay techniques and DNA detection from faeces are examples of such methods. Indirect detection, through evidence of a previous immune response (serology) is another technique of use, especially to epidemiologists. As might be expected, seroprevalence rates tend to be higher than frequencies determined by oocyst detection.

All human infections of cryptosporidiosis are considered to be due to *C. parvum*, the oocysts of which typically occur in surface waters at a concentration of *c.* 0.01-100 per litre. The oocysts of *C. parvum*, measured from human faeces ranged from 3.8-6.0 x 3.0-5.3μm with a mean size of 5.0 ± 0.25 x 4.5 ± 0.26 μm, a shape index (major / minor diameter) of 1.1, and a specific gravity of 1.05. Their small size enables them to penetrate through sand filters used in water treatment works. A pore size of no greater than 3μm is required to prevent their passage in membrane filters. Importantly, a certain plasticity of oocyst morphology has been demonstrated. *C. parvum* oocysts from calves were statistically significantly larger after recovery from experimentally infected baby rats (Beyer & Sidorenko, 1993).

Containing four naked sporozoites, the near spherical oocysts are enclosed within a thick wall that serves a protective function by isolating the parasite from the external environment. In contrast, the thin-walled oocysts, which are produced in fewer numbers (~20%) posses a fragile (single-unit) membrane that is easily ruptured by vigorous sporozoite movement (Current & Reese 1986). Subsequently, thin-walled oocysts are rarely, if ever, found in the egested faeces.

The physical surface properties of the oocysts have also been investigated, primarily in order to estimate the efficiency of microfiltration systems designed to remove such particles from surface waters. Measurements of electrophoretic mobility have demonstrated zeta potentials (the potential at the hydrodynamic plane of shear a small distance beyond the cell surface) for both *Cryptosporidium* oocysts and *Giardia* cysts to be similar to other particles in surface waters: at neutral pH zeta potentials are -25 to -35 mV; the charge can be neutralised by addition of H^+ ions, approaching zero (net) surface charge at around pH 3; the addition of excess positive ions will reverse the charge (Ongerth, & Pecoraro 1996). A slight decrease in zeta potential over time (1 month storage) was noted by Drozd and Schwartzbrod (1996), who also determined a zeta potential of -25mV at neutral pH and in river water with conductivity of around $300\mu S$ cm^{-1}, as well as an isoelectric point (pH at which the net charge and electrophoretic mobility is zero) of around 2.5. The hydrophobicity of oocysts has been measured, for example by the measurement of oocyst adhesion to octane. Drozd and Schwartzbrod (1996) found the hydrophobicity of *Cryptosporidium* to be low, especially at very low suspension conductivities ($<200\mu S$ cm^{-1}), in agreement with the findings of Musiel *et al.* (1987) who found a preferred adhesion of oocysts to glass rather than to hydrophobic plastic materials. Hydrophobicity was also measured against pH, the lowest mean hydrophobic potential (%A) was at neutral pH. This information has implications for the substrate and solution used for the ROT measurements of oocysts. Preference should be given to solutions of neutral pH and to substrates of hydrophobic plastic rather than glass to avoid adhesion.

It is of interest to note that the isoelectric point of eukaryotic cells (calculated by isoelectric focusing) has been shown to distinguish between viable and non-viable eukaryotic cells, the surface charge increasing when the cells become non-viable leading to a lower pI (Righetti, 1976). It was suggested that this change due to a rearrangement or conformational change on the cell surface was possibly a result of shielding of thiol groups. Also it was noted that isoelectric focusing (IEF) and cell electrophoresis, two methods to measure the pI value, give slightly different results by 2-3 pH units, as IEF probes 5nm further into the cell surface.

3.2.3.1   Oocyst wall

TEM studies show the (thick) oocyst wall of *Cryptosporidium* as composed of two electron-dense layers separated by an electron-lucent space (Reduker, Speer & Blixt 1985a) a diagram of which is presented in Figure 3.2. The outer layer is thin and moderately coarse, the inner layer is thicker and appears finely granular. This bilayered structure serves as a barrier to the sporozoites within. Of particular interest, TEM measurements revealed a range of 31.6-72.9 nm for the oocyst wall thickness (Reduker *et al.*, 1985a).

External face

Outer layer

Electron-lucent space

Outer zone (with electron-lucent mid region)

Inner layer

Inner zone

10nm

Internal face with plasma membrane
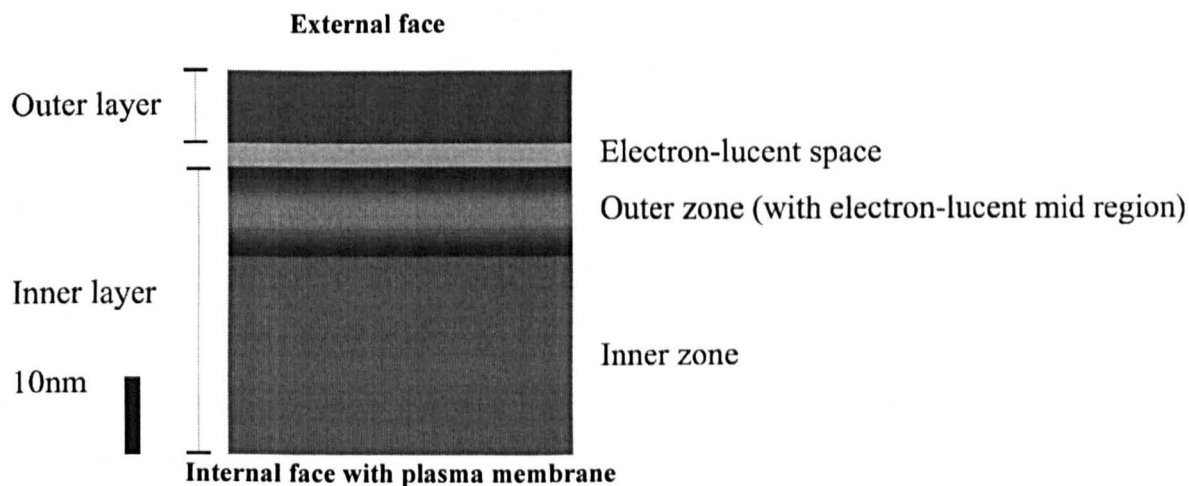
Figure 3.2 Diagram summarising the TEM observations of the oocyst wall structure of *Cryptosporidium parvum*, showing the relative widths of each layer, using the mean values from Reduker *et al.* (1985a) see Table 3.1.

	Mean width ± 1 SD (nm)	Range
Outer layer	10.0 ± 3.3	5.1 - 16.6
Electron-lucent space	2.5 ± 0.8	1.6 - 5.1
Inner layer - OUTER ZONE	11.6 ± 2.7	6.6 - 15.3
INNER ZONE	25.8 ± 5.3	16.1 - 41.0
Total oocyst wall	49.7 ± 11.5	31.6 - 72.9

Table 3.1 Values from TEM study of oocyst wall dimensions for *Cryptosporidium parvum* by Reduker *et al.* (1985a).

The electron-lucent space between the outer and inner layers of the oocyst wall originates from two unit membranes that form during development simultaneously external to the plasmalemma (plasma membrane) while the sporont separates from the feeder/attachment organelle.

Unlike other coccidia the oocyst wall of *Cryptosporidium* spp., has a suture at one pole spanning 1/3 to 1/2 the circumference of the oocyst (Reduker *et al.* 1985b). This dissolves at one end during excystation, providing an exit for the sporozoites.

The values given by Reduker *et al.* for oocysts of *C. parvum* listed in Table 3.1 are in sharp contrast to a study by Current & Reese (1986) who described the dimensions of the inner (210- 255nm) and outer wall (180-600nm) of unsporulated thick walled oocysts still contained in parasitophorous vesicles within the host epithelial cells.

As well as dimensional data, which is important for dielectric modelling and interpretation of electrorotational studies, some information is available on the composition of the oocyst wall. In contrast to *Eimeria* (another coccidian that develops in the gastrointestinal tract of vertebrates through all their lifecycle) whose wall is composed of a single glycoprotein, the walls of *Cryptosporidium* appear to

contain a number of proteins. One method, involving surface labelling of intact oocysts, identified a range of 5 proteins, of 15 - 96 kDa molecular weight (Lumb, Lanser & O'Donoghue, 1988).

Some of these proteins appear to be glycosylated. The reactivity of a monoclonal antibody (mAb 1B5) to 41 and 44kDa bands from oocyst walls were reduced by periodate ($NaIO_4$) treatment, suggesting that the epitopes are glycosylated (MacDonald, McCrossan & Petry, 1995). Other epitopes have been shown not to be glycosylated, i.e. they were insensitive to periodate digestion. The even fluorescence produced from fluorescently labelled mAbs directed towards oocyst surface epitopes suggest a uniform distribution of epitopes.

Other evidence of the composition of the wall comes from studies of lectin binding to intact oocysts. Lectins (from seaweed) specific to N-acetyl-D-glucosamine (GlcNAc) were shown to agglutinate intact oocysts from four clinical *C. parvum* isolates, suggesting that this sugar moiety is present on the oocyst outer wall (Llovo *et al.*, 1993) whether present in polysaccharides or glycoproteins was not determined. Others, using lectin-binding and lectin-inhibition studies, have demonstrated the presence in the outer wall of *C. parvum* both galactose/galactosamine and glucose/glucosamine residues, possibly with both *N*- and *O*-linked glycosylation (reviewed by Tilley & Upton, 1997).

3.2.4 Resistance of oocysts to various agents

The robustness of the oocysts was personally encountered when difficulties were found making ultramicrotone sections during a TEM study of *C. parvum* oocysts. Survival rates in water also demonstrated the resistance of these particles, a proportion surviving six months suspension in water (Robertson *et al.* 1992). This property of the oocyst also helps them withstand man-made physical and chemical stresses.

Resilience to various physical disinfection factors has been reported, including exposure to temperature extremes, ultra violet (UV) light, pulsed light and to air-drying. Figure 3.3 summarises studies that have investigated the effect of temperature on the survival of oocysts. Whereas most of these studies investigated combinations of temperature and time that was close to the critical boundary (either side of which large changes in survival were obtained), the sensitivity of dielectrophoresis (DEP) was clearly tested on some very crudely killed oocysts (Archer, Betts & Haigh, 1995). An autoclave was used, which subjected the oocysts to a temperature of 121°C for 10 minutes, at a pressure of 1.05 bar, whereas previously it was established (Fayer, 1994) that heating to 72.4°C (in a DNA thermocycler set to 75°C) for 1 minute was sufficient for oocyst inactivation (in water free of debris). In Fayer's study inactivation was determined by detection of infection in six sites in 36 mice, following doses of 150 000 oocysts, where the minimum infective dose had been calculated as being 25 oocysts. Oocyst inactivation by heating to 72.4°C for 1 minute was therefore shown to inactivate 150 000 oocysts to between 0 and 25 oocysts. It was noted that other suspending media may alter the temperature or time required for this inactivation.
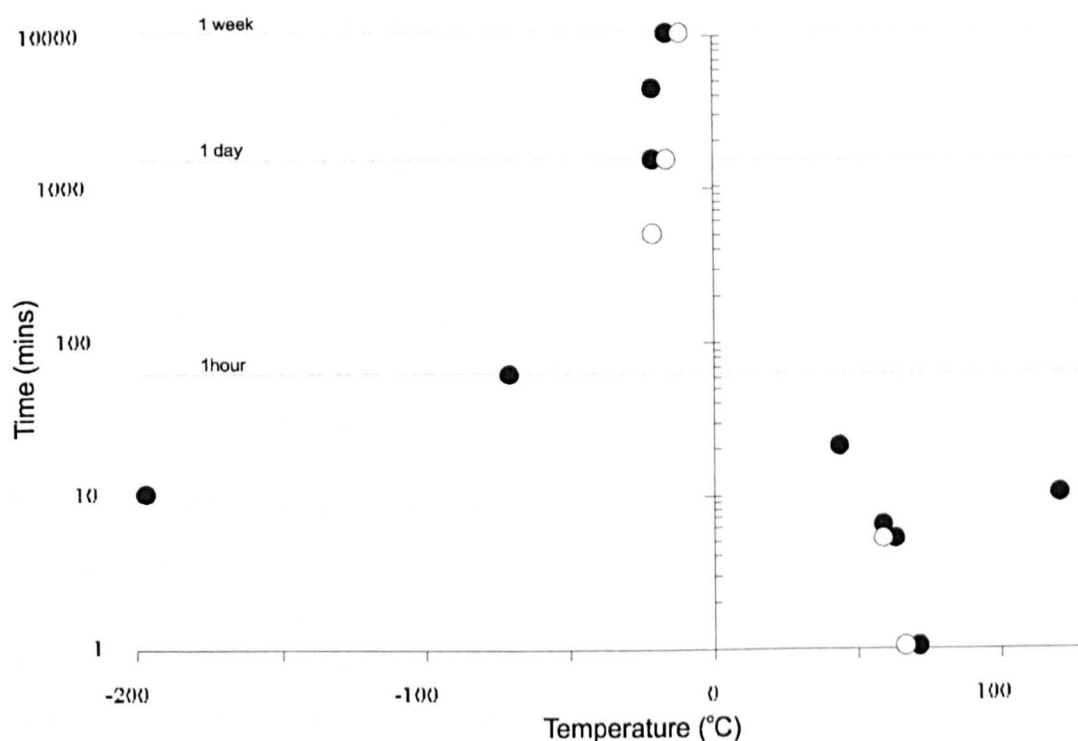
Figure 3.3 Summary of laboratory studies investigating the survival limits of oocysts exposed to heat and cold.
Results, non-infectious (•), infectious (O) as determined by *in vivo* testing in mice
(or * by DEP) data from Fayer *et al.* 1997.

One study of the UV disinfection of oocysts found that 150 minutes exposure to UV light at a strength of 15 Ws^{-1} was required for complete inactivation of a thin layer oocyst suspension (10 ml in a normal Petri dish) containing 2500 oocysts ml^{-1} (Lorenzolorenzo *et al.* 1993). Concerns were raised, however, as this is somewhat higher than the exposure level recommended by the U.S. Public Health Service.

Chemical disinfection has also been tested. Oocysts of *C. parvum* have shown considerable resistance against the effects of most commercial disinfectants. Although chlorine and other related halogen compounds can greatly reduce the ability of oocysts to excyst or infect, relatively high concentrations (which are therefore very expensive or quite toxic) and long exposure periods are required, limiting practical application. Ozone has been suggested as one of the most effective chemical disinfectants that may have application against oocysts in water. On average 4.5 mg min/l CT (concentration x time) at temperatures of between 20 and 25°C were required for 99% oocyst inactivation (measured by mouse infectivity) (reviewed by Rose, Lisle & LeChevallier, 1997). As well as criticisms of the timing of the method of CT calculation, based on the concentration of reactants at the end of the contact time (which overestimates the concentration required by a factor of about two), Korich *et al.* (1992) noted that each CT value calculation should be based on several disinfection concentrations. Importantly, of the eight

ozone disinfection studies listed by Rose *et al.* (1997) only two (Parker, Greaves & Smith 1993; Finch *et al.* 1993) were performed at a temperature below 10°C, an important point considering that most water treated would be below this temperature.

Synergistic strategies may also offer a solution. Combinations of treatments, for example ozone and monochloramines, produce inactivation greater than the sum of their effects examined separately (Finch *et al.* 1994).

Ideally, disinfection would only be required for water samples containing infectious oocysts. Viability is a prerequisite but not necessarily a perfect indicator of the potential infectious nature of an oocyst. Current detection and monitoring methods are discussed in the next section.

3.2.4.1 Detection and Monitoring - current status

The waterborne route for the transmission of *Cryptosporidium* is of great importance. Outbreaks of waterborne cryptosporidiosis, such as those in Milwaukee USA (1993) and in Devon UK (1995) have led to much interest in monitoring of water for the presence of oocysts. Environmental monitoring for these parasites is made problematic by their small size, their relatively low concentrations in most waters and the inability to augment their numbers by *in vitro* culture. There are also difficulties in identifying them amongst other particles and debris; for example, oocysts are often extracted from complex media such as water concentrates, sand, sludges and effluents.

A typical nationally recommended procedure for extraction includes:
'filtering a large volume of water through either a membrane or cartridge filter; releasing and eluting the trapped parasites from the filter matrix; concentrating the eluate to a small volume, possibly with a clarification procedure for dirty samples; and examining the final concentrate or a proportion thereof by fluorescence microscopy' (Smith, Robertson & Ongerth, 1995).

Within such a time-consuming, labour-intensive series of steps, the possibility to incur oocyst losses exists. Moreover, the microscopy in particular, requires full-time, well-trained and patient personnel.

Potential improvements to these detection methods could easily include the automation of fluorescence detection. Monoclonal antibodies bound to fluorogenic dyes (usually fluorescein isothiocyanate (FITC)) are currently used to highlight the oocysts wall aiding confirmation, as are several nucleic acid reactive fluorogenic dyes which highlight the nuclei (Grimason *et al.* 1994). A cooled, slow-scan, charge-couple device (CCD) has shown the potential to be used for routine screening of water samples for *Cryptosporidium* oocysts (Campbell *et al.* 1992). Contamination, however, from debris in the sample concentrate often hinders imaging methods (the ratio of particles of similar size to oocysts may easily be as high as 10^9:1 in 100 litres raw water) (in Smith *et al.* 1995).

Other methods of detection include those based upon antibody selection (although these often suffer from cross-reactivity and antigenic variability within clinical isolates) and those based upon nucleic acid recognition (e.g. polymerase chain reaction).

Although sensitive (typical limit of <200 oocysts) few PCR based detection methodologies give direct information on oocyst viability. One method that did give such information, was based on an *in vitro* infectivity assay (of cell monolayers) whose infections were detected by a *C. parvum* specific reverse transcriptase PCR of extracted mRNA, targeting the heat shock protein 70 (*hsp70*) gene (Rochelle *et al.* 1997). Importantly a single infectious oocyst was detected by this experimental procedure, and the use of concentrated samples obtained from 250 litres of finished water had no observable effect on either the integrity of the cell monolayers or on the infectivity of oocysts seeded into the concentrate. The status of PCR for *Cryptosporidium* detection from various media was reviewed by Morgan & Thompson (1998). An outline of the best (by sensitivity) of the PCR protocols for each source is given in Table 3.2.

Although the potential benefits of PCR seem great, high sensitivity, ease of use, ability to analyse large numbers of samples at one time, relatively low cost, ability to speciate oocysts (thus eliminating false positives encountered with cross-reactions of antibodies to non-pathogenic protozoan species) and 'strain typing' potential (thus allowing the source of the infection to be determined) the technique is not without its limitations. Only one reported the ability to determine viability, and the fastest method for detection from water samples was 3-4 hours to process 10-20 samples.

Oocyst source	Target	Sensitivity to oocysts	Specificity	Time to extract nucleic acids (10-20 samples)	Strain differentiation/ quantitation/ viability	Comments
DNA	DNA fragment	~200	cross-reacted with *Eimeria* and weakly with *Giardia*	several days	Nil/ND/ND	-
Purified oocysts	wall protein gene	40	poor	4 - 5 h	Nil/ND/ND	-
Milk	protein gene	poor	good	3 - 4 h	Nil/ND/ND	Failed to detect one human isolate of *C. parvum*
Faeces	Random Amplified Polymorphic DNA (RAPD)	1-10	good	1 - 2 h	Differentiates directly between human and bovine *C parvum*/ND/ND	-
Water	various	1-10	good	3 - 4 h	Nil/ND/ND	Multiplex PCR for the simultaneous detection of *Cryptosporidium* and *Giardia*
Waste-water	wall protein gene	poor (100 using nested PCR)	numerous non-specific bands	4 - 5 h	Nil/ND/ND	-

Table 3.2 Outline of best-published protocols for the PCR detection of *Cryptosporidium parvum* oocysts, categorised by source (Adapted from Morgan & Thompson, 1998). ND = not determined, RAPD = Random Amplified Polymorphic DNA.

3.2.5 Conclusions

Since it was first demonstrated that *C. parvum* could cause human disease, in a 3 year old child (Nime *et al.* 1976), the importance of this parasite has grown, with the Milwaukee epidemic of 1993 clearly highlighting this fact. Unlike other diarrhoeal agents cryptosporidiosis is generally more protracted, with a patent period of generally up to 20 days (or 30 days depending on the study). The immune deficient, immune naive or those with acquired immune syndrome are especially vulnerable to persistent infection, although AIDS patients are no more at risk from suffering the effects of a primary infection of cryptosporidiosis than other individuals.

Whereas normally, if you are going to catch an infectious disease, there are advantages to living in an industrialised country, this is not necessarily the case with cryptosporidiosis. Treatments, which may only be available in richer countries, have not been developed. Secondly, the geographic advantages of living in a temperate region such as an absence of a vector, such as with malarial infections and the *Anopheles* mosquito, do not apply. Indeed, where ingestion of contaminated water is the mode of transmission, those in temperate regions may actually be at a disadvantage because oocyst survival rates are greatly increased by storage at lower temperatures.

Several features of the biology of *Cryptosporidium* help the transmission cycle. Assisting with the persistence of the host infection are the auto-infecting thin-walled oocysts (~20% of those produced). The diarrhoea that cryptosporidiosis induces, means that the oocysts (that are fully sporulated and ready to initiate infection upon egestion) may be released from the host dispersed in a liquid phase, aiding transmission. The release of around 10^{10} oocysts during a typical infection, increases the likelihood of new host infection, or reinfection of the current host, even following dilution in a media such as surface waters, in which oocysts occur at concentrations of 0.01 to 100 l^{-1}.

The robust structure of the thick walled oocyst protects it from many chemical and physical disinfection methods employed to treat drinking water. These methods must be sufficient to enable a reduction of infectious oocysts to below the infectious dose, which is very low at around 30 oocysts for humans.

A sensitive detection method for the oocysts of *Cryptosporidium* would be a useful tool, especially for the water industry. Ideally a test would be automated, work at the single organism level, give information on viability and the identification of the oocyst. Automation is of particular importance as not only does this reduce the time of trained microscopists, but introduces standardisation where currently there may be an element of subjectiveness. The following chapters of this thesis describe in detail electrorotation (ROT) analysis of the thick walled oocysts of *C. parvum*. Both automation and the ability to work at the single organism level have previously been demonstrated. The ability of the ROT technique to satisfy the requirement for viability information and identification are explored.

In Chapter 7 a device is described that may assist in extracting low numbers of oocysts from various sources, possibly including faecal matter, that may improve the sensitivity of techniques such as PCR.

3.3 References

Archer, G.P. Betts, W.P. & Haigh, T. (1993) Rapid differentiation of untreated, autoclaved and ozone treated *C. parvum* oocysts using DEP. *Microbios.* **73:** 165-172.

Beyer T.V. & Sidorenko N.V. (1993) One more biological characteristic of coccidia in the genus *Cryptosporidium* (Sporozoa: Apicomplexa). *Parasitologia.* **27:** 309-319.

Blewett, D.A., Wright, S.E., Casemore, D.P., Booth, N.E. & Jones, C.E. (1993) Infective dose size studies on *Cryptosporidium parvum* using gnotobiotic lambs. *Water Science & Technol.* **27:** 61-64.

Campbell, A.T., Haggart, R., Robertson, L.J. & Smith, H.V. (1992) Fluorescent imaging of *Cryptosporidium* using a cooled charge couple device (CCD). *Journal of Microbiological Methods.* **16:** 169-174.

Casemore, D.P. (1991) Laboratory methods for diagnosing cryptosporidiosis. *ACP Broadsheet* **128:** 445-451.

CDC. (1982) Cryptosporidiosis: assessment of chemotherapy of males with acquired immune deficiency syndrome (AIDS). *Morbidity & Mortality Weekly Report.* **31:** 589-682.

Crawford, F.G. & Vermund, S. H. (1988) Human cryptosporidiosis. *CRC Critical Reviews in Microbiology.* **16:** 113-159. CRC Press Inc. Boca Raton, Florida, USA.

Current W.L. & Reese, N.C. (1986) A comparison of endogenous development of three isolates of *Cryptosporidium* in suckling mice. *Journal of Protozoology.* **33:** 98-108.

DuPont, H.L., Chappell, C.L., Sterling, C.R., Okhuysen, P.C., Rose, J.B. & Jakubowski, W. (1994) Infectivity of *Cryptosporidium parvum* for adult humans. Presented at the Clinical Research Meeting of the Association of American Physicians, Baltimore, Maryland. April 29 - May 2, 1994.

Du Pont, H.L., Chappell, C.L., Sterling, C.R., Okhuysen, P.C., Rose, J.B. & Jakubowski, W. (1995) Infectivity of *Cryptosporidium parvum* for adult humans. *New England Journal of Medicine.* **332:** 855-9.

Drozd, C. & Schwartzbrod, J. (1996) Hydrophobic and electrostatic cell surface properties of *Cryptosporidium parvum. Applied and Environmental Microbiology.* **62:** 1227-1232.

Fayer, R. & Ungar, B.L.P. (1986) *Cryptosporidium* and cryptosporidiosis. *Microbiology Reviews.* **50:** 458-483.

Fayer, R. (1994) Effect of high temperature on infectivity of *C. parvum* oocysts in water. *Applied and Environmental Microbiology.* **60:** 2732-2735.

Fayer, R., Speer, C.A. & Dubey J.P. (1997) The general biology of *Cryptosporidium.* In *Cryptosporidium* and cryptosporidiosis. (Ed. R. Fayer) CRC Press. Boca Raton. p.1-42.

Finch, G.R., Black, E.K. Gyurek, L.L. & Belosevich, M. (1993) Ozone inactivation of *Cryptosporidium parvum* in demand-free phosphate buffer determined by *in vitro* excystation and animal infectivity. *Applied and Environmental Microbiology.* **59:** 4203.

Finch G.R., Kathleen, B. & Gyurek, L.L. (1994) Ozone and chlorine inactivation of *Cryptosporidium.* In : *Proceedings of the American Water Works Association's Water Quality Technology Conference.* (San Francisco, CA, Nov. 6-10,1994). American Water Works Association, Denver, CO. 1303.

Fricker, C.R. & Crabb, J.H. (1998) Waterborne cryptosporidiosis: Detection methods and treatment options. in Opportunistic Protozoa in Humans. (Ed. S. Tzipori). *Advances in Parasitology* **40:** 242.

Grimason, A.M., Smith, H.V., Parker, J.F.W., Bukhari, Z., Campbell, A.T. & Robertson, L.J. (1994) Application of DAPI and immunofluorescence for enhanced identification of *Cryptosporidium* spp. oocysts in water samples. *Water Research.* 28: 733-736.

Korich, D.G., Mead, J.R. Modore, M.S. Sinclair, N.A. & Stirling, C.A. (1990) Effects of ozone, chlorine dioxide, chlorine, and monochloramine on *Cryptosporidium parvum* oocyst viability. *Applied and Environmental Microbiology.* 56: 1423-1428.

Lisle, J.T. & Rose, J.B. (1995) *Cryptosporidium* contamination of water in the USA and UK - a minireview. *Journal of Water supply research and technology-aqua.* 44: 103-117.

Llovo, J., Lopez, A., Fabregas, J. & Munoz, A. (1993) Interaction of lectins with *Cryptosporidium-parvum. Journal of infectious diseases.* 167: 1477-1480.

Lorenzolorenzo, M.J., Aresmazas, M.E., Dematurana, I.V.M. & Duranoreiro, D. (1993) Effect of ultraviolet disinfection of drinking water on the viability of *Cryptosporidium parvum* oocysts. *Journal of Parasitology.* 73: 67-70.

Lumb, R. Lanser, J.A. & O'Donoghue, P.J. (1988) Electrophoretic and immunoblot analysis of *Cryptosporidium* oocysts. *Immunology and cell biology.* 66: 369-376.

McDonald, V., McCrossan, M., & Petry, F. (1995) Localisation of parasite antigens in *Cryptosporidium parvum* Infected Epithelial-Cells Using Monoclonal-Antibodies. *Parasitology.* 110: 259-268.

MacKenzie, W.R., Hoxie, N.J., Proctor, M.E., Gradus, M.S., Blair, K.A., Peterson, D.E., Kazmierczak, J.J., Addiss, D.G., Fox, K.R., Rose, J.B. & Davis, J.P. (1994) A massive outbreak in Milwaukee of *Cryptosporidium* infection transmitted through the public water-supply. *New England Journal of Medicine.* 331: 161-167.

Meisel, J.L., Perera, D.R., Meligro, C,. & Rubin, C.E. (1976) Overwhelming watery diarrhoea associated with a *Cryptosporidium* in an immunosuppressed patient. *Gastroenterology.* 70: 1156.

Miller, R.A., Brondson, M.A. & Morton, W.R. (1990) Experimental cryptosporidiosis in a primate model. *Journal of Infectious Diseases.* 161: 312-315.

Morgan, U.M. & Thompson, R.C.A. (1998) PCR detection of *Cryptosporidium*: The way forward? *Parasitology Today.* 14: 241-245.

Musiel, C.E. Arrowood, M.J., Sterling, C.R. & Gerba, C.P. (1987) Detection of *Cryptosporidium* in water by using polypropylene cartridge filters. *Applied and Environmental Microbiology.* 53: 687-692.

Nime, F.A., Burek, J.D. Page, D.L., Holsher, M.A. & Yardley, J.H. (1976) Acute enterocolitis in a human being injected with the protozoan *Cryptosporidium. Gastroenterology.* 70: 592.

Ongerth, J.E. & Pecoraro, J.P. (1996) Electrophoretic mobility of *Cryptosporidium* oocysts and *Giardia* cysts. *Journal of Environmental Engineering-Asce.* 122: 228-231.

Parker, J.F.W., Greaves, G.F. & Smith, H.V. (1993) The effect of ozone on the viability of *Cryptosporidium parvum* oocysts and a comparison of experimental methods. *Water Science & Technology.* 27: 93-96.

Reduker, D.W., Speer, C.A. & Blixt, J.A. (1985a) Ultrastructural-changes in the oocyst wall during excystation of *Cryptosporidium parvum* (Apicomplexa, Eucoccidiorida). *Canadian Journal of Zoology.* 63: 1892-1896.

Reduker, D.W., Speer, C.A. & Blixt, J.A. (1985b) Ultrastructure of *Cryptosporidium parvum* oocysts and excysting sporozoites as revealed by high-resolution scanning electron-Microscopy. *Journal of Protozoology*. 32: 708-711.

Righetti, P.G. (1976) IEF of cells, subcellular particles, bacteria and viruses. In: Chap 5 pp. 527-529. Laboratory techniques in biochemistry and molecular biology. (Eds. P.G. Righetti & J.W. Drysdale) 5: pt. 2. Elsevier, New York.

Robertson, L.J., Campbell, A.T. & Smith, H.V. (1992) Survival of oocysts of *Cryptosporidium parvum* under various environmental pressures. *Applied and Environmental Microbiology*. 58: 3494-3500.

Robertson, L.J., Campbell, A., & Smith. H.V. (1993) *In vitro* excystation of *Cryptosporidium parvum*. *Parasitology*. 106: 13-19.

Rochelle, P.A., Ferguson, D.M., Handojo, T.J., DeLeon, R., Stewart, M.H. & Wolfe, R.L. (1997) An assay combining cell culture with reverse transcriptase PCR to detect and determine the infectivity of waterborne *Cryptosporidium parvum*. *Applied and Environmental Microbiology* 63: 2029-2037

Rose, J.B., Lisle, J.T. & LeChevallier (1997) Waterborne Cryptosporidiosis: Incidence, Outbreaks, and Treatment Strategies. In: *Cryptosporidium* and cryptosporidiosis. (Ed. R. Fayer) CRC Press. Boca Raton. p. 93-110.

Slavin, D. (1955) *Cryptosporidium meleagridis* (Sp. Nov). *Journal of Comparative Pathology*. 65: 262.

Smith, H.V., Patterson, W.J., Hardie, R., Greene, L.A., Benton, C., Tulloch, W.J., Gilmour, R.A., Girdwood, R.W.A., Sharp, J.C.M. & Forbes, G.I. (1989) An outbreak of waterborne cryptosporidiosis caused by post-treatment contamination. *Epidemiology & Infection*. 103: 703-715.

Smith, H.V., Robertson, L.J. & Ongerth, J.E. (1995) Cryptosporidiosis and Giardiasis: The Impact of Waterborne Transmission. *Journal of Water Supply Research and Technology-Aqua*, 44: 258-274.

Spano, F. Putignani, L., McLauchlin, J., Casemore, D.P. & Crisanti, A. (1997) PCR-RFLP analysis of the *Cryptosporidium* oocyst wall protein (COWP) gene discriminates between *C. wrairi* and *C. parvum*, and between *C. parvum* isolates of human and animal origin. *FEMS Microbiology Letters*. 150: 209-217.

Tilley, M. & Upton, S.J. (1997) *Biochemistry of Cryptosporidium*. In: *Cryptosporidium* and cryptosporidiosis. (Ed. R. Fayer) CRC Press. Boca Raton. p.163-180.

Tyzzer, E.E. (1907) A sporozoan found in the peptic glands of the common mouse. *Proceedings of the Society for Experimental Biology in Medicine*. 5: 12.

Weber, R., Bryan, R.T., Bishop, H.S., Wahlquist, S.P., Sullivan, J.J. & Juranek, D.D. (1991) Threshold of detection of *Cryptosporidium* oocysts in human stool specimens: evidence for low sensitivity in current diagnostic methods. *Journal of Clinical Microbiology*. 29:1323-1327.

Chapter 4
Electrorotation of the cysts of *Giardia* species.

4.1   Introduction to *Giardia* species
4.1.1 Historical aspects
Giardia was probably the first described intestinal protozoan. Antoni van Leeuwenhoek in 1681 observed and described what was later to be termed the trophozoite (feeding stage) of this parasite in his own stool sample. However, it was not until the twentieth century that the association of *Giardia* with disease symptoms was established (Nash, 1987).

This parasite is also well known as one of the most primitive eukaryotic organisms (e.g. Alberts *et al.*, 1994). As well as structural evidence (no mitochondria, chloroplasts, normal endoplasmic reticulum or Golgi apparatus) nucleotide sequencing studies indicate that *Giardia* is related almost as closely to bacteria as it is to other eukaryotes, from which it must have diverged very early in evolution (Sogins *et al.*, 1989).

4.1.2 Taxonomy

Taxonomically *Giardia* is described as outlined below;

Kingdom	Protozoa	single-celled eukaryotic organisms,
Phylum	Sarcomastigophora	containing sarcodines (amoebae) and flagellates,
Sub-phylum	Mastigophora	flagellated protozoans,
Class	Zoomastigophorea	animal-like flagellated protozoans,
Order	Diplomonadida	bilaterally symmetrical body, two nuclei, up to eight flagella
Family	Hexamitidae	axially symmetrical, eight flagella,
Genus	*Giardia*	two equal nuclei side by side.

The class zoomastigophora contains other parasites of economic importance, for example *Trypanosoma* spp. which causes sleeping sickness in man and domestic animals and *Leishmania* spp. that causes leishmaniasis. Although these two genera may cause more deaths *per annum* than giardiasis, the prevelance rate for *Giardia* is much higher with 200 million people infected at any one time, varying between 2-5% of the industrialised world and up to 20-30% of the developing world. Prevelence rates are 24 million for American trypanosomiasis and 1.2 million for leishmaniasis, based on the estimates of the WHO between 1975 and 1986 (Markell, Voge & John 1992).

The nomenclature of the *Giardia* species has undergone many changes. Three 'type-species' of *Giardia*, *G. agilis*, *G. muris*, and *G. duodenalis*, were identified by Filice (1952) based upon the appearance of

organelles in the cytoplasm of the trophozoite, known as the median bodies. According to Filice's classification, those of the *duodenalis* type cause infection and disease in human beings. However, not all *Giardia* of the *duodenalis* species cause infection in man. To clarify, those of the *duodenalis* type may be subdivided into those that infect man *G. intestinalis* (Stiles, 1915) and those that do not (but are not of the *agilis* or *muris* type) termed *G. lamblia* (Lambl, 1859).

Until the middle of the twentieth century it was common practice to assign *Giardia* species names using traditional criteria, namely on the basis of host specificity and on differences in various trophozoite dimensions. In 1952, Frances Filice published a monograph describing the results of his *Giardia* studies. Amongst other things he addressed the problems of taxonomy, and concluded that host specificity and body dimensions were untrustworthy criteria in this genus as little evidence supported this. Woo & Paterson (1986) demonstrated in meticulous cross-transmission studies, that some *Giardia* are apparently highly host specific, and that others are capable of infecting several different animal species.

Twenty-six years after Filice's work, Kulda & Nohynkova (1978), in a review, were able to list references to more than forty *Giardia* 'species'. Indeed, representatives of this genus appear to exist in virtually every mammalian species in which they have been systematically sought. Whereas those forty almost certainly do not represent distinct species, three clear morphological groups can be assigned to members of the genus, based on the shape and position of the median bodies (intracellular organelles composed of microtubules) in the trophozoite and in some cases the shape of the trophozoite, outlined in Table 4.1 below.

Feature	Species 'type'		
	Giardia duodenalis	*Giardia muris*	*Giardia agilis*
Host groups	Mammals, birds, reptiles	Rodents, birds, reptiles	Amphibians
Median body*	typically double claw hammer	small rounded	tear-drop shape
Cyst dimensions (μm)	8 - 12 x 7 - 10	9 x 6 (cited Sauch 1984)	no data found

Table 4.1. Features of the three *Giardia* morphological types as described by Filice.
*= disassembled ventral disc of trophozoite

The overlap in the dimensions of closely related species as shown in Table 4.1, may result in uncertainty when identifying cysts from the environment, so that accurate risk assessment is not possible.

Using host specificity as criteria for naming species is also complicated by the dynamic host-parasite interaction, whereby the initiation of infection depends on both host and parasite factors (Nash *et al.*, 1987). In the study described, two groups of human volunteers were challenged with two *Giardia* isolates obtained from humans. One isolate proved uniformly infectious; the other isolate failed to infect any of the challenged volunteers.

More recently chemotaxonomic methods have been applied to the species identification problem. Three key approaches have been taken, namely analysis by antigenic comparisons, isozyme analysis, and by DNA analysis.

A potential problem with the antigenic comparison method was highlighted by Aggarwal & Nash (1988) who found that a single *Giardia* trophozoite can give rise, *in vivo* as well as *in vitro*, to trophozoites with varying surface antigens. This strategy of variable surface antigens is observed in other parasites, such as trypanosomes, where it is thought to assist with host immunity evasion.

4.1.3 Life cycle

The life cycle of members of the genus *Giardia* involves a single host, see Figure 4.1. On examination the life cycle reveals several important features which assist in making this a successful and problematic parasite.
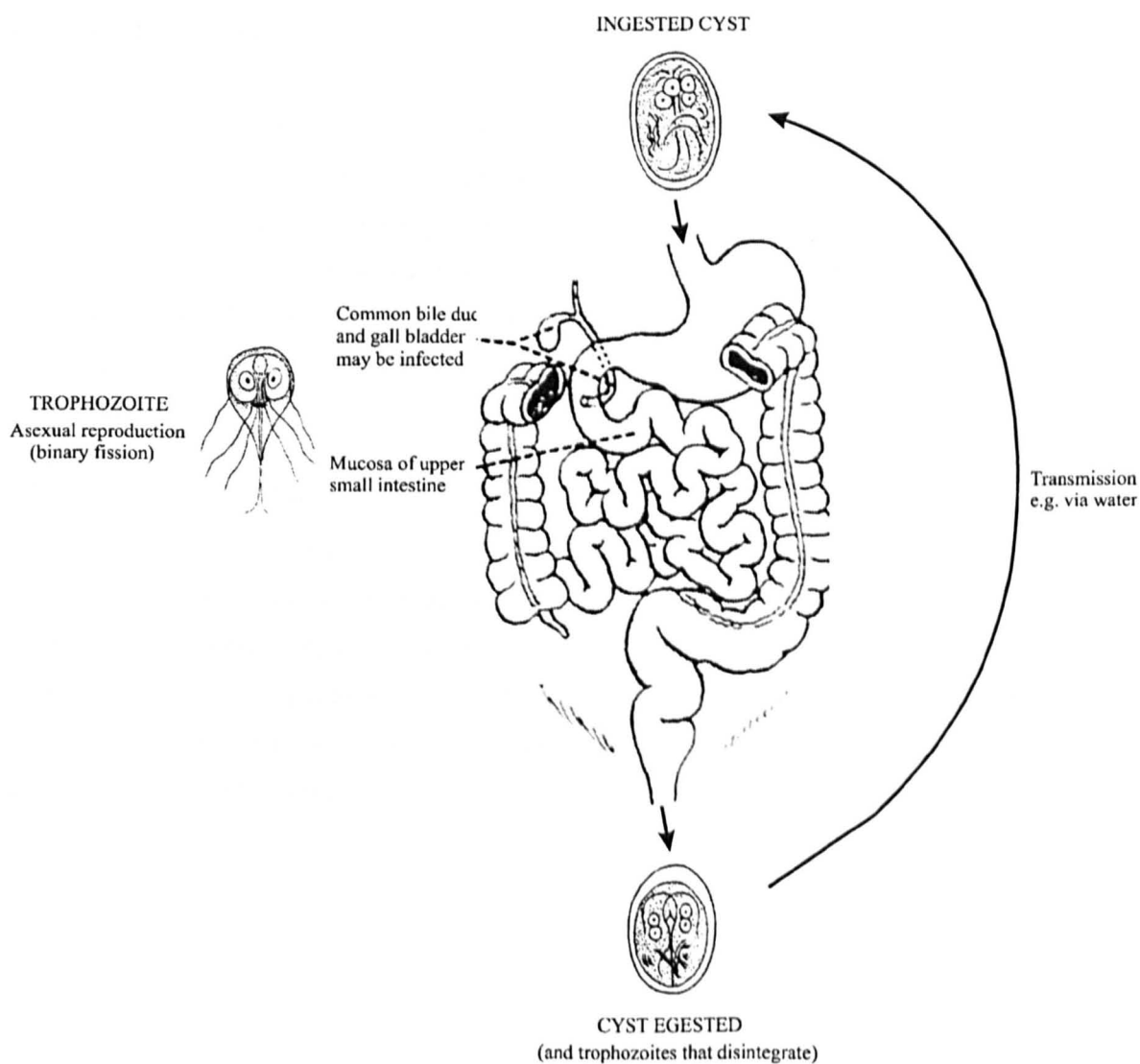
Figure 4.1 The life cycle of *Giardia lamblia* in the gastrointestinal tract. (Adapted from Markell *et al.*, 1992).

Giardia has a simple monoxenous life cycle. The parasite has two stages: the vegetative trophozoite that inhabits the small intestine of the host and is responsible for causing disease and the environmentally resistant cyst that is responsible for the transmission of the parasite among susceptible hosts. The main modes of infection are ingestion of contaminated water or faecal contaminated food. Cysts that have been freshly egested with faeces, typically only have two nuclei. In most *Giardia*, on maturation, the cyst contains four nuclei having undergone karyokinesis. Cytokinesis, whereby the cytoplasm divides to form two binucleate trophozoites, does not occur until (during or immediately after) excystation.

After ingestion, excystation begins in the acidic environment of the stomach (optimum pH 1.3 to 2.7 for *G. duodenalis*). Following emergence (which is stimulated by chymotrypsin, trypsin and pancreatic fluid) the emergent trophozoites colonise the upper small intestine where the conditions for survival and proliferation are optimal. The 12-15μm long trophozoites, swimming rapidly with eight flagella, attach via their ventral adhesive disc to the external surface of villi of the small intestine, and occasionally the bile duct and gall bladder.

In severe infections, trophozoites can cover the free surface of every cell lining the upper small intestine lumen. Unlike *Cryptosporidium* there is no sexual stage, reproduction is instead by binary fission which rapidly increases the number of *Giardia* present in the gut; consequently, a single diarrhoeic stool can contain 14 billion parasites. A prepatent period of 10 to 36 days before organisms could be detected in the stools has been observed, with a mean incubation period before clinical illness of 8 days (Markell *et al.*, 1992).

4.1.3.1 Encystation

From animal models the regions in the intestine where the cysts are formed have been mapped. Gillin *et al.* (1987) who used *G. lamblia* in a mouse model, found cysts rarely in the duodenum, the majority occurring in the lower jejunum and ileum. High concentrations of nutrients are to be found in the jejunum and so it is thought to be the favoured site for the trophozoites. Cysts would therefore be expected to form on leaving this region as the conditions become less favourable as in the ileum most of the nutrients have been absorbed.

The trigger for encystation is now thought to be cholesterol depravation, and not bile salts as was once thought, however, the precise mechanism by which this trigger causes encystation is not known. Two mechanisms have recently been proposed by Luján, Mowatt & Nash (1998):

- High levels of cholesterol available to *Giardia* in the duodenum and jejunum might repress the transcription of encystation specific genes. In the ileum naturally lower levels of cholesterol and the blocking of cholesterol uptake by excess bile micelles may allow gene activation.

- Cholesterol concentration in the trophozoite membrane alters its fluidity. Membrane related activities such as permeability and enzyme and receptor function may be affected, modulating some protein activity. Directly or indirectly this altered activity might trigger a cascade of signal transduction mechanisms that culminates in encystation-specific gene expression.

The changing conditions in the small intestine that lead to encystation are outlined below,

DUODENUM
bile salts released $[cholesterol]^{high}$ ───────────────▶   encystation blocked
into proximal
duodenum $[bile]$rising

JEJUNUM
major site of fat $[cholesterol]^{high}$ ──────────▶   encystation blocked
absorption in gut
aided by bile salts $[bile]^{high}$

ILEUM
bile salts actively $[cholesterol]_{low}$ ─ ─ ─▶◆   encystation triggered
reabsorbed in
distal ileum $[bile]^{excess}$
                                      ─────────▶│
                                      blocks uptake of
                                      cholesterol
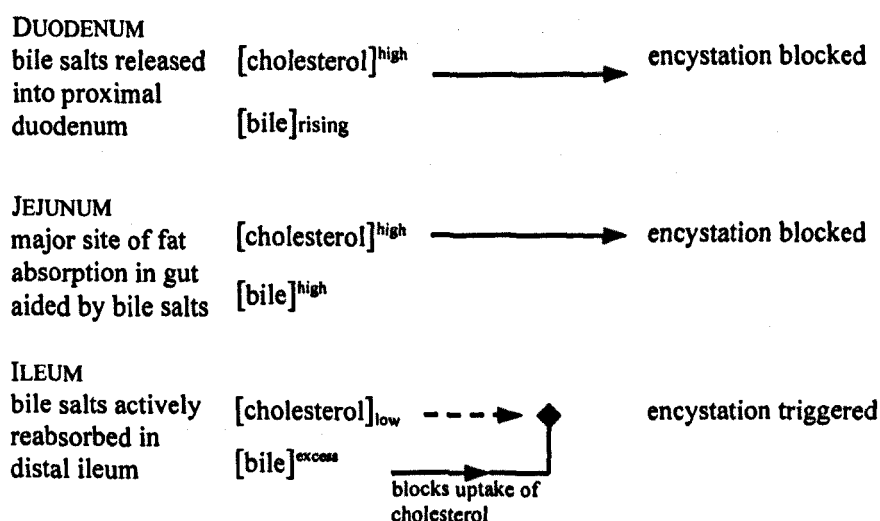
Cyst wall formation takes approximately 40 to 70 h, on completion both nuclei divide simultaneously.

4.1.3.2   The Cyst

Essentially a trophozoite surrounded by a cyst wall, those cysts of human source *Giardia* are ovoid and elliptical in appearance, see Table 4.1 for dimensions. The ultra structure of *Giardia* sp. cysts and the process of excystation have been described in detail (Sheffield & Bjorvatn, 1977; Bingham & Meyer, 1979). The cyst wall is thought to function as a selective barrier to the movement or diffusion of molecules found in the environment as well as a supportive exoskeleton (Coggins & Schaefer, 1986). Transmission electron microscope (TEM) studies show the cyst wall as consisting of 2 distinct layers, an outer consisting of a thin fibrous layer interspersed with fine particles, and an inner layer consisting of the plasma membrane which borders a thin cytoplasmic layer which is continuous with the main cytoplasm (Sheffield & Bjorvatn, 1977; Luchtel, Lawrence & DeWalle, 1980). This peripheral cytoplasm contains

many vacuoles, and is separated discontinuously from the main cytoplasm by a lacunar system which is seen as material of low electron density. The lacunar space is more pronounced at the posterior of the cyst.
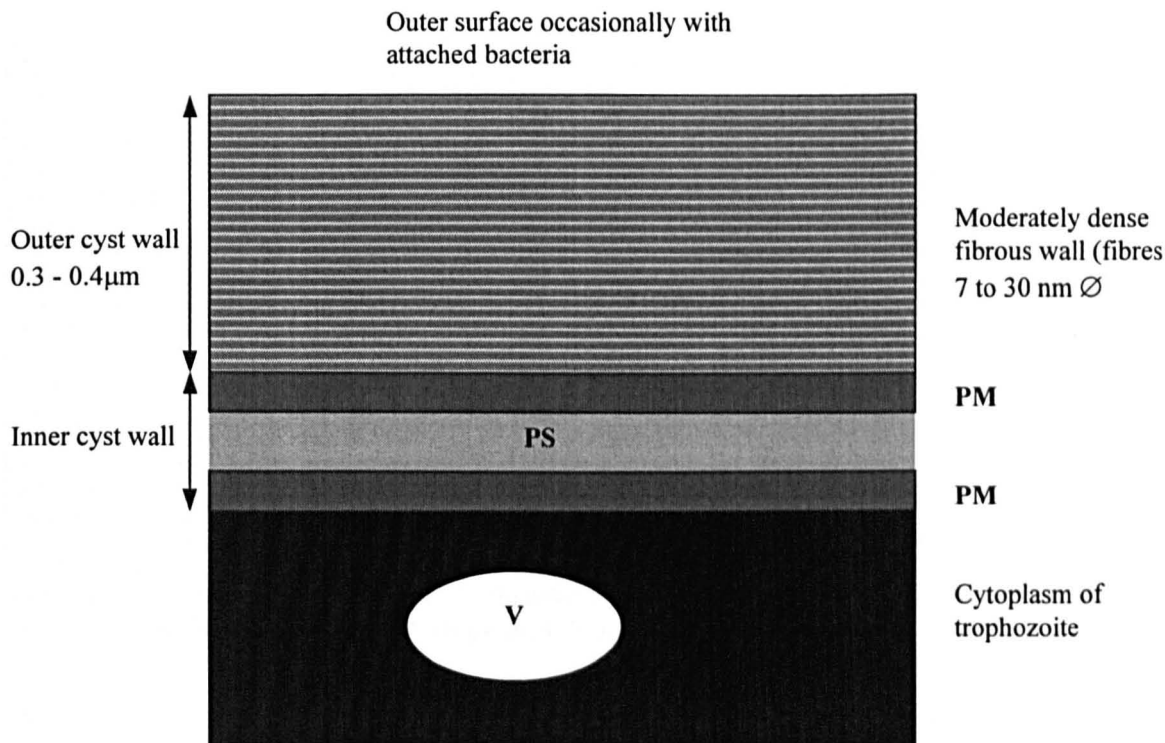
Figure 4.2. Summary of the TEM studies of the cyst wall structure of *Giardia muris*.
V = Intracellular peripheral spaces, PM = Plasma membrane, PS = Peritrophic/lacunar space (cytoplasm).

Upon examination by TEM, the cyst wall is approximately 0.3-0.5μm thick and composed of layers of fibrils (7-30nm in width) arranged in a felt-like web. By high-resolution low-voltage SEM, fine details of the cyst surface are visible (Erlandsen, Bemrick & Pawley, 1989). Fibrils of similar width but of undetermined length are seen. Both the *muris* and *duodenalis* morphological types as described by Filice (1952) possess a similar filamentous structure.

It has been reported that the cyst wall of *G. duodenalis* and *G. muris* contain chitin based on lectin binding analysis (Ward *et al.*, 1985). However, Jarroll *et al.* (1989) questioned the presence of chitin in the cyst wall. Their studies, using gas chromatography and mass spectrometry on *G. muris* and two human source *Giardia* cyst isolates, demonstrated that *n-acetyl galactosamine* was the primary amino sugar of the cyst wall. They were unable to detect *n-acetyl glucosamine*, the primary amino sugar of chitin. Glucose is the major sugar in the remainder of the cyst, present as glycogen. Proteins have also been demonstrated in the cyst wall by the hybridisation of cyst wall-specific antibodies to specific bands on Western immunoblots.

4.1.3.3 Transmission

The transmission of waterborne giardiasis is facilitated by several features of its biology. These are summarised in Table 4.2 below.

Feature	For *Giardia*
Large numbers of cysts excreted by infected hosts	Excretion rates vary substantially. Up to 1.44×10^{10} cysts per day can be excreted by an infected human.
Lack of, or reduced, host specificity increases the potential for environmental spread and contamination	*G. duodenalis* infections reported from a variety of animals including human beings, domestic livestock and wild animals
Robust nature of cysts enhances their survival for long periods of time in favourable environments before ingestion by potential hosts	Cyst survival is enhanced in moist, cold environments (such as those found in temperate regions) - e.g. viable cysts can survive, suspended in water, for 1-2 months.
Environmental robustness of cysts enables them to survive some water treatment processes	Waterborne outbreaks indicate that cysts can survive water treatment processes. Cysts are sensitive to some disinfectants commonly used in water treatment.
Small size of cysts aid their penetration through sand filters	$8 - 12 \times 7 - 10$ µm (length x width).
Low infectious dose means that few viable cysts need to be ingested for infection to establish in susceptible hosts	Median infectious dose in man is 25-100 cysts (10 cysts initiated infection 2 volunteers. Rendtorff, 1979). Some human-source isolates can vary their ability to colonise other human beings.
Egestion of cysts in faeces facilitate spread to water by water-roosting refuse feeders	Sewage/carrion feeders may transport viable cysts.

Table 4.2 Features of the biology of *G. intestinalis* which may facilitate waterborne transmission. (Adapted from Smith, Robertson & Ongerth, 1995).

Large numbers of cysts are egested from the host during the patent period with numbers approaching 10^7 cysts per gram of faeces (Nash, 1992). Although diluted to low densities in the aquatic environment, epidemic outbreaks of waterborne disease can arise from consumers ingesting cyst-contaminated potable water, as the infective dose of cysts is small (~10) (Rendtorff, 1979).

Although always transmitted by the faecal-oral route, the precise means of transmission varies in different parts of the world. Other than consumption of contaminated drinking water (Craun, 1986), transmission methods include the ingestion of contaminated food (difficult to determine) and from person to person contact. As a result giardiasis is a frequent cause of diarrhoeal illness in day-care centres for children, backpackers, travellers and homosexual men.

Assessment of the potential for cysts to cause epidemic waterborne outbreaks of giardiasis would be greatly facilitated by the availability of a system for defining viability of the small number of cysts isolated from water samples (Smith & Smith, 1989). Insufficient numbers are available for infectivity studies, therefore *in vitro* methods must be adopted.

Complicating the prevention of giardiasis in man is the zoonotic spread of the disease, whereby man may develop the disease from ingesting *Giardia* cysts derived from some animal hosts.

4.1.4 Giardiasis: the disease

The status of *Giardia intestinalis* has changed in the last 50 years from that of (i) harmless commensal to (ii) potential pathogen to (iii) one of the 10 major parasites of humans. Awareness by scientists, physicians and more recently the general public due to coverage of giardiasis outbreaks by the press has assisted this rise in status in recent years, as has the reduction of other serious diseases.

Backpackers and children in day care centres are high-risk groups, however, individuals with acquired immunodeficiency syndrome (AIDS) are not. In a study of AIDS patients, *Giardia* was found in none of 10 AIDS patients without diarrhoea and in only 3 of 22 patients with diarrhoea (Smith *et al.*, 1988). Asymptomatic infections with *Giardia* are also possible. Some investigations have indicated that between 30 - 70% of *Giardia* infections can be asymptomatic (Birkhead & Vogt, 1989; Lopez *et al.*, 1980). Indeed Koch's postulates* can not always be applied to *Giardia*, as it does not always cause disease. Since Rendtorff's studies involving experimental infections of humans with human source *Giardia* in 1954 there was a gap of 33 years before the next human-to-human infection studies. Nash *et al.* (1987) attempted to infect volunteers with two different isolates of *Giardia* (GM/S and Isr) derived from human infections. Inoculated via a polyvinyl tube as trophozoites directly into the small intestine, only one of the isolates was successful in producing infection documented by the recovery of cysts/trophozoites in the volunteer's stools. This was the first fulfilment of Koch's postulates for human *Giardia*.

4.1.4.1   Prevelance

Giardia is the most frequently detected parasite in faecal samples from man. World-wide in distribution, giardiasis occurs in high prevalence in the developing world, where prevelence rates reach 20-30% of the population. *Giardia* is currently the most frequently identifiable causative agent in waterborne outbreaks of diarrhoeal disease in the U.S.A. and in recent decades, documented waterborne giardiasis has been on the increase. Bennet *et al.* (1987) suggested that approximately 60% of giardiasis cases are aquired via the waterbourne route. In the U.K. detection of *Giardia lamblia* cysts in stools screened by the Public Health Laboratory (PHL) has stayed at a high level for the last decade.

---

* Koch's postulates - the ground rules for proving an organism causes a disease first applied experimentally by Robert Koch in 1876 with anthrax:
- the microorganism must be present in every case of the disease
- the microorganism must be isolated from the diseased host and grown in pure culture
- the specific disease must be reproduced when a pure culture of the microorganism is inoculated into a healthy susceptible host
- the microorganism must be recovered once again from the experimentally infected host
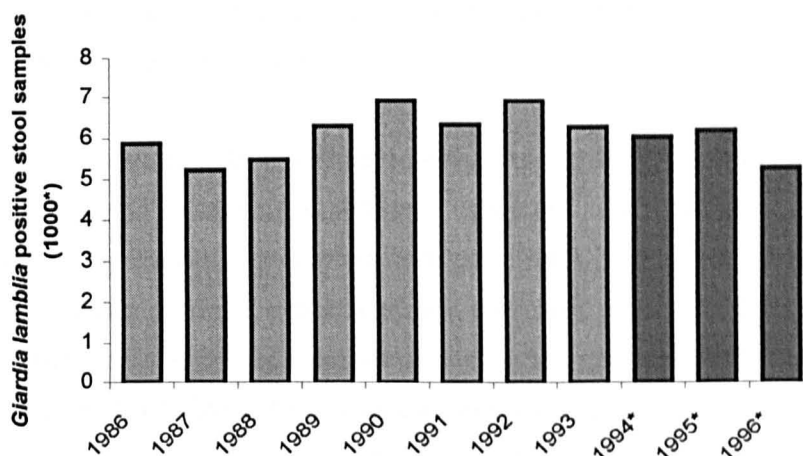
Figure 4.3 **Laboratory reports of *G. lamblia* to Communicable Disease Surveillance Centre (CDSC), all identifications for England and Wales.**

* Provisional data
Source: http://www.phls.co.uk/CDSC/site, fr3.htm

4.1.4.2 Symptoms

Following the consumption of sufficient cysts to initiate infection, there is the prepatent period before organisms are detected in the faeces. Disease symptoms may predate cyst excretion. Common clinical features range from mild diarrhoea, abdominal cramps, flatulence and anorexia to steatorrhoea and full blown malabsorption syndrome. Fortunately, treatment is available in the form of Timidazole (treatment of choice in the US) and Albendazole which also has worming qualities and is therefore often the choice in developing countries. Both of these treatments are based on a single dose, which is an important quality for treatments in developing countries where in disperse communities access to medical attention may be irregular. Previous treatments consisted of the antiprotozoal drug Metronidazole (Flagyl™) or Quinacrine hydrochloride (Atabrine™) both of which required a 5 day course to be effective (Markell *et al.*, 1992).

4.1.5 Control of Giardiasis

Although treatment is effective, prevention of the disease is better than its cure. That infections occur after consumption of treated water, implies that conventional water treatment processes are not always sufficient. However, chlorine, the most widely used drinking water disinfectant, has been shown to be partially effective against Giardia cysts. For example, the concentration and time (CT) required for a 2 log inactivation at pH 7 and 5°C is about 100 mg l^{-1} min^{-1} (Clark, 1989). The chlorine concentration required at higher temperatures is less, falling below 10 mg l^{-1} min^{-1} for 25°C (pH 7). Using ozone treatment, a 2 log inactivation of *Giardia* cysts at pH 7 was achieved by a CT of 0.53 mg l^{-1} min^{-1} at 5°C

and a CT of 0.17 mg l⁻¹ min⁻¹ at 25°C (Wickramanayake *et al.*, 1984). However, as outlined in Table 4.2, the sheer numbers of cysts, possible sources, long survival time, small size (enabling them to pass through filters) and low infectious dose, all mean that minor faults with a treatment facility may allow cysts to pass through treatment works.

Recognising that infections with *Giardia* often result from ingesting viable cysts in contaminated water and food, may help to devise control measures. Prevention of contamination of water and food with cysts, destroying or removing cysts which manage to reach water or food, reducing the number of clinically asymptomatic chronic cyst passers, and improving personal hygiene to reduce the risks of person-to-person transmission, are examples of such control measures. Specific control measures may not be suitable for all individuals, for example, in developing countries the cost of fuel is a major limiting factor in the use of this otherwise simple method of water purification.

Tests for water quality are required to ensure drinking water safety. For a test to be of use, not only must the cysts be detected, but also information on their infectivity should be available, as only viable cysts carry a potential risk with them.

4.1.5.1   Current methods for the determination of viability.

Determination of cyst viability is not as easy as for the feeding stage (trophozoite) since the cysts are not motile. Various methods have been assessed for determining cyst viability, including the use of animal models for infectivity, *in vitro* excystation, vital stains and differential interference contrast microscopy (Schupp & Erlandsen 1987a). All these techniques have been assessed for both *G. muris* and *G. duodenalis* types apart from the morphological assessment which has only been reported for *G. muris*. These are all lengthy procedures and are subject to inaccuracies.

The mouse model, first described by Roberts-Thompson *et al.* (1976) has proved a suitable method for viability testing of cysts and correlation with the various *in vitro* viability techniques (Schupp & Erlandsen, 1987b). Faecal cyst shedding indicates the establishment of an infection. However, *in vivo* methods are expensive, and while they give information about populations of cysts, none is obtained about individual cysts.

In vitro excystation would seem to be an indicator of the viability of *Giardia* cysts since trophozoites must be released from the cysts to infect the host (Bingham & Meyer, 1979). Problems exist with the somewhat subjective definition of excystation used, which even includes aborted attempts of trophozoite emergence from the cysts, making this method likely to overestimate the true infectious ability of the cysts.

The simultaneous use of the fluorogenic stains fluorescein diacetate (FDA) and propidium iodide (PI) were shown to be good indicators of cell viability (Jones & Senft, 1985). Later they were demonstrated as viability indicators of both *G. muris* (Schupp & Erlandsen, 1987b) and *G. intestinalis* (Smith & Smith, 1989) cysts. Those of the muris type are useful in that they can be used for comparisons of staining with infectivity, either directly (Schupp & Erlandsen, 1987b) or to quantify an inactivation procedure such as treatment with ozone (Labatiuk *et al.*, 1991). Stains have also been used in conjunction with indirect fluorescent antibody detection of *Giardia* cysts (Dowd & Pillai, 1997) which has important implications for water samples, where both detection and viability determination of cysts are required.

There are criticisms, however, of the use of these fluorogenic stains. For example, in Schupp & Erlandsen's study (1987b) mice were inoculated with (1000 and 50000) FDA positive cysts, others were inoculated with (5000 and 50000) PI positive cysts. Although the fluorogenic stains correlated well with Giardia infectivity in mice, no information was gained about individual cysts.

In a comparison between PI staining and *in vitro* excystation for *G. muris* cysts following chemical inactivation, the reliability of the staining procedure was questioned (Sauch *et al.*, 1991). No significant correlation between lack of excystation and PI inclusion was found for cysts exposed to two commonly used drinking water disinfectants, chlorine and monochloramines. Non-staining of some cysts has also been reported, both for the occasional *G. muris* cyst (Schupp & Erlandsen, 1987a) and for one of four human isolates of *G. duodenalis* cysts tested (Smith & Smith, 1989).

Giardia cysts have been shown to remain viable in natural, tap and distilled water for periods of up to several weeks. Survival is enhanced by cold temperature, other water quality factors seem not to be important. The maximum survival time for *G. lamblia* in unchlorinated tap water was 77 days at 8°C and for *G. muris* in natural water between 56 and 84 days at 3.3°C (Wallis, 1994) although it was noted that these were maximum survival times and that very few cysts were left alive after the exposure times quoted. Cyst survival follows a decay curve that does not begin to drop significantly for at least 50 days in very cold water, after which cyst mortality rapidly increases. Survival times at warmer temperatures are considerably shorter.

The electrorotation (ROT) assay has been successfully used to differentiate viable and non-viable yeast cells (Huang *et al.*, 1992), bacteria biofilms (Zhou *et al.*, 1995) and animal cells (Gundel *et al.*, 1989). The principal characteristics of cell rotation, namely the sense and maximum angular frequency of rotation, are expressed over a relatively narrow frequency range of the applied electric field. ROT is particularly sensitive to changes in the electrochemical, physico-chemical and structural integrity of the cell membrane (Pethig, 1991), as occurs when biological cells of all types die. This *in vitro* method is potentially more sensitive in at least two ways because it is based on non-invasive observations of individual cysts, and the information is gained in less than one hour from any purification steps.

4.2 Methods

Not all the cysts that are recovered from potable water supplies are of the type that is infectious to man. To avoid false positives it is important to be able not only to determine viability, but to also distinguish between the types that are infectious to humans and those that are not. Electrorotation (ROT) data was therefore collected from cysts of both human source *Giardia* (*G. intestinalis*) and those from a murine host (*G. muris*) which are not infective to humans.

4.2.1 *G. intestinalis* material

G. intestinalis cysts were obtained from diarrhoeic samples screened at the local Public Health Laboratory (PHL) at Gwynedd Hospital, Bangor. After microscopic examination, positive faecal samples were stored at 4°C for collection. Two samples obtained within 2 days of examination at the PHL were purified by formol-ether sedimentation, followed by a sucrose density flotation method (Smith & Smith, 1989) and then stored in water at 4°C.

4.2.2 Formalin - ethyl acetate sedimentation (concentration).

After thoroughly mixing the faecal suspension, 5ml was strained through a metal gauze over a beaker. Distilled water was added to make a total volume of 15ml, which was then mixed and centrifuged (1500g for 10 mins) and the supernatant decanted. 10 ml of 10% formalin was mixed with the sediment then 4 ml of ethyl acetate was added. The tube was stoppered, and shaken vigorously in an inverted position for 30 s. After careful removal of the stopper, the suspension was centrifuged (500g for 10 mins). A plug of debris from the top of the tube was freed by ringing the sides with an applicator stick. The top layers of supernatant were decanted and using a cotton swab adhering debris from the sides of the tube was removed. The sediment was washed immediately 3 times with water (10mins at 1500g) to remove ether (only once if sucrose flotation was then to be used) mixed well, and stored at 4°C.

4.2.3 Sucrose density flotation (purification).

10ml of washed oocyst suspension (in 50ml centrifuge tube) was underlayed with an equal volume of cold sucrose (4°C) of specific gravity 1.18 by needle and syringe. Following centrifugation (1500g for 15 mins) a 10ml mid-layer was collected with a hypodermic syringe. The sucrose was removed from the collected suspension by washing in distilled water (centrifugation for 10mins at 1500g). The purified suspension was then enumerated by haemocytometer, and stored at 4°C for subsequent use.

4.2.4 *G. muris* material

Mice (BKTO and CBACA) from the University animal house were checked for the presence of *Giardia* infections over a two-month period, as a possible source for experimental material. The formol-ether concentration method was used to aid detection of cysts from the mice droppings, collected within 1 hour of egestion. Although gut sections had previously been reported as containing *Giardia* trophozoites, extensive searches in droppings from 3 and 5 week, as well as 7 ½ month old thymectomised and 5 month immunosuppressed (with corticosteroids) mice all proved negative. Requested checks at animal

houses in London, Glasgow and Edinburgh also proved negative. Subsequently, material from Waterborne Inc. (USA) Louisiana USA was obtained via Prof. H.V. Smith at the Scottish Parasite Diagnostic Laboratory (SPDL), arriving ice packed as a stock solution of 7 million cysts in 1ml of reverse-osmosis water. On arrival (10 days post egestion) the suspension was washed in ultra pure water and stored at 4°C until required.

4.2.5 Fluorogenic vital staining

The fluorogenic dye fluorescein diacetate (FDA) has been shown to stain viable cysts of *Giardia* (Schupp & Erlandsen, 1987b). In a twin fluorogenic dye assay, they showed that FDA positive cysts were observed to excyst, whereas those staining propidium iodide (PI) positive were never observed to excyst. Non-polar FDA molecules enter cysts by diffusion and are catalysed by non-specific esterases (breaking ester linkages) releasing free fluorescein which diffuses through intact bilipid membranes slowly thus accumulating within living cells (Jones & Senft, 1985). It has been established that an intact lipid bilayer slows the leakage of the fluorochrome from intact cells, while injured cells cannot retain or accumulate the fluorochrome. In cysts of *G. muris*, the fluorescein is observed to accumulate both within the trophozoite and within the space between the trophozoite membrane and the cell wall. It has also been established that FDA and PI are non-toxic at the concentrations used during these staining procedures.

PI only stains non-viable cysts, as it cannot traverse intact biological membranes. On traversing damaged membranes PI intercalates with nucleic acids producing a x25 increase in fluorescence emission (Jones & Senft, 1985). This was the only stain used with the *G. intestinalis* sample, as inconsistent FDA staining was observed with these cysts, indeed Smith & Smith (1989) reported that 9.3-19% of cysts from 3 human isolates failed to stain with either FDA or PI.

The FDA working solution was made up prior to each experiment by diluting the stock solution (10mg/ml FDA in acetone, stored in the dark at 4°C) 1:1000 in phosphate buffered saline (PBS). PI working solution (1mg PI in 50ml PBS) was stored in the dark at 4°C until used. On excitation with an appropriate light frequency (FDA 450 - 490nm; PI 530 - 545nm) viable cysts fluoresce apple green through an appropriate filter block (Nikon B2A for FDA), and non-viable cysts fluoresce orange/red (Nikon G for PI).

10 μl of each of the above solutions were incubated with 1×10^4 cysts in 100 μl of PBS for 30 mins in a preheated water bath at 37°C.

4.2.6 Preparation of the cysts for electrorotation

Following any fluorogenic staining, the suspensions were diluted with ultra pure water, vortexed and microcentrifuged (Microcentaur 13 500 revs/min for 2 minutes). The supernatant was then removed to 100μl, refilled to 1.5ml with ultra pure water (conductivity 1μS cm⁻¹) vortexed and re-microcentrifuged. After four washes, the suspension was resuspended in dilute PBS solution (typically 10μS cm⁻¹). The conductivities of these solutions were measured using a Whatman CDM 4010 meter, with a calibrated

chamber of cell constant 0.12 cm^{-1} and volume 300µl. Typical working concentrations of particles were of 3×10^4 cysts ml^{-1} as determined by haemocytometer.

After conductivity adjustment, the cyst suspension was vortexed for 30s then 20µl were pipetted onto the ROT chamber manufactured on a glass slide, for observation with a Nikon Labophot microscope with fluorescent attachment. The apparatus set up is shown in Figure 4.4.
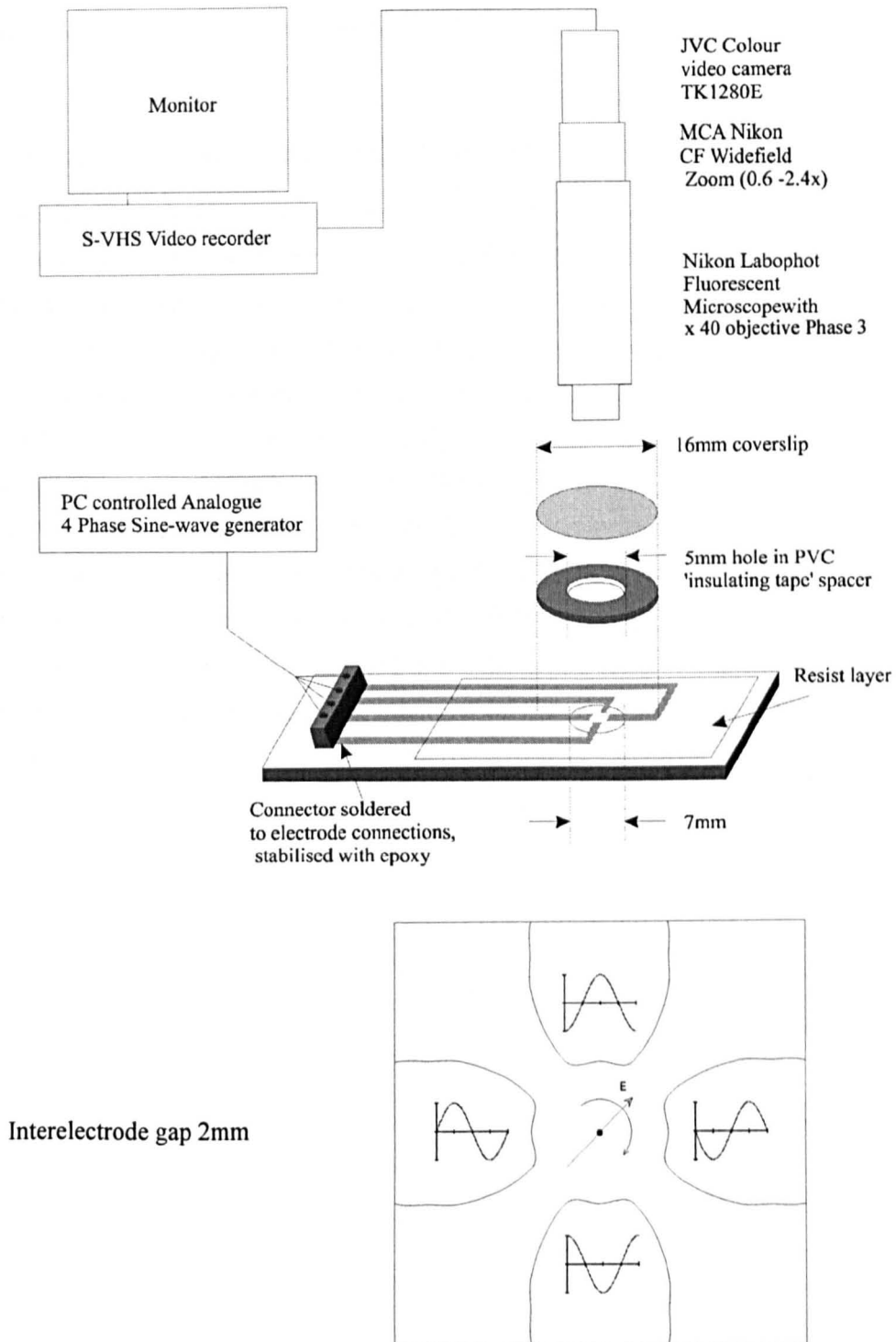
Figure 4.4 ROT apparatus and view of electrode tips with 'bone' end profiles.
The sine waves applied as shown creates a clockwise rotating field.

The gold electrodes constructed via photolithography onto a glass slide were stored in ultra pure water before use to minimise adhesion. Their 'bone-shaped' end profile assists in creating a uniform field in the central region of the interelectrode gap, as using low conductivity suspending media results in disruptive positive DEP forces over a wider frequency range than are observed for higher conductivity solutions. Indeed, for high conductivity media, negative DEP may be observed over the whole frequency range of interest, in which case highly angular electrode tips are an advantage as they assist in keeping the particles in the centre of the chamber (Fuhr *et al.*, 1994).

4.2.7 Recording and Measuring the Rotation Rates

After 1min (to allow particle sedimentation onto the glass) particles within the middle 1/3 of the ROT chamber and greater than 3 particle diameters from other particles were selected for the full frequency ROT spectrum. In this manner, up to six rotating particles could be recorded simultaneously in a field of view. 20 approximately equidistant frequency points (on a log scale) were chosen between 100Hz and 5MHz, and the rotation of the particles recorded for around 10 s at each frequency, for later analysis with a stopwatch. The applied field was kept on while changing frequencies as this helped prevent particle-substrate adhesion. As electrophoretic effects (causing particle drift) were more noticeable at lower frequencies (<1kHz) each spectrum was recorded from high to low frequency. There was no significant difference between a spectrum recorded in this manner and one recorded with a random frequency order. Particles that drifted more than 3 diameters over recording time were discarded.

Following each full frequency sweep a fresh particle suspension was used. In between each aliquot, the chamber was washed under pressure with ultra pure water from a hand held bottle, then dried under a stream of N_2 gas.

4.2.8 Modelling of results

In electrical terms, a cell in suspension often resembles an aqueous sphere or ellipsoid (the cytoplasm) surrounded by a non-conducting membrane. For particles such as protozoal cysts, the cyst membrane is in turn surrounded by a conducting cyst wall. Thus, a cyst can be represented as a number of concentric shells with differing (dielectric) properties. This concentric-spheroid model of a cell was used (Irimajiri, Hanai & Inouye, 1979) to calculate the effective electrical properties of cells in suspension, and later adapted (Fuhr, 1985) for the calculation of the ROT torque on a cell in a rotating electric field. The model used in this work is based on a two-shelled (Kakutani, Shibatani, & Sugai, 1993) ellipsoidal (Zhou *et al.*, 1996) model.

Written in MatLab (The Maths Works™) the program enables one to both predict trends for the ROT (and DEP) response of a particle as a function of a variable, or to find the values of various parameters by fitting a curve to an experimental ROT spectrum.

Dielectric Parameters	Value	Physical Dimensions	Value
$\varepsilon_{interior}$	70 *	Membrane thickness	6 nm **
$\varepsilon_{membrane}$	8 *	Wall thickness	300 nm #
ε_{wall}	60 **	Major radius	4.5 μm #
$\varepsilon_{suspending\ medium}$	79	Minor radius	3.0 μm #
$\sigma_{interior}$	0.5 *		
$\sigma_{membrane}$	1x 10^{-6} *		
σ_{wall}	0.01 *		

σ = conductivity (S m⁻¹); ε = relative permittivity

Table 4.3 Constants used in the ellipsoidal multishell model to predict trends of electrorotation spectra.
* Fitted values; ** Huang *et al.* (1992); # Coggins & Schaefer (1986).

The MatLab program
(modified from Zhou *et al.* 1996).

```
%shelled ellipsoid with semi-axes a,b,c
%prolate spheroid where a>b=c
%ellipticity factor e=a/b (e>>1)
%a,b,and c directed along x,y,and z,respectively
%rotation field applied in x-y plane
%Ellipsoid rotates about the minor z-axis

clear;

%Constants and parameters
f=logspace(2,7);
zeroline=f-f;
w=2*pi*f;
p0=8.854e-12;

%G. muris a0=4.5e-6 ;b0=3e-6;
%G. duodenalis a0=5 ;b0=8e-6;
%C. muris a0=3.7e-6; b0=2.8e-6;
%C. parvum a0=2.5e-6; b0=2.25e-6;
%C. baileyi a0=3.1e-6; b0=2.3e-6;

d1=2e-7; d2=8e-9;
a1=a0-d1; a2=a1-d2;
b1=b0-d1; b2=b1-d2;

%permittivities
%internal; membrane; wall; medium
kp1=70*p0;
kp2=8*p0;
kp3=60*p0;
kp4=79*p0;

%conductivities live;dead
%internal; membrane; wall; medium
kc1=0.5; %kc1=0.02
kc2=1e-6; %kc2=1e-5
kc3=0.0250;
kc4=100e-4;

%complex terms
k1=kp1-i*kc1 ./w;
k2=kp2-i*kc2 ./w;
k3=kp3-i*kc3 ./w;
k4=kp4-i*kc4 ./w;

%Volume of concentric ellipsoids
v1=a1*b1^2/(a0*b0^2);
v2=a2*b2^2/(a1*b1^2);
vc=4*pi*a0*b0^2/3;

%depolarizing factors A0x, A1x, A2x &
    A0y, A1y, A2y;
zhou0=0.5*(a0*b0^2/(sqrt((a0^2-
    b0^2)^3)));
xiao0=log((2*a0^2-b0^2+2*a0*sqrt(a0^2-
    b0^2))/b0^2);
feng0=b0^2/(a0^2-b0^2);
A0x=zhou0*xiao0-feng0;

zhou1=0.5*(a1*b1^2/(sqrt((a1^2-
    b1^2)^3)));
xiao1=log((2*a1^2-b1^2+2*a1*sqrt(a1^2-
    b1^2))/b1^2);
feng1=b1^2/(a1^2-b1^2);
A1x=zhou1*xiao1-feng1;
```

```
zhou2=0.5*(a2*b2^2/(sqrt((a2^2-b2^2)
    ^3)));
xiao2=log((2*a2^2-b2^2+2*a2*sqrt(a2^2-
    b2^2))/b2^2);
feng2=b2^2/(a2^2-b2^2);
A2x=zhou2*xiao2-feng2;

keffx2=k2    .*(k2+(k1-k2)    *(A2x+v2*(1-
    A1x)))  ./(k2+(k1-k2)*(A2x-v2*A1x));

keffx3=k3 .*(k3+(keffx2-k3)*(A1x+v1*(1-
    A0x)))         ./(k3+(keffx2-k3)*(A1x-
    v1*A0x));

Px=(keffx3-k4) ./((keffx3-k4)*A0x+k4);

A0y=0.5-0.5*A0x;
A1y=0.5-0.5*A1x;
A2y=0.5-0.5*A2x;

keffy2=k2        .*(k2+(k1-k2)*(A2y+v2*(1-
    A1y))) ./(k2+(k1-k2)*(A2y-v2*A1y));

keffy3=k3 .*(k3+(keffy2-k3)*(A1y+v1*(1-
    A0y)))         ./(k3+(keffy2-k3)*(A1y-
    v1*A0y));

Py=(keffy3-k4) ./((keffy3-k4)*A0y+k4);

imP=imag(Px+Py);
reP=real(Px+Py);

%Calculation of Viscous drag (Rv)
%Viscosity of water at 20c = 0.01002
    poise (gm/sec.cm)
%ie nu=1.002e-3 Kg/sec.m

nu=1.002e-3;
Rv=2*vc*nu*((a0^2+b0^2)/(a0^2*A0x+b0^2*
    A0y));

%applied field strength (E);
E=3.5e3;

%ROT equation
rot=0.5*p0*79*(vc/Rv)*E^2*imP;

ratio=1;
rot=ratio*rot;

twave=reP.*(-rot);
for i=1:50
 if reP(i)>0
  twave(i)=0;
 end
end

%Plotting
AXIS([2 7 -3 5])

plot(log10(f),-rot,'k-',log10(f),
    zeroline,'k-');
plot(log10(f),reP,'r.');
plot(log10(f),twave,'b:');

hold on
end
```

4.3 Results

Initial spectra of 10 day old fluorescently stained *G. muris* cysts revealed a field frequency range at which viable and non-viable stained cysts rotated in opposite directions. The mid-frequency of this range (500kHz) was then used as a quick test to judge the viability of the cyst population on 5 of the following 40 days, for a direct comparison with the fluorescent dyes. The viability estimations at 500kHz, based on the first $n \geq 50$ cyst observations are presented in Table 4.4a and in Figure 4.5. On two additional days, viability was determined by ROT alone, see a summary Table 4.4b.

Through days 10 to 48 a total of $n=50$ full ROT spectra were recorded over the frequency range 100Hz to 5MHz. Only spectra were recorded for cysts where it was also possible to see the fluorescent stains, as not all cysts included the stains. Empty cyst shells were recorded as a separate category. The ROT spectra are presented in Figures 4.6 to 4.8.

Cyst age (no.)	Stain result FDA / PI	ROT assay (500kHz)		
		Antifield rotation	Non-rotating	Co-field rotating
Day 10	+ / -	91	2	0
(n=104)	- / -	2	0	0
	+ / +	0	0	9
Day 12	+ / -	40	0	0
(n=50)	- / -	2	0	0
	+ / +	0	0	8
Day 22	+ / -	14	2	0
(n=50)	- / -	1	0	0
	+ / +	0	0	38
Day 36	+ / -	1	0	0
(n=57)	- / -	0	0	1
	+ / +	0	0	56
Day 48	+ / -	0	0	0
(n=50)	- / -	0	0	0
	+ / +	0	0	50

(a) Days 10-48

Day (cysts checked)	% Viable by FDA+/PI-	ROT
10 (104)	89.4	89.4
12 (50)	80.0	84.0
20 (44)	*	42.0
22 (50)	32.0	30.0
30 (50)	*	2.0
36 (57)	1.8	1.8
48 (50)	0.0	0.0

(b) Summary

Table 4.4 Comparison between fluorogenic vital stains and ROT.
* = staining procedure was not used.

Of the cysts (n=311) checked by both stains and ROT on these five days, it was possible to judge the viability of all cysts by at least one method. There may therefore be an advantage in using the two techniques in conjunction, as 10 cysts (out of 311) that were subjected to both techniques could only be judged by one method. In all these 10 cases, the result from the method that did work agreed with morphological indicators using phase contrast microscopy (Schupp *et al.*, 1987a).

It is worth noting that it is possible to design a ROT chamber in which all cysts will spin, *i.e.* one which does not have contact with the substrate using a combination of negative DEP with ROT, for example the field cage (Schnelle *et al.*, 1993). This experiment should therefore be viewed as an indicator of the potential of the ROT technique. There was good agreement between sense of ROT and morphology as determined using the criteria set out by Schupp & Erlandsen (1987a).
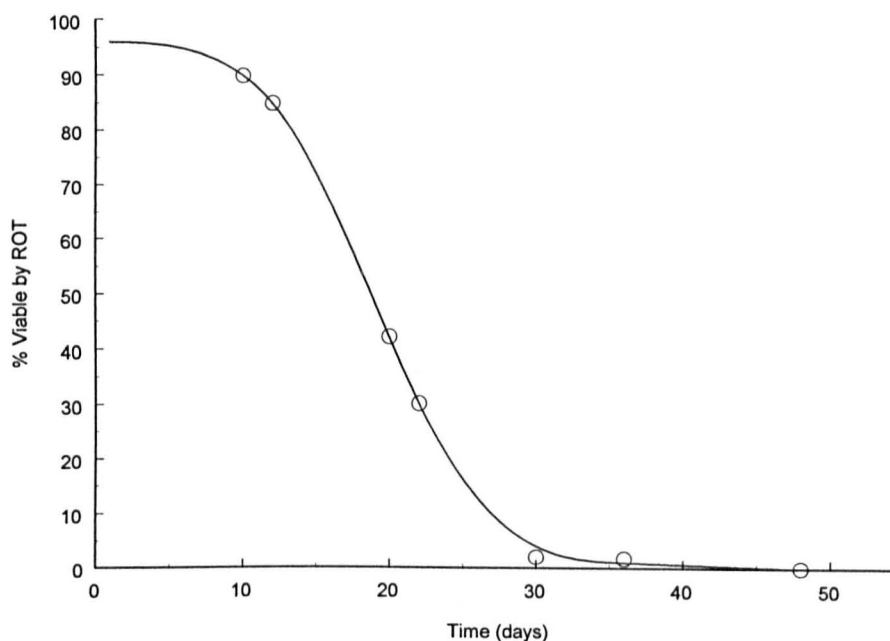
Figure 4.5 Viability of *G. muris* cysts as a function of storage time in ultra pure water (4°C) as determined by ROT ($\sigma_{sus\ med}$=5µS cm^{-1} f=500kHz) and morphological indicators. Each data point (O) based on $n \geq$ 44 observations.

The shape of the decay curve fits well with the description of Wallis (1994), although the rapid drop was centred about 18 days (i.e. average storage time ST_{50}=18) and not 50 days. A sigmoidal decay curve would be consistent with an approximately normal distribution of energy stores within individuals of a population. A few cysts with a small amount of stores would die sooner than average, large numbers in the population would die around the average time having average storage contents, finally a few would surivive longer than average time having greater storage reserves. These values are in close agreement with the fluorogenic vital dyes FDA and PI.
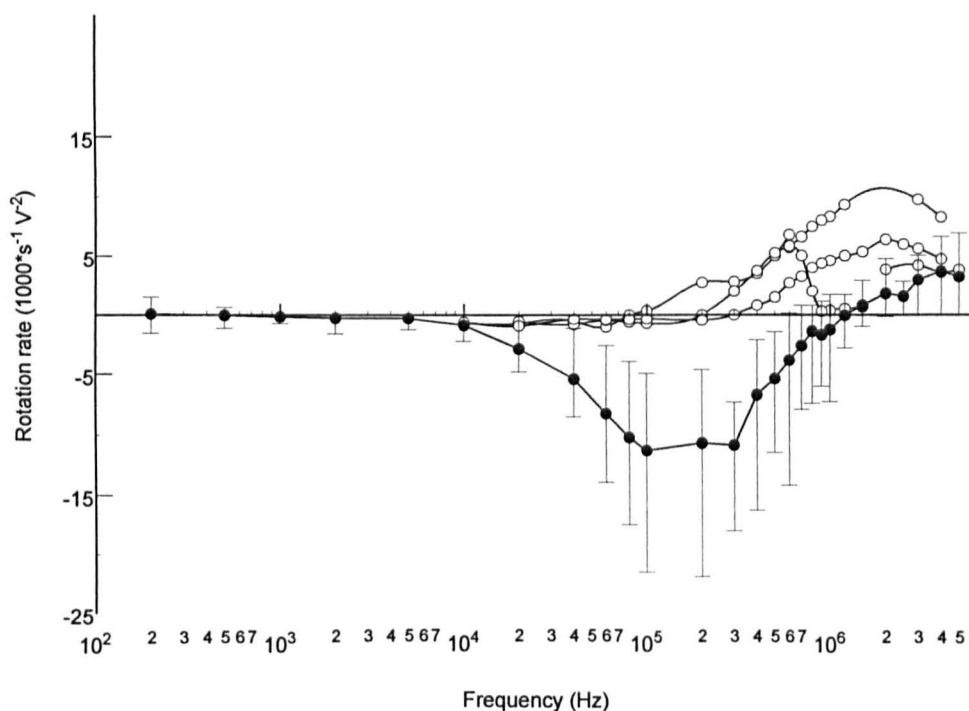
Figure 4.6 Electrorotation spectra of (*n*=37) viable (•) and (n=5) non-viable (o) *G. muris* cysts.
No overlap was observed between the rotation rates for the viable and non-viable *G. muris* cysts between
the frequencies 50kHz and 800kHz. Between 400kHz and 700kHz, the sense of rotation for the viable
and non-viable cysts was different. A single frequency, for example 500kHz, may therefore be used as a
simple test to determine the physiological state of a cyst, by the sense of its rotation. This method was
used to judge the population viability over time as shown in Figure 4.5.
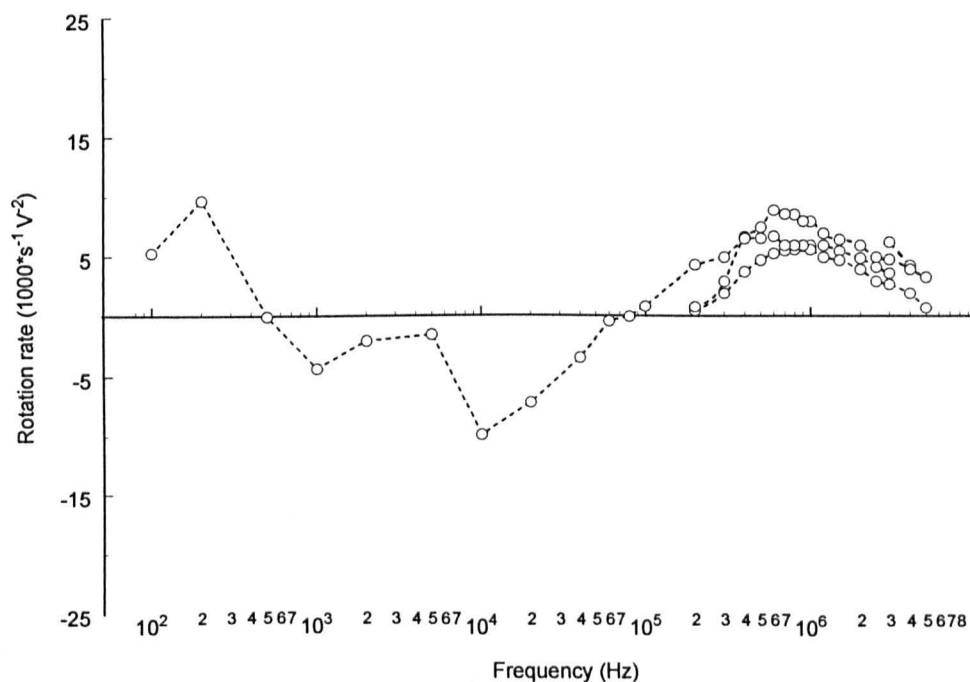
Figure 4.7 Electrorotation spectra of *G. muris* cyst ghosts.

The term 'cyst ghost' is used in this work to describe an empty (unless otherwise stated) cyst with visible hole at one end, through which excystation may have occurred. The high frequency crossover point in the spectra (the crossover from antifield to cofield rotation at around 100 - 200 kHz) was undetectable in three of four ghosts observed as below 200kHz these were either stuck on the substrate or failed to rotate. One ghost, from which a full spectrum was obtained, had a very irregular spectrum a feature of which was a secondary antifield peak at 1kHz not observed for any other particle investigated in this thesis. The presence of the secondary peak was checked during experimentation to ensure it was not due to experimental error.
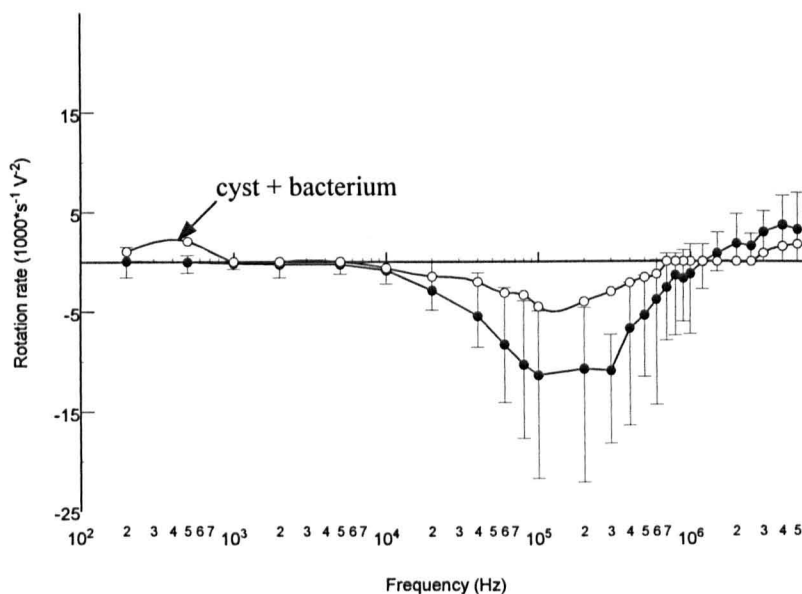
Figure 4.8 Range of electrorotation rates observed for non-sticking clean (*n*=37) viable cysts (•) of *G. muris* for comparison with a viable cyst with a single bacterium attached to its surface (o).

The cyst with bacterium adhering to the surface had a reduced rotation rate compared with the viable clean cysts for frequencies above 1kHz. Interestingly, for this cyst at 500Hz there is a cofield rotation peak that is distinct from the other 37 cysts observed. This indicates that the effect on the spectrum cannot be explained purely in terms of an increase in drag due to the adherent bacterium which could have explained the reduction in rotation rate at higher frequenices.

4.4   Variability in size

Measures of the inherent variability of the cysts, that may affect the ROT response, are variations in cyst size or shape. Using a haemocytometer grid for calibration, and an eye piece graticule, the major and minor axis of 73 cysts were measured from the initial stock solution of a *G. muris* isolate obtained from Waterborne Inc. stored in reverse osmosis water for 12 days. Measurements were taken after the cysts had settled onto the slide surface. From the size distribution of *G. muris* cysts shown in Table 4.5 and graphically in Figure 4.9, it is clear that there is considerable variation both in size and ellipsicity. All measurements were taken from cysts in the same solution, and so were all under the same osmotic stress. Like plant cells cysts possess a retaining wall that restricts their size. The net influx of water into the cyst through the process of osmosis, is countered by the cyst wall. The cyst while intact, through this turgor pressure, is held close to their maximum natural dimensions. This may also explain why some of the

cysts described as non-viable have smaller dimensions, their leaky membranes not allowing the build up of the turgor pressure.

The mean cyst dimensions (*n*=73) were 7.2 x 10.7 μm. A measure of ellipsicity is given by the major to minor axis ratio, which for this sample had a mean of 1.49 ±0.13.

G. muris cysts (*n*=73)	Minimum	Maximum	Mean	Standard deviation
Major axis	7.40	13.30	10.73	0.82
Minor axis	5.60	8.40	7.21	0.51
Ratio	1.15	2.02	1.49	0.13

Table 4.5 Size and ellipsicity of *G. muris* cysts stored in reverse osmosis water.

As shown in Figure 4.9 there is considerable overlap between the sizes of the viable and non-viable cysts observed. This is to be expected, as when the cyst dies the cyst contents simply shrink away from the cyst wall, little altering the size or shape of the cyst.
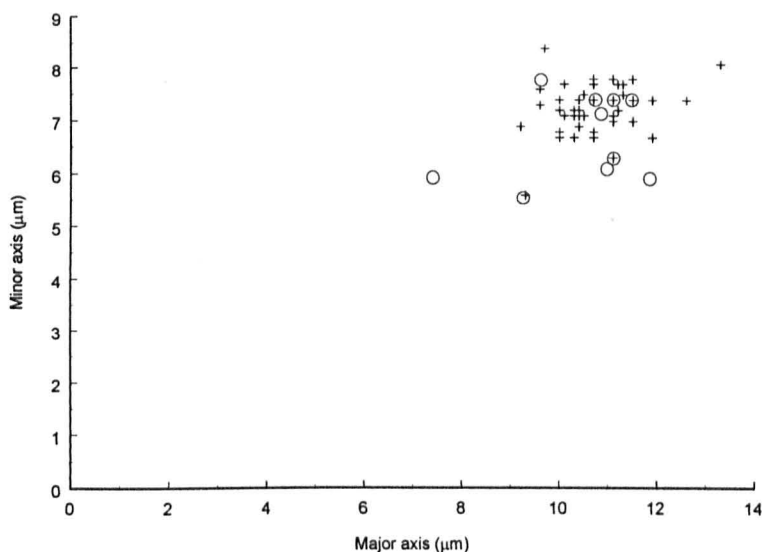
Figure 4.9 Size distribution of (*n*=73) *G. muris* cysts from the Louisiana isolate.

Cysts were judged viable (+) and non-viable (O) by morphological indicators and the inclusion of the fluorescent dyes FDA and PI.

The effect of particle size on the ROT spectra was modelled, using representative dimensions from those shown in figure 4.9, within which the majority of values fall. A fixed particle ellipsicity (length to width ratio = 1.5) is shown in figure 4.10 for two extremes of volume. The extremes of particle ellipsicity observed was also modelled, for a fixed particle volume, figure 4.11.
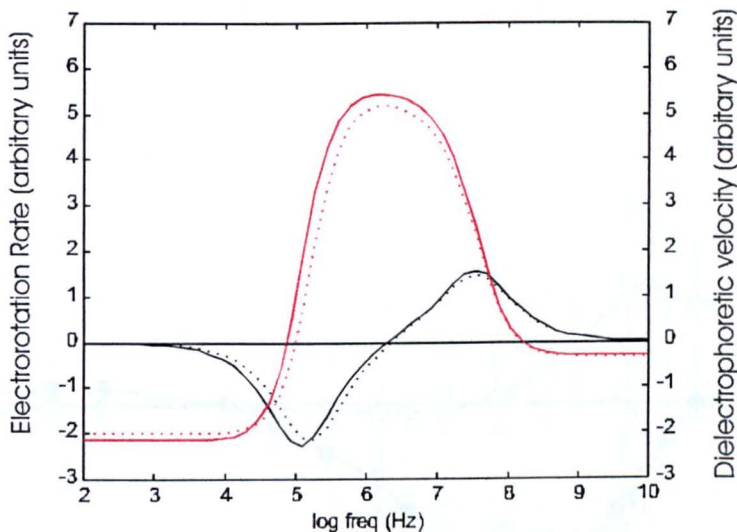
Figure 4.10 Effect of particle volume on the ROT and DEP response for *G. muris* cysts.
Fixed aspect ratio (r) of 1.5 parameters: small volume $170\mu m^3$ (.) radii = 4.5 x 3µm; larger volume $402\mu m^3$ (-) radii = 6 x 4.
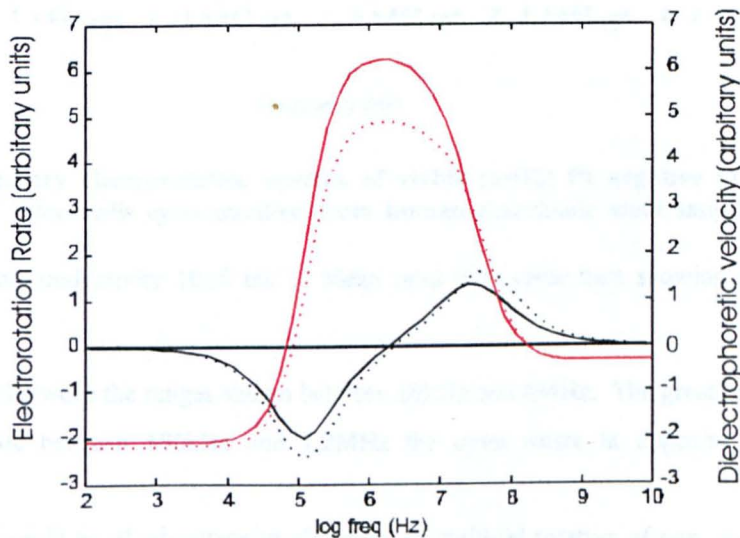
Figure 4.11 Effect of particle ellipsicity on the ROT and DEP response for *Giardia muris* cysts.
Fixed volume ($282\mu m^3$) parameters: r = 1.16 (··) radii = 4.5 x 3.875 for r = 2.02 (-) radii = 6.5 x 3.2µm.

The predicted trends are that smaller particles have crossovers that occur at slightly higher frequencies, with little effect on the magnitude. Ellipsicity decreases the ROT rate (for the antifield peak) while increasing the magnitude of the positive DEP force. That wider ranges in the rotation rates occur (see viable cyst ranges Figures 4.6 and 4.8) implies that the variation is due to something other than size or shape.

From the two isolates of *G. intestinalis* of human origin, *n* = 54 spectra were obtained within 10 days of egestion. Spectra obtained are presented in figures 4.12, 4.15 & 4.15.
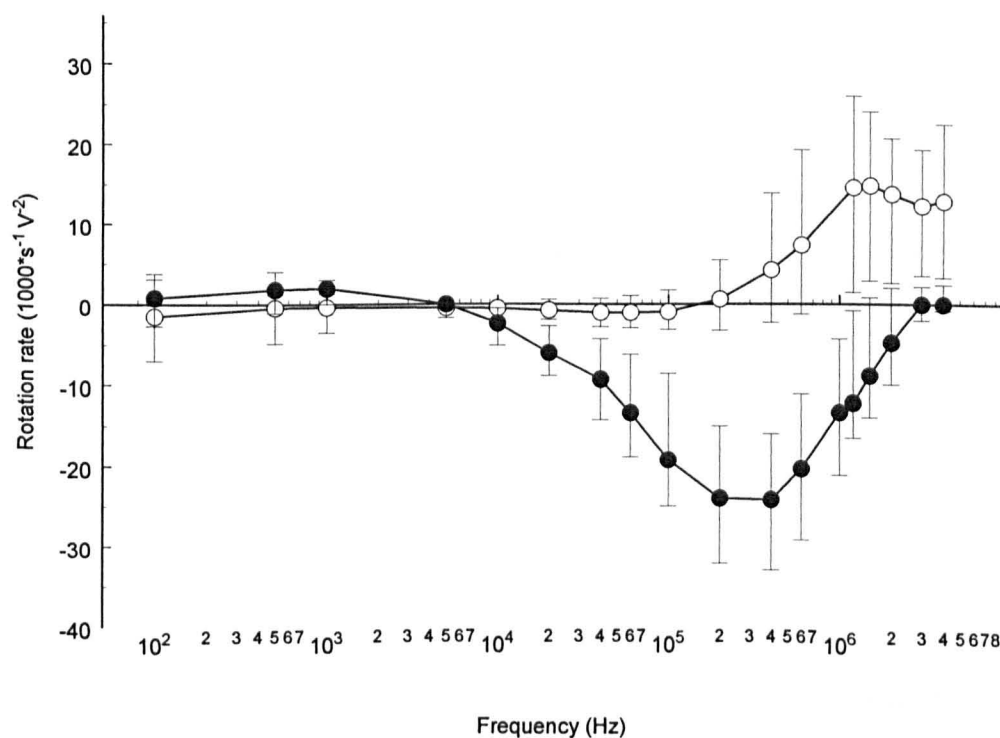
Figure 4.12 Summary electrorotation spectra of viable (n=32) PI negative (•) and non-viable (n=15) PI+ (o) *G. intestinalis* cysts purified from human diarrhoeic stool samples, PHL Bangor (isolate 1).
Suspending medium conductivity 10μS cm^{-1}. Mean rates with error bars showing the total range of observations.

There is no overlap between the ranges shown between 20kHz and 4MHz. The greatest difference in rate is at 400kHz, while between 800kHz and 1.2MHz the cysts rotate in opposite directions at this conductivity.

From these data it would be of advantage to eliminate all antifield rotation of non-viable cysts between 20kHz and 1MHz. This should be possible through increasing the medium conductivity. The effect of medium conductivity on the rotation rate of the cysts is shown through modelled spectra in the next figure.
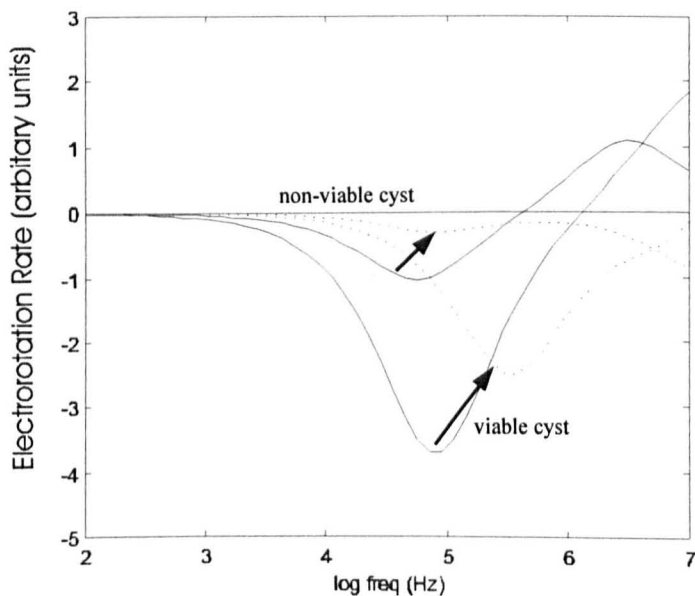
Figure 4.13 Effect of suspending medium conductivity on rotation rate of viable and non-viable *G. intestinalis* cysts, (-) 10μS cm⁻¹, (- -) 750 μS cm⁻¹.
Arrows indicate for both viable and non-viable cysts the change in the antifield peak from low to high conductivity medium.

Although not eliminating the antifield rotation of the non-viable cysts, a comparatively greater reduction is achieved by increasing the suspending medium conductivity. A disadvantage however, is observed in the crossover region of the spectra. The method would rely on detection of rotation only, and not on the direction.
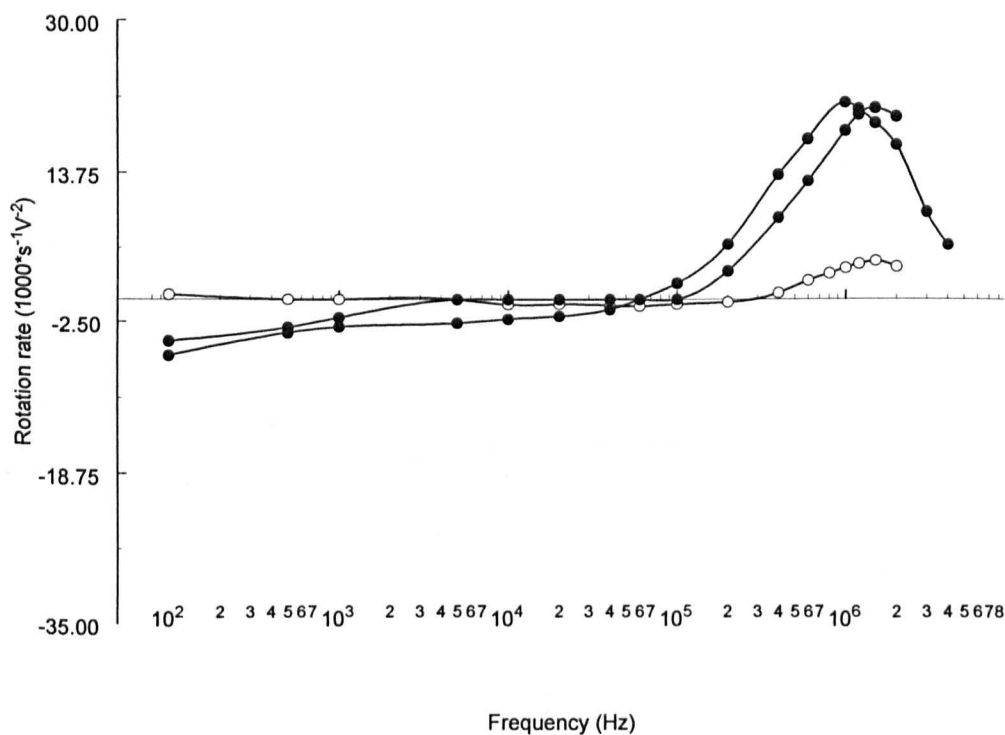
Figure 4.14 *G. intestinalis* **cyst ghosts with residium (•) and a non-motile trophozoite (o) recorded 10 minutes after excystation *in vitro*.**
Suspension medium conductivity 10μS cm⁻¹.

Cyst walls lacking cytoplasmic contents but with a PI staining residium (contracted cytoplasm) exhibit an antifield region below 100kHz, the rate of which increases to a maximum at 100Hz. It would have been useful to extend the frequency range used, but this was limited by the occurrence of electrolysis at the electrodes for f <100Hz. The strong cofield rotation at 1MHz is characteristic of the non-viable cysts shown in Figure 4.6 for *G. muris*.
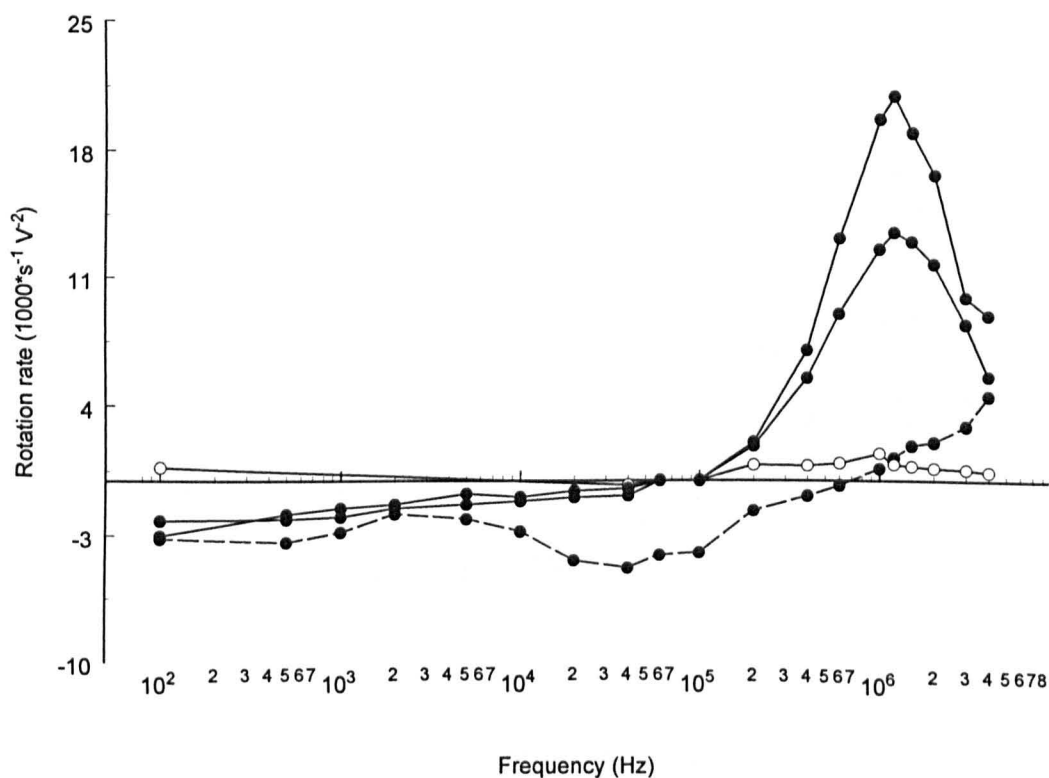
Figure 4.15 *G. intestinalis* cysts from Glasgow sample, SPDL (isolate 2).
Typical cyst with dark cytoplasm PI+ staining (- • -) non-motile trophozoite (o) and two examples of cysts with distinct shrunken cytoplasm (•). Suspension medium conductivity 10µS cm^{-1}.

Similar in appearance to the non-viable PI+ staining *G. muris* cysts, these *G. intestinalis* non-viable cysts exhibit a large cofield ROT at around 1MHz. However, the peaks are more pronounced than those of *G. muris*.
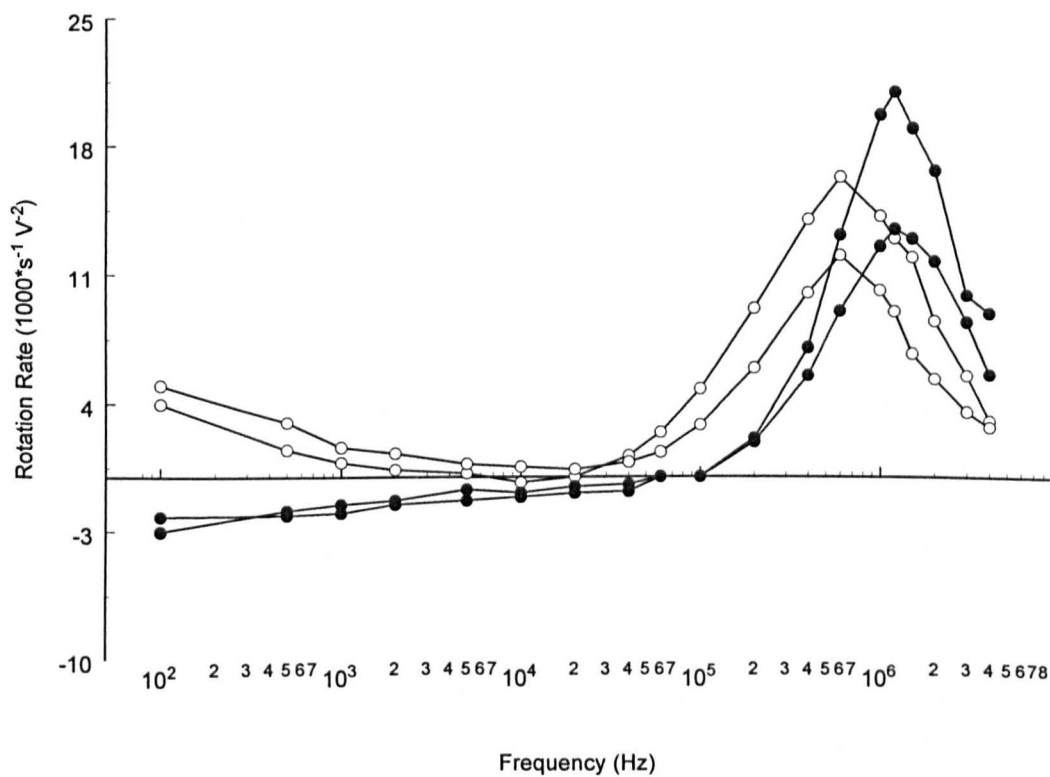
Figure 4.16 Cysts from two isolates of *G. intestinalis*.
Morphologically similar non-viable cysts with shrunken granular cytoplasm, isolate 1(o) isolate 2(•). Suspended in 10µS cm⁻¹ PBS.

There are two notable differences between the spectra of cysts with shrunken cytoplasm obtained for the isolates obtained from Glasgow. The high frequency peaks are at 600kHz and 1.2 MHz respectively. More noticeably, below 7kHz the isolates rotate in opposite directions, the difference being pronounced at lower frequencies.

4.5   Conclusions

A specific and rapid viability test for the small number of cysts isolated from water samples is currently seen as an important tool for assessing the potential for contracting various diseases including giardiasis in man. If such a test could distinguish between cysts of different species (cysts of *G. muris* are not infective to man) then this would be of further use in identifying the source of environmental contamination, as well as further indicating the risk potential.

The results presented in this chapter demonstrate that ROT does give an indication of the viability of individual cysts of both *G. muris* and *G. intestinalis*. Good agreement was found between fluorogenic vital dyes and ROT, for *G. muris* cysts at 500kHz (5µS cm^{-1}) over a period of 48 days. A small advantage of ROT was observed, in that it was possible to judge viability by ROT of 1.9% (6 of 311) cysts that were unstained. 1.3% (4 of 311) cysts, however, did not rotate but did stain. Using both techniques in conjunction it was possible to judge all 311 cysts. For *G. intestinalis* between 800kHz and 1.2MHz (10µS cm^{-1}) good agreement was found between ROT and PI inclusion / exclusion. As the species were investigated at slightly different suspending medium conductivities (5 and 10µS cm^{-1}) it is not possible to make direct comparisons between the two species. From modelling work, potential improvements to the method through increasing the medium conductivity were suggested. Both species however, exhibited cofield and antifield rotation < 1kHz. ROT spectra of non-viable trophozoites and ghosts were also described for completeness.

The effect of a bacterium adhering to a viable *G. muris* cyst was found not only to affect the magnitude of the rotation, which would be expected through increased viscous drag, but also to alter the shape of the spectrum. At 500Hz, for example, this cyst exhibited a much faster rotation rate than all the other 37 cysts. Electrophoretic effects may explain this observation, as this occurred at a relatively low frequency. It would be of interest to determine the bacteria species involved and then compare the electrophoretic mobilities of a clean viable cyst and of a bacterium.

Interestingly significant rotational differences were noted between the cysts of two *G. intestinalis* isolates of human source. Below 7kHz non-viable cysts of the two isolates rotated in different directions, as well as the cofield peaks occurring at distinct frequencies. Again, it would be useful to compare electrophoretic mobilities of the two isolates.

Of potential interest for further dielectric studies, are the cysts of species found in voles and muskrats (Feely, 1988). In contrast to the cysts of other *Giardia* species, those of *G. microti* (Kofoid & Christiansen, 1915) contain two differentiated trophozoites, each having a mature ventral disk. This would be a useful particle for studying the presence of intracellular structures; presumably effecting obtained spectra at frequencies above the normal Maxwell-Wagner relaxation. Distinguishing between these and other cysts found in environmental samples would be of benefit, as sequences of the small subunit rRNA from these cysts have been shown to differ from the cysts that parasitise humans (VanKeulen *et al.*, 1998).

4.6   References

Alberts B., Bray, D., Lewis, J., Raff, M, Roberts, K. & Watson J.D. eds. (1994) Eukaryotic cells depend on mitochondria for their oxidative metabolism. In Chapter 1 : The Evolution of the cell. *Molecular biology of the Cell.* 3rd edn. Garland Publishing. New York. Chapter 1. pp. 3-41.

Aggarwal, A. & Nash, T.E. (1988) Antigenic variation of *Giardia lamblia in vivo. Infection and Immunity.* **56:** 1420-1423.

Anon (1986) Laboratory reports of *G. lamblia* to the Communicable Disease Surveillance Centre (CDSC) all identifications for England and Wales. http://www.phls.co.uk/CDSC/site, fr3.htm

Bennet, J.V., Holmsberg, S.D., Rogers, M.S. & Solomon, S.M. (1987) Infectious and Parasitic Diseases data selection. *American Journal of Preventative Medicine.* **3:** suppl. 102-114.

Bingham A.K. & Meyer E.A. (1979) *Giardia* excystation can be induced *in vitro* in acidic solutions. *Nature* **277:** 301-302.

Birkhead, G., & Vogt, R. (1989) Epidemiologic surveillance for endemic *Giardia lamblia* infection in Vermont. *American Journal of Epidemiology.* **129:** 762-768.

Clark, R. (1989) Analysis of inactivation of *Giardia lamblia* by chlorine. *American Society for Civil Engineers Journal of Environmental Engineers Division.* **115:** 80-90.

Coggins, J.R. & Schaefer, F.W. (III) (1986) *Giardia muris:* ultrastructural analysis of *in vitro* excystation. *Experimental Parasitology.* **61:** 219-228.

Craun, G.F. (1986) Waterborne giardiasis in the united-states 1965-84. *Lancet.* **2:** 514

Dowd S.E. & Pillai, S.D. (1997) A rapid viability assay for *Cryptosporidium* oocysts and *Giardia* cysts for use in conjunction with indirect fluorescent antibody detection *Canadian Journal of Microbiology.* **43:** 658-662.

Erlandsen, S.L., Bemrick, W.J. & Pawley, J. (1989) High resolution electron-microscopic evidence for the filamentous structure of the cyst wall in *G. muris* and *G. duodenalis. Journal of Parasitology* **75:** 787-797.

Feely, D.E. (1988) Morphology of the cyst of *Giardia-microti* by light and electron-microscopy. *Journal of Protozoology.* **35:** 52-54.

Filice, F.P. (1952) Studies on the cytology and life history of a *Giardia* from the laboratory rat. *University of California Publications on Zoology.* **57:** 53-146.

Fuhr, G. (1985) Über die Rotation Dielektrisher Körper in Rotierenden, Feldern PhD dissertation, Humboldt Univerität.

Fuhr, G., Glasser, H., Muller, T. & Schnelle, T. (1994) Cell manipulation and cultivation under AC electric field influence in highly conductive culture media. *Biochimica Biophysica Acta.* **1201:** 353-360.

Gillin, F.D., Reiner, D.S., Gault, M.J., Douglas, H., Das, S., Wunderlich, A. & Sauch, J.F. (1987) Encystation and expression of cyst antigens by *G. lamblia in vitro. Science* **235:** 1040-1043.

Gundel, J., Wicher, D. & Matthies, H. (1989) Electrorotation as a viability test for isolated single animal cells. *Studia Biophysica* **133:** 5-18.

Huang Y., Holzel, R., Pethig, R. & Wang, X.B. (1992) Differences in the A.C. electrodynamics of viable and non-viable yeast cells determined through combined dielectrophoresis and electrorotation studies. *Physics in Medicine and Biology.* **37:** 1499-1517.

Irimajiri, A., Hanai, T. & Inouye, A. (1979) A dielectric theory of Multi-stratified shell model with its application to a lymphoma cell. *Journal of Theoretical Biology.* **78**: 251-269.

Jarroll, E.L., Manning, P., Lindmark D.G., Coggins, J.R. & Erlandsen, S.L. (1989) *Giardia* cyst wall-specific carbohydrate - evidence for the presence of galactosamine. *Molecular and Biochemical Parasitology.* **32**: 121-131.

Jones K.H. & Senft J.A. (1985) An improved method to determine cell viability by simultaneously staining with fluorescein diacetate and PI. *Journal of Histochemistry and Cytochemistry.* **331**: 77-79.

Kakutani, T., Shibatani, S. & Sugai, M. (1993) Electrorotation of nonspherical cells - theory for ellipsoidal cells with an arbitrary number of shells. *Bioelectrochemistry and Bioenergetics.* **31**: 131-145.

Kulda, J. & Nohynkova, E. (1978) Flagellates of the human intestine and of intestines of other species. p2-38. In: *Parasitic Protozoa*, vol. II. Intestinal flagellates : histomonads, trichomonads, amoeba, amoeba, opalinids, and ciliates (Ed. J.P. Krier) Academic Press. Inc. New York.

Labatiuk, C.W., Schaefer, F.W., Finch, G.R., & Belosevic, M. (1991) Comparison of animal infectivity, excystation, and fluorogenic dye as measures of *Giardia-muris* cyst inactivation by ozone. *Applied and Environmental Microbiology.* **57**: 3187-3192.

Lopez, C.E., Dykes, A.C., Juranek, D.D., Sinclair, S.P., Conn, J.M., Christie, R.W., Lippy, E.C., Schultz, M.G. and Mires, M.H. (1980) Waterborne giardiasis: a community outbreak of disease and a high rate of asymptomatic infection. *American Journal of Epidemiology.* **112**: 495-507.

Luján, H.D., Mowatt, M.R. & Nash, T.E. (1998) The molecular mechanisms of *Giardia* encystation. *Parasitology Today.* **14**: 446-450.

Luchtel, D.L. Lawrence, W.P. & DeWalle, F.B. (1980) Electron microscopy of *Giardia lamblia* cysts. *Applied and Environmental Microbiology.* **40**: 821-832.

Markell, E.K., Voge, M. & John D.T. eds (1992) Lumen dwelling protozoa. In *Medical Parasitology.* *7th edn.* Saunders, Philadelphia.

Nash, T.E. (1992) Surface antigen variability and variation in *Giardia lamblia. Parasitology Today* **8**: 229-234.

Nash, T.E., Herrington, D.A., Losonsky, G.A. & Levine, M.M. (1987) Experimental human infections with *Giardia lamblia. Journal of Infectious Diseases.* **156**: 974-984.

Pethig, R. (1991) Application of A.C. Electrical fields to the manipulation and characterisation of cells. Automation in Biotechnology. ed. I Karube (Amsterdam: Elsevier). pp. 159-85.

Rendtorff, R.C. (1979) The experimental transmission of *Giardia lamblia* among volunteer subjects. In: *Waterborne Transmission of Giardiasis* (Eds. W. Jakubowski & J.C. Hoff), U.S. Environmental Protection Agency. Office of Research and Development, Environmental Research Centre, Cincinnati, Ohio 45268, USA, EPA-600/9- 79-001. pp 64-81.

Roberts-Thomson, I.C., Stevens, D.P., Moahmoud, A.A.F., & Warren, K. S. (1976) Giardiasis in the mouse: An animal model. *Gastroenterology* **7**: 57-61.

Sauch, J.F. (1984) Purification of *G. muris* cysts by velocity sedimentation. *Applied and Environmental Microbiology.* **48**: 454-455.

Schupp, D.G. & Erlandsen, S.L. (1987a) Determination of *G. muris* cyst viability by differential interference contrast, phase, or brightfield microscopy. *Journal of Parasitology.* **73**: 723-729.

Schupp, D.G. & Erlandsen, S.L. (1987b) A new method to determine *Giardia* cyst viability: correlation of Fluorescein Diacetate and Propidium Iodide Staining with animal infectivity. *Applied and Environmental Microbiology.* **53**: 704-707.

Schnelle, T.; Hagedorn, R.; Fuhr, G.; Fiedler, S.; Muller, T. (1993) 3-Dimensional Electric-Field Traps for Manipulation of Cells Calculation and Experimental-Verification *Biochimica et Biophysica Acta* **1157: 127-140.**

Sheffield, H.G. & Bjorvatn, B. (1977) Ultra structure of the cyst of *Giardia lamblia. American Journal of Tropical Medicine and Hygiene* **26**: 23-30.

Smith, A.L. & Smith, H.V. (1989) A comparison of fluorescein diacetate and propidium iodide staining and *in vitro* excystation for determining *Giardia intestinalis* cyst viability. *Parasitology* **99**: 329-331.

Smith, H.V., Robertson, L.J. & Ongerth, J.E. (1995) Cryptosporidiosis and Giardiasis: The impact of waterborne transmission. *Journal of Water Supply Research and Technology-Aqua.* **44**: 258-274.

Smith, P.D., Lane, H.C., Gill, V.J., Manischewitz, J.F., Quinnan, G.V., Fauci, A.S. & Masur, H. (1988) Intestinal infections in patients with the acquired immune deficiency syndrome (AIDS). *Annals of International Medicine.* **108**: 328-333.

Soggins, M.L., Gunderson, J.H., Elwood, H.J., Alonso, R.A. & Peattie, D.A. (1989) Phylogenetic meaning of the kingdom concept: an unusual ribosomal RNA from *Giardia lamblia. Science* **243**: 75-77.

VanKeulen, H., Feely, D.E., Macechko, P.T., Jarroll, E.L., Erlandsen, S.L. (1998) The sequence of *Giardia* small subunit rRNA shows that voles and muskrats are parasitised by a unique species *Giardia microti. Journal of Parasitology.* **84**: 294-300.

Wallis, P.M. (1994) Abiotic transmission - is water really significant? In: *Giardia: from molecules to disease.* (Eds. R.C.A. Thompson, J.A. Reynoldson, & A.J. Lymbery) CAB International, Oxon.

Ward, H.D., Alroy, J., Lev, B.I., Keusch, G.T., & Pereira, M.E.A. (1985) Identification of chitin as a structural component of *Giardia* cysts. *Infection and Immunity..* **49**: 629-634.

Wickramanayake, G.B., Alan, J.R. & Otis, J.S. (1984) Inactivation of *Giardia lamblia* cysts with ozone. *Applied and Environmental Microbiology.* **48**: 671-672.

Woo, P.T.K., & Paterson, W.B. (1986) *Giardia lamblia* in children in day-care-centers in Southern Ontario, Canada, and susceptibility of animals to *Giardia lamblia. Transactions of the Royal Society of Tropical Medicine and Hygiene.* **80**: 56-59.

Zhou, X-F., Markx, G.H., Pethig, R. & Eastwood, I.M. (1995) Differentiation of viable and non-viable bacterial biofilms using electrorotation. *Biochimica et Biophysica Acta* 1245:85-93.

Zhou, X-F., Markx, G.H. & Pethig, R. (1996) Effect of biocide concentration on electrorotation spectra of yeast cells. *Biochimica et Biophysica Acta-Biomembranes.* **1281**: 60-64.

Chapter 5

Electrorotation of *Cryptosporidium parvum* oocysts.

5.1   Introduction

Electrorotation (ROT) data obtained from any species will show a certain amount of variation. Differences observed are reflected in both the magnitude and frequency response represented in the ROT spectra. This chapter explores the extent to which the observed variation in the ROT spectra is due to real differences between individuals within a species, using *Cryptosporidium parvum* oocysts as the model particle.

Oocysts of *C. parvum* are suitable for such studies as they are very uniform in size distribution, are near spherical and are available in large numbers commercially as well as being readily obtainable from clinical samples via the Public Health Laboratories.

There are at least two possible causes for variation in the observed ROT spectra from oocysts of the same species. The first, intraspecific variation, may involve physical, and or, chemical differences between the oocysts. Size or variation in the composition of the structures of the oocysts are examples of intraspecific variation. A second cause of variation in the observed ROT spectra, is that from experimental conditions.

As was noted in Chapter 3 the conductivity of the suspending medium relative to that of the particle will affect the magnitude and direction of the induced dipole in an AC electric field. For each particle there will therefore be a unique ROT response for each suspending medium conductivity. If the electrorotation assay is to be of any practical use for characterising a particle, then either the effect of different values of suspending medium conductivity must be precisely known for that particle, (so that it can be accurately measured and accounted for) or the conductivity value must be accurately controlled.

Three features of the ROT spectra of *C. parvum* oocysts are explored in this chapter as a function of the suspending medium conductivity, highlighted in Figure 5.1, namely, the antifield-peak frequency, the antifield-peak magnitude and the high frequency crossover frequency.
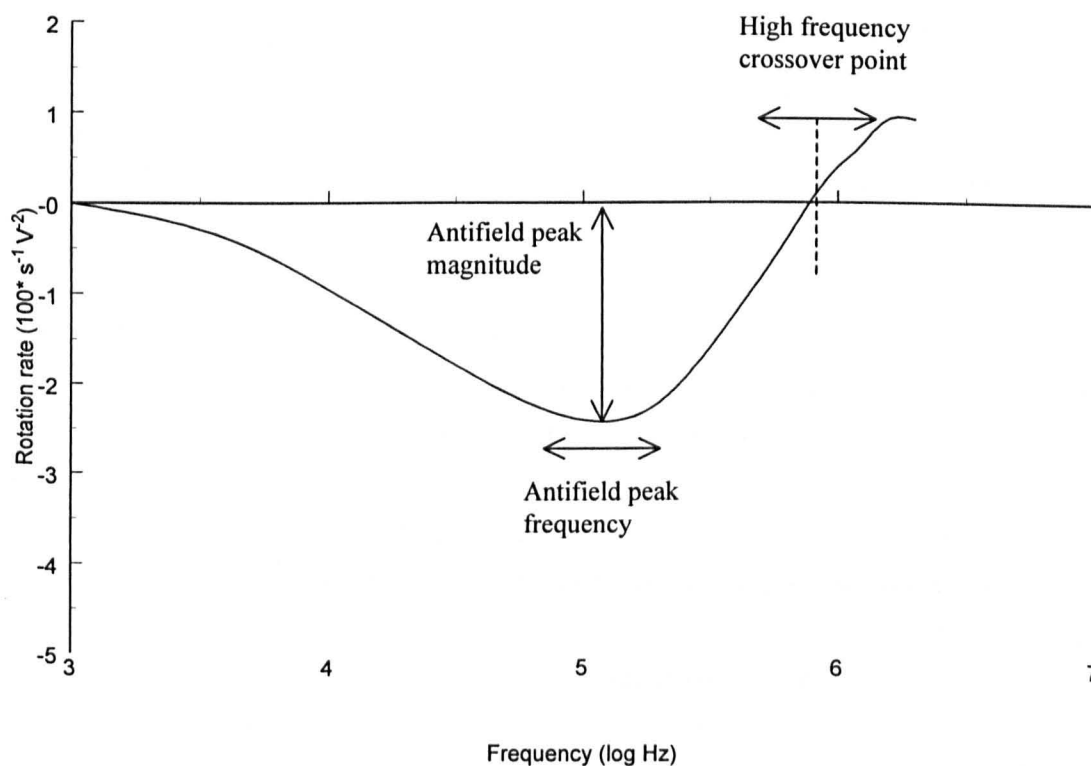
Figure 5.1 Typical Electrorotation spectrum highlighting the features explored in this chapter as a function of suspending medium conductivity.

Also in section 5.7, ROT as a method to determine oocyst viability is explored, in a direct comparison with a twin fluorogenic vital dyes method. These are referred to as dyes (as opposed to stains) because they highlight specific features rather than show the presence or absence of structures.

5.2 Oocyst Material and Methods

To quantify the effect of suspending medium conductivity on the electrorotation response of *C. parvum* oocysts, spectra from both viable and non-viable oocysts were obtained. The oocysts obtained for these experiments were from a commercially available cervine-ovine isolate maintained by passage through lambs (Moredun Research Institute, Edinburgh, UK) see table 9.2. Prior to the electrorotation experiments the oocysts were incubated with two fluorogenic vital dyes, the trypanocide 4',6-diamidino 2-phenylindole (DAPI) and propidium iodide (PI) according to the method of Campbell, Robertson & Smith (1992).

This viability assay for oocysts of *Cryptosporidium parvum* is based on the inclusion or exclusion of the fluorogenic vital dyes. Developed using several different isolates of oocysts, the assay was shown to correlate with viability measured by *in vitro* excystation assay (calculated correlation coefficient of 0.997).

DAPI binds irreversibly to DNA. It binds to nucleic acids of double stranded DNA but not to RNA or single-stranded DNA (usually). Two binding sites have been recognised on DNA, in both, the DAPI molecule is bound with its long axis approximately parallel to the grooves of the DNA helix (Kubista *et al.*, 1987). The DAPI working solution was made up by dissolving 2mg DAPI in 200µl methanol. PI preparation was as described in Chapter 4 for *Giardia* cysts.

10 µl of each of the DAPI and PI solutions were incubated with 1×10^4 oocysts in 100 µl of PBS for 30 mins in a preheated water bath at 37°C. Samples were then viewed under a fluorescent microscope with appropriate filter blocks, Nikon UV for DAPI fluorescence, Nikon G for PI.

The oocyst fluorescence observed are explained in Table 5.1. Oocysts are considered DAPI+/PI- only if they do not include PI and if the nuclei of the sporozoites fluoresce a distinctive sky blue under the UV filter block. Those oocysts which are neither PI+ nor ghosts and which show either a rim fluorescence or an absence of fluorescence under the UV filter block are considered DAPI-/PI- .

Type of oocyst	Contents seen by phase contrast* microscopy	Inclusion of: PI	Inclusion of: DAPI	Viability status
Ghost	No	No	No	Dead
PI+	Yes	Yes	Yes	Dead
DAPI+/PI-	Yes	No	Yes	Viable at assay
DAPI-/PI-[a]	Yes	No	No	Viable after further trigger
(DAPI+)[b]/PI-	Yes	No	Yes[b]	Dead

Table 5.1 Correlation of oocyst viability, visualisation of oocyst contents by phase contrast microscopy, and exclusion or inclusion of DAPI and PI.
[a] = DAPI-/PI- oocysts can be converted to DAPI+/PI- oocysts and vice versa. These oocysts are also more resistant to acid or alkali treatment,
[b] = Cytoplasmic DAPI staining - not solely nuclear staining
* = Nomarski microscopy is preferred method

5.2.1 Preparation of the oocysts for electrorotation

Following any fluorogenic staining, the suspensions were diluted with ultra pure water, vortexed and microcentrifuged (Microcentaur 13 500 revs/min for 2 minutes). The supernatant was then removed to 100μl, refilled to 1.5ml with ultra pure water (conductivity 1μS cm^{-1}) vortexed and re-microcentrifuged. After four washes, the suspension was resuspended in dilute PBS solution (typically 10μS cm^{-1}). The conductivities of these solutions were measured using a Whatman CDM 4010 meter, with a calibrated chamber of cell constant 0.12 cm^{-1} and volume 300μl. Typical working concentrations of particles were of 3x10^4 cysts ml^{-1} as determined by haemocytometer.

After conductivity adjustment, the cyst suspension was vortexed for 30s then 20μl were pipetted onto the ROT chamber manufactured on a glass slide, for observation with a Nikon Labophot microscope with fluorescent attachment. The apparatus set up is shown in Figure 4.4.

The lower limit of suspending medium conductivity investigated was around 1 μS cm^{-1} (0.1 mS m^{-1}) corresponding to water freshly obtained from a Milli_RO $^®$ 60 Water Purification System (Millipore) with a reading of resistivity equal to 18 x10^{6}Ω.cm (conductivity = 0.055 μS cm^{-1}). The increase in conductivity between the *in situ* meter of the purification system and that obtained in the storage vessel occured instantly and was due to factors such as atmospheric and pipe / vessel contact.

The upper limit suspending medium conductivity investigated was in the order of 750 μS cm^{-1} (75 mS m^{-1}). This range encompasses the reported values for river water (300 to 700μS cm^{-1}) (Drozd & Schwartzbrod, 1996) one potential source of oocysts. Above this value the electrodes were seen to visibly undergo electrolysis. Although lower voltages could have been used, which reduces electrolysis, this would have reduced the rotation rate and here considerably slowed down the acquisition of data.

5.3 The Antifield-Peak Frequency as a function of Suspending Medium Conductivity, for viable and non-viable oocysts.

Initial investigations using different suspending medium conductivities revealed a conductivity dependent frequency shift in the antifield peak. Variation of the peak frequency for oocysts within a single sample must arise from biological or indeed physiological variation. The range of variation was typically between 0.1 and 0.3 decades of frequency. Initial results suggested that greater variation was observed for non-viable oocysts.

Figure 5.2 shows these ranges from initial data obtained from a commercially available cervine/ovine isolate. It was found that an increase from 5 to 35 μS cm^{-1} (3.5mS m^{-1}) was required to produce a sufficient shift so that there was no overlap in the ranges of peak frequencies. This implies that at least at low conductivities, it is very important to accurately measure the suspending medium conductivity of the sample.
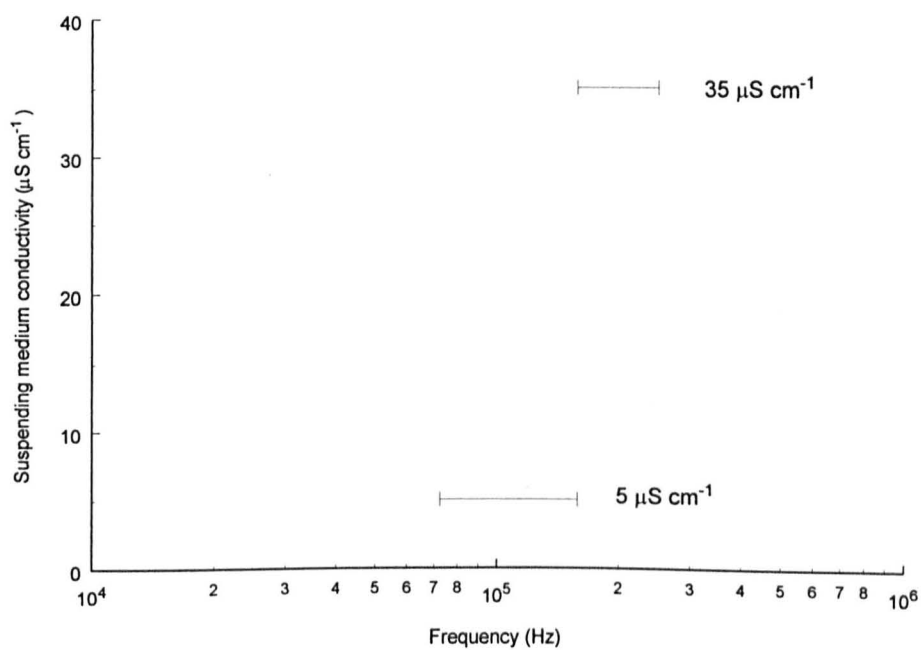
Figure 5.2 The effect of suspending medium conductivity on the observed antifield peak frequency. Ranges are shown for (n = 3) viable oocysts.

Figure 5.3 shows the antifield peak frequencies for viable oocysts over a wider conductivity range, with a trend line. Also shown are values for non-viable oocysts. From this data it can be seen that the antifield peak frequencies for both groups decreased with decreasing conductivity. For conductivities over approximately 150 μS cm^{-1} the viable peak frequencies were consistently higher than those for the non-viable oocysts.
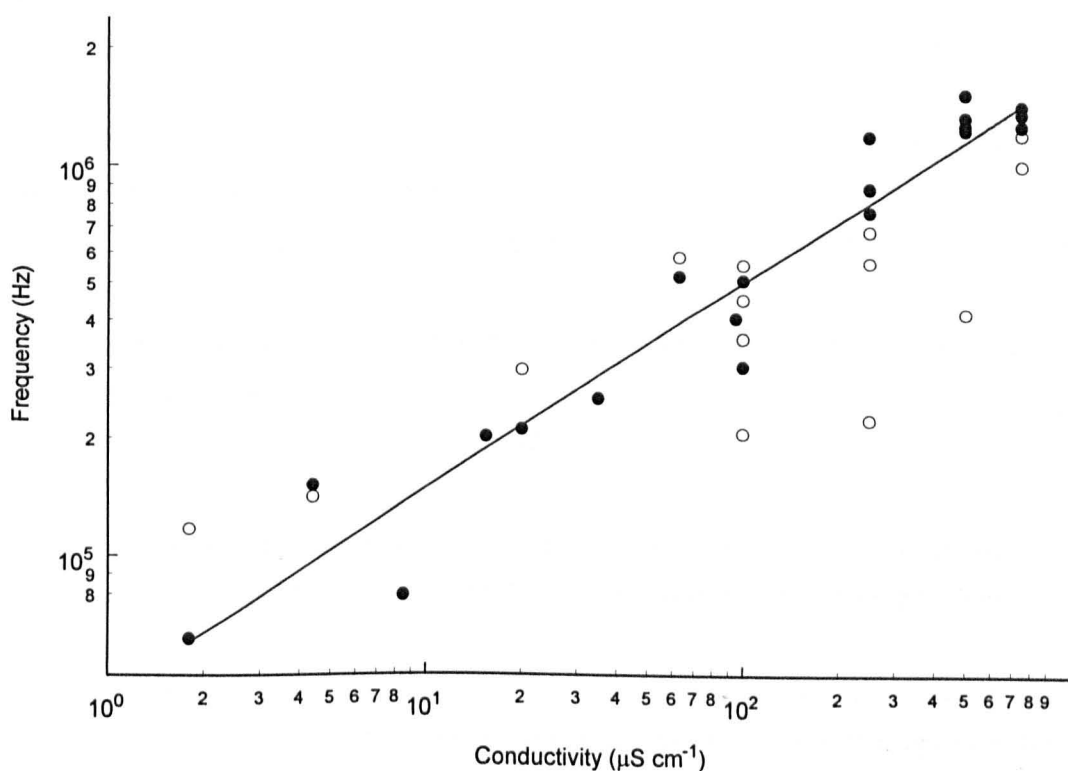
Figure 5.3 Antifield peak frequency for viable oocysts (•) as a function of suspending medium conductivity, with trend line.
Also shown are values obtained for non-viable (o) oocysts. Viability was determined by DAPI/PI.

5.4   The Antifield-Peak Magnitude as a function of Suspending Medium Conductivity, for viable and nonviable oocysts.

The magnitude as well as the frequency of the antifield-peak may vary considerably within a sample of oocysts. Magnitudes of rotation rates observed (at the peak frequency) for all the isolates investigated, range from 0 to -3 rotations s^{-1}. Due to limitations in the equipment (frequency generator) the data collected at different frequencies was not always at the same voltage. As the ROT rate has been shown to scale with the square of the applied voltage (an effect which was checked) the rates were normalised by dividing by V^2 as shown in equation 5.1.

$$ROT_{rate} = 100 * \left(\frac{\left(\frac{Rotations}{Time} \right)}{\left(V_{pk} \right)^2} \right) \tag{5.1}$$

Figure 5.4 shows the magnitude of the antifield peak as a function of suspending medium conductivity. Several trends are apparent from the data;

- the magnitudes of peak rotation rates is greater at lower conductivities for both viable and non-viable oocysts,

- the viable peak magnitude is always greater than that for the nonviable peak magnitude,

- the difference between the rotation rates is greatest at lower conductivities, the viable oocysts rotating at 2.3 times the velocity of the nonviable oocysts at 4 µS cm^{-1} compared with 1.8 times the velocity at 750 µS cm^{-1}.

These observations are of importance because they show that the difference between oocysts of different physiological state become more pronounced with lower suspending medium conductivity.

Plotted with the conductivity on a log scale, the slopes of the best fit lines are both close to the horizontal. Over the 2.75 decades shown, the viable oocysts show a decrease from 4.25 to approximately 2.5 units, whilst for the nonviable oocysts there is a decrease from 1.8 to 1.3 units, slopes of -0.0023 and -0.0007 respectively.
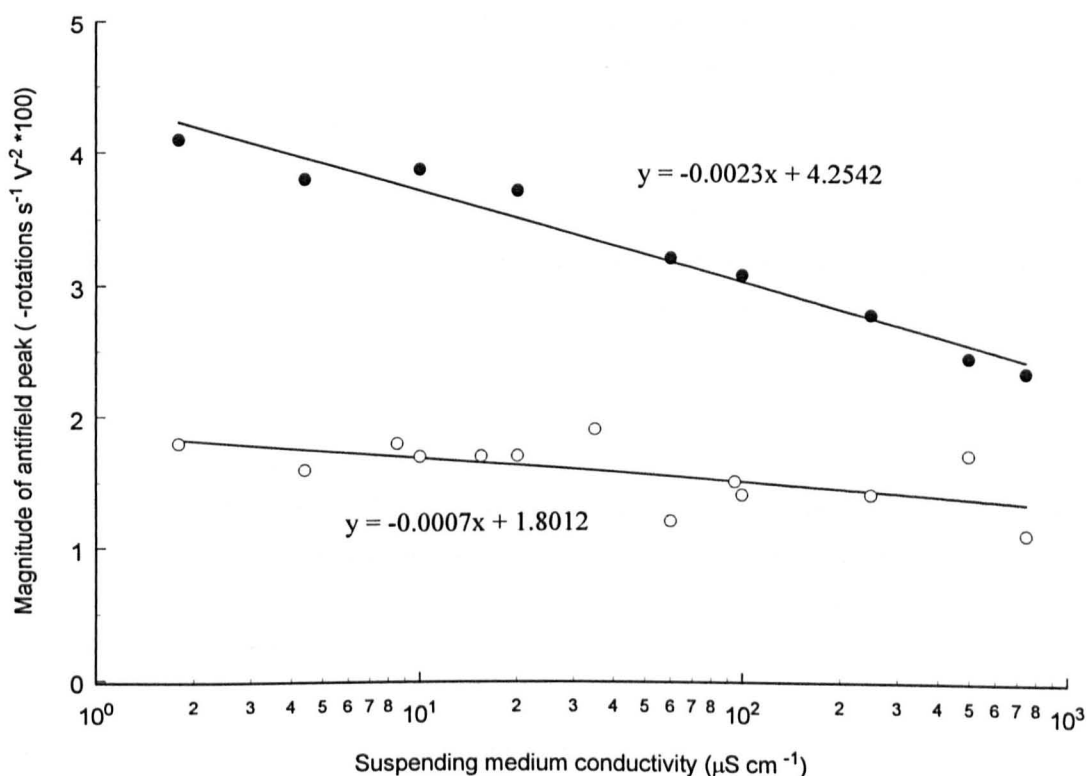
Figure 5.4 Antifield peak magnitudes for viable (•) and non-viable (o) oocysts as a function of suspending medium conductivity.

From these data it is possible, if the antifield peak rotation rate and conductivity are accurately known, to distinguish between the two physiological types by antifield peak magnitude alone. Interestingly a cut-off rate of 2 units could be used to separate the two groups over the whole range of conductivity investigated. This would be an example of a conductivity independent method of distinguishing them, which would simplify any diagnostic test, in that fewer or less stringent steps would be required in sample handling/preparation with regards to the conductivity control.

The increase in rotation rates at lower conductivites, and the pronounced differences between the two physiological types, suggests that the optimum conductivity for the electrorotation assay should be as low as possible. In this complex system however, optimising one variable might affect others. Potential problems associated with using this method for distinguishing between oocysts are discussed in section 5.4.1.

5.4.1 Complications noted for the use of low conductivity solutions to maximise the electrorotation rate

Particles in a ROT chamber are subjected to dielectrophoretic forces as well as rotating fields. The magnitude of the dielectrophoretic force on a particle is greater when it is either closer to the electrodes (which may be due to a smaller interelectrode gap) or if the applied field is stronger (ignoring electrode geometry effects and particle properties).

Positive DEP effects are generally deleterious to the recording of electrorotation spectra as they cause translational motion of the particle towards the electrodes, which is a greater problem at low conductivities. Conversely negative DEP effects are advantageous as they keep particles in the central region of the chamber.

It has been demonstrated for many cell types, for example viable and non-viable yeast cells (Markx, Talary & Pethig, 1994) that the DEP force experienced by particles decreases with increasing suspending medium conductivity. Unless superposition of frequencies can be used, whereby an additional frequency is added that decreases the DEP force while not influencing the rotation rate, it is better to use higher conductivities as this reduces interfering DEP effects.

In section 5.4 it was suggested that the optimum conductivity for distinguishing between physiological types of oocysts was as low as possible. A compromise between a fast rotation rate and minimal interference from DEP effects would be to use an intermediate conductivity. Alternatively, as was chosen for these studies, one should record electrorotation spectra only from particles in the central region between the electrodes. This strategy works well for reasonable cell concentrations.

Large interelectrode gaps, greater than 1mm , were also found to minimise these DEP problems as well as maximising the usable area, which assists in acquiring data from samples with low concentrations of particles, as is typically the case for *C. parvum* oocysts from purified environmental or clinical samples.

5.4.2 Complications due to bacteria adhering to the oocyst surface

In many environmental and clinical samples containing *C. parvum* oocysts, numerous bacteria are also present. One source of bacteria, the same as the oocysts, is the mammalian intestinal lumen.

Whereas the small intestine does not provide favourable conditions for the growth of bacteria, the large intestine, through which the oocysts must travel to exit the body, harbours an extremely large resident flora. Bacterial species found in the large intestine include *Escherichia coli*, *Streptococcus faecalis* and *Bacteroides* spp.. In the faeces there may be as many as 10^{10} to 10^{11} bacteria per gram of stool (Stanier *et al.*, 1976a) which significantly increase the probability of oocyst-bacteria interactions.

Some bacteria, for example species of the genus *Caulobacter*, which occur in both fresh and salt water, produce an adhesive extracellular holdfast, by which they attach nonspecifically to substrates, including the cell walls of other micro-organisms, algae, protozoa, and other bacteria (Stanier *et al.*, 1976b). This is thought to enable them to utilise organic materials secreted by the organisms to which they adhere.

In most samples of oocysts obtained, bacteria were also observed. These included the highly purified samples obtained from Moredun Research Institute. Complicating the conclusions drawn from electrorotation spectra of the oocysts, are oocysts with bacteria attached to their surface. The size and shape matched that of non-adherent bacteria present in the samples. Checks by plating out small aliquots of the samples of the oocyst suspensions onto sterile general purpose agar were also conducted. After 3 days incubation bacterial colonies were always detected.

The effect of bacteria adhering to the surface of viable and non-viable oocysts were investigated at several conductivities. Examples of the electrorotation spectra obtained are shown in Figures 5.5, 5.6 and 5.7.

The effect on the electrorotation spectrum of these adherent bacteria, is only on the magnitude of the rotation rates for the frequencies investigated here. In Figure 5.5 it can be seen that the addition of a bacterium on the surface of this viable oocyst at a suspending medium of 100 μScm^{-1} reduced its rotation rate at all frequencies by a factor of approximately 0.4. By applying a simple scaling factor of 1.65, the spectrum of the 'oocyst plus bacterium' can be made to align closely with the spectrum of the clean viable oocyst. It is suggested that the effect on the rotation rate could therefore be due most simply to an increase in the viscous drag on the oocyst. A change in dielectric properties, in contrast, might have caused a frequency as well as a magnitude change in the spectra.

With reference to the viable and nonviable oocyst peak magnitudes in Figure 5.4 and the non-viable spectrum shown in Figure 5.5 it is noted that the magnitude of this viable oocyst with adherent bacteria could easily be confused with a nonviable if distinguished by peak magnitude alone. This would generate a false negative result, which would not be acceptable in a test of this sort.

Further evidence of the effect of bacteria adhering to the surface of oocysts is provided in Figure 5.6, at 250μS cm^{-1}, where it was observed that two bacteria on the oocyst surface reduced the rotation rate by a factor greater than 0.5. Figure 5.7 also shows this, but at the higher conductivity of 750μScm^{-1}. Again the shape of the scaled electrorotation spectrum closely matches the spectra obtained for the clean viable oocysts.
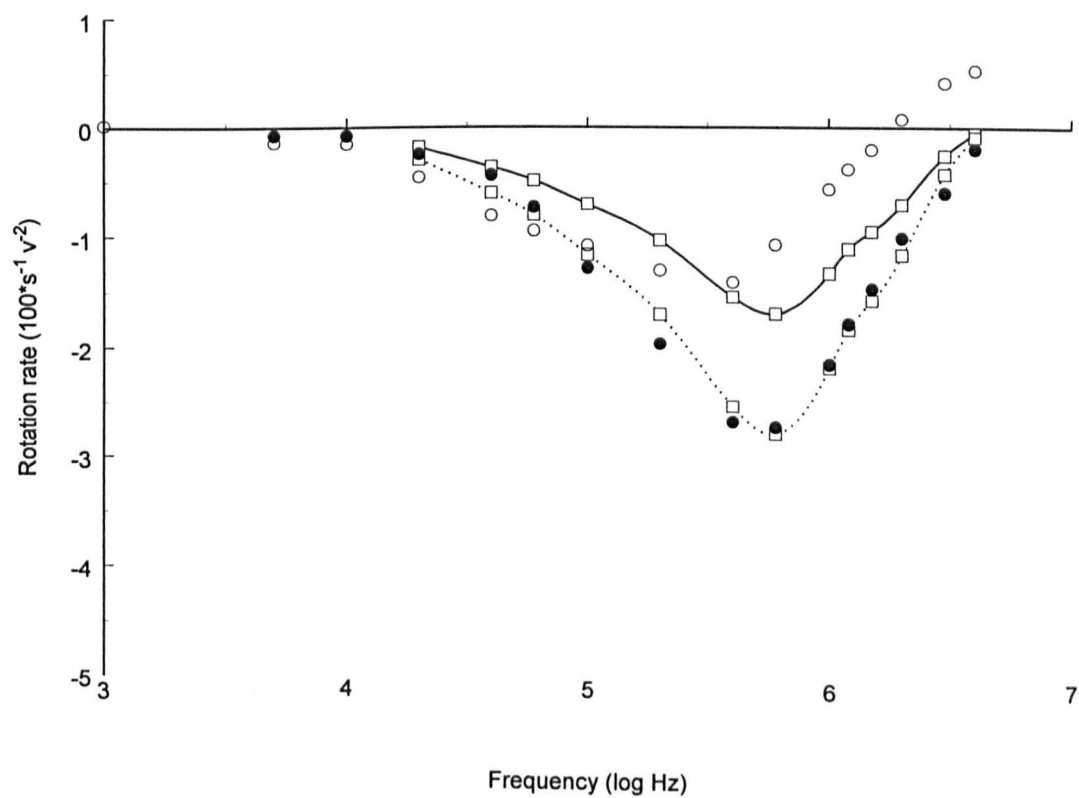
Figure 5.5 ROT spectra for a viable (•) and nonviable (o) oocyst for comparison with a viable oocyst with a bacterium adherent on its surface before (-□-) and after scaling x1.65 (- -□- -). Suspending medium conductivity 100μS cm⁻¹.
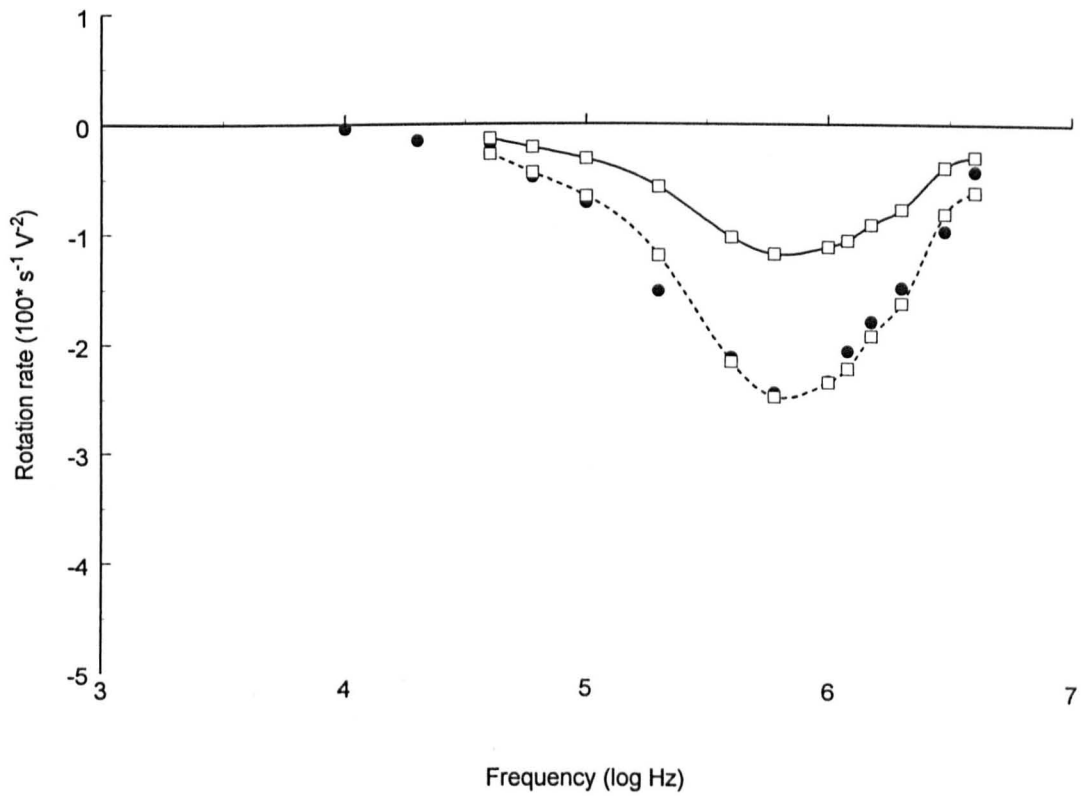
Figure 5.6 ROT spectra of a viable (•) oocyst for comparison with a viable oocyst with 2 bacteria adherent to its surface before (-□-) and after scaling x2.1 (- -□- -).
Suspending medium conductivity 250μS cm⁻¹.
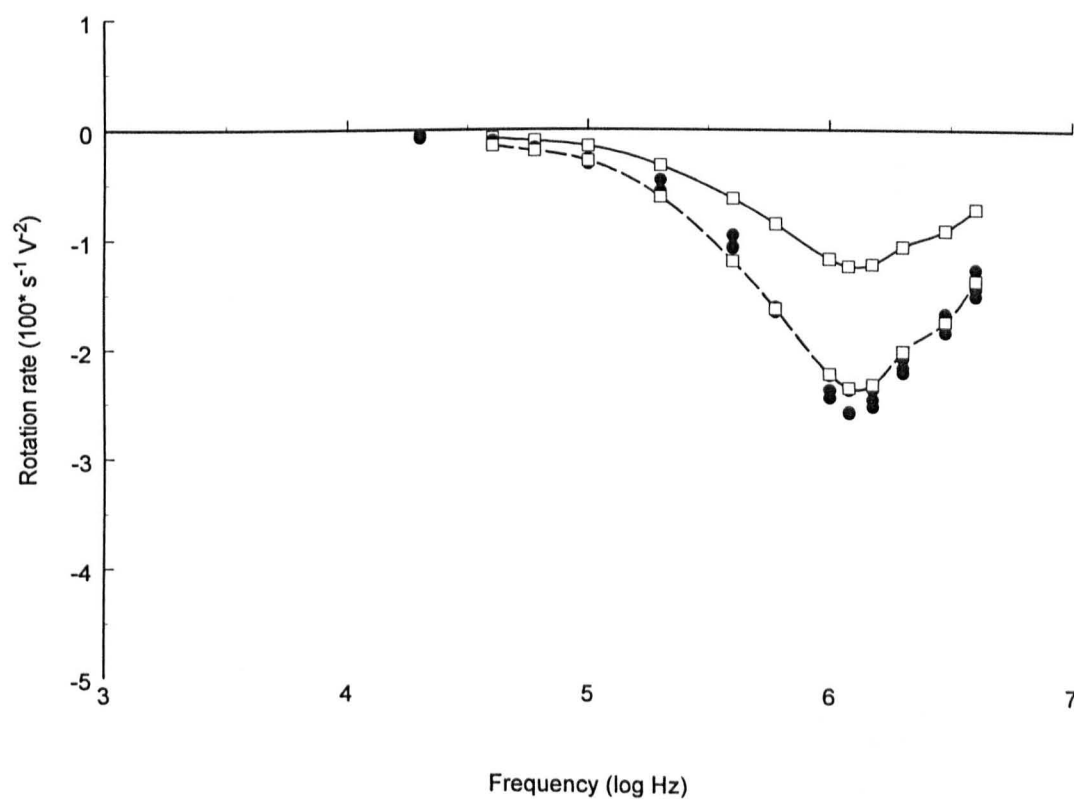
Figure 5.7 **Electrorotation spectra of (n=3) clean viable (•) oocysts and viable oocyst with a single bacterium adhering to its surface before (-□-) and after scaling x1.9 (- -□- -).** Suspending medium conductivity 750μS cm⁻¹.

5.4.3 Suspending Medium Conductivity induced changes in the High Frequency Crossover Point

Cumulative data from several isolates on the high frequency crossover point as a function of suspending medium conductivity are shown in Figure 5.8. There is a clear trend below 100 μS cm^{-1} where the difference between the viable and non-viable oocysts increase with decreasing conductivity. At 750μS cm^{-1} the crossover frequencies for the non-viable oocysts exceeds that of the viables.
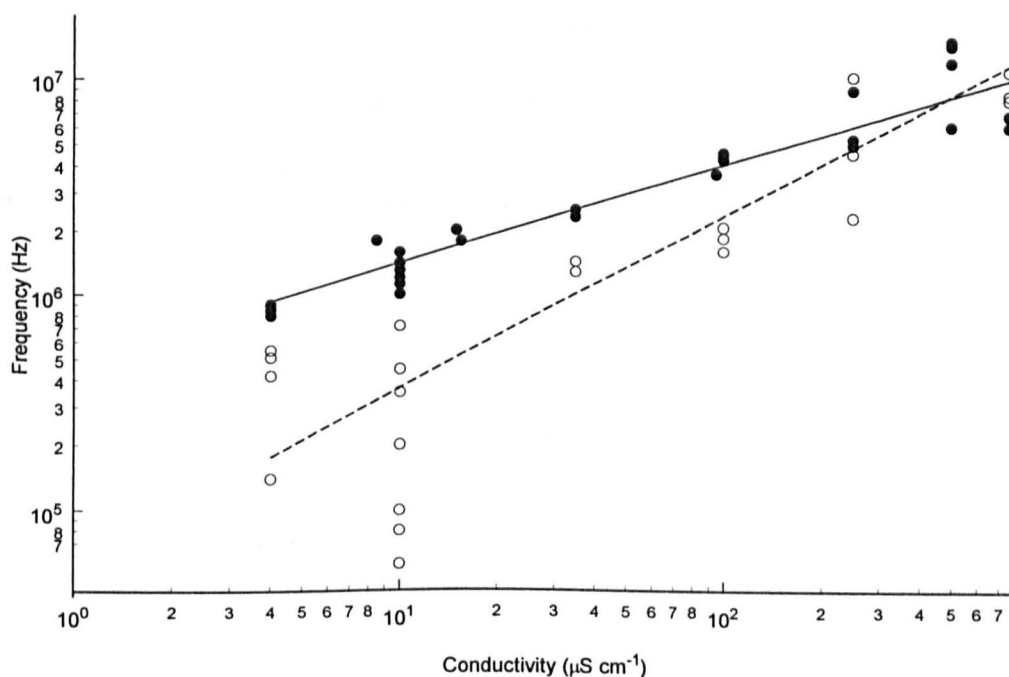
Figure 5.8 The high frequency ROT crossover frequency point for viable (•) and nonviable (o) _C. parvum_ oocysts as a function of suspending medium conductivity.

5.5 Modelling of the ROT response with respect to Suspending Medium Conductivity

Using the MatLab multishelled model described in Chapter 4, predicted trends were generated for the ROT spectra as a function of suspending medium conductivity. The constants used are listed in table 5.2 below.

Dielectric Parameters	Value	Physical Dimensions	Value
$\varepsilon_{interior}$	70 *	Membrane thickness	6 nm **
$\varepsilon_{membrane}$	8 *	Wall thickness	60 nm ***
ε_{wall}	60 **	Major radius	2.5 µm ***
$\varepsilon_{suspending\ medium}$	79	Minor radius	2.25 µm ***
$\sigma_{interior}$	0.5 *		
$\sigma_{membrane}$	1×10^{-6} *		
σ_{wall}	0.01 *		

σ = conductivity (S m^{-1}); ε = permittivity

Table 5.2 Constants used in multishell model to predict trends of electrorotation spectra as a function of suspending medium conductivity.
* Fitted values; ** Huang *et al.* (1992); *** Reduker, Speer & Blixt (1985)

5.5.1 Modelling the Antifield-Peak Frequency for viable oocysts

Using the constants in Table 5.2, the trend shown in Figure 5.9 was predicted by the model. In agreement with the observed trends (*cf.* Figure 5.3) the predicted antifield peak frequency shifts to higher frequencies with increased conductivity in a near linear manner.
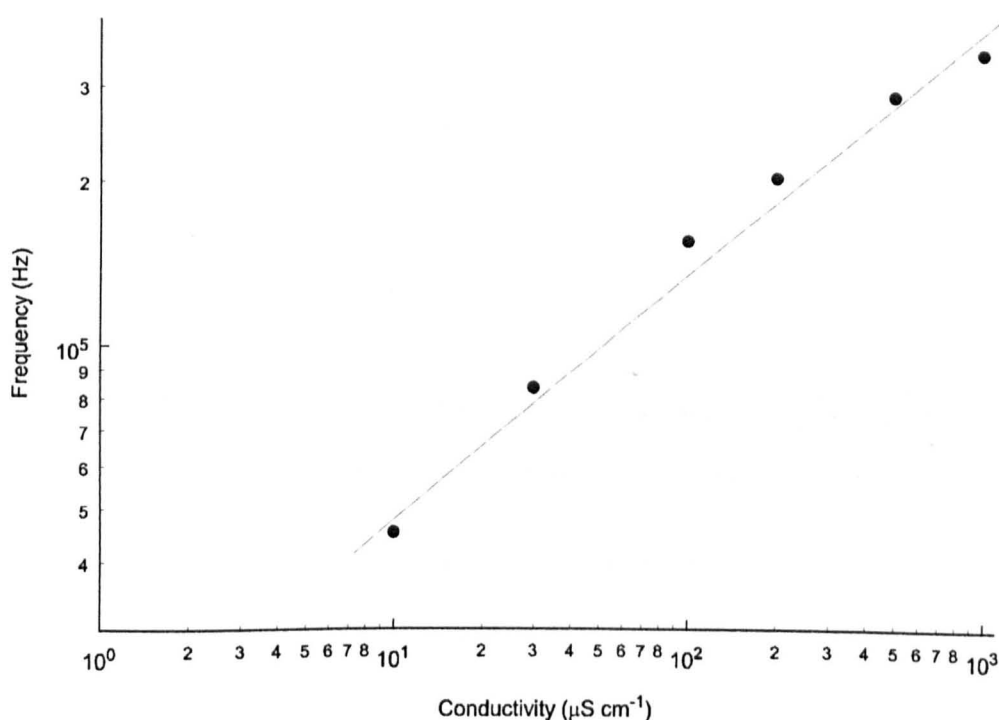
Figure 5.9 The effect of suspending medium conductivity on the antifield peak frequency, predicted by a multishelled model.

5.5.2 Modelling the Antifield-Peak Magnitude

Predictions for the antifield-peak magnitude from the model are shown in Figure 5.10. Although not linear as in Figure 5.4, overall the trend is one of a decrease in magnitude of the antifield peak with conductivity. One criticism of the model may be due, for simplicity, to the assumed constant wall conductivity, which for walled particles such as Gram positive and negative bacteria (Carstensen *et al.* 1965) and yeast cells (Markx *et al.* 1995) has been shown to vary with suspending medium conductivities. Carstensen *et al.* suggested that at low suspending medium conductivities the conductivity of the wall has a lower limit determined by counterions of the fixed charge of the cell wall, whereas for higher conductivities, ions from the medium invade the cell wall causing an increase in its conductivity so that it takes on values roughly proportional to that of the suspending medium. The model used in this study was a simplified one for ease of use and as most of the work described is performed in low medium conductivities an assumption was made that the wall conductivity would be a constant near to its lower limit.
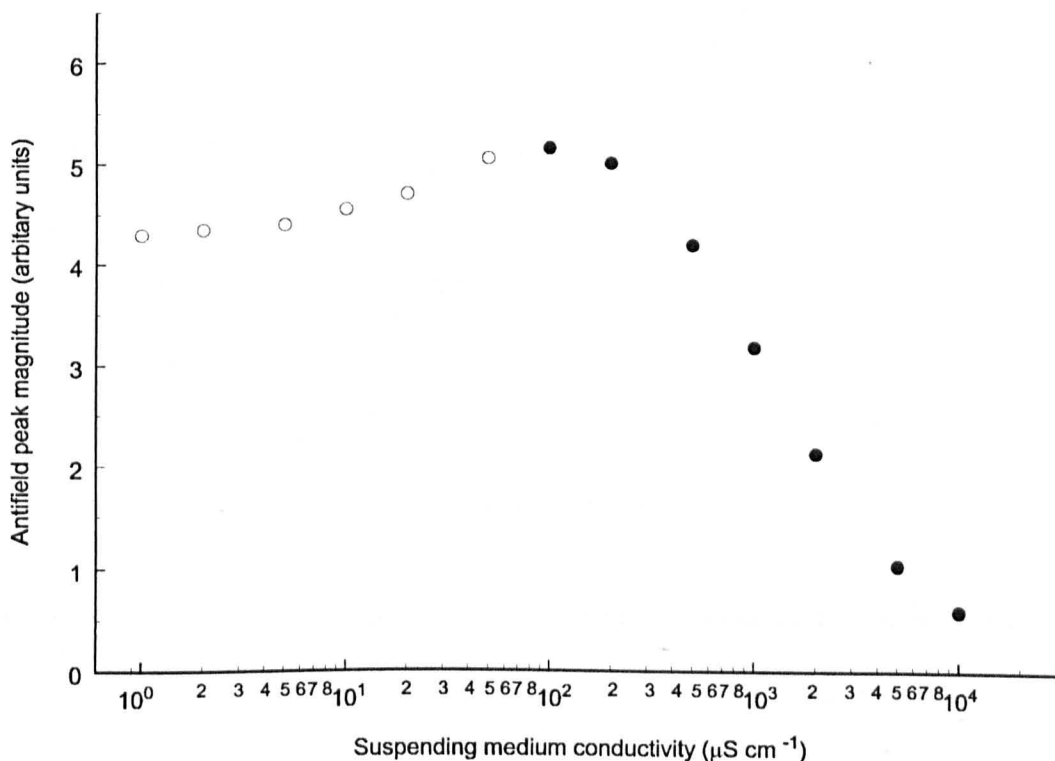
Figure 5.10 The effect of suspending medium conductivity on the antifield peak magnitude, predicted by the multishelled model.
Predictions in agreement (•) and not in agreement (o) with experimental observations.

5.5.3 Modelling the High Frequency Crossover point.

In close agreement with the observed trends Figure 5.8, the predicted high frequency crossover points shown in Figure 5.11 shift to higher frequencies with increased conductivity.
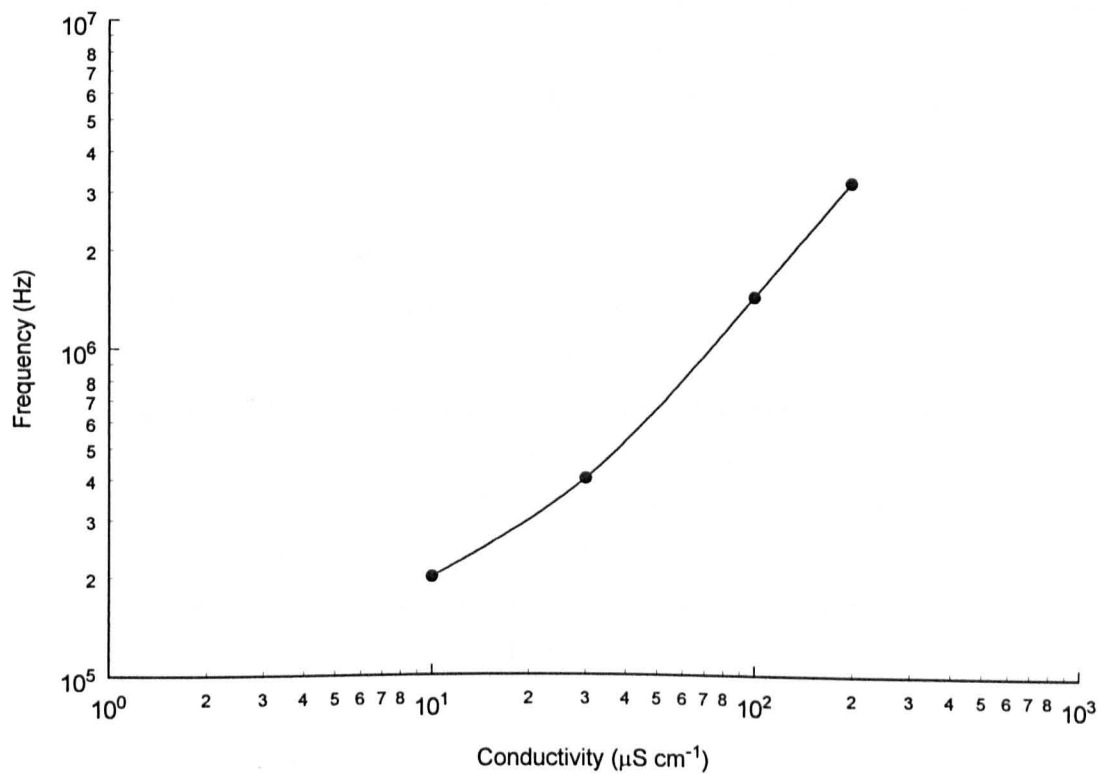
Figure 5.11 The high frequency crossover point for a viable oocyst modeled as a function of suspending medium conductivity.

5.6   Suspending Medium Conductivity Conclusions

The extent to which the observed variation in the ROT spectra is due to intraspecific variation has been explored, using *Cryptosporidium parvum* oocysts as test particle. Oocysts stained with the fluorogenic vital dyes DAPI and PI were observed as a function of frequency and of suspending medium conductivity over the range 1 to 750 μS cm^{-1}. Trends and conclusions are drawn from analysis of three features of the ROT spectra highlighted in Figure 5.1, both from experimental and theoretical (modelled) data.

Peak Frequency conclusions

The frequency of the antifield peak has been found to increase with suspending medium conductivity, for both viable and nonviable oocysts. The multishelled model used in this study for generating trends, is in agreement with these findings. Also bacteria found on the oocyst surface were found not to affect the peak frequency of the ROT spectra.

Peak Magnitude conclusions

The magnitude of the antifield peak (measured at constant applied voltage for all samples) was found to increase with decreasing suspending medium conductivity, for both viable and nonviable oocysts, which is in broad agreement with the model. Interestingly, however, the shape from the model differs from that of the observations. Clean viable oocysts consistently had faster rotation rates than non-viable oocysts, whereas protrusions decreased the magnitude of rotation, possibly by increasing the drag forces on the particle. The effect of the bacteria was found to increase with the number observed on each oocyst. A consequence of this observation is the potential problem of distinguishing between oocysts of different physiological states by the magnitude of their peak rotation rate, as suggested above.

Crossover Frequency

A relationship between the high frequency crossover point and suspending medium conductivity was observed for *C. parvum* oocysts, in agreement with other studies. For both viable and nonviable oocysts, the crossover frequency increases with increasing conductivity. This general trend is consistent with predictions from the model, as described in section 5.5.3. Viable oocysts have a consistently higher crossover frequency point than the non-viable oocysts below a suspending medium conductivity of 250μS cm^{-1}, the difference being greater at lower conductivities.

Also, greater variations were observed for the nonviable oocysts. This can be explained in terms of the deterioration of the oocysts. Structures present in oocysts that have been dead for different lengths of time will be in various states of decay, which will result in a range of dielectric responses. Viable oocysts in comparison are confined to a narrower range, all being above a certain threshold. Methods for reducing viability that do not cause gross morphological changes (as observed for naturally decaying oocysts) should be tested. These include ozone and UV disinfection studies. Whereas ozone causes structural changes such as holes in the oocyst wall, UV disinfection reduces viability at the DNA level.

UV of the appropriate wavelength is absorbed by the DNA bases and can produce chemical changes such as covalent bonds between adjacent thymine (pyrimidine) residues in one strand of DNA. These thymine-thymine dimers interfere with both transcription and replication of DNA, resulting in a more subtle destruction of the oocyst.

The overriding conclusion from the work described on the effects of suspending medium conductivity is the importance of its accurate measurement when recording electrorotation data, as at least the three features of the spectrum described here have been shown to vary as a function of the conductivity. A new aspect has been revealed here, namely the effect of bacteria adhering to the surface of the oocysts on the ROT spectra. This is of relevance to all electrorotation experiments, and especially to the potential confusion when determining the physiological states of oocysts, dealt with in the next section.

5.7   Comparison between ROT and a twin fluorogenic vital dye assay

Typical ROT spectra recorded over this frequency range, for a viable and nonviable C. parvum oocyst suspended in water of 0.5 mS m^{-1}, are shown in Figure 5.12. Spectra from oocysts in three states of deterioration are also shown: intact dead with no discernible sporozoites but with contents, intact dead with no discernible contents (empty), and dead empty oocyst with a gape at the suture (similar to a Pacman). Depending on the frequency, typical rotation rates observed are between -3 and +1.5 rotations per second for a viable C. parvum oocyst subjected to a rotating field of around 10 kV m^{-1} (pk).

The viability of stocks of C. parvum oocysts was assessed by the fluorogenic vital dye assay of Campbell et al. (1992) which has demonstrated good correlation with in vitro excystation. In the fluorogenic vital dye assay, oocysts are suspended in aqueous solutions of two fluorogens: 4'6-diamidino-2-phenyl indole (DAPI) and propidium iodide (PI). Viable oocysts take up only the nuclear fluorogen DAPI (DAPI+/PI-) whereas dead oocysts take up both DAPI and PI (DAPI+/PI+). In order to determine whether the incorporation of vital dyes affected spectra obtained with ROT, washed, stained oocysts were mixed with an equal number of unstained oocysts from the same oocyst stock, suspended in low conductivity water, and placed in the ROT chamber. 35 full spectra were obtained for oocysts stained by the fluorogenic vital dyes: 26 of these were from viable (DAPI+/PI-) oocysts and 9 from dead (DAPI+/PI+) oocysts. Spectra from 32 unstained oocysts were also recorded, of which, 27 were from oocysts judged to be viable, morphologically using phase contrast microscopy at a magnification of 400. Figure 5.13 shows the range of rotation rates observed for the viable (DAPI+/PI-) and non-viable (DAPI+/PI+) oocysts which had incorporated the fluorogenic vital dyes. The fluorogenic vital dyes exerted no significant effect on the rotation rates of C. parvum oocysts. Figure 5.14 compares the rotation rates of viable, stained (DAPI+/PI-) and unstained oocysts. Also from Figure 5.13 we concluded that it should be possible to assess oocyst viability by ROT at a single frequency (around 900kHz). A direct comparison between ROT and the fluorogenic vital dyes at this frequency is presented in table 5.3.

Oocysts from 7 human isolates of *C. parvum*, as well as 3 non-human (cervine-ovine, bovine) isolates have been investigated using ROT, described in later chapters of this thesis. The spectra presented in Figures 5.12-5.14 are derived using oocysts purified from a bovine source.
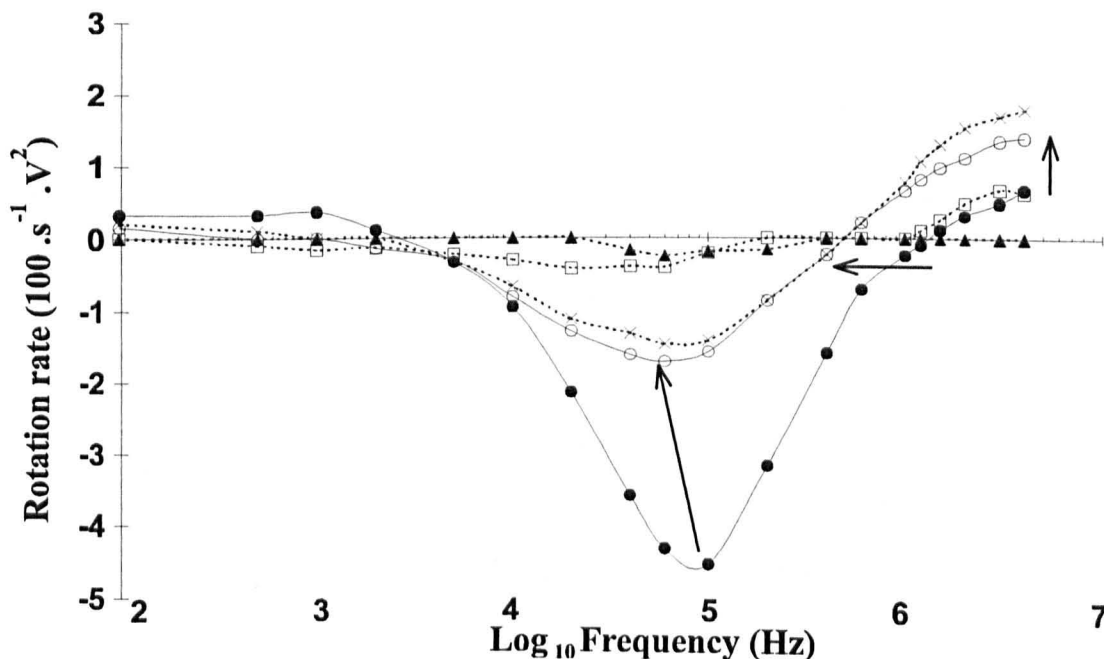
Figure 5.12 ROT spectra of individual *C. parvum* oocysts.

ROT spectra are shown for individual viable (•) and dead (o) oocysts. Trend arrows highlight the important differences between these spectra. Importantly in transition from a viable to a non-viable oocyst spectrum there is (a) a large reduction in the antifield rotation peak accompanied by a small shift to a lower frequency (b) a large shift in the frequency at which the oocyst does not rotate and (c) a small increase in the higher frequency cofield rotation region. Of these differences the second (b) is of greatest use in distinguishing between viable and non-viable oocysts. Between the frequencies at which the viable and dead oocysts do not spin, they will both spin but in opposite directions. Spectra from oocysts with no discernible sporozoites (--) are also shown: intact with residual body (◻), intact and empty (x) and empty oocyst with a gape at the suture (similar to a Pacman ◖) (▲).
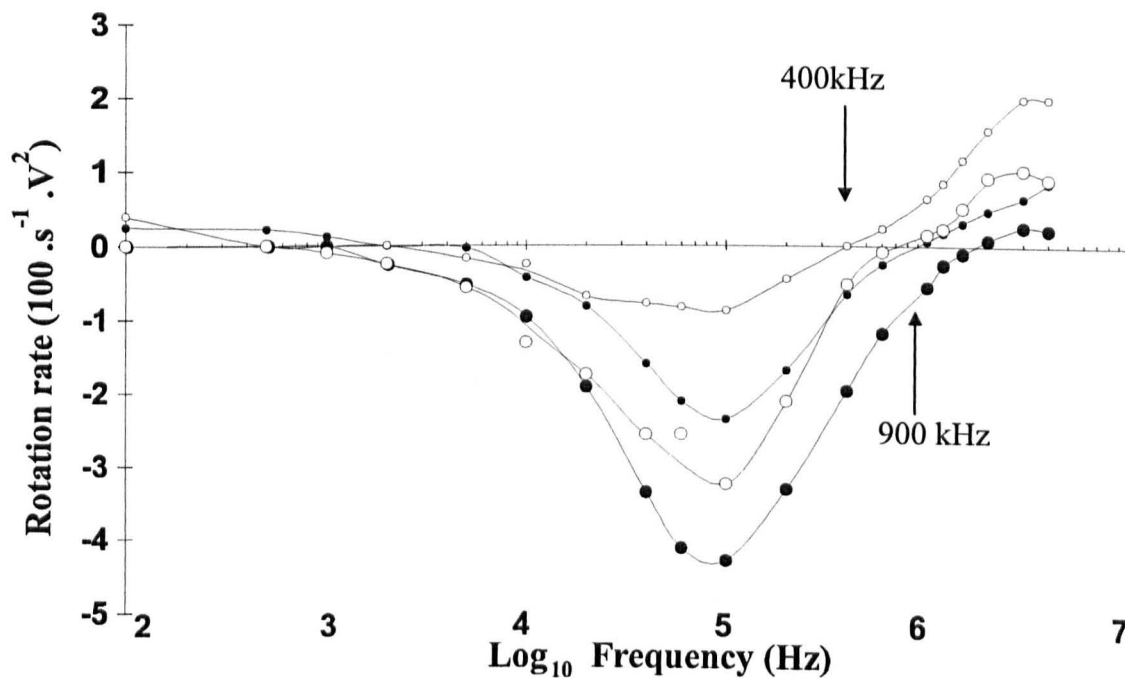
Figure 5.13 **ROT spectra of viable and dead oocysts determined using fluorogenic vital stains (DAPI and PI).**

The limits to the range of rotation rates observed for viable (DAPI+/PI-) oocysts (n=26) are denoted by (•) and (●), and for dead (DAPI+/PI+) oocysts (n=9) by (o) and (O). For field frequencies above 400kHz the ranges of spectra for the viable and dead oocysts do not overlap. Importantly at 900kHz all the viable oocysts rotate in the opposite direction to the dead oocysts.
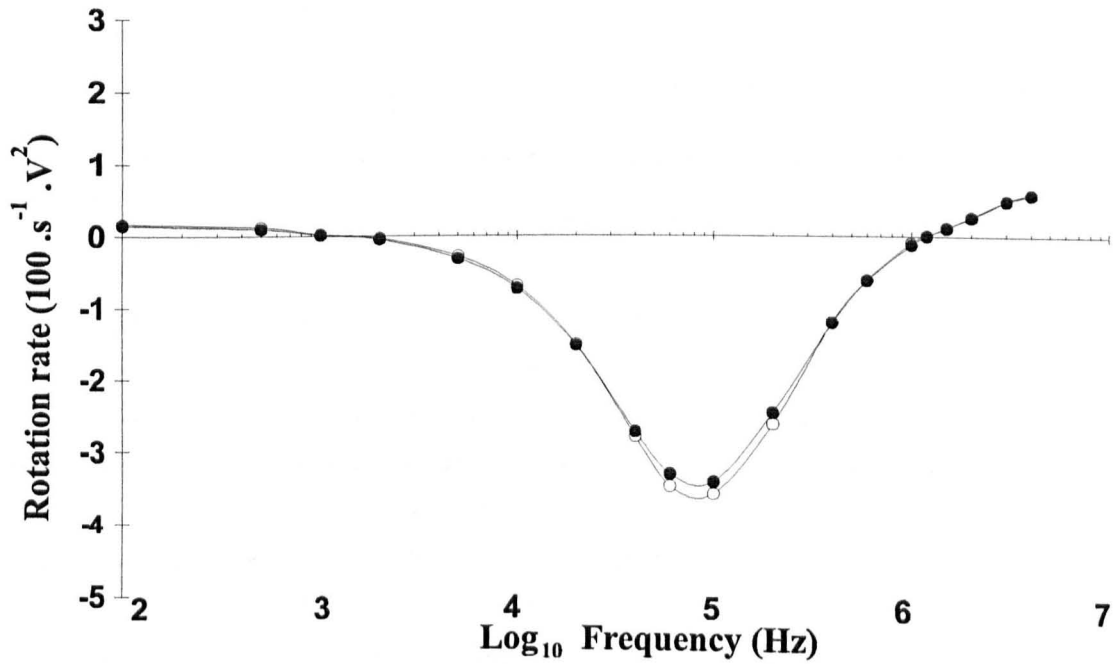
Figure 5.14 Comparison of the spectra of viable oocysts, determined using fluorogenic vital stains (DAPI and PI) or morphology.

These spectra show that there are no significant differences between the mean rotation rates observed for oocysts whose viability has been determined with either fluorogenic vital stains (n=26) denoted by (•), or by morphological criteria (n=27) denoted by (o). The oocysts for this comparison were from the same stock as used for the data in figure 5.13.

	[+]ROT viable	[+]ROT dead
Viable by fluorogenic vital dyes (DAPI+/PI-) & [*](DAPI-/PI-)	285 + [*]8	0
Dead by fluorogenic vital dyes (DAPI +/PI+)	0	207

[+]Medium conductivity 0.5± 0.1 mScm[-1].

Table 5.3 A direct, single frequency (930 kHz) comparison between ROT and the fluorogenic vital dyes, of viability of 500 oocysts from a bovine isolate.
Results from a comparison of viability of individual oocysts, using ROT at a single frequency and the fluorogenic vital dyes on 500 oocysts. The specific frequency (930kHz) at which a 100% correlation between the two methods was found to be very sensitive to the suspending medium conductivity. Oocysts were exposed to the fluorogenic vital dyes (without pre-acidification) according to Campbell *et al.* (1992) then prepared as before for the ROT chamber. The comparison between ROT (930kHz) and the fluorogenic vital dyes is presented in Table 5.3. Of the 500 oocysts, eight did not take up either DAPI or PI (DAPI-/PI-) but were judged viable by ROT. Four oocysts adhered to the glass substrate and did not rotate at first, but were deemed viable (DAPI+/PI-) by the fluorogenic vital dyes. These can be 'unstuck' by briefly switching the field to 100kHz where the oocysts are subjected to a greater torque and then rotated at the desired frequency. The intact oocysts which remained unstained (DAPI-/PI-) in the fluorogenic vital dye assay are termed 'potentially viable', and can be converted to viable type (DAPI+/PI-) following a further trigger (pre-acidification incubation for 1 hour in at pH 2.7) as described by Campbell *et al.* (1992). ROT can determine the viability of DAPI-/PI- oocysts without the need for pre-acidification for 1 hour.

5.7.1 Overcoming potential limitations of ROT

For determining the viability of oocysts present in water concentrates, the requirement to resuspend oocysts in low conductivity water prior to analysis by ROT can be seen as a limitation. A combination of immunomagnetisable separation (IMS), and dielectrophoretic concentration of oocysts can achieve efficient concentration and extraction of oocysts from water concentrates (data not shown). The need to use low conductivity solutions for ROT assays can compromise the integrity of more delicate organisms including vegetative and endogenous stages of protozoan parasites, which may rupture due to osmotic shock. In order to overcome this problem, cells can be washed and resuspended in a solution of sucrose or mannitol (280mM) (Huang *et al.,* 1993) which is used to increase the osmolarity of the suspending medium thus supporting the survival of the organisms without compromising the requirement for low conductivity.

5.8 Conclusions

The quantifiable results of the electrorotation technique described demonstrate several important features, the most important of which is the real-time assessment of viability of individual oocysts, which correlates closely with the fluorogenic vital dye technique of Campbell *et al.* (1992). As well as the rapid (a few seconds per oocyst), straightforward assessment of the viability of individual oocysts, the viability of larger numbers of oocysts (e.g. 30 oocysts in a field of view at a magnification of 400) can also be assessed simultaneously. To assist the analyst, automatic measurement of the rotation rate at one frequency or over a range of frequencies to create a full spectrum is possible (Schnelle *et al.,* 1997; Zhou, Burt & Pethig, 1998; DeGaseperis, *et al.* 1998; Budde *et al.,* 1999). A ROT spectrum, which can be thought of as a 'fingerprint' for each oocyst, provides information not only about the viability of the oocyst, but also the conductivity and permittivity of the various 'compartments' within the oocyst structure. Following ROT analysis, the oocyst remains intact and unchanged. As ROT is a non-invasive method, the oocyst can be subjected to further holistic or destructive analytical methods. Although *C. parvum* is nearly spherical, this is not a prerequisite for ROT analysis as shown by the ROT investigations with the larger ellipsoidal cysts of *Giardia duodenalis* and *G. muris* described in Chapter 4.

A variety of particle types, including the transmissive stages of parasites can be investigated by this technique. Indeed, whereas there is often the need to develop viability stains, molecular methods or excystation protocols for determining the viability of newly investigated cell types, ROT probes a common difference between all dead and viable cells, namely membrane integrity.

5.9 References

Budde, A., Grummer, G. & Knippel, E. (1999) Electrorotation of cells and particles: An automated instrumentation. *Instrumentation Science and Technology*. 27: 59-66.

Campbell, A.T., Robertson, L.J. & Smith, H.V. (1992) Viability of *Cryptosporidium parvum* oocysts: correlation of *in vitro* excystation with inclusion/exclusion of fluorogenic vital dyes. *Applied and Environmental Microbiology*. 58: 3488-3493.

DeGasperis, G., Wang, X.B., Yang, J., Becker, F.F. & Gascoyne, P.R.C. (1998) Automated electrorotation: dielectric characterization of living cells by real-time motion estimation. *Measurement Science and Technology*. 9: 518-529.

Drozd, C. & Schwartzbrod, J. (1996) Hydrophobic and electrostatic cell surface properties of *Cryptosporidium parvum*. *Applied and Environmental Microbiology*. 62: 1227-1232.

Huang, Y., Wang, X-B., Tame, J.A. & Pethig, R. (1993) Electrokinetic behaviour of colloidal particles in travelling electric fields: Studies using yeast cells. *Journal of Physics D-Applied Physics*. 26: 1528-1535.

Kubista, M., Akerman, B. & Norden, B. (1987) Characterisation of interaction between DNA and 4',6-diamidino-2-phenylindole by optical spectroscopy. *Biochemistry* 26: 4545-4553.

Markx, G.H., Talary, M.S. & Pethig, R. (1994) Separation of Viable and Nonviable Yeast using Dielectrophoresis. *Journal of Biotechnology* 32: 29-37.

Markx, G.H., Zhou, X-F. & Pethig, R. (1995) Dielectrophoretic manipulation of micro-organisms in micro-electrode arrays. *Institute of Physics Conference Series* No. 143. International Conference on Electrostatics, York.

Reduker, D.W., Speer, C.A. & Blixt, J.A. (1985) Ultrastructural-Changes in the Oocyst Wall During Excystation of *Cryptosporidium parvum* (Apicomplexa, Eucoccidiorida) *Canadian Journal of Zoology*. 63: 1892-1896.

Schnelle, T., Glasser, H. & Fuhr, G. (1997) Opto-electronic technique for automatic detection of electrorotational spectra of single cells. *Cellular Engineering*. 2: 33-41.

Stanier, R.Y., Adelberg, E.A. & Ingraham, J.L. eds (1976a) General Microbiology. Chapter 28 Symbiotic Associations between two non-photosynthetic partners. pp783. MacMillan Press.

Stanier, R.Y., Adelberg, E.A. & Ingraham, J.L. eds (1976b) General Microbiology. Chapter 19 Gram-Negative Bacteria : Aerobic chemoheterotrophs. pp 598-602. MacMillan Press.

Zhou, X-F, Burt, J.P.H. & Pethig, R. (1998) Automatic cell electrorotation measurements: Applied to studies of the biological effects of low-frequency magnetic fields and of heat shock. *Physics in Medicine and Biology* 43: 1075-1090.

Chapter 6

Travelling-Wave Dielectrophoresis of *Cryptosporidium parvum* oocysts.

6.1 Introduction

A particle in solution experiences many forces that may affect its motion. Summarising, these are: a random thermal force $\underline{F}_{RAND}$ from Brownian motion; the buoyancy force $\underline{F}_B$ related to the gravitational force and the difference in the particle and solution densities; the viscous drag force $\underline{F}_{DRAG}$ due to the fluid; and the diffusion force $\underline{F}_{DIFF}$, related to the thermal energy of the system and the concentration gradient, if any. In addition to these, for a particle undergoing dielectrophoresis (DEP) there will be a dielectrophoretic force $\underline{F}_{DEP}$; the total force $\underline{F}_T$ on the particle (Green & Morgan 1998) can be written as the sum of a number of independently acting forces:

$$\underline{F}_T = \underline{F}_{DEP} + \underline{F}_{RAND} + \underline{F}_B + \underline{F}_{DRAG} + \underline{F}_{DIFF} \qquad (6.1)$$

In spatially non-uniform AC electric fields, dielectric particles move as a consequence of the interaction of the applied field gradient and the dipole induced in the particle. The time averaged dielectrophoretic force (Pethig, 1979a) on a particle is found to be:

$$\left\langle \underline{F}_{DEP} \right\rangle = 2\pi\varepsilon_m \alpha^3 \operatorname{Re}\{f(\omega)\} \nabla \left| \underline{E}_{rms} \right|^2 \qquad (6.2)$$

where ε_m is the suspending medium permittivity, a is the particle radius, $\nabla \left| \underline{E}_{rms} \right|^2$ is the gradient of the square of the *rms* electric field, and Re{} indicates the real part of and $f(\omega)$ the Clausius-Mossotti factor given by:

$$f(\omega) = \frac{(\varepsilon^*_p - \varepsilon^*_m)}{(\varepsilon^*_p + 2\varepsilon^*_m)} \qquad (6.3)$$

where ε^*_p and ε^*_m are the complex permittivities of the particle and the medium respectively. The complex permittivity is $\varepsilon^* = \varepsilon - j\,(\sigma/\omega)$ where $j = \sqrt{-1}$, ε is the permittivity and σ is the conductivity of the dielectric. The Clausius-Mossotti factor thus describes the frequency dependent behaviour of the induced dipole. From equation (6.3) it is noted that the Clausius Mossotti factor may only take theoretical values of between +1 and -0.5.

From equation (6.2) it is seen that the DEP force on a particle is dependent on its volume, subsequently, for DEP of particles greater than 1μm in diameter, the effects of $\underline{F}_{DIFF}$ and $\underline{F}_{RAND}$ are generally ignored in the total force equation. If the particle is more dense than the suspending medium, as is generally the case for viable *C. parvum* oocysts (specific gravity=1.05) the buoyancy force acts downwards and the

particle sinks until it comes to rest on the glass substrate or on the electrodes, and the buoyancy force can also be neglected. There is now, of course, an extra drag term due to the friction between the particle and the surface. The sinking rate for a viable oocyst suspended in deionised water was observed to be approximately $50\mu m$ min^{-1} with generally a slower rate for non-viable oocysts.

Viscous drag and particle-surface friction are of importance when translational motion is induced in the particle, as can be achieved by several electrokinetic methods. Traditionally, electrophoresis has been used to move particles over greater distances than DEP. One reason is that the DEP force on a particle drops off rapidly with increasing distance from the electrode. A near constant force, however, over any distance is achieved by DEP, if it is combined with the technique of ROT, in the hybrid technique termed travelling wave dielectrophoresis (TWD) (Fuhr *et al.*, 1991).

TWD is achieved by applying AC potentials, with staggered phases sequentially, to arrays of parallel electrodes. For the case of a particle moving down the middle of an open channel lined by such electrodes, the TWD force (on a spherical particle) is given (Hughes, Pethig & Wang, 1996) by the equation:

$$F_{TWD} = -\frac{4\pi^2 \varepsilon_m a^3}{\lambda} \text{Im}\{f(\omega)\}\underline{E}^2 \qquad (6.4)$$

where λ is given by the number of phases in the signal multiplied by the periodic spacing of the electrodes, which, for the electrodes used in this work is 4 x $20\mu m$. E is the applied electric field, Im{} indicates the imaginary part of and $f(\omega)$ is the Clausius-Mossotti factor given by equation (6.3) which describes the frequency dependent behaviour of the induced dipole. It is important to note that the particle also experiences a dielectrophoretic force as well as the TWD force (Huang *et al.*, 1993). Unhindered movement due to TWD will occur if the particles are repelled from the electrodes by negative DEP.

If one assumes that negative DEP conditions are sufficient to prevent particle-surface contact, there is no extra drag term due to their interaction. For particle motion by TWD under these conditions, the force F_{TWD} must exceed opposing forces from the fluid such as the viscous drag. For a spherical particle in a fluid of viscosity η, the viscous drag force in equation (6.1) is given by Stoke's law (Shaw, 1996):

$$\underline{F}_{DRAG} = 6\pi\eta\, a\, \underline{v} \qquad (6.5)$$

where $\underline{v}$ is the velocity of the particle. The terminal velocity V_{TWD} of a spherical particle in a medium of viscosity η is therefore given by

$$V_{TWD} = -\frac{2\pi\varepsilon_m a^2}{3\eta\lambda}\mathrm{Im}\{f(\omega)\}\underline{E}^2 \qquad\qquad (6.6)$$

As shown by Fuhr (1985) and Sauer & Schlogl (1985) dielectrophoretic forces acting on particles in AC electric fields are directly proportional to the *real* component of the induced dipole moment, whereas rotations created by rotating electric fields are proportional to the *imaginary* component. From equations (6.4) and (6.6) it is clear therefore that TWD is essentially electrorotational in nature, a fact not reflected in the name.

To summarise, there are a large number of variable factors describing the TWD force, which, with the frequency dependence of the Clausius-Mossotti factor makes TWD an extremely versatile technique for separating different particle types from a mixture. Small differences in particle size and dielectric properties have been exploited for manipulation and separations using TWD (Talary *et al.*, 1996; Morgan *et al.*, 1997) a brief introduction to which is given in section (2.13) and which includes examples of applications. In addition, the same technique has also been used in micro-systems for electrohydrodynamic pumping of fluid (Fuhr *et al.*, 1994).

The biological particles investigated to date with the TWD technique are by no means as extensive as those investigated by DEP and ROT (*cf.* tables 2.4 with 2.1 and 2.3). Importantly it has not been demonstrated for any protozoans, some of which are of major economic importance.

Having characterised the 'near spherical' *Cryptosporidium parvum* oocysts by ROT as a function of suspending medium conductivity (described in Chapter 5) it should be possible to predict their behaviour in a TWD field, if first a DEP spectrum is obtained. In this chapter ROT, DEP and TWD spectra are described for viable *C. parvum* oocysts for comparison with modelled results.

6.2   Experimental Materials and Methods

6.2.1 The particles

Cryptosporidium parvum oocysts (Iowa isolate) were supplied as a suspension (1×10^6 ml^{-1}) in deionised water. After storage at 4°C, they were incubated with the fluorescent vital stains DAPI and PI at 37°C for 30mins, then washed four times in ultra pure water as described in chapter 5. Finally, they were centrifuged and resuspended at various dilute concentrations in phosphate buffered saline (PBS) solutions.

6.2.2 Electrode designs

Three electrode geometries were used for investigating the electrokinetic properties of the *C. parvum* oocysts.

(a) ROT Electrodes

Electrorotation measurements were made for each solution conductivity, using the 2mm bone electrodes described in chapter 4, with field strengths of 20V (pk-pk). These relatively 'large' microelectrodes provide a large area of homogenous field, thereby reducing variability in the rotation rate due to spatial differences in field strength. The greater area allowed lower concentrations of particles to be used, which in turn, lead to greater spacing of particles, reducing potential particle-particle interactions.

(b) DEP Electrodes

To measure the DEP force on the oocysts as a function of frequency and suspending medium conductivity, hyperbolic 'polynomial' electrodes (Huang & Pethig, 1991; Wang *et al.*, 1993; Hughes *et al.*, 1994) of internal diameter 400μm were used. The chosen polynomial design consisted of four electrodes, the simplest useful case of the polynomial type electrodes, which may consist of 2n electrodes.

A voltage signal, up to 10V pk-pk, was applied to two of the electrodes diametrically opposite each other, with the inverse of the signal applied to the remaining two electrodes. The hyperbolic nature of the electrodes is useful because the electric field resulting from the electrodes has a uniform gradient over most of the central area, allowing particle manipulation either towards the electrodes by positive DEP or towards the centre of the electrode gap by negative DEP. Velocities of individual oocysts were measured relatively close to the electrode tips over a distance of 35μm. This was achieved by timing the oocyst between two markers on a calibrated television screen at 35 and 70μm from the centre of an electrode tip. A simple switch enabled the duration of the applied field, and therefore position of the particle, to be accurately controlled. The zero force point or 'cross-over' corresponding to the frequency at which the movement of the particle was not governed by the DEP force, was measured for a number of particles in each suspension to find the maximum variation.

(c) TWD Electrodes

As shown by Talary *et al.* (1996) it is possible to observe TWD of particles in at least two frequency bands. The lower of these frequency bands, where antifield ROT of the particle is typically observed, was used in the following experiments as the ROT data previously obtained is more detailed in this region.

For the TWD experiments, offset comb-type electrodes, as described by Huang *et al.* (1993) were used. Designed for simplicity of field calculations, these electrodes allow TWD to be observed in two modes in the same field of view; between electrode tips in a channel, and over parallel electrode arrays. These planar electrodes, manufactured in two dimensions on a flat glass substrate, had the following dimensions: electrode width 10 μm; spacing 10μm; channel width 30μm. Opposing combs each had 10 electrode fingers, providing 2.5 periods of the travelling wave. Field strengths of between 0.4 V to 4V (pk-pk) were applied to the travelling wave electrodes in phase sequence as shown in Figure 6.1. Both viable and nonviable oocysts were observed over the frequency range 500Hz to 10MHz. A three way four-pole switch enabled close control of the field from the 'Rotogen' signal generator, allowing on-off switching as well as reversals in the direction of the travelling wave. This proved more efficient than switching the field at signal generator level via a PC keyboard.
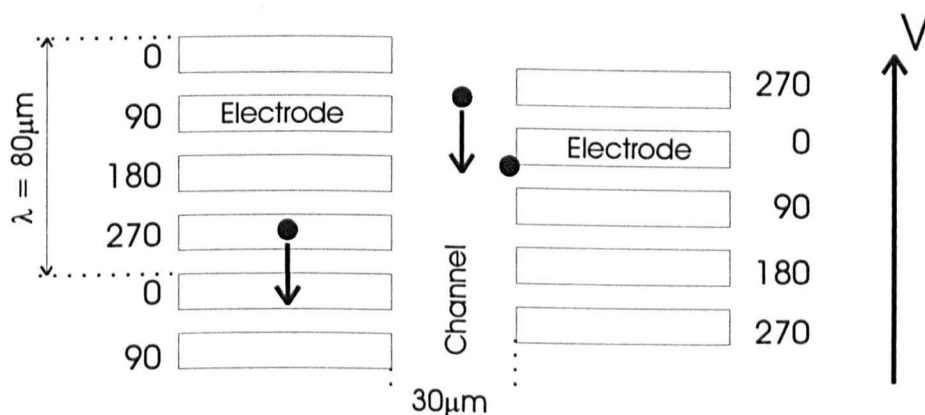
Figure 6.1 The 'comb' geometry microelectrodes used to investigate the TWD of the oocysts.
Travelling electric fields, of propagation direction indicated by the arrow V and of periodic length 80μm, were established by addressing the electrodes with the phase sequences (in degrees) shown. Under TWD, the particles moved over the electrodes and along the channel in the direction opposing that of the travelling field. A third particle is shown held at an electrode tip by positive dielectrophoresis.

6.3 Results

Typical ROT and DEP spectra for viable *C. parvum* oocysts at two suspending medium conductivities, 18 and 95 μS cm⁻¹, are shown in Figure 6.2.

6.3.1 ROT of viable *C. parvum* oocysts

The ROT spectra of viable *C. parvum* oocysts, show the characteristic features, described in the previous chapter, of an antifield peak at several hundred kilohertz, followed by a change in the sense of direction in the low megahertz frequency region. At higher suspending medium conductivities, an increase in the frequency of the crossover is accompanied by a reduction in the magnitude of the antifield peak. In previous samples of this isolate, a small co-field rotation was observed below 5kHz, possibly related to surface charge effects. Little or no rotation was observed from this sample.

6.3.2 DEP of viable *C. parvum* oocysts

As observed for many other particles, for example plant protoplasts and viable yeast cells (Pethig & Markx, 1997) a positive dielectrophoretic force was observed for viable *C. parvum* oocysts at frequencies around 1 MHz, Figure 6.2. The DEP force reduced in magnitude and became negative for frequencies below around 100kHz. Interestingly, at both conductivities shown in Figure 6.2, for frequencies of 20kHz and below there was an 'apparent' increase in the magnitude of the negative DEP force, the effect of which was greater for the higher conductivity solution. This unexpected observation is discussed in detail in section 6.3.2.1.
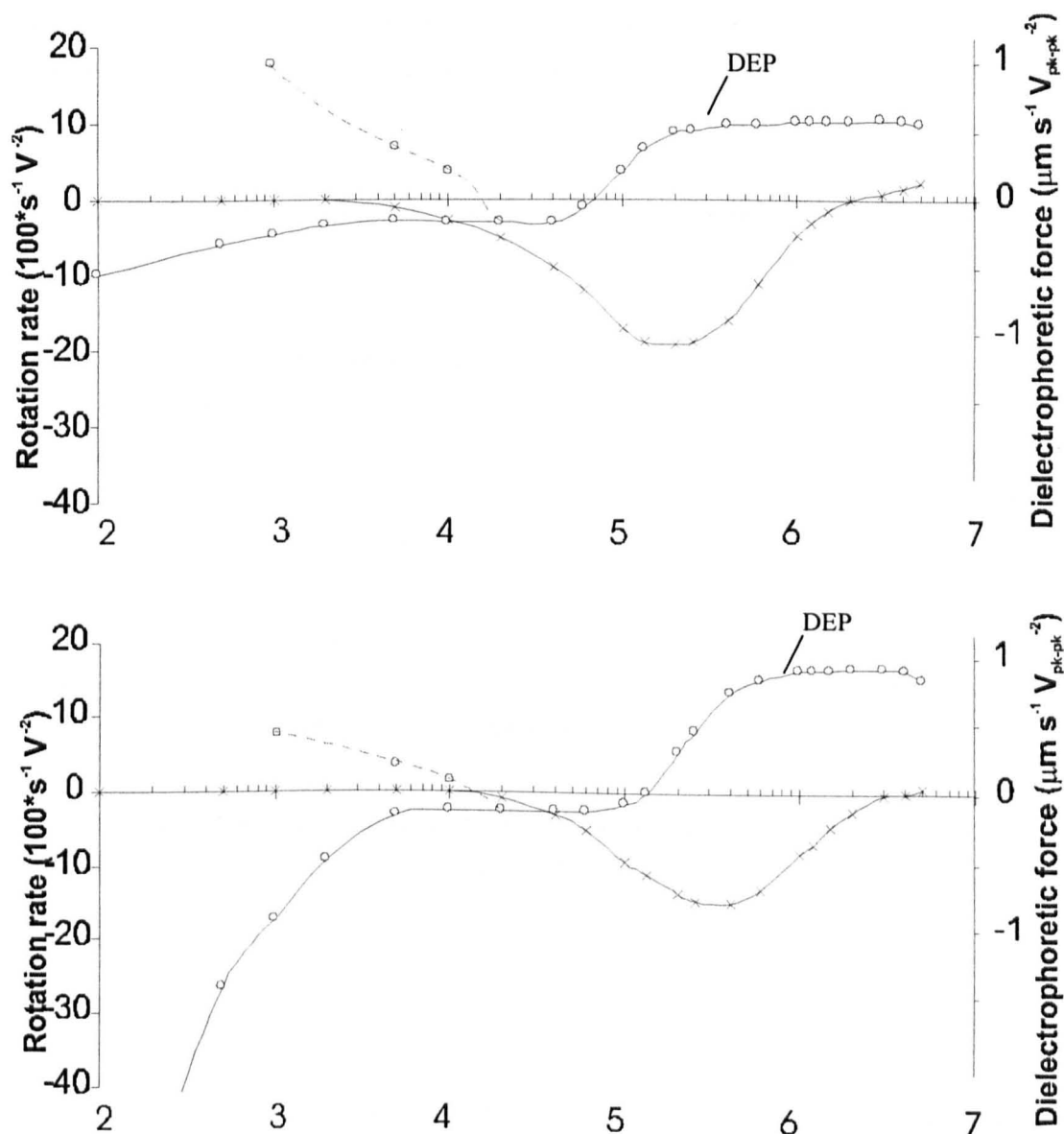
Figure 6.2 Experimental data for ROT (x) and DEP (o) spectra for viable *C. parvum* oocysts at two suspending medium conductivities 18μS cm⁻¹ (top) and 95 μS cm⁻¹ (below). Relative values for the anomalous positive DEP force (- -) are also given.

For the higher conductivity, a range of DEP crossovers frequencies were observed between 85 and 135kHz.

6.3.2.1 Anomalous observations

The measurement of the DEP force at low frequencies (<20kHz) appeared to be complicated by another force, possibly fluid flow, directing the oocysts away from the electrodes towards the centre of the electrode free space. That another force, other than a dielectrophoretic force, was present, was indicated by a boundary line some 15μm from the electrode tip. On the application of the AC field (<20 kHz) oocysts within this boundary moved towards the electrode while those beyond moved toward the centre of the inter-electrode gap, indicating two forces working in opposite directions. It was concluded, from

the observed change in particle velocity, that inside the boundary the dielectrophoretic force was greater, while beyond the boundary the fluid flow was greater resulting in a near constant motion of the particles. The boundary was therefore a line at which the DEP and the opposing force from the fluid flow balanced.

The distance of the boundary from the electrode edge varied with suspending medium conductivity. For the higher conductivity investigated (95µS cm^{-1}) a distance of 15 µm was recorded at 10kHz. At the lower conductivites, for example 18µS cm^{-1}, the distance of the boundary from the electrode was greater, 38µm at 10kHz increasing to 80µm at 1kHz.

Experimentally, if the oocysts were strongly attracted to the electrode edge, briefly switching the field to 40kHz was found to repel the oocysts. This was found to work at any distance from the electrode, i.e. no boundary was observed for frequencies of 40 kHz or higher.

As well as this strong repulsion from the electrodes, at and below 200Hz, oocyst vibration of around two diameters occurred along a path perpendicular to the electrode edge. These vibrations were due to electrophoretic effects related to the surface charge of the oocysts.

Clues to the origin of the strong repulsive force involved come from the quality of the particle motion. A consideration of the other potential phenomena and problems reported at low frequencies is relevant at this point.

6.3.2.2   Electrode polarisation

There are complications in the accurate measurement of DEP and ROT forces on particles at low frequencies. Electrode polarisation for example, is an effect which is prominent at low frequencies and modifies the field distribution within the solution by the formation of an ionic double-layer at the electrode-solution interface. The effects are an increase in the measured capacitance between the electrodes and a decrease in the field magnitude perceived by the particle (Grant, Sheppard & South 1978). In simple terms the electrode polarisation effect can be represented as a series RC equivalent circuit (with an associated time constant, τ, for that circuit) where R is the resistance of the bulk liquid and C is the effective capacitance of the ionic double-layer at the electrode surface (Lawton, 1992). Electrical measurements have to be performed at a frequency above the reciprocal of the time constant, RC, if electrode polarisation effects are to be avoided. Methods to overcome electrode polarisation thus include: reducing the conductivity of the solution as much as possible; roughening the electrode surfaces or depositing a layer of platinum black onto the electrode surfaces to increase their surface area. Increasing the surface area can reduce electrode polarisation effects by as much as four orders of magnitude. The effect of electrode polarisation on the DEP and ROT spectra is a decrease in their respective magnitudes, so knowing the reduction caused one can allow for this when constructing ROT

spectra (Zhou *et al.*, 1995). The increase in velocity of the particles from the electrodes with decreasing frequency is therefore unlikely to be caused directly by electrode polarisation effects, indeed electrode polarisation has the effect of reducing the magnitude of the ROT rate.

6.3.2.3   Properties of the particle

As briefly described in Chapter 2, the surface charges of the particle attract ions of opposite charge, counter-ions, from the bulk solution creating an electrical double-layer (figure 2.1). It was noted that distortions of the double layer by an AC electric field could follow changes in field direction to frequencies of around 50kHz, that is, within the frequency range of interest.

Miles and Robertson (1932) proposed the idea that the double-layer would affect the dielectric properties of the medium around the particle and, as a direct consequence, the effective dipole moment. Experimentally, a large dispersion, or change in polarisability, at a frequency lower than the Maxwell-Wagner relaxation frequency was described for a suspension of 188nm polystyrene particles (Schwann *et al.*, 1962). This dispersion was centred around 20kHz. Dispersions of this type have the prefix 'α' to distinguish them from the interfacial (Maxwell-Wagner) or β-dispersions, occurring at higher frequencies.

The mechanism behind the α-dispersion was considered by Schwarz (1962) who presented the idea (at least for a highly charged solid colloidal particle) that counter-ions are strongly bound by electrostatic attraction to the surface. In order to escape from the surface into free solution, they have to overcome a high potential barrier. Along the surface, however, they can be moved much more easily. Thus, they will be moved tangentially by an external field, polarising the ion atmosphere and inducing an electric dipole moment of the particle. Einolf and Carstensen (1971) extended this theory to cover the case of a porous particle with a uniform volume distribution of fixed charges, in an attempt to model more closely, the properties of a bacterium with porous cell wall. The concept of the polarisability of colloid particles in electrolytes being associated with surface counter-ion conductivity effects has been considered by many others. The nature and dynamic properties of the electrical double layer vary between the theories proposed, discussed in (Pethig, 1979b). More recently, it has been shown (Burt *et al.*, 1990; Pethig *et al.*, 1992) that for frequencies below 10kHz the DEP behaviour of colloidal particles is influenced by the magnitude of the electrical charge on the particle surface. Electrophoretic motion of the particles at and below 200Hz indirectly suggests that the oocysts posses a considerable surface charge. Maier (1997) emphasised the importance of surface conductivity on the ROT rate, not only at low frequencies, but also at Maxwell-Wagner frequencies. He concluded from studies with 9.67μm diameter latex particles investigated at different pH, that for the case where the conductivity of the particle is small compared to that of the surrounding liquid, the effect may be so drastic that it can invert the direction of rotation.

6.3.2.4   Properties of the fluid

Fluid flow caused by the electric field in microelectrodes has been reported previously (Muller *et al.*, 1996) without a detailed attempt being made to characterise the behaviour. It has been described as either a disruptive effect or something that assists dielectrophoretic collection in the case of polynomial electrodes. Controlled fluid flow has been used to assist particle separations (Markx, Pethig & Rousselet, 1997).

Essentially, power dissipation in a liquid gives rise to temperature gradients in the liquid, which in turn produce inhomogeneities in the permittivity and conductivity of the liquid. The permittivity of the liquid changes by about -0.4% °C^{-1}, and the electrical conductivity by about 2% °C^{-1} (Muller *et al.*, 1996). Consequently volume forces occur, driving fluid motion.

Green (1998) described two frequencies; a lower range where coulombic forces arising from gradients in conductivity dominate, and a higher range where dielectric forces from permittivity gradients dominate. In an experiment with 557nm diameter latex spheres on hyperbolic polynomial electrodes (10μm inter-electrode distance) fluid flow was readily observed and a line described at which fluid-flow balanced the DEP force, close to the electrode edge. Green described the coulombic forces causing this effect as being approximately ten times stronger than the dielectric force. In contrast to this description, the observations made for *C. parvum* oocysts on 400μm polynomial electrodes were made in the inter-electrode gap. Motion of the oocysts was in the opposite direction, from the electrode edges towards the centre of the inter-electrode gap.

The magnitude of the oocyst motion away from the electrodes was stronger than the motion due to the DEP force at higher frequencies. The direction and levitation of the particles (which occurred at 1kHz at the centre of the inter-electrode gap) is consistent only with higher frequency fluid motion described. Further work on this would be required to identify the true origins of the forces involved, as the observed phenomena occurred at low (<20kHz) frequencies. One potential method that would enable determination of the fluid motion during the experiment uses sub-micron test particles, from which it would be possible to make more accurate calculations of the true DEP force.

6.3.3 TWD of oocysts

An example of the TWD motion of a viable oocyst in the electrode gap is shown in Figure 6.3 at a suspending medium conductivity of 40μS cm^{-1}. In this sequence, one oocyst is shown held at an electrode tip by positive DEP, while the other travels in the centre of the gap. The travelling oocyst stained DAPI +/PI- and was therefore considered viable, while the oocyst held at the electrode tip was nonviable staining DAPI+/PI+. Differences in the motion of these two oocysts can be explained by different magnitudes of DEP force, at this frequency and conductivity. The DEP force for viable oocysts in these conditions was more negative than for the nonviable oocyst.

Viable oocysts having a more negative DEP force were also observed at the higher conductivity of 95µS cm⁻¹. Using the travelling wave electrodes energised at a frequency of 100kHz, levitation of a viable oocyst (due to a sufficient negative DEP force) over the electrode arrays, was observed at an applied voltage of 2 V_{pk-pk} whereas for a nonviable oocyst 3V_{pk-pk} was required.

TWD spectra of viable *C. parvum* oocysts at two conductivities are shown in Figure 6.4. These show that translational motion of the oocysts by TWD was observed both in the channel and over the electrode arrays. Not shown in Figure 6.4 for the lower conductivity solution is a frequency, 2kHz, at which the oocysts travelled over the electrodes at velocities of 70 to 80µm s⁻¹ V⁻² . Apart from this single observation, the maximum velocity attained was greater in the channel. The frequency range over which travelling wave dielectrophoresis occurred was found to widen as the conductivity of the suspending medium was increased, in agreement with the work of Huang *et al.* (1993).

In general, the occurrence of TWD *usually* coincided when both a rotational component and negative DEP conditions were met, in agreement with Huang *et al.* (1993). At the frequency at which a weak positive DEP force was observed, oocysts in the gap moved to and travelled along the electrode tips, exhibiting the 'fundamentally unstable' (FUN) regime originally described by Huang *et al.* (1993). This occurs when the trapping and translational forces are of similar magnitudes.

Also of interest was the ejection of the oocysts from the end of the channel to distances of around 30µm. This observation is exploited in Chapter 7, for the injection of oocysts into a rotation chamber.
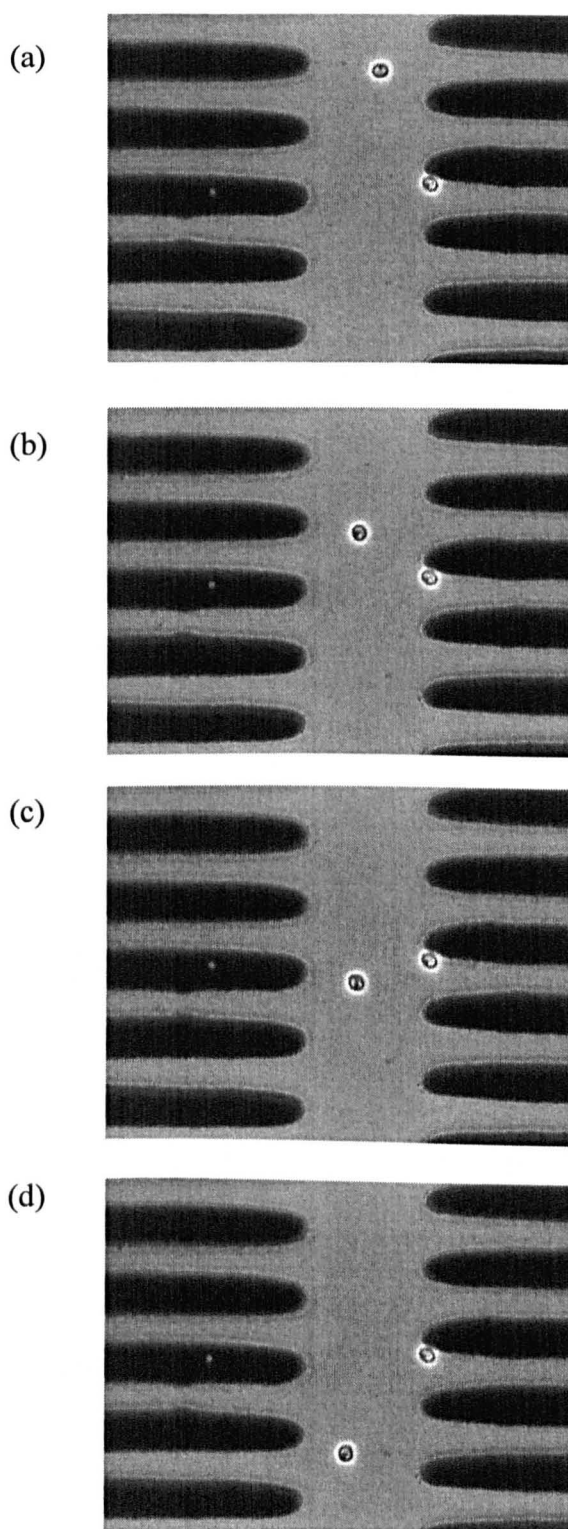
Figure 6.3 In time sequences (a)-(d) of separation of around 1 s, two *C. parvum* oocysts between two comb microelectrode arrays.

One oocyst is shown moving under TWD along the central region of the channel, in the opposite direction to the travelling wave. A 30 kHz voltage, 1V (pk-pk), was applied to the electrodes and the suspending medium was of conductivity 4.0 mS m^{-1}. The second oocyst is held at the tip of an electrode, under the influence of positive DEP.
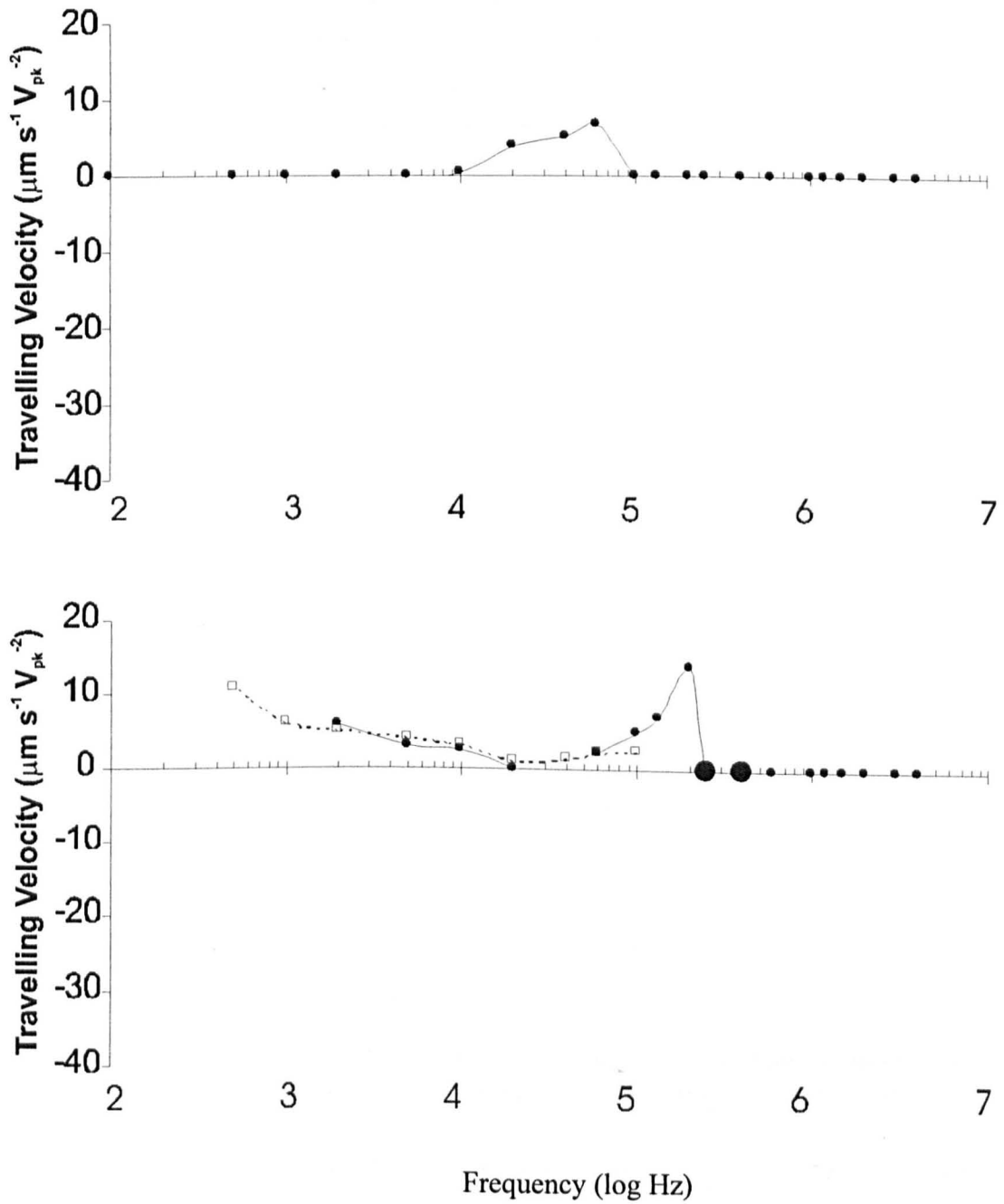
Figure 6.4 For comparison with Figure 6.2, the TWD spectra obtained in the channel (•) and over the electrode arrays (- □ -) for viable *C. parvum* oocysts at 2 suspending medium conductivities 18μS cm⁻¹ (top) and 95 μS cm⁻¹ (below).
Also shown are two examples of frequencies at which the fundamentally unstable regime was observed

(⬤).

6.3.4 Modelling of results.

Using the MatLab model the results obtained for the ROT and DEP data were modelled, presented in Figure 6.5 below. The ROT modelling is in close agreement with the experimental results. Differences between the observed and modelled DEP spectra obtained are as follows. Whereas the crossover frequencies are in close agreement, the magnitudes of the forces differ, also below 20kHz the model does not show the anomalous part of the spectrum observed.
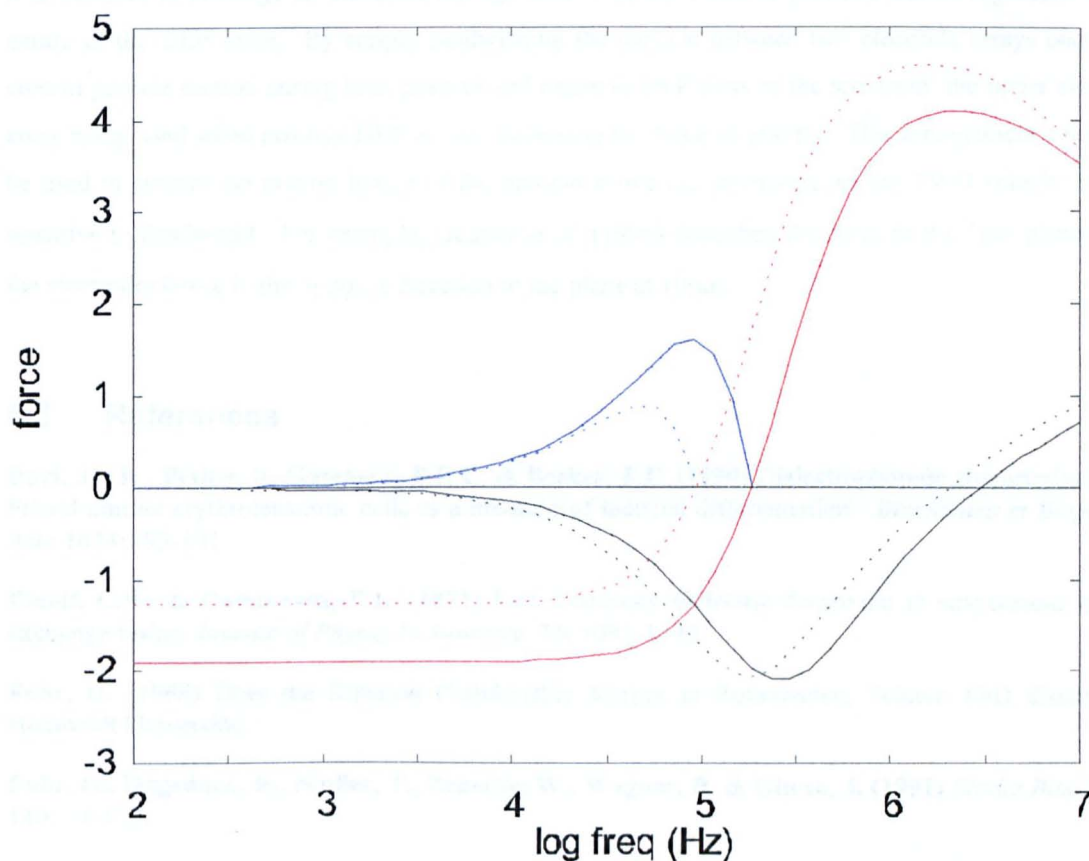
Figure 6.5 Modelled data for the ROT (black), DEP (red) and TWD (blue) responses of viable *C. parvum* oocysts at two suspending medium conductivities, 18 μS cm⁻¹ (- -) and 95μS cm⁻¹(—).

For modelling purposes the magnitude and direction of the V_{TWD} was calculated as proportional to the ROT rate, once the requirement for negative DEP condition had been met, see section 6.3.2. Magnitudes and frequency responses of the predicted TWD spectra are in close agreement with the experimentally observed spectra, at least for TWD in the channel, above 20kHz. As with the DEP spectra differences exist between the observed and expected spectra below this frequency. The model therefore gives a reasonable estimation of the TWD spectra above 20kHz.

6.4   Conclusions

The restriction on the part of the frequency spectrum at which the TWD 'window' is seen has both advantages and disadvantages. A small frequency band is useful if differential mobility of particles is required. However, the lower frequency band observed for particles to date, occurs at frequencies where the rotational component is less than half its full value. One potential solutions to widen the frequency band at which TWD occurs is outlined below.

It is possible to envisage an electrode arrangement whereby TWD of particles occurs regardless of the nature of the DEP force. By simply sandwiching the particle between two electrode arrays one could control particle motion during both positive and negative DEP parts of the spectrum; the upper electrode array being used when positive DEP occurs, balancing the force of gravity. This arrangement could also be used to control the precise height of the particle above the electrodes, as the TWD velocity is very sensitive to this height. For example, Hughes *et al.* (1996) described the force in the 3µm plane above the electrodes being in the opposite direction to the plane at 10µm.

6.5   References

Burt, J.P.H., Pethig, R. Gascoyne, P.R.C. & Becker, F.F. (1990) Dielectrophoretic characterisation of Friend murine erythroleukemic cells as a measure of induced differentiation. *Biochimica et Biophysica Acta* 1034: :93-101.

Einolf, C.W. & Carstensen, E.L. (1971) Low-frequency dielectric dispersion in suspensions of ion-exchange resins. *Journal of Physical Chemistry.* 75: 1091-1099.

Fuhr, G. (1985) Über die Rotation Dielektrisher Körper in Rotierenden, Feldern PhD dissertation, Humboldt Universität.

Fuhr, G., Hagedorn, R., Muller, T., Benecke, W., Wagner, B. & Gimsa, J. (1991) *Studia Biophysica.* 140: 79-102.

Fuhr, G., Schnelle, Th. & Wagner, B. (1994) *Journal of Micromechnics and Microengineering* 4: 217-226.

Grant, E.H. Sheppard, R.J. & South, G.P. (1978) In: Dielectric Behaviour of Biological Molecules in Solution. Clarendon Press, Oxford. Chap 3 The measurement of permittivity. p63.

Green, N.G. (1998) Dielectrophoresis of sub-micrometre particles. *Ph.D. Thesis*, Glasgow.

Green, N.G. & Morgan, H. (1998) Separation of submicrometre particles using a combination of dielectrophoretic and electrohydrodynamic forces. *Journal of Physics D- Applied Phys.* 31: L25-L30.

Huang, Y. & Pethig, R. (1991) Electrode design for negative dielectrophoresis. *Measurement Science and Technology.* 2: 1142-1146.

Huang, Y. Wang, X-B., Tame, J.A. & Pethig, R. (1993) Electrokinetic behaviour of colloidal particles in travelling electric fields: Studies using yeast cells. *Journal of Physics D- Applied Phys.* 26: 1528-1535.

Hughes, M.P., Wang, X-B. Becker F.F., Gascoyne, P.R.C. & Pethig R. (1994) Computer-aided analyses of electric fields used in electrorotation studies. *Journal of Physics D- Applied Phys.* 27: 1564-1570.

Hughes, M.P., Pethig, R. & Wang, X-B. (1996) Dielectrophoretic forces on particles in travelling electric fields. *Journal of Physics D- Applied Phys.* **29:** 474-482.

Lawton, B.A. (1992) Some application of dielectric phenomena. *PhD. Thesis.* University of Wales. Bangor.

Maier, H. (1997) Electrorotation of colloidal particles and cells depends on surface charge. *Biophysical Journal.* **73:** 1617-1626.

Markx, G.H. Pethig, R. & Rousselet, J. (1997) The dielectrophoretic levitation of latex beads, with reference to field-flow fractionation. *Journal of Physics D- Applied Phys.* **30:** 2470-2477.

Miles J.B. & Robertson, H.P. (1932) The dielectric behaviour of colloidal particles with an electric double layer. *Physical Review* **40:** 583-591.

Morgan, H., Green, N.G., Hughes, M.P., Monaghan, W. & Tan, T.C. (1997) Large-area travelling-wave dielectrophoresis particle separator. *Journal of Micromechanics and Microengineering.* **7:** 65-70.

Muller, T., Gerardino, A., Schnelle, T., Shirley, S.G., Bordoni, F., De Gasperis, G., Leoni, R. & Fuhr, G. (1996) Trapping of micrometre and sub-micrometre particles by high-frequency electric fields and hydrodynamic forces. *Journal of Physics D- Applied Phys.* **29:** 340-349.

Pethig, R. (1979).(a) Dielectrophoretic studies of biomolecular systems. p.189, (b) Chap. 5 Interfacial dielectric phenomena in biological systems pp.173-175. In: *Dielectric and electronic properties of biological materials.* Wiley & Sons, Chichester.

Pethig, R., Huang, Y., Wang, X-B. & Burt, J.P.H. (1992) Positive and negative dielectrophoretic collection of colloidal particles using interdigitated castellated micro-electrodes. *Journal of Physics D-Applied Physics.* **25:** 881-888.

Pethig, R. & Markx, G.H. (1997) Applications of dielectrophoresis in biotechnology. *Trends in Biotechnology.* **15:** 426-432.

Sauer F.A. & Schlogl, R.W. (1985) Torques exerted on cylinders and spheres by external electromagnetic fields: A contribution to the theory of field induced cell rotation. *In: Interactions between electromagnetic fields and cells.* (Eds A.Chiabrera, C. Nicolini & H.P.Schwan) Plenum, New York. pp. 205-251.

Schwann, H.P., Schwarz, G.H. Maczuk, J. & Pauly, H. (1962) On the low-frequency dielectric dispersion of colloidal particles in electrolyte solution. *Journal of Physical Chemistry.* **66:** 2626-2635.

Schwarz, G. (1962) A theory of the low-frequency dielectric dispersion of colloidal particles in electrolyte solution. *Journal of Physical Chemistry.* **66:** 2636-2642.

Shaw, D.J. (1996) Kinetic properties. In: *Introduction to colloid and surface chemistry.* p22 Reed, Elsevier, Oxford.

Talary, M. S., Burt, J.P.H., Tame, J. & Pethig, R. (1996) Electromanipulation and separation of cells using travelling electric fields. *Journal of Physics D- Applied Phys.* **29:** 2198-2203.

Wang, X-B, Huang, Y., Burt, J.P.H., Markx, G.H. & Pethig, R. (1993) Selective dielectrophoretic confinement of bioparticles in potential energy wells. *Journal of Physics D- Applied Phys.* **26:** 1278-1285.

Zhou, X-F., Markx, G.H., Pethig, R. & Eastwood, I.M. (1995) Differentiation of viable and nonviable biofilms using electrorotation. *Biochimica et Biophysica Acta.* **1245:** 85-93.

Chapter 7

A Combined Travelling Wave Dielectrophoresis and Electrorotation Device: applied to the Concentration and Viability Determination of *Cryptosporidium* oocysts.

7.1 Introduction

The development of microelectrode devices for the electrokinetic-characterisation and selective manipulation of cells and other bioparticles is currently an active area of research. One important electrokinetic phenomenon is dielectrophoresis (DEP) (Pohl 1978) whereby translational motion of particles is induced by exposing them to non-uniform, stationary, A.C. electric fields. As described in Chapter 2, it is found that the magnitude and sense of the dielectrophoretic force depends on the nature of the dipole moments induced in the particles, and this in turn is a function of the dielectric properties of each particle and its surrounding medium. If, instead of a stationary electric field, a particle is subjected to a moving field, then under appropriate conditions it can be induced to move by the effect of travelling wave dielectrophoresis (TWD), an introduction to which has been given in Chapter 2, and initial investigations using *Cryptosporidium* oocysts are described in Chapter 6. Several laboratories have described the theory and practical demonstration of bioparticle manipulation using microelectrode structures to induce TWD (*e.g.* Masuda, Washizu & Iwadare, 1987; Hagedorn *et al.*, 1992; Huang *et al.*, 1993; Green *et al.*, 1997; Wang *et al.*, 1997). The microelectrodes have taken the form of either grid-like, periodic elements such as those used by Green, *et al.* (1997) or spiral electrode structures (Hagedorn *et al.*, 1992; Fuhr *et al.*, 1995; Wang *et al.*, 1997) fabricated using monolayer (*e.g.* Masuda *et al.*, 1987; Fuhr *et al.*, 1995; Huang *et al.*, 1993) or multilayer (Fuhr *et al.*, 1995; Talary *et al.*, 1996; Green *et al.*, 1997) techniques. The travelling waves can be produced, for example, by energising the electrode elements with phase-quadrature sinusoidal signals of frequencies between around 50 Hz and 100 MHz.

Another important electrokinetic effect is electrorotation (ROT), which is the induced rotation of particles exposed to a rotating electric field. The theoretical and experimental aspects of ROT have been developed in several laboratories (reviewed by Fuhr & Hagedorn 1996) and it has been shown to be a sensitive method for monitoring the physiological viability of cells. The rotating electric field is usually generated using four electrodes positioned at right angles to each other and energised with phase-quadrature signals of frequencies between around 50 Hz and 100 MHz.

The fact that TWD and ROT can be induced using similar electrical signals implies that they should be capable of integration into a single microelectrode structure. In this Chapter, two basic devices are described, and it is shown how they can be used to concentrate and determine the viability of relatively dilute concentrations of micro-organisms. The model Microorganism used in this study was the oocyst of *Cryptosporidium parvum*, which was previously characterised extensively by ROT as a function of

various experimental conditions, as described in Chapter 5. The presence of these oocysts, even at very low concentrations, in drinking water has led to outbreaks of human infection (cryptosporidiosis), which occurs as a self-limiting diarrhoea in healthy adults but may lead to death in infants and immuno-compromised people. AIDS patients with cryptosporidiosis often suffer persistent infections when their CD4 counts are less than 140 cells/mm^3 (Flanagan *et al.,* 1992). The current detection methods for the transmission stages of *Cryptosporidium* (also for *Giardia*) are outlined below.

As methods are not available for the routine culture of either *Cryptosporidium* or *Giardia* from water concentrates, detection relies upon direct examination. The procedure for detecting protozoan parasites in water can be divided into three basic sequential sections, namely concentration, purification and detection. The three most commonly used concentration methods are membrane filtration, calcium carbonate flocculation and cartridge filtration. Typical sample volumes are around 100 litres for a raw water and 1000 l for treated water with the cartridge filtration method, the other methods are only suitable for smaller volumes of water of 10-20 litres. All three methods end with a final step of centrifugation, typically resulting in a 2-3 ml concentrate, from water samples.

Purification of this concentrate is commonly by a density flotation method, with Percoll, Percoll-sucrose or sucrose (1.18g/ml). Factors such as turbidity may have a significant effect on the recovery of oocysts (or cysts) using this method, as they may bind to larger particles of dense material, and so will be lost. Flow cytometry together with fluorescently activated cell sorting (FACS) has been found suitable for sorting oocysts from background debris but is expensive. Immunomagnetic separation (IMS) is also possible, whereby microbeads with an iron core are coated with antibody specific to the target organism, which after mixing and binding with the target can be removed by a nearby magnet.

Final detection usually relies on direct microscopical examination, which requires experienced and patient staff. Aids to the detection such as fluorescent labelling are prone to cross reactions with other organisms or to other particulate matter in the sample and so can lead to inaccuracies.

The generic device described in this Chapter addresses the problem of the final concentration step for assessment, which could be scaled to handle 2-3 ml concentrates, while also incorporating a method for determining viability in the same apparatus.

7.2   Spiral Electrode Designs

TWD has been shown to operate in two different ways, between 'comb-like' arrays, see for example the device described by Huang *et al.* (1993) or above parallel electrode elements as used by Morgan *et al.* (1997). Using monolayer construction of the electrodes it is technically easier to make the required electrode connections if one repeats the same four parallel elements by arranging the electrodes in a spiral. Experiments using two different designs of spiral are described, namely square-sided and circular designs. Also, various dimensions, with up to 40 spiral turns per electrode, were investigated. Schematics of the two basic microelectrode arrays are shown in Figure 7.1 and 7.2. When the four spiral

electrode elements are energised with sinusoidal voltages of relative phase difference shown in these figures, a travelling electric field is generated that travels radially from the centre towards the periphery of the spiral array. An anticlockwise rotating electric field is also generated in the central free space region. In the frequency range where a particle exhibits cofield electrorotation, any induced TWD motion will be in the direction of propagation of the travelling field, and *vice versa* (Huang *et al.*, 1993).

7.2.1 Square-sided Spiral Design

A square-sided spiral geometry (Hagedorn *et al.*, 1992; Fuhr *et al.*, 1995) as shown in Figure 7.1 was initially investigated. Designed using CorelDraw! (Version 5) electrode elements and gaps of 40μm were created, with a lambda (period of repeat) of 320μm and an electrode free central region of 160μm. Although simple to design, a problem with the square sided design was the trapping of the oocysts at the 90° corners. This can be explained by the greater interelectrode gap at the corners of 56.6 μm, along with an increase in the lambda to 452.56μm. One solution is by masking the corners and forming TWD channels, as described for example by Fuhr *et al.* (1995) but this reduces the surface area available for the concentration of the particles.
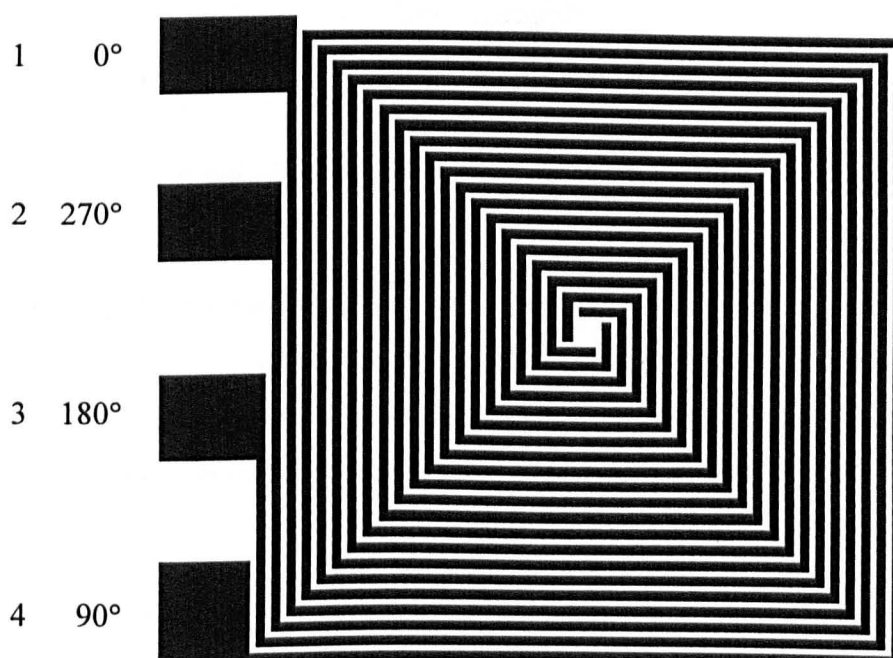
Figure 7.1 The TWD-ROT square spiral microelectrode design consisting of four parallel spiral elements.

7.2.2 Circular Spiral Design

The electrode elements of the circular spiral, Figure 7.21, were drawn using a macro in Autosketch 2.1 (Autodesk, Inc.). Elements of 15μm with gaps of 25μm created a lambda of 160μm, half that of the square spiral. The central region is also slightly smaller than that of the square design at 140μm. A total area of ~3 mm² was created with just 5 turns of the spiral. By simply increasing the number of turns, the surface area of this design can be increased to deal with larger volumes.
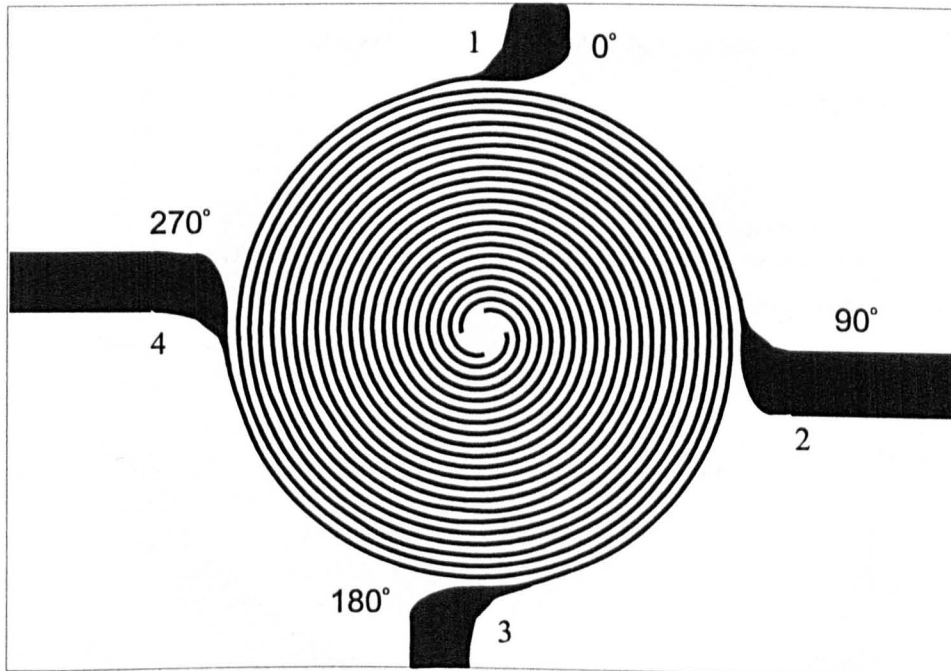
Figure 7.2 The TWD-ROT circular microelectrode design.

7.2.3 The Spiral Centre - Rotation Chamber

The travelling force from periodic electrode elements was found in the previous chapter to only exert a significant force on the oocysts when the particles were within 20μm of the end of the array. This can be explained by the particle predominantly perceiving the field from the nearest electrode, a reduced effect being perceived from the other electrodes as they are both further away and masked to some extent by the near electrode. To create a TWD-free region in the centre of the spiral it was considered a requirement to have an electrode free space of diameter greater than 40μm. In contrast to TWD fields, rotating fields are perceived by the particles at greater distances as shown by the ability to rotate particles with interelectrode gaps of 2mm. The major requirement for a rotating field is that the particle can 'see' each of the electrodes, preferably at equal distances. Termination of the electrodes in both designs was by a simple blunt 'square-ended' cut off, but in contrast to the design of Wang *et al.* (1997) the ends were arranged symmetrically about the centre, thus forming a rotating field in the centre.

A necessary requirement for reliable ROT measurements is that the rotating electric field should be as homogeneous as possible (Burt *et al.,* 1996) and as shown in Figure 7.3 the field over the central region is reasonably uniform. The field homogeneity can be improved by changing the electrode geometry, but the efficiency of particle injection by TWD into the centre of the spiral array is reduced.
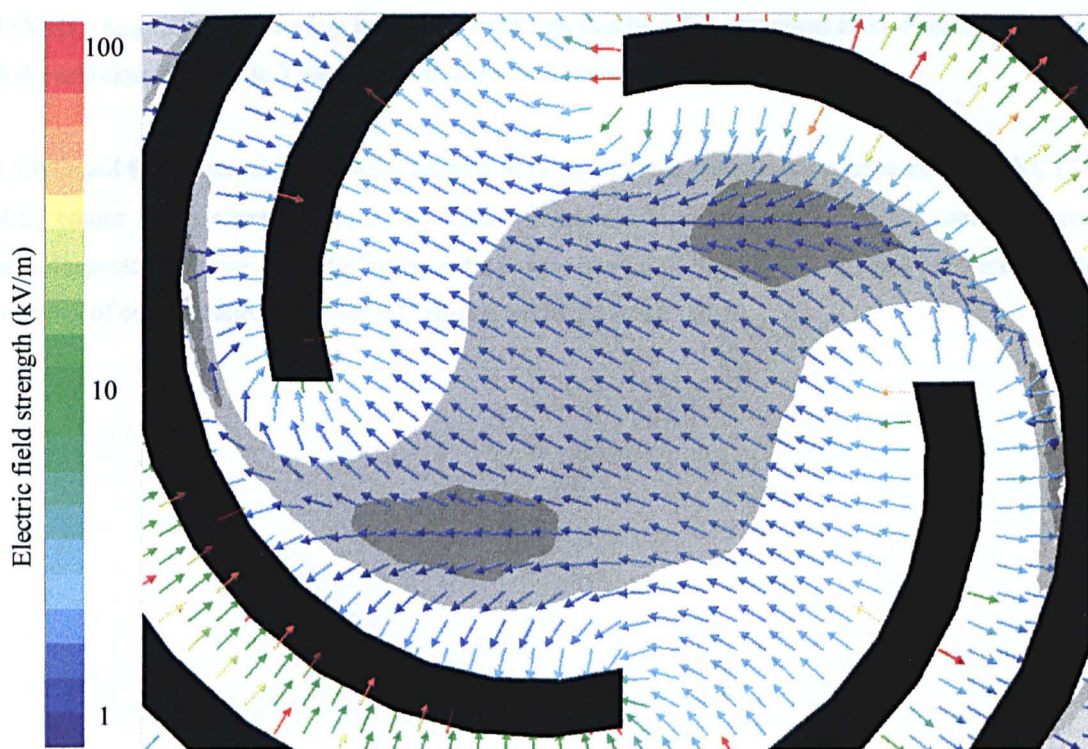
Figure 7.3 The electric field vectors and magnitude distribution at the centre of the spiral electrode array shown in Figure 7.2, calculated using the Maxwell 3D Field Simulator (Ansoft, Pittsburgh).

This result depicts the instant when electrodes 1, 2, 3 and 4 of Figure 1 are energised with 1 V_{RMS} sinusoidal voltages of phases 30°, 120°, 210°, and 300°, respectively. The field strength in the two darkly shaded regions is less than 2.5 kVm^{-1} and that within the region of lighter shading has values in the range 2.5 to 5.0 kVm^{-1}. The field strength within 1 μm of the electrode edges exceeds 100 kVm^{-1}.

7.3   Materials and Methods

The *C. parvum* oocysts of human origin, were a gift of Prof. H. V. Smith of the Scottish Parasite Diagnostic Laboratory, Stobhill NHS Trust, Glasgow. Averaging 5μm in diameter (Fayer, 1997) the oocysts were supplied as a suspension in deionised water, of concentration around 1.5×10^6 ml^{-1} as determined using an improved Neubauer haemocytometer. After storage at 4°C they were, stained according to the method of Campbell, Robertson & Smith (1992) with DAPI and PI, and washed as described in Chapter 5.

The microelectrode arrays were energised with phase-quadrature signals of frequencies between 100 Hz and 5MHz. Applied voltages of up to 2V rms were supplied by a PC controlled electrorotation generator, with the addition of a 4 pole 3 way switch that allowed reversal of the field direction.

The TWD and ROT characteristics were monitored using a Nikon Labophot-2 microscope and JVC (TK-1280E) colour video camera, coupled to a Matrox Meteor (Quebec) frame-grabber controlled using Matrox Inspector software. The following stills images shown in Figures 7.5, 7.7 and 7.8 were obtained for oocysts of concentration 3.8×10^4 ml^{-1} suspended in 3.5 mSm^{-1} PBS.

7.4   Results

To understand the following observations it is useful to briefly re-examine the ROT and DEP spectra of *C. parvum* oocysts. Spectra obtained from the Matlab model for both the ROT and DEP spectra of a viable *C. parvum* oocyst are shown in Figure 7.4.

At a conductivity of 35 μS cm^{-1}, for frequencies between around 10 kHz and a few MHz the rotation sense is predominantly anti-field, and so in this range any observed TWD motion should be against the travelling field and thus towards the centre of the spiral array.
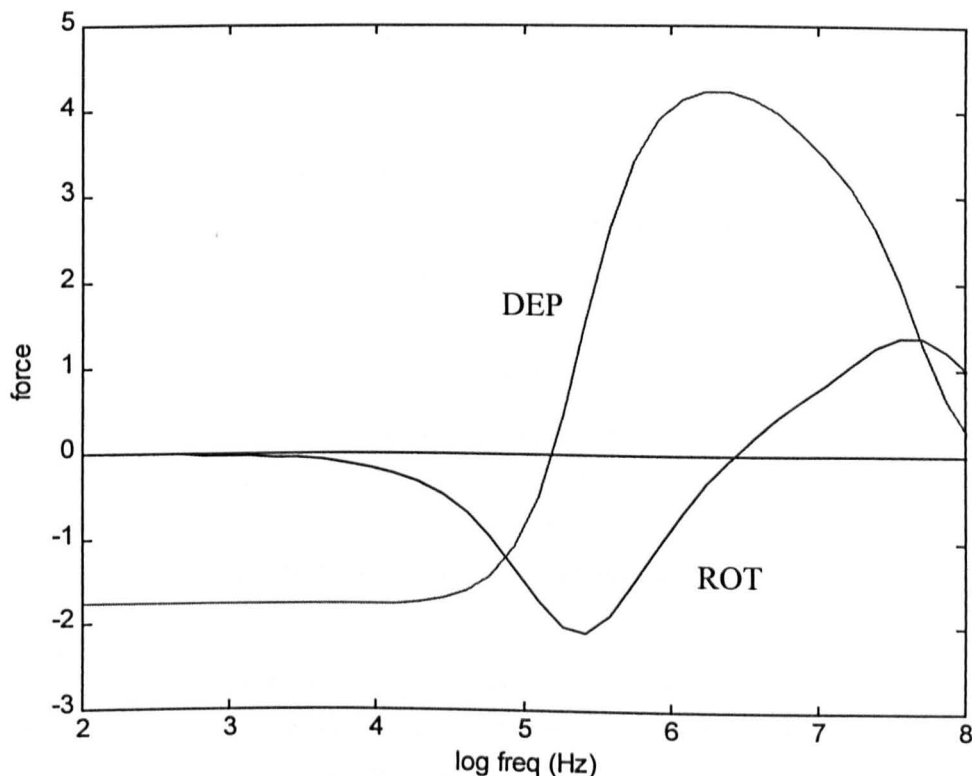
Figure 7.4 ROT and DEP spectra modelled for a viable *C. parvum* oocyst at a suspending medium conductivity of 35 μS cm^{-1}.
Cytoplasmic conductivity 0.5 S m^{-1}, membrane conductivity 1 μS m^{-1}.

The TWD motion is sensitive to the levitation height induced by negative dielectrophoresis (Wang *et al.*, 1997). As shown in Figure 7.4, negative dielectrophoresis is only expected below approximately 200kHz for this suspending medium conductivity. For frequencies greater than this, the oocysts are held at the electrode edges by positive dielectrophoresis, sometimes spinning as they are held. This fact was incorporated into the experimental procedure to aid collection of the oocysts described in section 7.4.1. As well as varying with frequency, the magnitude of negative dielectrophoresis is a sensitive function of the electrode dimensions for periodic electrode structures (Markx, Pethig & Rousselet, 1997).

7.4.1 Experimental sequence.

A sample of the oocyst suspension was micro-pipetted into a circular chamber enclosing the microelectrode array, constructed using 150 μm thick insulating tape. A coverslip (18mm circular) was placed over this chamber and the total enclosed volume of sample was 1.45 ± 0.02 μl, corresponding to on average 55 ± 1 oocysts being suspended within the field of influence of the microelectrodes.

Settling of the oocysts onto the plane of the electrodes was achieved either passively by gravity, which took up to 3 minutes for some oocysts, or actively by attracting the oocysts onto the electrodes over a period of 30 s by positive dielectrophoresis, using 1 MHz, 2 V_{RMS} applied voltages of relative phases shown in Figure 7.1.

For a suspension conductivity of 35 μS cm^{-1} the frequency was then reduced to 160 kHz (0.7 V_{RMS}) whereupon the oocysts were levitated above the electrodes under the influence of negative dielectrophoresis and travelled towards the centre at an average velocity of 10 μms^{-1} under the action of TWD, see sequence in Figure 7.5. At other values of the suspension conductivity, for example 12 and 100 μS cm^{-1}, optimum TWD motion towards the centre occurred at frequencies of 60 kHz and 240 kHz, respectively. For the 100 μS cm^{-1} suspensions, when the frequency was reduced to 1 kHz the oocysts reversed their TWD motion and moved to the periphery of the spiral array. This reflects a reversal of the electrorotation for frequencies below around 3 kHz, which is seen in ROT data collected from normal polynomial electrodes, but is not reflected in the modelled spectrum of Figure 7.4.

On reaching the central region, the oocysts move out of the influence of the TWD force, with its levitational component, and are injected into a predominantly rotating electric field. Without the levitational force, the oocysts fall to the glass surface within 15 seconds, a small distance from the electrodes, as seen for the particles in Figure 7.7 that are in the same plane as the electrodes.

The image shown in Figure 7.8 was obtained 2 mins after initiating the TWD transport. It can be seen that of the estimated 54 oocysts initially in suspension over the electrode array, 49 of them had been concentrated by TWD into the centre. This collection efficiency of around 90% was a reproducible finding. The final concentrating together of the oocysts was achieved by increasing the magnitude of the negative dielectrophoretic force acting on them, which required adjustment of the applied voltages to 60 kHz and 2V_{RMS}. At this stage, the ROT responses of the oocysts could be investigated by adjusting the applied voltages to 1.5 MHz and 1V_{RMS}. At 1.5 MHz the oocysts experienced not only a clockwise rotating field, but also a positive dielectrophoretic force causing them to slowly move back towards the electrodes. If this effect interfered with the ROT analysis, the oocysts were redirected towards the centre by briefly reducing the frequency to 60 kHz. As shown in Figure 7.9, at 1.5 MHz viable oocysts exhibit antifield rotation, whereas nonviable ones rotate in a cofield sense. Of the 51 oocysts shown in Figure 7.7, 27 exhibited antifield (anticlockwise) rotation and were deemed to be viable, whilst the

remaining 24 oocysts rotated in a cofield (clockwise) sense and were considered to be nonviable, in total agreement with fluorogenic vital dye checks performed on each oocyst at the same time. Although dipole-dipole interactions between the oocysts can influence the rotation rate, such interactions are not strong enough to *reverse* their sense of rotation.

(a)

(b)

(c)
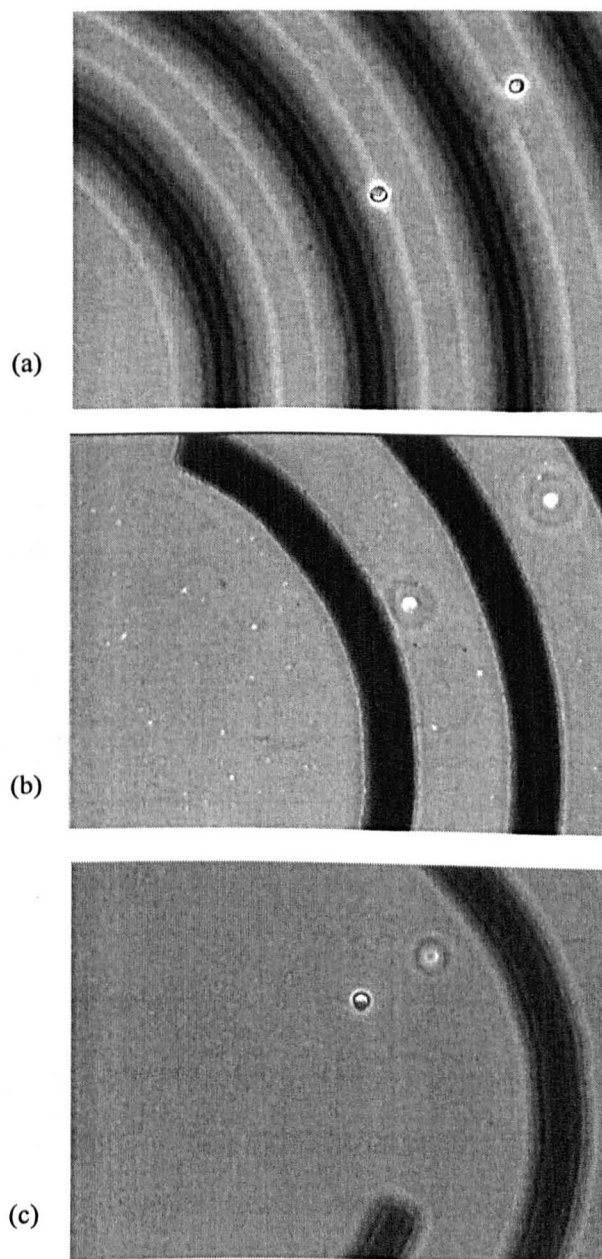
Figure 7.5 Movement of the oocysts into the centre of the array.
(a) Two oocysts levitated above the electrodes (out of focus) undergoing TWD motion towards the centre of the microelectrode array. (b) Image obtained 4 seconds later, with electrodes in focus, showing progress of TWD motion. (c) 4 seconds later, the leading oocyst has entered the inner electrode space and dropped down to the electrode plane, whilst the trailing oocyst remains levitated under the influence of TWD.
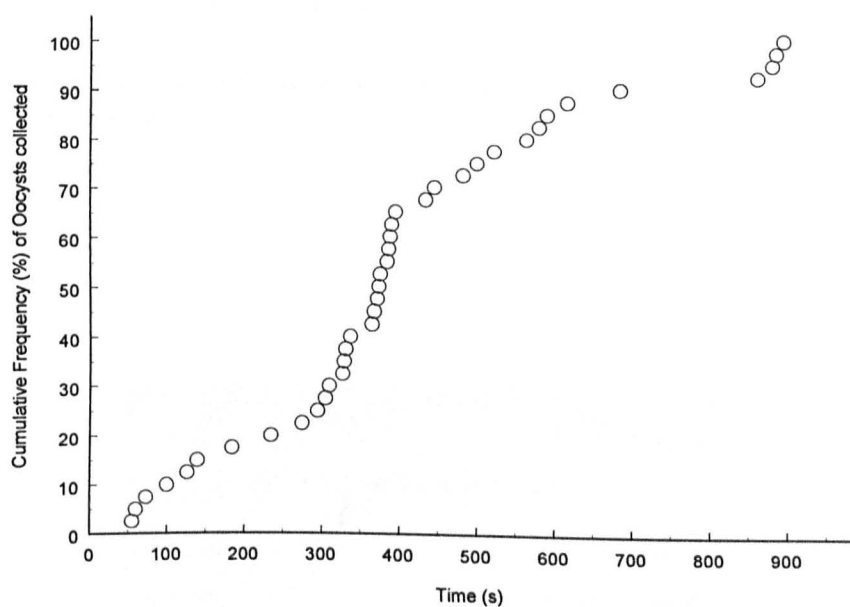
Figure 7.6 A typical collection profile of (n=40) oocysts into the central region using the circular spiral electrode array.
The total collection time was later improved to around 2 minutes by optimising the voltages and frequency.
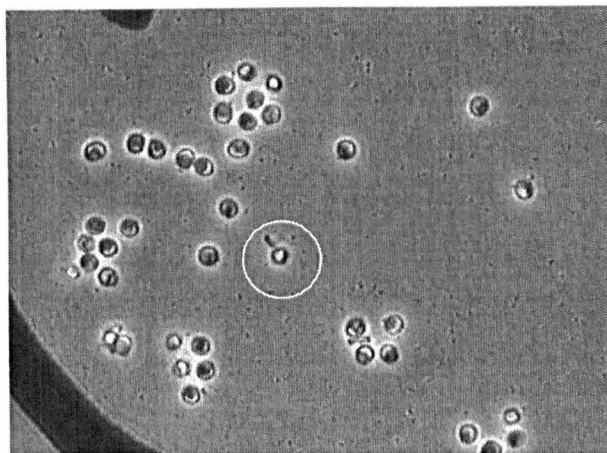
Figure 7.7 Oocysts injected into the centre, resting on the glass substrate.
The circle identifies an oocyst with an adherent bacterium.
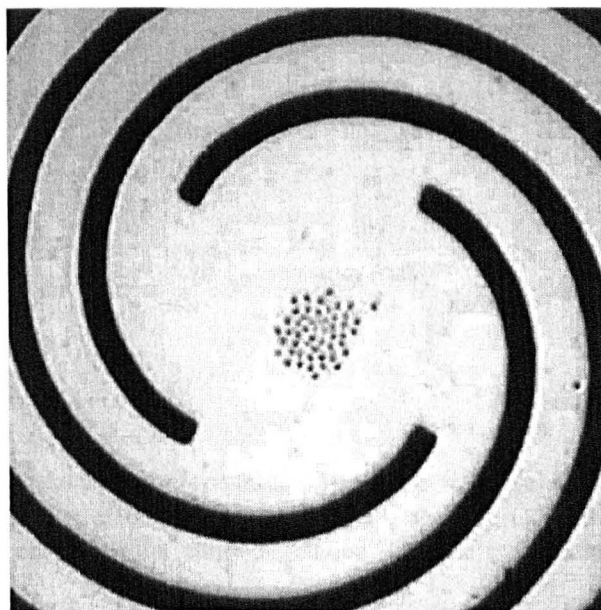
Figure 7.8 Concentration of the particles into the centre by increasing the negative DEP force (60 kHz, 2 V_{RMS}).
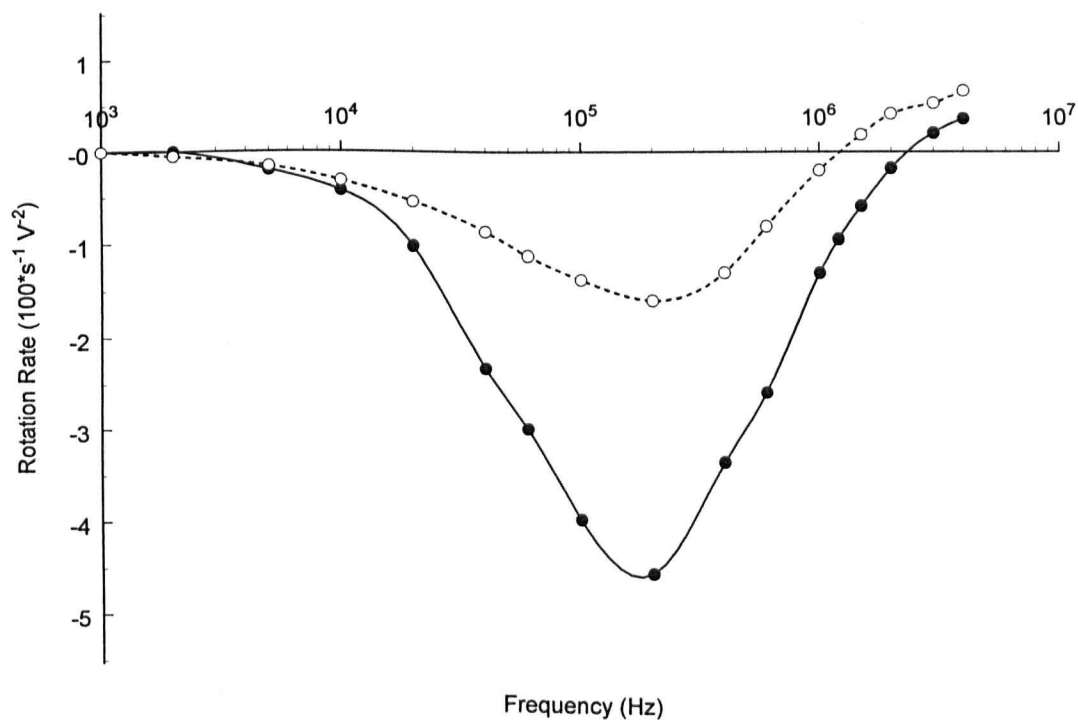
Figure 7.9 Electrorotation spectra for viable (•) and non-viable (o) *C. parvum* oocysts.
Suspended in PBS solution of conductivity $40\mu S$ cm^{-1}, obtained using the 2mm bone electrodes. At 1.5 MHz the viable oocysts exhibit antifield rotation, whilst the nonviable oocysts rotate in a cofield sense.

7.5   TWD - Differences between Viable and Non-viable oocysts

Viable and non-viable oocysts have different ROT and DEP spectra as shown in Figure 7.10 (for simplicity from modelled spectra). It should therefore be expected that their respective TWD forces and subsequent concentration rates would not be equal. At one extreme, it was observed that the oocyst ghosts or visibly deteriorated oocysts did not travel under the influence of TWD. This accounted for the ~10% of oocysts that failed to travel to the centre.

Between 10 and 100 kHz the magnitude of negative dielectrophoresis and rotational torque are less for the nonviable oocyst. This difference could be exploited by using the spiral electrodes to selectively concentrate the viable oocysts. This could easily be achieved by using a lower suspending medium conductivity, which would shift the negative DEP force to a more positive value. One could detect the number of viable oocysts in a sample using this method, by simply counting the oocysts that had entered the centre after a given time. It is often advantageous however, to know the percentage viability of a population, for example for comparison with vital dyes. This is the approach described in this Chapter.
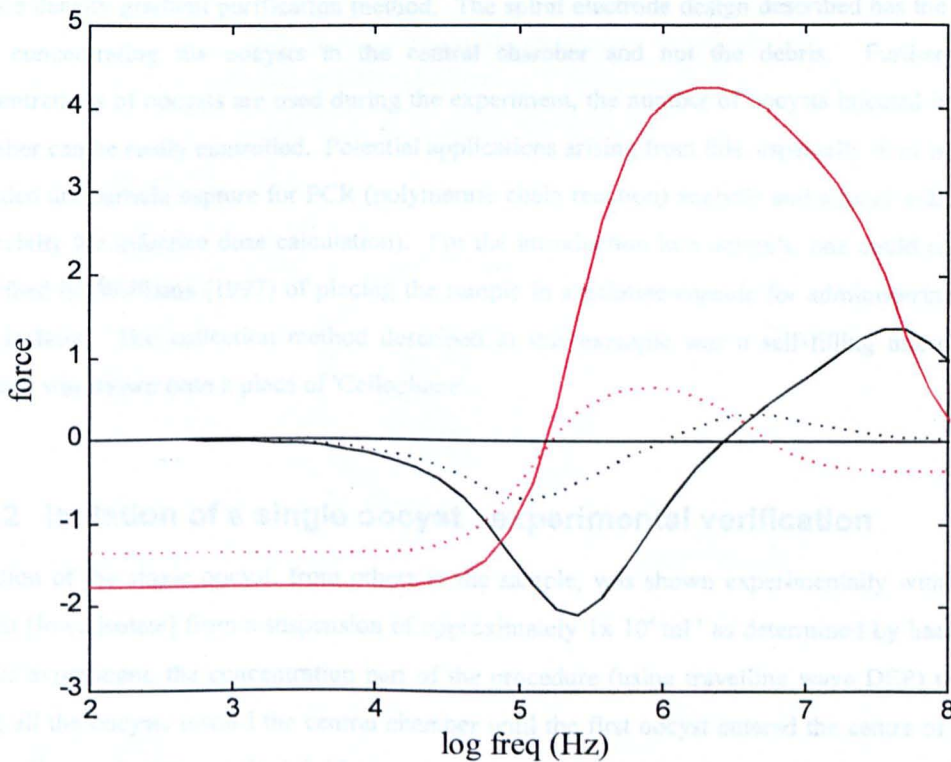
Figure 7.10 ROT (black) and DEP (red) spectra modelled for a viable (-) and nonviable (...)
C. parvum **oocyst at a suspending medium conductivity of 35 μS cm^{-1}.**
Viable and nonviable oocyst dielectric parameters; cytoplasmic conductivity 0.5 and 0.02 S m^{-1}, membrane conductivity 1 and 10 μS m^{-1} respectively.

7.6   Conclusions

To our knowledge this is the first reported operation of a "laboratory-on-a chip" device that incorporates the combined electrokinetic effects of travelling wave dielectrophoresis and electrorotation. Here it has been used to concentrate and then assay the viability of *C. parvum* oocysts, but other biomedical and biotechnological applications can be envisaged. The area of the spiral electrode array could readily be increased and we are exploring this aspect using laser ablation, which is capable of high-resolution patterning over large areas, to accuracy's of 2 µm over 20 cm (Marx, 1997). The device described, of effective capture area around 0.1 cm², can be used for particle concentrations of 10^4 ml^{-1} and so, in principle at least, it could be developed to handle particle concentrations of 10 ml^{-1} and less.

7.6.1   Developments arising from the spiral electrode design:

A common problem that is encountered in electrorotation experiments with oocysts of *Cryptosporidium* is that of working with low concentrations of organisms. Concentrating oocysts by conventional methods such as centrifugation, results also in the concentration of debris within the sample, a problem even when using a density gradient purification method. The spiral electrode design described has the advantage of only concentrating the oocysts in the central chamber and not the debris. Furthermore, if low concentrations of oocysts are used during the experiment, the number of oocysts injected into the central chamber can be easily controlled. Potential applications arising from this, especially if an isolation step is included are particle capture for PCR (polymerase chain reaction) analysis and animal infectivity studies (especially for infective dose calculation). For the introduction into animals, one could use the method described by Williams (1997) of placing the sample in a gelatine capsule for administering in a plastic-film isolator. The collection method described in this example was a self-filling micropipette, from which it was blown onto a piece of 'Cellophane'.

7.6.2   Isolation of a single oocyst : experimental verification

Isolation of the single oocyst, from others in the sample, was shown experimentally with a *C. parvum* oocyst [Iowa isolate] from a suspension of approximately 1x 10^4 ml^{-1} as determined by haemocytometer. In this experiment, the concentration part of the procedure (using travelling wave DEP) was utilised to bring all the oocysts toward the central chamber until the first oocyst entered the centre of the electrode array. Reversal of the applied field sequence using the 3 way 4 pole switch, changed the direction of travel for the oocysts remaining over the electrodes so they could be moved to the periphery of the electrode array approximately 900µm away from the centre. The oocyst in the centre was not under the control of the travelling wave as it was resting on the glass substrate. This was repeated successfully with six aliquots to demonstrate repeatability. Collection methods were then tested.

7.6.3 The method for collecting an isolated oocyst

The most reproducible method for collecting the isolated oocyst was through a circular 100 μm hole manufactured in the centre of the electrode array, allowing collection on a filter membrane. To achieve a hole of the desired dimensions, the electrode array was manufactured on a thin polyimide film (Kapton HN® 75 μm thick) using a procedure described below, Figure 7.11.
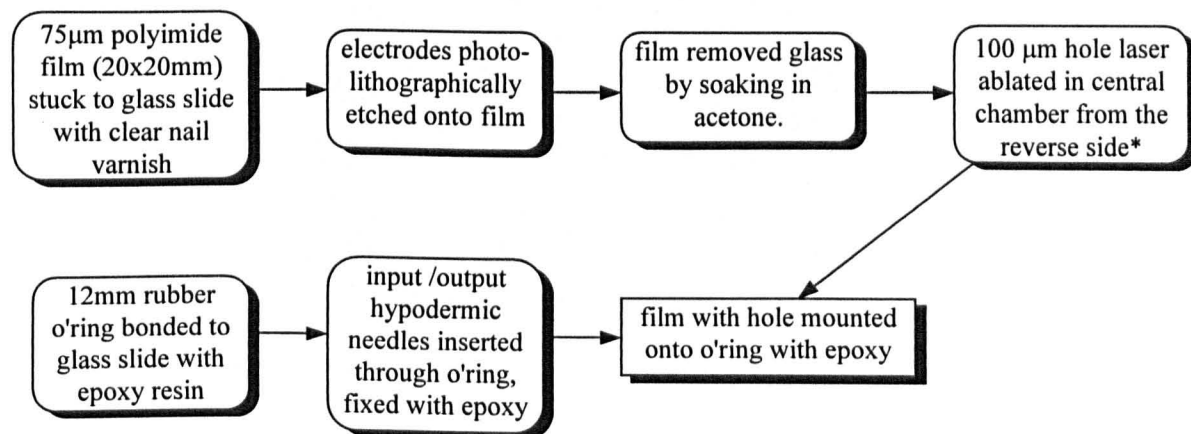
Figure 7.11 Sequence in manufacture of isolating chamber.
* avoids exit debris around hole on electrode face
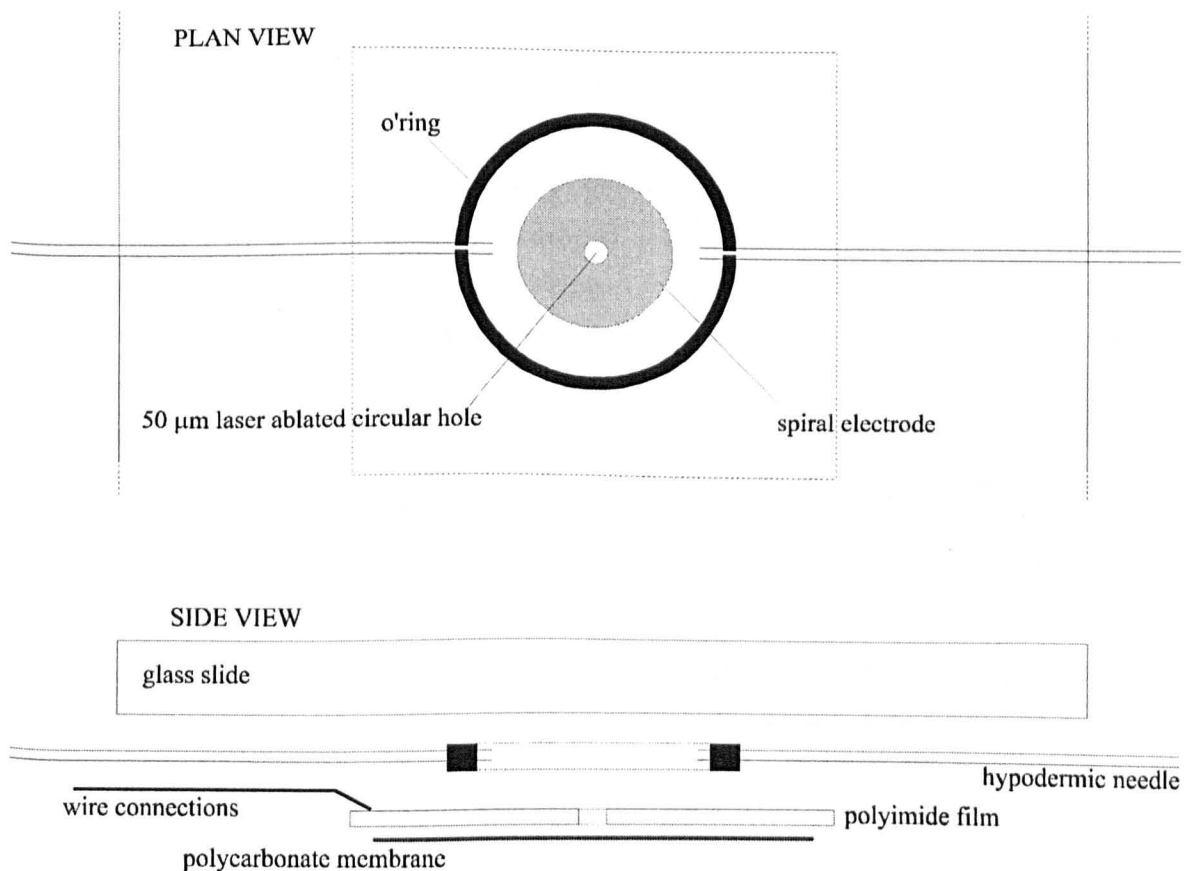
Figure 7.12 Diagram of isolating chamber mounted under a glass slide.
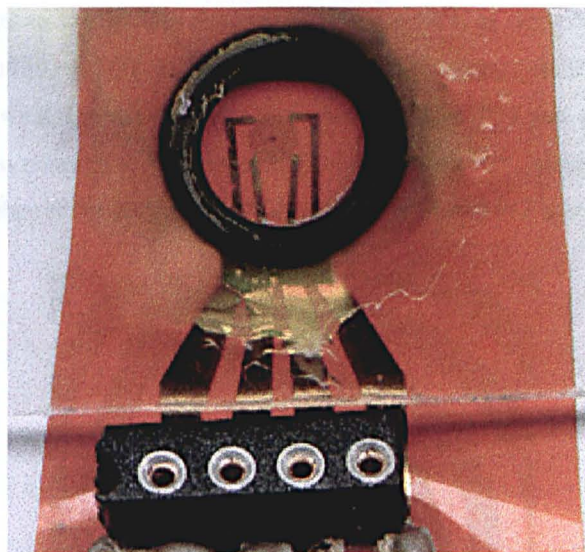
Figure 7.13 Image of the isolating device showing the electrodes with 4 pin SIL socket connector .

7.6.3.1 Excimer Laser Ablation of hole

The hole in the polyimide film was created by laser ablation, using an Exitech Series 8000 micro-machining workstation, incorporating a Lambda Physik Compex 110 krypton fluoride Excimer laser operating at $\lambda = 248$ nm. The term Excimer originates from the fact that pulsed high voltages are used to excite a dimeric gas, e.g. ArF, XeCl or KrF to a high electron state. These normally inert gases remain at an excited state for 5 to 15 ns, and on reforming at the ground state emit UV photons.

The beam delivery system contains beam shaping and homogenisation optics to create a uniform spot at the plane of a mask held on an open-frame CNC (computer numerically controlled) XY stage. For this work the mask was made simply by drilling a 400 μm hole in a thin Copper-Beryllium sheet. A projection lens of magnification 0.25 then transfers the pattern of the mask on to the workpiece, which is mounted on precision air-bearing XY stages.

Ablation occurs as the pulses of UV light interact with the polymer causing photochemical decomposition. Particles (mostly elemental carbon) are ejected at supersonic speeds accompanied by an audible acoustic crack.

7.6.3.2 Isolation Procedure

A 5ml syringe attached to the input hypodermic needle via a 20cm length of rubber tubing ($\varnothing = 6$mm) was used to fill the chamber mounted on a normal microscope stage. A shorter length of tubing attached to the output needle allowed all air bubbles to be removed, this was then clamped. The pre-wetted 13mm polycarbonate membrane (pore size 3μm) was placed under the polyimide film to capture the oocyst.

A dilute suspension of oocysts was injected into the inlet tubing via a hypodermic syringe. Then, the electrodes were energised to manipulate one oocyst to the centre, as described in section 7.6.2. After briefly checking the viability by ROT and with fluorescent microscopy (via DAPI / PI) the oocyst, under the influence of gravity went through the hole, presented in Figure 7.14 and onto the membrane. That a single oocyst was on the membrane was then checked by fluorescent microscopy. An example of an oocyst captured on the fibre of the polycarbonate membrane is shown in Figure 7.15.
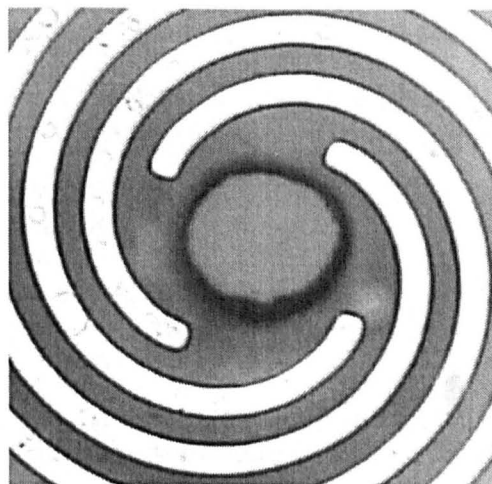
Figure 7.14 The 100 µm diameter hole in the centre of the spiral electrode array.

Figure 7.15 Highlighted region showing the 5 µm oocyst captured on a polycarbonate membrane fibre.

7.7 References

Burt, J.P.H., Chan, K.L., Dawson, D., Parton, A. & Pethig, R. (1996) Assays for Microbial-Contamination and DNA Analysis Based On Electrorotation. *Annales de Biologie Clinique*, **54**: 253-257.

Campbell, A., Robertson, L, & Smith, H.V. (1992) Viability of *Cryptosporidium parvum* oocysts - Correlation of *in vitro* excystation with inclusion or exclusion of fluorogenic vital dyes. *Applied and Environmental Microbiology.* **58**: 3488-3493.
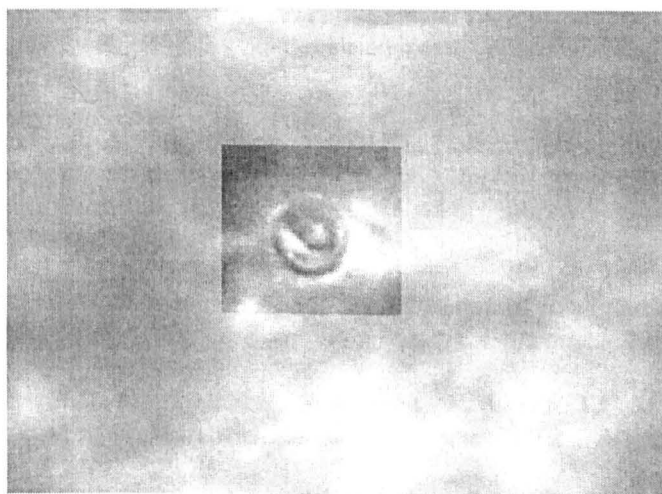
Flanagan, T., Whalen, C., Turner, J., Soave, R., Havlir, D. & Kotler, D. (1992) *Cryptosporidium* infection and CD4 counts. *Annals of International Medicine.* **116**: 840.

Fuhr, G., Schnelle, T., Müller, T., Glasser, H., Lisec, T. & Wagner, B. (1995) *Sensors Materials.* **7**: 131-146.

Fuhr, G. & Hagedorn, R. (1996) Cell Electrorotation. *In: Electrical Manipulation of Cells.* (Ed. P.T. Lynch & M.R. Davey) Chapman & Hall, New York pp37-70.

Goater, A.D., Burt, J.P.H. & Pethig, R. (1997) A combined travelling wave dielectrophoresis and electrorotation device: applied to the concentration and viability determination of *Cryptosporidium. Journal of Physics D-Applied Physics*, **30**: L65-L69.

Green, N.G, Hughes M.P., Monaghan W. & Morgan H. (1997) Large area multilayered electrode arrays for dielectrophoretic fractionation. *Microelectronic Engineering.* **35**: 421-424.

Hagedorn, R., Fuhr, G., Muller, T. & Gimsa, J. (1992) Travelling-Wave Dielectrophoresis of Microparticles. *Electrophoresis.* **13**: 49-54.

Huang, Y., Wang, X-B., Tame, J.A. & Pethig, R. (1993) Electrokinetic Behaviour of Colloidal Particles in Travelling Electric Fields - Studies Using Yeast-Cells. *Journal of Physics D-Applied Physics.* **26**: 1528-1535.

Markx, G.H., Pethig, R. & Rousselet, J. (1997). The dielectrophoretic levitation of latex beads, with reference to field-flow fractionation. *Journal of Physics D-Applied Physics.* **30**: 2470-2477.

Marx, B.R. (1997) *Laser Focus World* **33**: 19-20.

Masuda, S., Washizu, M. & Iwadare, M. (1987) Separation of small particles suspended in liquid by nonuniform travelling fields. *IEEE Transactions on Industry Applications.* **23**: 474-480.

Morgan, H., Green, N.G., Hughes, M.P., Monaghan, W. & Tan, T.C. (1997) Large-area travelling-wave dielectrophoretic particle separator. *Journal of Micromechanics & Microengineering.* **7**: 65-70.

Pohl, H.A. (1978) *Dielectrophoresis* Cambridge University Press, Cambridge.

Talary, M.S., Burt, J.P.H., Tame, J.A. & Pethig, R. (1996) Electromanipulation and separation of acells using travelling electric fields. *Journal of Physics D- Applied Physics.* **29**: 2198-2203.

Wang, X-B., Huang, Y., Wang, X., Becker, F.F. & Gascoyne, P.R.C. (1997) Dielectrophoretic manipulation of cells with spiral electrodes. *Biophysical Journal.* **72**: 1887-1899.

Williams, R.B. (1997) A self-filling micropipette for the isolation of single coccidial oocysts. *Research in Veterinary Science.* **62**: 301.

Chapter 8

Electrorotation of oocysts from *Cryptosporidium* species not infective to humans.

8.1 Cryptosporidium species other than *C. parvum*

As described in section 3.2.1 at least seven valid species of *Cryptosporidium* have been identified. Several isolates have also been recognised by various techniques. As only the oocysts of *C. parvum* are infective to man it is useful, not only to determine viability, but also to distinguish between the different species for predicting the disease-causing potential of oocyst-contaminated environmental samples.

8.1.1 *C. muris*

The type species of the genus *Cryptosporidium* (Tyzzer, 1910) *C. muris* is not infective to humans. As well as mice (the original host) infection with *C. muris* has been found in various species, including camels, cattle and other rodents. Dogs are not considered good hosts, cats have a single reporting. Isolate differences have been noted, for example *C. muris* from cattle was not found infectious to a variety of rodents (Koudela, Modry & Vitovec, 1998). As well as possessing much larger oocysts, *C. muris* differs from *C. parvum* in its site of development. *C. muris* develops higher up the gut than *C. parvum*, in the gastric-epithelia of mice (Current & Reese, 1986). In cattle, *C. muris* infections occur in the peptic and pyloric glands, and lesions include dilation of glands and hypertrophy of the gastric mucosa. The abomasum of severely infected animals can be two to three times the normal weight (Anderson, 1987). High prevalence rates have been reported in cattle, positive samples were found at 68% out of 150 dairies and 80% out of 30 feedlots investigated in the US (Anderson, 1991). Although not infectious to man, they can be of economic significance; cows shedding *C. muris* oocysts produced significantly less milk (approximately 3.2 kg/d) (Esteban & Anderson, 1995). *C. muris* has also been reported from cattle in the UK (Bukhari & Smith, 1996) although at a low prevelence rate (4/109 adult cattle). From the same 109 cattle 21 were found to be shedding *C. parvum* oocysts.

8.1.2 *C. baileyi*

A third species that is often, through domestic poultry, in close contact to man is *C. baileyi* first described by Current, Upton & Haynes (1986). Originally found in broiler chickens (*Gallus domesticus*) the life cycle of this species differs slightly from that of *C. parvum* in having 3 generations of shizonts (compared with 2 generations) containing 8, 4 and 8 merozoites respectively. Stages were found sequentially in the microvillus regions of the enterocytes of the ileum, large intestine, cloaca and Bursa of Fabricius, as well as causing upper respiratory infections when challenged at this site. Indeed, *C. baileyi* may enhance the severity of respiratory disease caused by other avian pathogens such as infectious bronchitis virus (IBV) (Blagburn *et al.*, 1991). Oocysts of *C. baileyi* have also been identified in turkeys and in the wild, chicks

of black-headed gulls (*Larus ridibundus*) (Pavlasek, 1993). Interestingly, oocysts of this species have been successfully cultured in embryonated chicken eggs (Wunderlin, Wild & Eckert, 1997).

In addition to host specificity's, other features that have been used to distinguish the species of *Cryptosporidium* include their morphology. Dimensions of oocysts from six *Cryptosporidium* spp. are given in Table 8.1 and summarised graphically in Figure 8.1.

Species	Original Host	Author	Oocyst length (μm)	Oocyst width (μm)	Shape index (l/w)
C. muris	Mus musculus	Tyzzer, 1910	6.6-7.9 (7.4)	5.3-6.5 (5.6)	1.1-1.5 (1.3)
C. parvum	Mus musculus	Tyzzer, 1912	4.5-5.4 (5.0)	4.2-5.0 (4.5)	1.0-1.3 (1.1)
C. meleagridis	Meleagridis gallopavo	Slavin, 1955	4.5-6.0 (5.2)	4.2-5.3 (4.6	1.0-1.3 (1.1)
C. serpentis	Elaphe guttata	Levine, 1980	5.6-6.6 (6.2)	4.8-5.6 (5.3)	1.0-1.3 (1.2)
C, nasorum*	Naso literatus	Hoover, 1981	3.5-4.7 (4.3)	2.5-4.0 (3.3)	0.9-1.9 (1.3)
C. baileyi	Gallus gallus	Current et al., 1986	6.0-7.5 (6.6)	4.8-5.7 (5.0)	1.0-1.8 (1.3)

Table 8.1 Morphometric features of oocysts from *Cryptosporidium* species.
Ranges with mean values in parenthesis (adapted from Arrowood, 1997).
* = Calculations based on electron micrograph measurements, so possible error due to shrinkage during dehydration procedure.
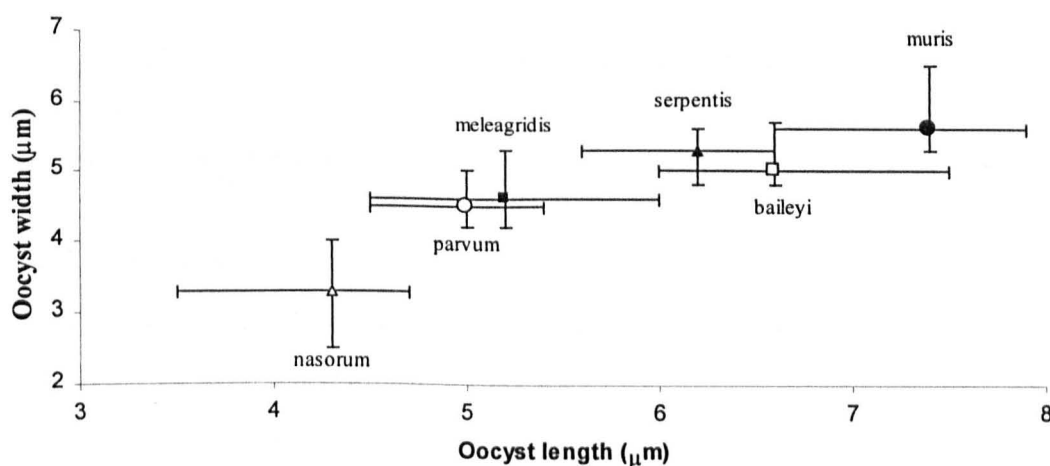
Figure 8.1. Mean (symbols) maximum and minimum (error bars) dimension observed for oocysts of six *Cryptosporidium* species.

From Figure 8.1 it can be seen that there is overlap between the oocyst dimensions of *C. baileyi* and *C. muris*. Although noted by some (H.V. Smith pers. com.), these data do not show an overlap between the oocysts of *C. parvum* and *C. baileyi*, however, there is overlap in their widths. Unless the oocysts are lying flat on the substrate, there could be some confusion in the measurements taken, for example an oocyst attached to some debris might only reveal an end on profile. Dielectrophoretic alignment of particles, as seen with pearl chaining, could assist with this potential problem. Of these three species, based on dimensions alone it is only possible to clearly distinguish between *C. parvum* and *C. muris* (i.e. no overlap in either axis).

As morphology is unable to distinguish some species, other more reliable methods are required. Analysis by PCR has shown promise. PCR products from a 1750 base pair product of the *Cryptosporidium* 18S rRNA gene were resolved electrophoretically into RFLP profiles that were distinct for *C. muris*, *C. parvum* and *C. baileyi* (Leng, Mosier & Oberst, 1996). This method did not, however, give information on the viability of the oocysts, which for *C. muris* and *C. baileyi* would be of use for studies of the infective dose or the effect of disinfectants. PCR is also a destructive method, whereby the speciated oocysts are not available for analysis by other techniques.

Electrorotation data collected from oocysts of *C. baileyi* and *C. muris* are presented in this chapter, for interspecific comparisons.

8.2 Electrorotation of *C. baileyi* oocysts as a function of storage time at 4°C.

A suspension of *C. baileyi* oocysts in tap water were obtained from the SPDL (Glasgow). After washing in deionised water, the oocyst suspension was stored at 4°C before use. At days 1, 14, 23, 31 and 40 storage, 100μl of the stock suspension was washed as described in previous chapters. A total of 63 ROT spectra were obtained, at a suspending medium conductivity of 5μS cm^{-1}. As no viability stains have been reported as tested on the oocysts of *C. baileyi*, none were used in this work. It was noted, that in a mixed sample of *C. baileyi* and *C. parvum* that had been incubated with DAPI and PI that only the *C. parvum* oocysts stained consistently.

The *C. baileyi* oocysts observed were categorised morphologically into five groups;

- oocysts containing distinct sporozoites, intact oocyst walls (considered potentially viable by phase contrast microscopy)

- oocysts with dark granular cytoplasm contracted from oocyst wall (considered non-viable)

- ghosts (oocyst walls) with protruding sporozoites

- ghosts containing residium (contracted cytoplasm)

- empty ghosts

8.2.1 Results

ROT spectra for each category are presented in Figures 8.1 to 8.4, individual features of which are compared in Table 8.1 below.

Feature	Oocyst category					
	Empty ghost	Ghost with residual body	Ghost with protruding sporozoite	Intact dark granular cytoplasm	Viable by morphology <23 days storage	Viable by morphology >23 day
ROT rate at 100Hz (rotations s⁻¹ V⁻²*100)	0-2.7	0-2.5	2.3	0.3-2.6	1.4-2.9	0.3-1.7
Low frequency crossover (kHz)	4	5	2	2-3	4	5
Range of anti-field peak magnitude (-rotations s⁻¹ V⁻²*100)	0.4-1.9	0.9-3.2	4	1.2-3.5	2.0-4.3	2.6-4.2
Anti-field peak (kHz)	100	60-100	100	40-200	100-200	100-200
High frequency crossover (MHz)	<0.6	0.6-1	1	0.4-0.6	1.0-1.5	1.0-2.5
Co-field peak (MHz)	2	2	2	1.5-3	>4	>4

Table 8.2 Summary of ROT data for the six *C. baileyi* oocyst categories.

8.2.2 Rotation rate at 100Hz

An applied frequency of 100Hz was the lowest at which ROT measurements were undertaken on *C. baileyi* oocysts. Co-field rotations observed at this frequency, showed considerable variation in magnitude, from not rotating (which were checked for adhesion to surface by observing Brownian motion) to ~1.3 rotations /s at 20 V_{pk-pk}.

Of the six oocyst categories, the intact oocysts that were judged viable by morphology showed the only trend with storage time. The rotation rates observed at 100Hz fell in magnitude with increasing storage time, an effect which is clearest if the spectra are grouped into days 1-23, and days 24-40 storage as in Figures 8.4(a) and (b). This drop, which is more clearly shown by a histogram in a direct comparison of the mean ROT rates in Figure 8.6, may be due to a decrease in surface charge, as ions diffuse from the oocyst into the deionised storage media.

8.2.3 Low frequency crossover

The low frequency crossover point, for four of the six categories, was consistently at 4 or 5kHz. For two categories, however, the oocyst ghosts with protruding sporozoites and the intact oocysts with granular cytoplasm, reduced crossovers of 2 to 3kHz were observed.

8.2.4 Anti-field peak magnitude

The two viable categories had generally greater anti-field peaks than the other categories. Inconsistent with this however, was an oocyst ghost with protruding sporozoite that also had a substantial anti-field peak (-0.4 x 10^3 rotations s⁻¹V⁻²). Also, the presence of contents in oocyst ghosts increased the antifield peak rotation rate compared with the ghosts without such bodies. The increase in magnitude due to the residual body was less than for the protruding sporozoites (maximum rates; empty shell -0.19, with residual body -0.32, with protruding sporozoite -0.4).

8.2.5 Anti-field peak frequency

Upper ranges for intact oocysts were higher at 200kHz compared with the three oocyst ghost categories, however, there was considerable overlap. Only the ghosts with residual bodies and the dark cytoplasmic oocysts had anti-field peaks below 100kHz.

8.2.6 High frequency crossover point

Oocysts viable by morphology viewed under phase contrast microscopy, had higher frequency crossover points. There was overlap between the viable oocysts and the ghosts with either a residual body or with a protruding sporozoite, but these are easily distinguished. Importantly there was no overlap between the viable oocysts and the intact (but with dark cytoplasm) oocysts.

8.2.7 High frequency co-field peak

No true co-field peaks for the viable categories were observed as the frequencies investigated were too low; a limitation of the equipment used. All other categories had peaks at approximately 2 MHz. The intact but dark granular oocysts showed a range of values which would be consistent with oocysts at different stages of deterioration.
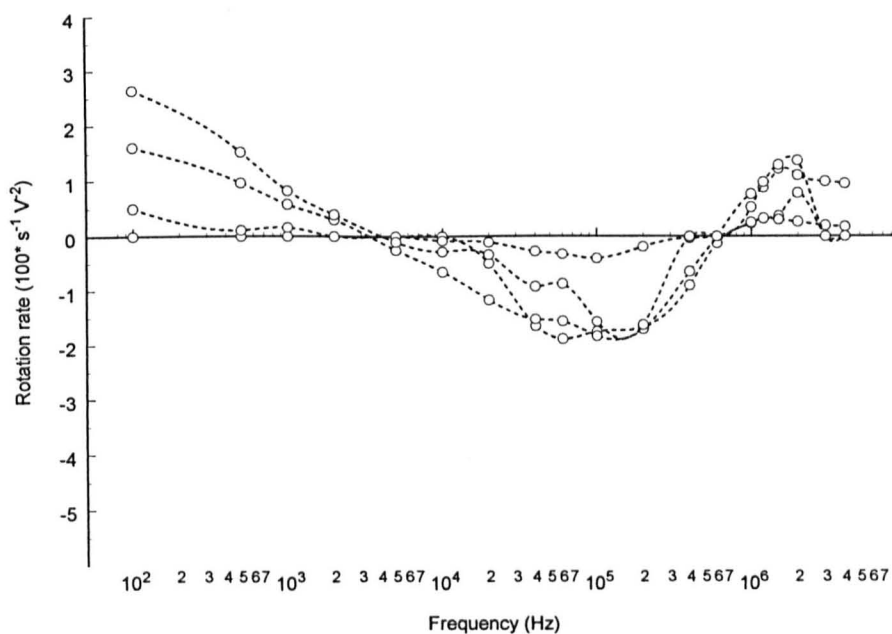
Figure 8.2 Four ROT spectra of empty *C. baileyi* oocyst ghosts.
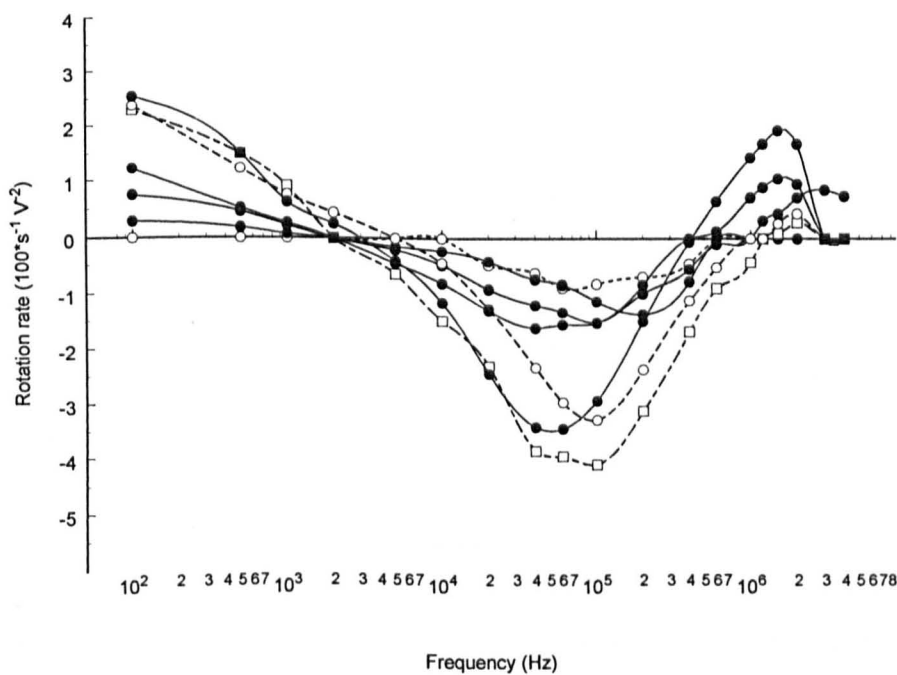
Figure 8.3 ROT spectra of two oocyst ghosts with residual bodies (- o -), a ghost with protruding sporozoite (- □ -) and four oocysts with non-refractile dark granular contents (•).
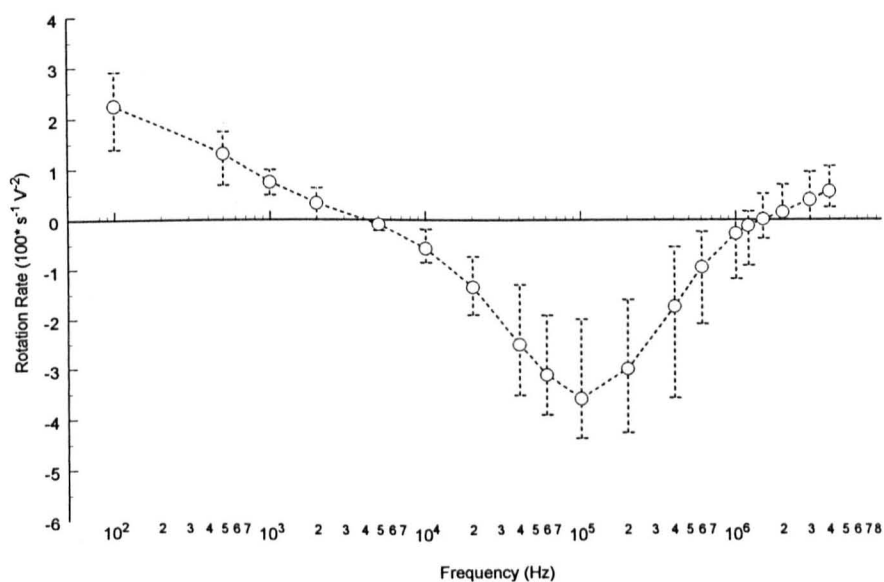
Figure 8.4(a) Mean ROT rates (- o -) with ranges shown for (n=29) *C. baileyi* oocysts with distinct sporozoites and intact oocyst walls, which were considered viable by morphological indicators assessed by phase contrast microscopy, <23 days of storage in ultra pure water.
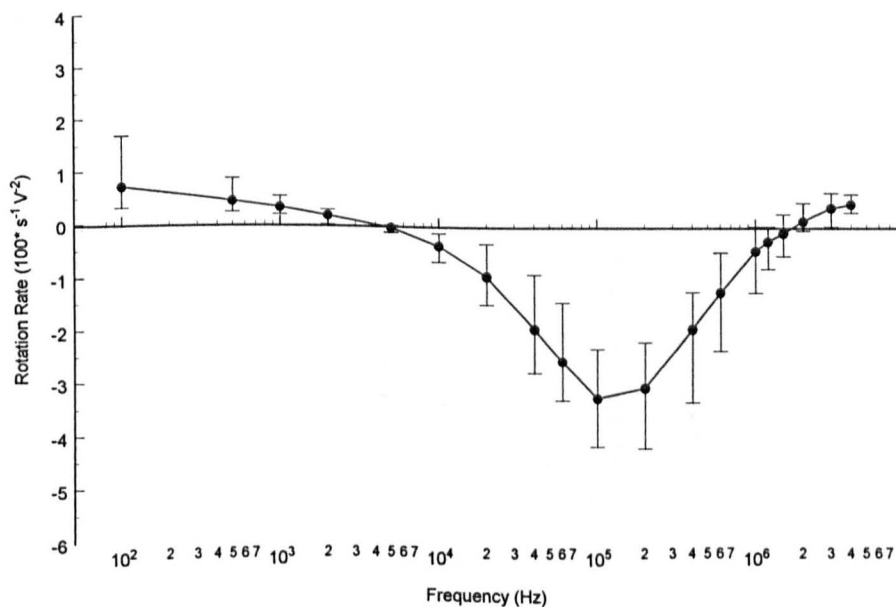
Figure 8.4(b) Mean ROT rates with ranges shown for (n=24) oocysts after 24-40 days storage in ultra pure water.
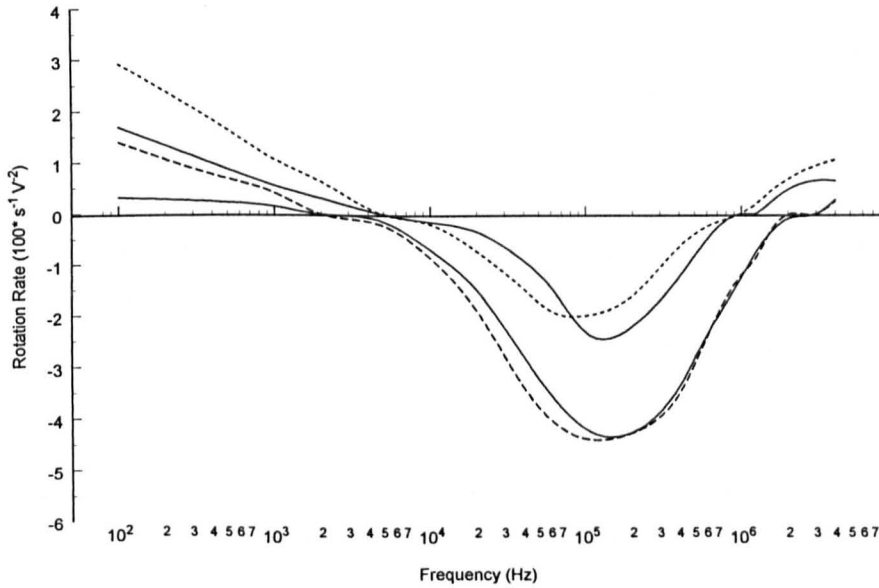
Figure 8.5 A direct comparison between the ranges of ROT rates for viable *C. baileyi* oocysts after days 1-23 (between upper and lower - - lines) and days 24-40 (between upper and lower — lines) storage.
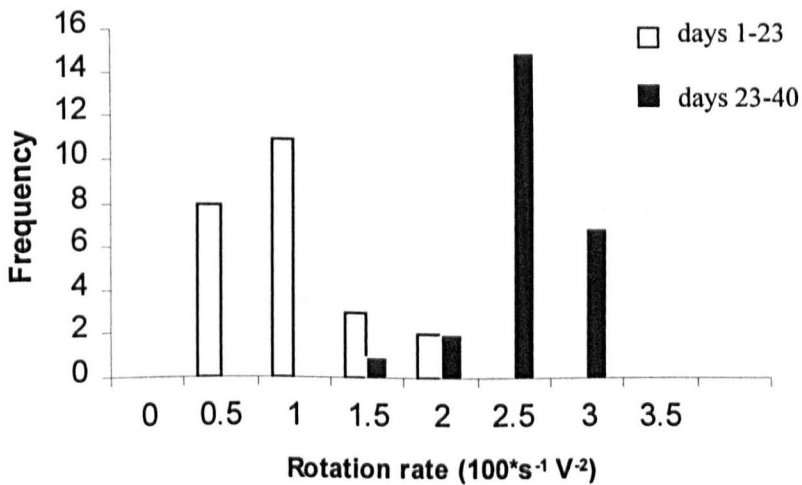
Figure 8.6 Histogram comparing the rotation rates of viable *C. baileyi* oocysts at at 100Hz.

8.3 Electrorotation of *C. muris* oocysts

A suspension of *C. muris* oocysts stored in tap water was obtained from the SPDL, Glasgow. After washing in ultra pure water, by centrifugation, the oocyst suspension was stored at 4°C before use (storage time = 0). At days 1, 2, 9, 23 and 40 storage, 100μl of the stock suspension was washed as described in previous chapters. A total of 68 ROT spectra were obtained, at a suspending medium conductivity of 5 μS cm^{-1}.

As with the oocysts of *C. baileyi*, no viability stains have been optimised for the oocysts of *C. muris*. It was observed, however, that in mixed samples of *C. muris* and *C. parvum* oocysts that had undergone the DAPI and PI staining procedure, without the acidification step, a proportion (>50%) of the *C. muris* oocysts did indeed include one or both of the stains and so the viability of this proportion could be assessed. In the following experiments the staining procedure was used, to test if the ROT technique could reveal any differences between those that do and those that do not stain. The pre-acidification step was not used as oocysts failing to stain was considered an interesting category from which to collect data for comparison. The ROT spectra obtained were categorised as follows:

- intact oocysts with distinct sporozoites whose nuclei include DAPI, which were also considered viable by morphological indicators such as intact oocyst walls, observed by phase contrast microscopy

- intact oocysts that included both DAPI and PI, considered non-viable

- intact oocysts considered viable by morphology but which failed to stain with either DAPI or PI

- ghosts with protruding sporozoites (staining with PI)

- ghosts containing residium (contracted cytoplasm)

- empty ghosts

ROT spectra for each category are presented in Figures 8.7 to 8.11, individual features of which are compared in Table 8.3 below.

Feature	Oocyst category					
	Empty ghost	Ghost with residual body	Ghost with protruding sporozoites	Morphologically viable but non-staining	Non-viable by DAPI and PI stains	Viable by DAPI and PI staining
ROT rate at 100Hz (rotations s^{-1} V^{-2}*100)	0-0.5	0-0.5	0.6	0.1-1.7	0.0-0.6	0.1-1.0
Mean low frequency crossover (kHz)	1	1-2	2	2	1	2
Range of anti-field peak magnitude (-rotations s^{-1} V^{-2}*100)	0.0-1.4	0.2-3.2	1.5	2.2-4.4	1.0-2.4	1.9-4.5
Anti-field peak (kHz)	100	60-200	100	60-100	100	100
High frequency crossover (MHz)	<1.0	0.2->4	0.4	0.8-1.5	0.4-0.9	0.9-2.5
Co-field peak (MHz)	1.5	>4	3	>4	>4	>4

Table 8.3 Summary of ROT data for the six *C. muris* oocyst categories.

8.3.1 Rotation rate at 100Hz

As with the oocysts of *C. baileyi*, rotations of *C. muris* oocysts observed at 100Hz were all in the cofield direction, however, the magnitudes of rotation were significantly lower. Only 2 of 68 oocysts exceeded a rate of 0.1×10^3 rotations s^{-1} V^{-2} compared with 35 of 60 *C. baileyi* oocysts. Unlike *C. baileyi*, no trend with storage time was noticed for the magnitude of the rotation at 100Hz for *C. muris*. A correlation was observed however, between oocysts that appeared morphologically viable but failed to stain viable, those not staining had much higher rotation rates.

8.3.2 Low frequency crossover

Three of the four comparable *C. muris* categories had significantly lower crossover frequencies, when compared with those for oocysts of *C. baileyi*. For each of these a drop in frequency of around 3kHz was found. The low frequency crossover for the other category that was common to both species stayed at around 2kHz.

8.3.3 Anti-field peak magnitude

Like other oocysts investigated from this genus, *C. muris* oocyst types can be ranked according to their anti-field peak magnitudes. Empty ghosts had the lowest magnitudes, followed by ghosts containing a residual body or a protruding sporozoite, non-viable oocysts and finally the viable class. Again, the appearance of bacteria on the surface of the oocysts was shown to reduce the rotation rate when present on both viable oocysts and on an oocyst ghost, illustrated in figures 8.7, 8.9. and 8.11.

8.3.4 Anti-field peak frequency

No significant differences were observed between the antifield peak frequencies of *C. muris* and *C. baileyi* oocysts.

8.3.5 High frequency crossover point

Differences between viable and non-viable oocysts were again found at the high frequency crossover point. A frequency of 900kHz at this medium conductivity ($5\mu S$ cm^{-1}) distinguished the two types, with the exception of a ghost containing a residual body which failed to show a crossover even at 4MHz, therefore it also did not exhibit a co-field peak.

8.3.6 Co-field peak frequency

Co-field peaks were only observed for empty shells (1.5MHz) and for a shell with a protruding sporozoite (3MHz). For all other categories no co-field peaks were observed below 4MHz. This is in contrast to the observations of the oocysts of *C. baileyi* for which co-field peaks were observed for all non-viable groups.
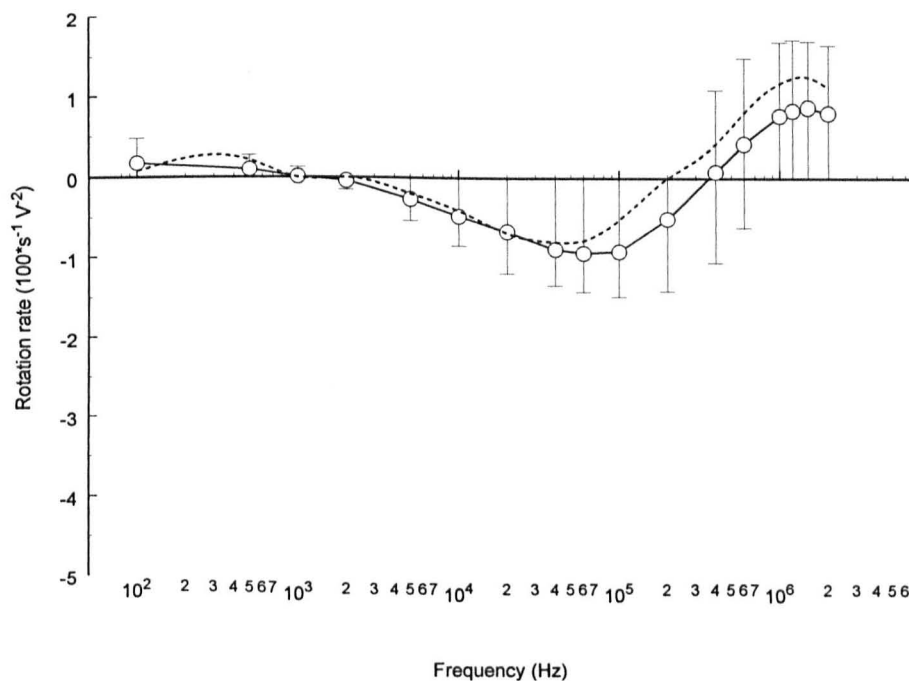
Figure 8.7 **Mean ROT rates (-o-) with ranges shown for (n=12) empty *C. muris* oocyst ghosts and one with adherent bacteria (- -).**
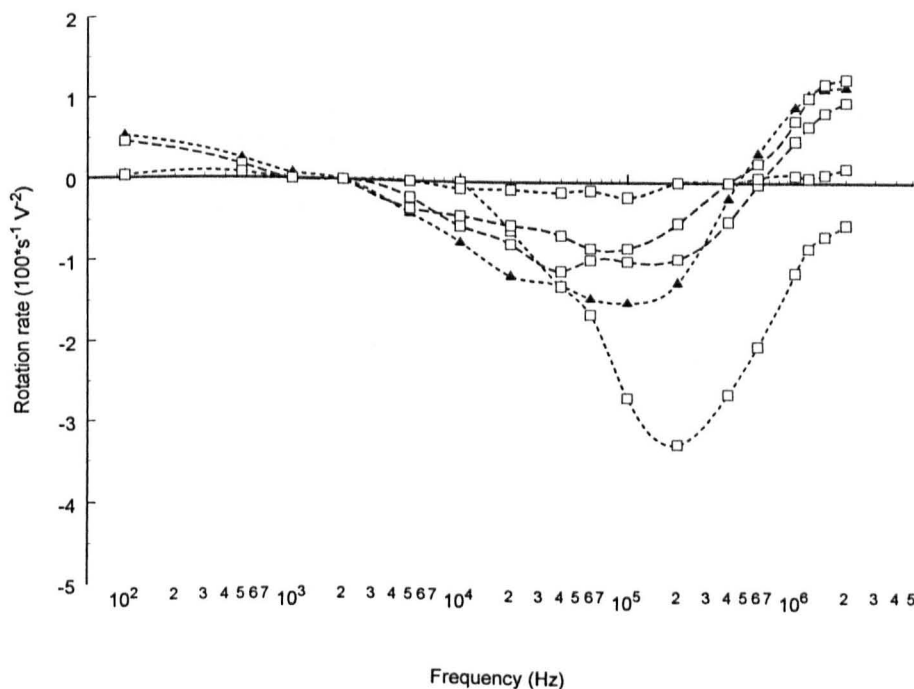
Figure 8.8 **ROT spectra of four *C. muris* oocyst ghosts with residual bodies (- □ -) and a ghost with a protruding sporozoite (- ▲ -).**
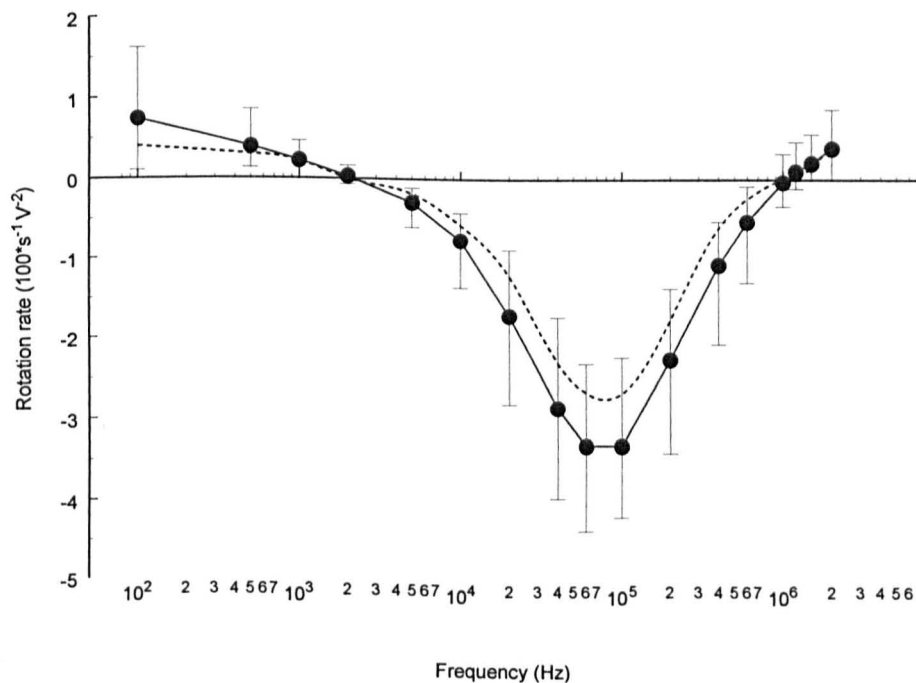
Figure 8.9 Mean ROT rates (-•-) with ranges shown for (n=20) *C. muris* oocysts considered viable by phase contrast microscopy (distinct sporozoites and intact oocyst walls) that were exposed to the full staining procedure (DAPI /PI) but failed to stain.
Also shown is one, as above, but with a bacterium adherent to the oocyst surface (- -) (also unstained).
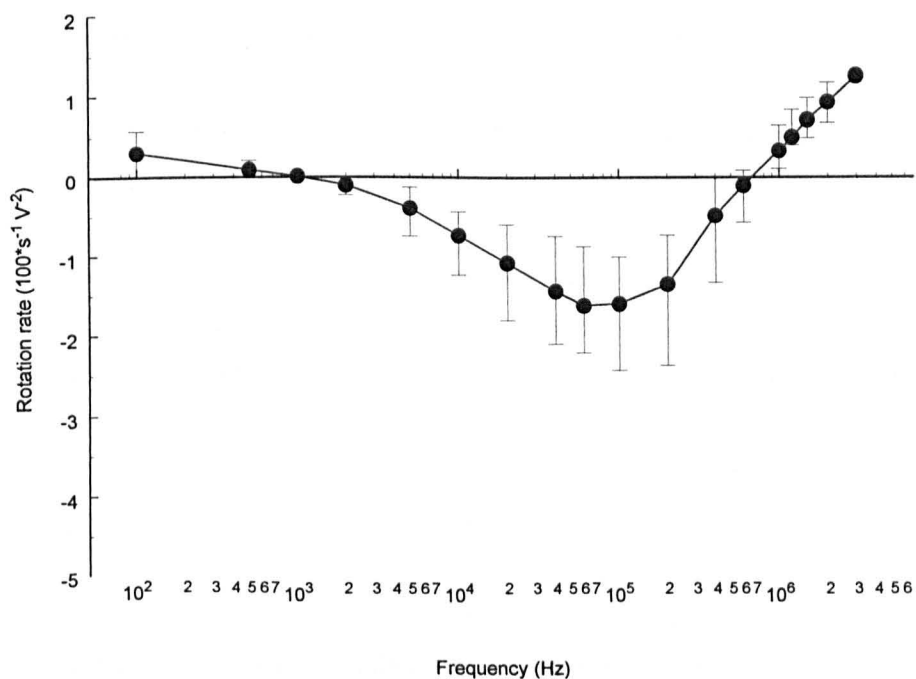
Figure 8.10 Mean ROT rates (•) with ranges shown for (n=10) *C. muris* oocysts considered non-viable by inclusion of both DAPI and PI.
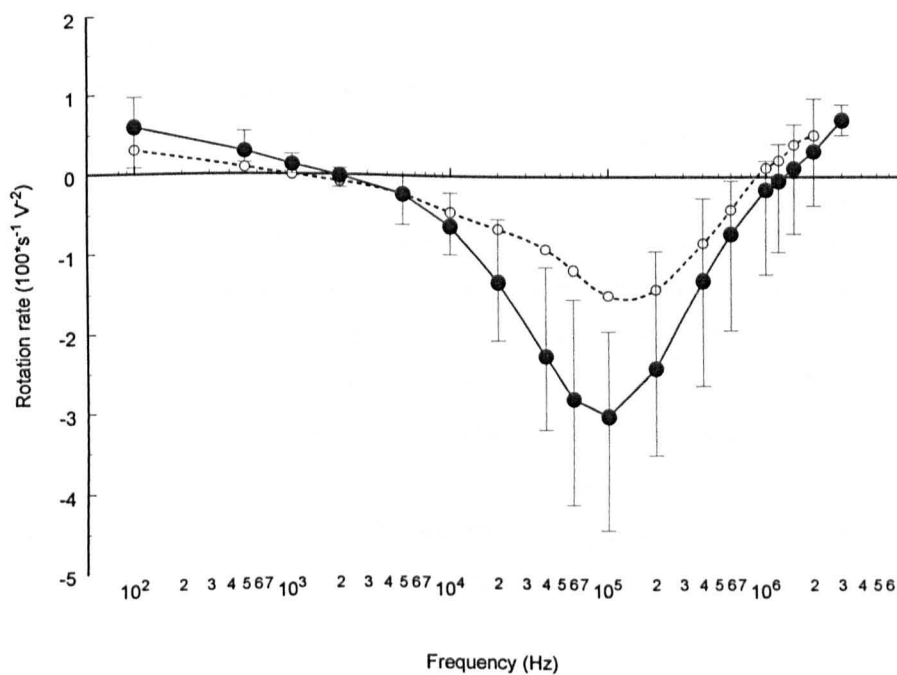
Figure 8.11 Mean ROT rates (•) with ranges shown for (n=13) viable *C. muris* oocysts (DAPI+/ PI-). Also shown is a spectrum for a viable oocyst with an adherent bacterium (- o -) demonstrating a reduced rotation rate.

8.4 Conclusions

C. baileyi spectra

The general pattern of ROT spectra for *C. baileyi* is the same as seen for *C. parvum*. Interestingly an effect of storage time was noted, whereby the magnitude of the low frequency co-field rotation decreased. Summarised in Figures 8.5 and 8.6, this effect was pronounced when the magnitude was recorded before and after 23 days storage. One possible explanation is the amount of energy stores left in the oocyst over time.

For example, if there was an active maintenance mechanism of the oocyst wall then energy would be required. As finite energy resources are available within the oocyst, maintenance of the oocyst wall can only be sustained for a limited period. Thereafter a deterioration in the state would be expected, which could result in a change in the electrical properties of the wall. Similarities between this work and that of Drozd & Schwartzbrod (1996) who measured zeta potentials (a measure of the surface potential) of *C. parvum* oocysts over time are noted. They reported that purified oocysts showed no significant decrease in zeta potential after 2 weeks storage in deionised water, but a slight decrease after 1 month.

Overlaps between the spectra of the different categories occur at most frequencies, however, the spectra for the viable oocysts had one distinguishing feature, the absence of a co-field peak below 4 MHz. The difference in behaviour of the viable oocysts can be explained in terms of a lower membrane conductivity in parallel with a higher oocyst interior conductivity.

The presence of either a residium or a protruding sporozoite alters the spectrum of an oocyst ghost, so that they overlap with healthy looking oocysts. That they are visually distinct prevents confusion, as does the presence of a co-field peak below 4MHz. Any automated system would therefore need the ability for image recognition.

Comparing *C. parvum* viable oocysts with adherent bacteria (Figures 5.7 and 5.8) with the *C. baileyi* ghosts with protruding sporozoite (Figure 8.3) one can see that different effects are caused by the secondary particle in each case. The primary particle (oocyst) in the *C. parvum* example was viable, the bacteria causing a reduction in rotation rate but little change in the shape of the spectra. This can be explained almost entirely in terms of increased friction between the particle and the medium. With the *C. baileyi* ghost with the protruding sporozoite however, (*cf* Figure 8.2 for examples of ghost only spectra) an increase in the antifield rotation rate from 2 to 4 units, along with an increase in the crossover frequency from 700kHz to 1.2MHz was observed. This is an example of a spectrum shape change as well as a scaling change and so the dielectric properties of the secondary particle must therefore be influencing the rotation response, as well as (minor) frictional effects. Although only based on one example, these are distinct changes in the spectra to a typically more viable type spectra, possibly indicating the physiological state of the sporozoite involved.

C. muris spectra

The effect of an adherent bacterium on the *C. muris* ghost oocyst shown in Figure 8.7 was not significant. Although the spectrum lies to the non-viable side of the mean (of 12 spectra) it was within the range of the empty ghosts.

The ghosts with residual contents (Figure 8.8) had a wide range of response, exhibiting from typically viable to typically non-viable spectra. An oocyst ghost with protruding sporozoite, in contrast to that of the *C. baileyi* example, exhibited a non-viable type spectra, again possibly indicating the viability of the sporozoite involved.

Two examples of viable *C. muris* oocysts with bacterium attached were described (Figures 8.9 and 8.11). These follow the trend observed for *C. parvum* (Figures 5.7 and 5.8) showing a negative scaling effect only due to increased viscous drag.

A comparison between the viable oocysts that did and did not take up the dyes revealed a difference at 100Hz. Higher rates were observed for the non-staining group (maximum of 1.7 cf. 1.0).

No trend with storage time at 100Hz was observed unlike those of *C. baileyi*, suggesting differences in the cyst walls due to surface charge.

If one considers the different host environments from which the oocysts were derived, mammalian versus avian intestinal tracts, then one can see that the oocysts may be subjected to different selection pressures resulting in oocyst walls of slightly different composition.

The avian lower intestine compared with that of mammals differs in a number of respects such as typically large, laterally joining cecae and a generally much shorter rectum (Duke, 1976). These features probably have little influence on the oocysts survival, however, the avian cloaca may affect the oocysts. This chambered structure at the end of the intestine serves the digestive, urinary and reproductive tracts resulting in contact between the faecal matter and the urine, which is of different physical characteristics to that from mammals (Sturkie, 1976). Bird urine, which is usually cream coloured, contains thick mucoid with much uric acid and is hyperosmotic.

8.5   References

Anderson, B.C. (1987) *Veterinary Pathology*. 24: 235.

Anderson, B.C. (1991) Prevalence of *Cryptosporidium muris*-like oocysts among cattle populations of the United-States - preliminary report. *Journal of Protozoology* 38: S 14-S 15.

Arrowood, M.J. (1997) Diagnosis. In : *Cryptosporidium* and Cryptosporidiosis (Ed. R. Fayer) CRC, Boca Raton. p 43-64.

Blagburn, B.L., Lindsay, D.S., Hoerr, F.J., Davis, J.F. & Giambrone, J.J. (1991) Pathobiology of Cryptosporidiosis (*C. baileyi*) in broiler chickens. *Journal of Protozoology* 38: S 25-S 28.

Bukhari, Z. & Smith, H.V. (1996) Detection of *Cryptosporidium muris* oocysts in the faeces of adult dairy-cattle in Scotland. *Veterinary Record.* 138: 207-208.

Current W.L. & Reese, N.C. (1986) A comparison of endogenous development of three isolates of *Cryptosporidium* in suckling mice. *Journal of Protozoology*. 33: 98-108.

Current, W.L., Upton, S.J. & Haynes, T.B. (1986) The life-cycle of *Cryptosporidium baileyi* N. Sp. (Apicomplexa Cryptosporidiidae) infecting chickens. *Journal of Protozoology*. 33: 289-296.

Duke, G.E. (1976) Alimentary canal: Anatomy, Regulation of Feeding, and Motility. In: *Avian Physiology* 4th edn. (Ed. P.D. Sturkie) Springer-Verlag, New York pp 269-288.

Esteban, E. & Anderson, B.C. (1995) *Cryptosporidium muris* - Prevalence, persistency, and detrimental effect on milk-production in a drylot dairy. *Journal of Dairy Science*. 78: 1068-1072.

Koudela, B., Modry, D. & Vitovec, J. (1998) Infectivity of *Cryptosporidium muris* isolated from cattle. *Veterinary Parasitology* 76:181-188.

Leng, X.G., Mosier, D.A. & Oberst, R.D. (1996) Differentiation of *Cryptosporidium parvum, Cryptosporidium muris,* and *Cryptosporidium baileyi* by PCR-RFLP analysis of the 18s ribosomal-RNA Gene. *Veterinary Parasitology* 62: 1-7.

Pavlasek, I. (1993) Black-Headed Gull (*Larus ridibundus* L.), a new host of *Cryptosporidium baileyi* (Apicomplexa, Cryptosporidiidae) *Veterinarni Medicina* 38: 629-638.

Sturkie, P.D. (1976) Kidneys, extrarenal salt excretion, and urine. In: *Avian Physiology* 4th edn. (Ed. P.D. Sturkie) Springer-Verlag, New York. pp 359-383.

Wunderlin, E., Wild, P. & Eckert, J. (1997) Comparative reproduction of *Cryptosporidium baileyi* in embryonated eggs and in chickens. *Parasitology Research* 83: 712-715.

Chapter 9
Electrorotation of human and other animal
Cryptosporidium parvum isolates.

9.1 Introduction to *Cryptosporidium parvum* isolates

Many species exhibit intra-specific variations. An extreme example is that of the parasitic nematode genus *Trichinella*, which includes *T. spiralis* (the cause of a serious and often fatal disease in man known as *trichinosis*). This has a very wide geographical distribution and a large range of host species. As a result more than 300 isolates of the genus are available for laboratory study (Wakelin & Goyal 1996).

Since the first description of the genus *Cryptosporidium* by Tyzzer in 1907 a number of species (*see Table 8.1*) have been recognised. Of these, *C. parvum*, with its world-wide distribution, is a significant cause of diarrhoeal illness in a variety of animals including humans. The zoonotic potential (ability to infect different host species) of *C. parvum* is extensive, its oocysts having been found infectious for virtually all mammal species systematically investigated (>79 to date) (O'Donaghue, 1995). Domestic livestock, pets, feral and wild mammals have all been shown to excrete oocysts of *C. parvum*. Importantly, evidence implying waterborne bovine oocysts as a source of infection and disease in consumers of potable water has been provided (Smith *et al.*, 1989). *Cryptosporidium* oocysts from other vertebrate classes, such as from reptiles and birds have been shown not to infect mammals.

On the basis of a review of cross-transmission studies Levine (1984) concluded that the species *C. parvum* was not valid, instead grouping it within the *C. muris* species, despite occupying a different niche within the type host *Mus musculus*. Now considered a valid species (Fayer, Speer & Dubey 1997) the question has arisen of whether it can be futher subdivided taxonomically. Although no traits of great enough significance within *C. parvum* have yet been reported to merit other taxon status (i.e. sub-species or strains), distinct genotypes have been identified within the species, for example evidence for two distinct human transmission cycles has been given (Peng *et al.*, 1997) based on genetic polymorphisms observed at the thrombospondin-related adhesion protein gene. Morgan *et al.* (1998) have suggested, based on sequences from the 18S DNA and the acetyl CoA synthetase gene, that humans are infected with two distinct genotypes, one common to isolates from cattle, sheep and goats, referred to as 'calf' derived *Cryptosporidium* genotype, another as 'human' derived genotype. They noted also that humans are susceptible to infection with the 'calf' genotype.

So that information of host origin is not lost, oocysts of *C. parvum* from different host species or individuals are referred to as isolates. Differentiating between isolates would provide valuable information, as both population density and land use for animal production increase, there is greater potential for oocysts from septic tanks or run-off from farms, and grazing lands to contaminate water supplies. Contamination can be limited only if the source of oocysts can be traced. A useful test, for

example, would be one that distinguished between oocysts of *C. parvum* from human and from bovine sources.

9.2   Current methods to distinguish isolates

As with other protozoan species, both genotypic and phenotypic polymorphisms have been described for *C. parvum*. Phenotypic differences between isolates have been determined by a number of techniques. In addition to virulence variation between isolates, differences in the resistance to storage in 2% potassium dichromate at 4°C were noted both between human isolates, and between oocysts of human and bovine source (Pozio, 1992). Although many antigens associated with *Cryptosporidium* sp. appear to be conserved, two-dimensional gel electrophoresis highlighted isolate specific sporozoite proteins (Mead *et al.*, 1990). Oocyst antigen extracts analysed by immunoblotting with monoclonal antibodies following sodium-dodecylsulphate polyacrylamide gel electrophoresis (SDS-PAGE) separation, showed differences between isolates of *C. parvum*, with two different banding types found in human isolates, and other banding types seen in calf and lamb isolates (Nichols, McLauchlin & Samuel, 1991). In contrast to the study by Nichols *et al.*, few antigenic differences were found between a number of isolates of *C. parvum* using immunoblotting by Nina *et al.* (1992).

Isozyme typing, has been shown to be effective in identifying species and examining strain variation in related parasites. *Plasmodium falciparum* (one of the four *Plasmodium* species responsible for malaria in man) from different countries were distinguished using isozyme analysis (Walliker, 1985) as were strains of the coccidian *Eimeria* spp. (Shirley, 1986). Differentiation between three species within the *Cryptosporidium* genus was demonstrated with this technique based on Glucose Phosphate Isomerase (Ogunkolade *et al.*, 1993) and later more importantly between human and animal strains of *C. parvum* (Awad-El-Kariem, 1995).

More recently genetic analysis has also shown to be of use. Similar to the results of the antigenic analysis by Nichols (1991), a PCR-RFLP assay distinguished not only between calf and human isolates, but also between two groups of human isolates (Bonnin, 1996). Potentially complicating such methods are the findings of a recent study by Carraway *et al.* (1997) that showed, through RFLP analysis, a possible plasticity of the genetic profile of *C. parvum* isolates following transmission from bovine to human hosts.

A significant drawback of traditional methods for genotypic and phenotypic characterisation, including the methods described above such as Western immunoblotting, and the isoenzyme assay, is the requirement for a relatively large number of parasites. Immunoblotting requires between 10^4 and 10^6 oocysts (Smith H.V. pers comm.) while to yield detectable bands in the starch-gel-electropherograms, between 10^7 and 10^8 excysting oocysts per sample were required (Ogunkolade *et al.*, 1993). Isoenzyme electrophoresis is therefore probably impractical for environmental samples, although it may be useful for clinical samples where oocysts are available in larger quantities. PCR protocols, although generally more sensitive, suffer because of their sensitivities to contaminants. Those tested on material from water were

attributed sensitivities of 1-10 oocysts (Stinear *et al.,* 1996; Rochelle *et al.,* 1997) however, this greatly decreased (at least 5-10 fold) for environmental samples. The lack of an *in vitro* system (as is often possible for bacteria) capable of expanding *C. parvum* isolates for further analysis makes more sensitive methods necessary for analysing oocysts from environmental samples.

Two methods based on observations of individual oocysts, have been reported as showing variations between oocysts from different isolates; namely differences in the excystation rates of oocysts (Robertson, Campbell & Smith 1993) and variations in permeability to the fluorescent vital-dye 4'6-diamidino-2-phenylindole (DAPI) (Campbell, Robertson & Smith 1992).

As the ROT technique has been shown to highlight some differences between *Cryptosporidium* spp., described in the previous chapter, it may also be possible to distinguish between isolates. Supporting this suggestion are findings such as another PCR-RFLP assay, based a fragment of the *Cryptosporidium* oocyst wall protein (COWP) gene, originally sequenced by Lally *et al.* (1992), that has been shown to discriminate between *C. parvum* isolates of human and animal origin (Spano *et al.,* 1997) and the variation in oocyst permeability to vital dyes described above. It is possible, however, that the genotypic differences, such as those found in the COWP gene may be found in the intron regions of the sequence (as opposed to the exons) and so may not necessarily produce a phenotypic change in the oocyst wall protein. In this way, sequence based techniques may always have a potential advantage over phenotypic detection methods such as ROT. As it is being used in these experiments ROT is only probing the products of expressed genes and not differences in the DNA sequence itself, which may or may not be expressed in eukaryotes. Introns are such non-coding regions in eukaryotic genes that once transcribed into RNA molecules are excised by RNA splicing when mRNA is produced. Oocyst permeability variation, as detected by vital dyes, are more likely to be detected by ROT as they both relying on probing the same structures, namely the wall / membrane of the oocyst.

This chapter describes the wider application of electrorotation to a number of *C. parvum* isolates of human and other animal origin. This will further test the use of the ROT assay for *C. parvum* as a means for determining viability while also potentially revealing any isolate differences in the spectra.

9.3   Methods

9.3.1 The isolates

A list of the 10 isolates, and purification procedures used on each sample is given in Table 9.1, as is the approximate age of the oocysts when investigated and storage medium used. All oocyst isolates were purified from faecal samples. Those of human origin were clinical samples from patients that had been collected for diagnostic purposes and subsequently stored at 4°C. Those of isolate 1, from Moredun Animal Health (a division of Moredun Scientific Ltd., Edinburgh) were originally isolated from the faeces of red deer calves (*Cervus elaphus*). This commercial source, maintains the lifecycle by passage through lambs - hence *cervine-ovine*. Isolation and purification from the lamb faeces was by

sedimentation and differential centrifugation according to the method described by Hill *et al.* (1990) whereupon they were stored in Hank's balanced salt solution (HBSS), containing antibiotics, at 4°C until used. The Iowa isolate was originally isolated from male neonatal Holstein calves (*Bos tauris*) by Harley Moon at the National Animals Disease Centre, Ames, Iowa.

9.3.2 Purification

As the electrorotation technique is based on observations of the oocysts induced motion, any debris in contact with the oocysts interferes with the results. A reasonable level of purification was therefore required. Oocysts originally obtained in faecal samples were purified by one of three methods; sucrose density flotation, caesium chloride flotation, or by repeated washes in water. The recovery by the latter technique was poor and so was only performed on two samples that had very high oocyst counts in the faeces, assessed by direct examination of faecal smears.

9.3.3 Determination of *C. parvum* oocyst viability using the fluorogenic vital dyes (DAPI and PI)

The twin fluorogenic dye method using DAPI and PI has been shown to correlate well with *in vitro* excystation (Campbell, Robertson & Smith, 1992). In this study it was used as the indicator of viability, as it has been shown to correlate well with the ROT assay (section 5.7).

Oocysts are considered DAPI+/PI- (viable) only if they do not include PI and if the nuclei of the sporozoites fluoresce a distinctive sky blue under the UV filter block. Those oocysts which are neither PI+ nor ghosts and which show either a rim fluorescence or an absence of fluorescence under the UV filter block are considered DAPI-/PI- (see table 5.1).

9.3.4 Staining with FITC-conjugated anti-*Cryptosporidium* spp. monoclonal antibody (mAb)

Purified oocysts stored at 4°C, were stained with DAPI and PI using the method of (Campbell *et al.*, 1992). In addition, for isolate 1 a fluorescein isothiocyanate (FITC)-conjugated anti-*Cryptosporidium* spp. monoclonal antibody (mAb) (Waterborne Inc.) was used. This genus specific fluorescent label is routinely used as an aid to identification. 100 µl of the working dilution of FITC-conjugated anti-*Cryptosporidium* spp. mAb was added to the 1.5ml microcentrifuge tube containing the stained oocysts and incubated at 37°C in the dark for a further 30 min.

9.3.5 Washing and final preparation

Following incubation with the dyes, the oocysts were washed in deionised water of conductivity 1µS cm⁻¹ four times (centrifugation for 1 minute 30 seconds at 13000g, supernatant removed to 100µl) before resuspension in a solution of water with conductivity of 5 µS cm⁻¹. The conductivity of this solution was adjusted with diluted concentrations of phosphate buffered saline (PBS) solution, monitored with a

Whatman CDM 4010 meter, with a calibrated chamber of cell constant 0.12 cm^{-1} and volume 300μl. Final oocyst concentrations were adjusted to typically 3×10^4 ml^{-1} in a final volume of around 200μl.

20μl of the final suspension was introduced into the electrorotation chamber using a micropipette. The chamber, with interelectrode spacing of 2mm, creates a rotating electric field via four electrodes energised with AC signals, each $90°$ phase shifted to its neighbour. Field strengths of 10 kV m^{-1}, and of frequencies between 100 Hz and 10 MHz were used, generated by a digitally controlled sine wave generator 'Rotogen'.

After introduction of the pipetted sample, a coverslip was placed over the chamber, being kept at a constant height by a spacer (insulating tape) of 150 μm. A minimum of 3 minutes was then allowed for the oocysts to settle onto the glass surface. The electrorotation and fluorescent characteristics of the oocysts in the interelectrode space were monitored using a Nikon Labophot-2 microscope and JVC (TK-1280E) colour video camera, coupled to a VCR for later analysis. Data was only collected for oocysts approximately > 250 μm from the electrode edges as only this area was considered to contain a uniform rotating field.

A direct simultaneous comparison between ROT and this twin stain method was performed initially on *C. parvum* oocysts from a clean known isolate source (isolate 1, Moredun, Edinburgh). A close correlation was found, and so the comparison was extended to a further nine isolates of both human and other animal origin. Effects of purification procedures are also described.

Isolate source	Origin	Oocyst age	Purification method from faeces	Storage media after purification	Total electrorotation spectra obtained
1. Moredun	Cervine-ovine	1 month	Repeated centrifugation	Water	8
2. *PHL Bangor	Human	2 weeks	Sucrose flotation	Water	26
3. **SPDL	Human	3 weeks +	Sucrose flotation	Water	62
4. Arizona [Iowa]	Bovine, passaged through calves	2 weeks to 2 months	CsCl flotation	Water / water + antibiotics[1] + tween	67
5. SPDL	Human	5 months	Sucrose flotation	Water	6
6. Vermont -	Bovine	4 to 15 months	Cs Cl flotation	Water	8
7. SPDL ref 270	Human female	1 month	Sucrose flotation or water wash	Water	29
8. SPDL ref 667	Human	8 months	Sucrose or water wash	Water	30
9. SPDL ref 062	Human	4 months	Sucrose	Water	14
10. SPDL ref 182	Human 2.5 month old male	1.5 months	Sucrose	Water	15

Table 9.1 Summary of the *C. parvum* isolates investigated with the ROT assay.

*PHL   Public Health Laboratory, Ysbyty Gwynedd, Bangor. Wales.

**SPDL   Scottish Parasite Diagnostic Laboratory, Stobhill NHS Trust, Glasgow, Scotland.

[1] Storage media - 0.01% Tween 20 (surfactant, as lots of clumping noted) antibiotics Penicillin-Streptomycin liquid; Gentamicin reagent solution.

9.4 Results

Key features of the spectra obtained are listed below in Tables 9.2 (viable oocysts) and 9.3 (non-viable oocysts) for comparison between the isolates. Of the ten isolates investigated, five had no detectable viable oocysts by the fluorogenic vital dye assay. This was probably due to the increased age of the samples (four of these five samples were ≥4 months old).

Isolate	Magnitude at 100Hz (rotations s^{-1} V^{-2} x 10^2)	Low frequency crossover (kHz)	Antifield peak frequency (kHz)	Antifield peak magnitude (rotations s^{-1} V^{-2} x 10^2)	High frequency crossover (MHz)	High frequency peak (MHz)
**1 (CO)	0.00	1.0-2.0	150-200	3.8-4.4	2.00-2.50	x
2 (Hu)	0.10	0.7-2.0	60- 80	3.4-4.2	1.00-1.50	>4
3 (Hu)	0.00-0.70	0.0-3.0	60-100	3.4-5.1	0.80-1.50	>2
4 (Bo)	0.00-0.40	1.0	100	2.9-4.2	0.80-1.00	>4
5 (Hu)	-	-	-	-	-	-
6 (Bo)	-	-	-	-	-	-
**7 (Hu)	0.00-0.70	2.5	60-100	3.1-4.2	0.90-1.10	x
8 (Hu)	-	-	-	-	-	-
9 (Hu)	-	-	-	-	-	-
10 (Hu)	-	-	-	-	-	-

Table 9.2 Summary of ROT spectra from all isolates (viable oocysts). Origin CO = Cervine-Ovine; Hu = Human; Bo = Bovine. (-) = no data.

Isolate	Magnitude at 100Hz (rotations s^{-1} V^{-2} x 10^2)	Low frequency crossover (kHz)	Antifield peak frequency (kHz)	Antifield peak magnitude (rotations s^{-1} V^{-2} x 10^2)	High frequency crossover (MHz)	High frequency peak (MHz)
**1 (CO)	0.00	0.5	80-250	1.5-3.5	0.80	1.8+
2 (Hu)	0.00	2.0	70	not observed or 1.7*	0.02-0.20	1+
3 (Hu)	0.00-0.52	1.0-5.0	20- 60	0.9-3.7	0.20-0.50	1+
4 (Bo)	0.00-0.40	1.0	60-100	0.8-3.3	0.40-0.70	2+
5 (Hu)	-0.20-0.50	2.0	40- 60	0.6-3.3	0.10-0.80	3+
**6 (Bo)	-0.20-5.20	1.0-4.0	200	3.8	1.10-1.20	6
**7 (Hu)	0.00-0.60	2.0	60	1.6-3.7	0.40-0.80	4
8 (Hu)	0.00- 0.70	2.0	40- 60	1.6-3.7	0.30-0.80	>4
9 (Hu)	0.00- 0.40	1.0	50-150	0.8-3.5	0.20-0.90	1.2+
10 (Hu)	0.50	1.0-2.0	60	1.5-1.7	0.22-0.60	1.2-1.5

Table 9.3 Summary of ROT spectra from all isolates (non-viable oocysts).
* heat killed (autoclave)
**35µS cm-1

9.4.1 Isolate 1

Figure 9.1 below shows possibly the clearest demonstration yet of the effect of membrane integrity on the electrorotation spectrum, showing a single oocyst before (o) and after (•) *in vitro* excystation. The most pronounced differences in the spectrum are in the higher frequency part, notably in the crossover and magnitude of the cofield region, which through modelling correspond to an decrease in the interior conductivity from around 0.5 to 0.2 S/m. This is consistent with the efflux of contents and influx of water during excystation. There is also a clear shift in the spectrum between 20kHz and 200kHz corresponding to an increase in wall conductivity from around 250 to 450 μS cm^{-1}. This could be due, for example, to the exposure of more ionisable groups as the wall is ruptured.
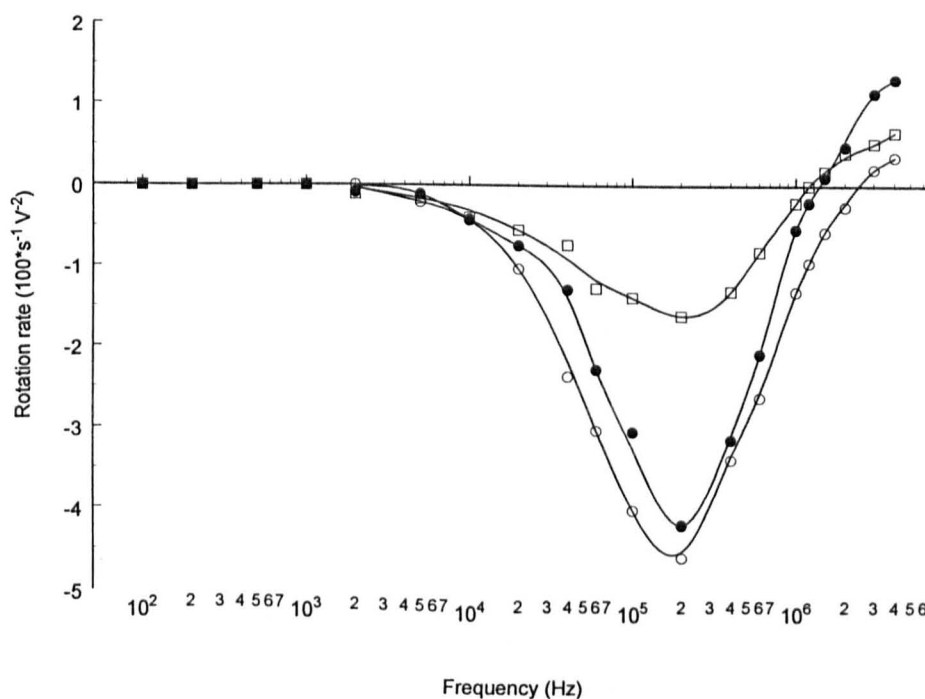
Figure 9.1 ROT spectra of a typical non-viable DAPI+/PI+ (□) oocyst from isolate 1.
Also shown is the transition of a single oocyst spectrum from viable DAPI+/PI- state before (o) and after excystation (•). The later spectrum was recorded within 5 minutes of excystation, the oocyst consisting then of a ghost with residual body. Suspending medium conductivity of 35 μS cm^{-1}. See Plate 3 for images of this excystation event.

Following excystation, the sporozoites were lysed within 30 seconds by the influx of water by osmosis from the suspending medium

Figure 9.2 below, demonstrates that additional antibody labelling of oocysts does not markedly interfere with the ability to distinguish spectra from oocysts of different viability states. Labelling, such as that with the monoclonal antibody (mAb) FITC conjugate (*Cryptosporidium* specific), may assist in the identification of oocysts. In addition these are useful because the antibody paratopes bind surface-exposed oocyst epitopes, the fluorescence visualised therefore defines the maximum dimensions of the organism assisting accurate morphometric analysis. Further assistance in the visualisation of *Cryptosporidium* spp. oocysts has been demonstrated by Campbell *et al.* (1992b) and Grimason *et al.* (1994) who showed that the nuclear fluorochrome 4'6-diamidino-2-phenyl indole (DAPI), which binds to sporozoite DNA, can be used as an adjunct to fluorescence-labelled mAbs for highlighting the four nuclei of the sporozoites in sporulated oocysts.
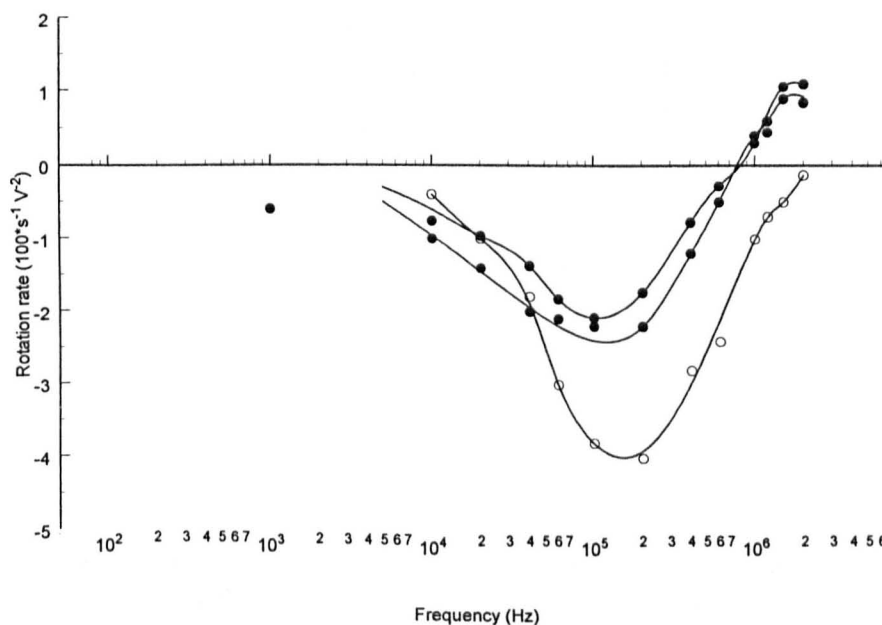
Figure 9.2 ROT spectra of fluorescent-antibody (FITC) labelled isolate 1 oocyst in both non-viable DAPI+/PI+ (•) viable DAPI+/PI- (o) state.
Suspending medium conductivity of 35 μS cm^{-1}.

A summary of all ROT spectra obtained for isolate 1 that had been stained with DAPI and PI, but not with the mAb, is shown in Figure 9.3 below.
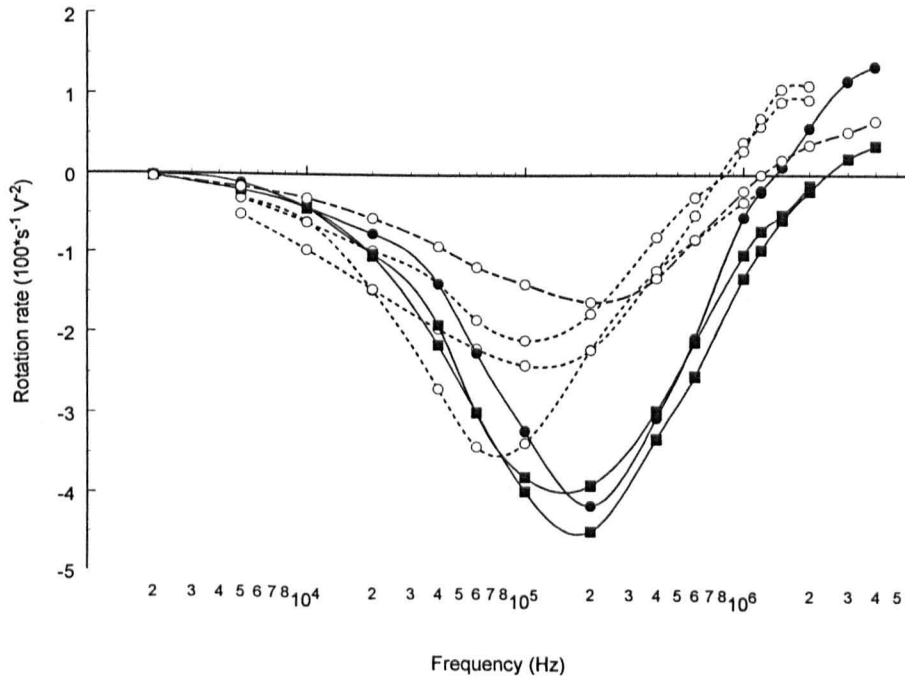
Figure 9.3 Comparison of ROT spectra of viable DAPI+/PI- (-■-) and non-viable DAPI+/PI+ (-o-) isolate 1 oocysts, as well as the freshly excysted oocyst spectrum (-•-).
Suspending medium conductivity of 35 μS cm^{-1}.

9.4.2 Isolate 2

Clear differences are shown between viable and non-viable oocysts of isolate 2 in Figure 9.4 below. Although all intact, the non-viable oocysts had very diffuse staining with both the DAPI and PI dyes. The spectra for this group resemble those seen previously for ghost oocysts. A less dramatic difference is seen between the viable and heat killed (autoclaved) spectra of Figure 9.5.
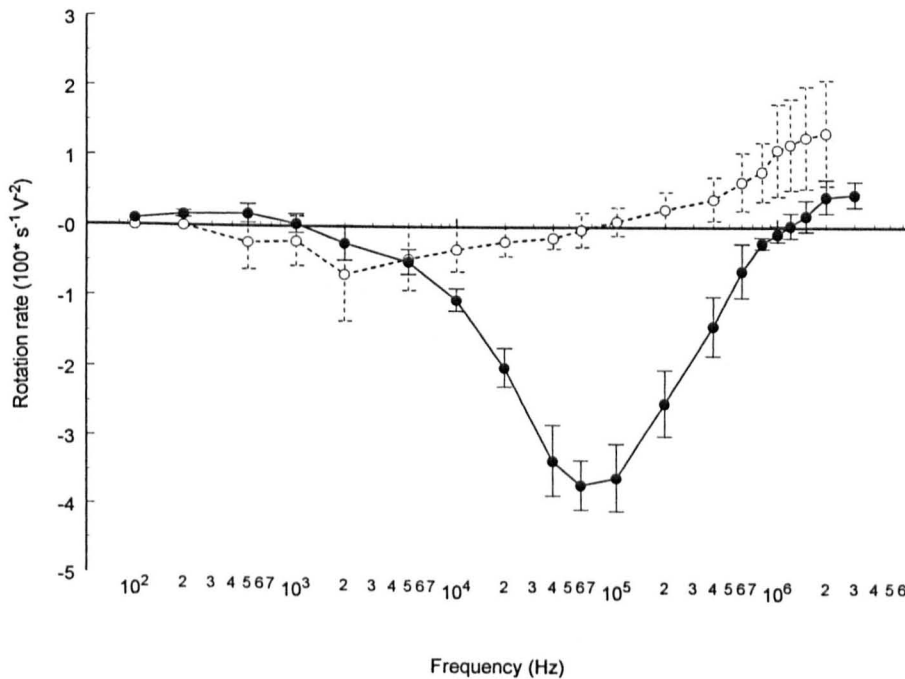
Figure 9.4 Mean rotation rates with error bars showing ranges for (n=12) viable DAPI+/PI- (•) and (n=12) non-viable DAPI+/PI+ (o) oocysts of isolate 2.
Suspending medium conductivity of 5 μS cm⁻¹.
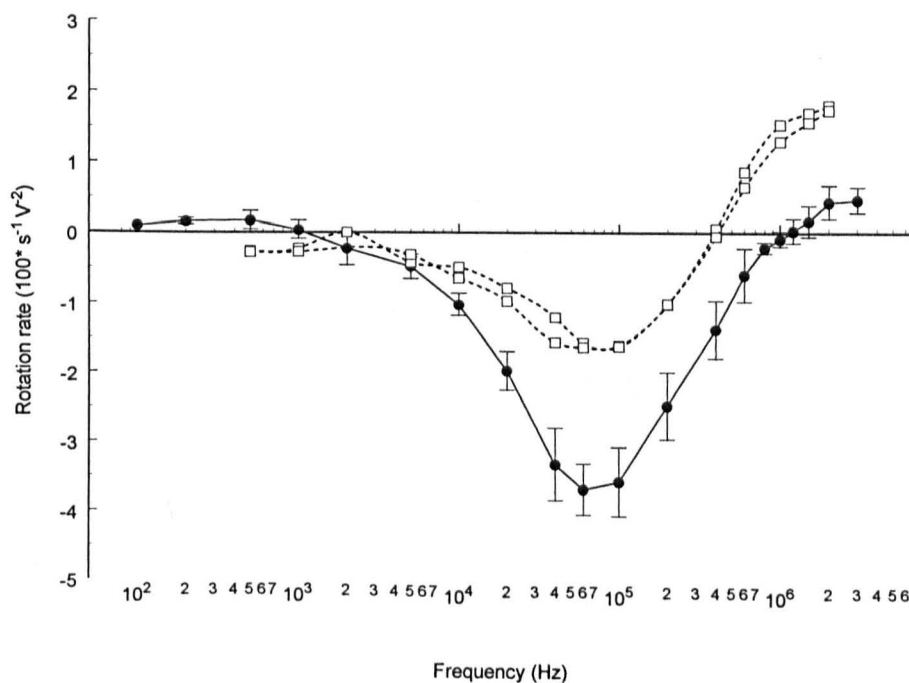
Figure 9.5 Comparison between the viable oocyst spectra and (n=2) heat killed non-viable DAPI+/PI+ (o) oocysts of isolate 2.

Suspending medium conductivity of 5 μS cm^{-1}.

9.4.3 Isolate 3

A total of 62 full ROT spectra were obtained from oocysts of isolate 3, which were observed on days 5, 19 , 33, 47, 57 after initial storage in water at 4°C. Of these 62 oocysts, 26 underwent the full staining procedure. Interestingly, the spectra from non-staining (DAPI-/PI-) but viable oocysts are somewhat different, having a clear shift to higher frequencies as shown in Figure 9.7.
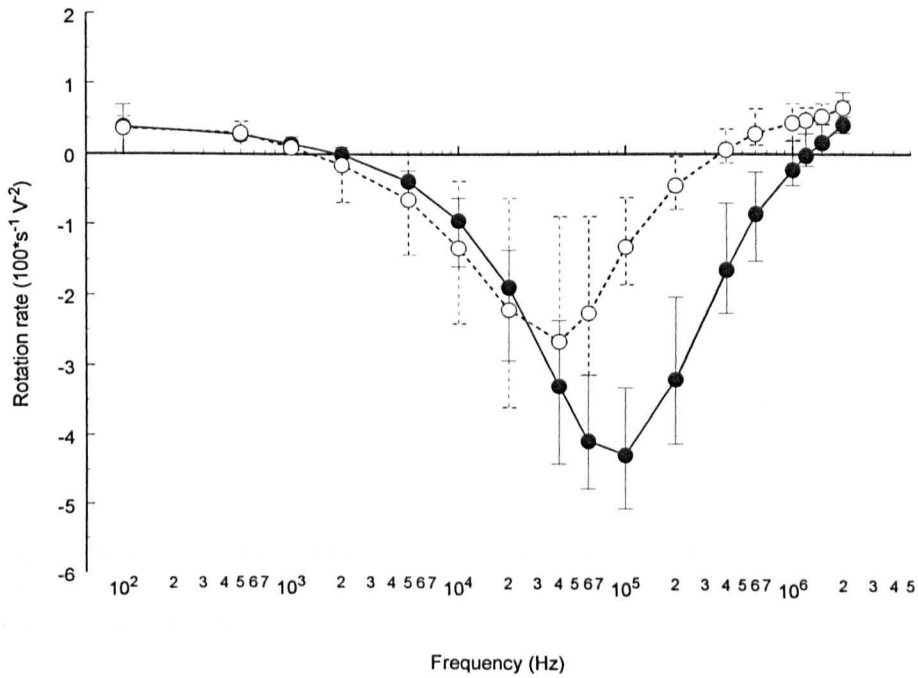
Figure 9.6 Summary of (n=9) DAPI+/PI- viable (•) and (n=5) DAPI+/PI+ non-viable (o) oocysts from isolate 3.
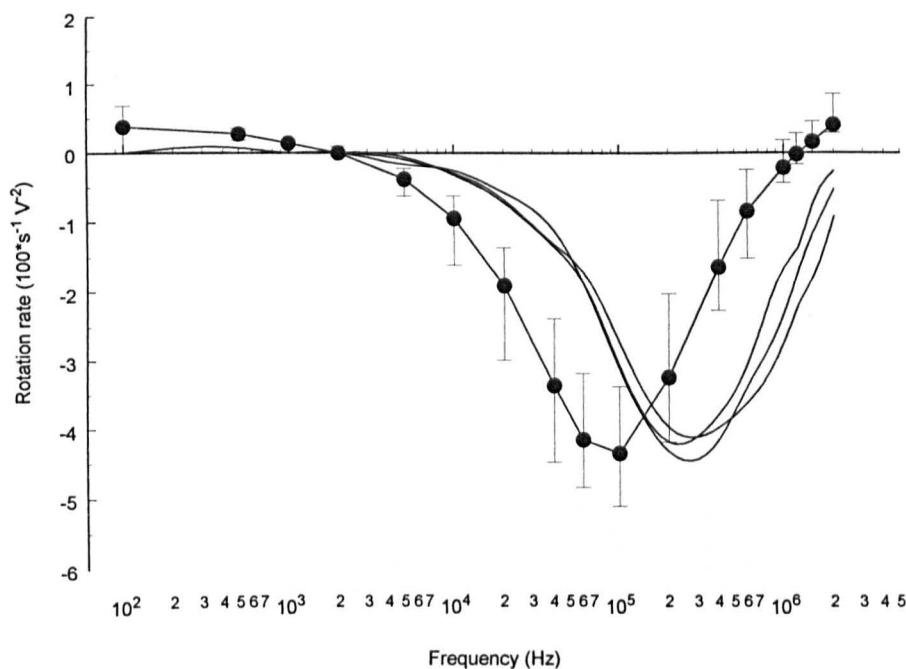
Figure 9.7 Mean values with error bars showing ranges, summarising (n=9) DAPI+/PI- viable oocysts (•) as in Figure 9.6 above, for comparison with (n=3) DAPI-/PI- but viable (by morphology) oocysts (—) from isolate 3.

Oocysts dye permeability is thought to be a dynamic situation (upon death or excystation), which is increased by acidic incubation (Campbell *et al.*, 1992) and reduced by incubation with saliva or storage in cow faeces (Robertson *et al.*, 1992). The decrease in permeability from storage in cow faeces may be due to a component such as a mucopolysaccharide inserting into the oocyst wall. Jenkins *et al.* (1998) have suggested a time- and temperature-dependent increase in oocyst wall permeability whereby oocysts become increasingly susceptible to environmental factors such as temperature and NH_3.

9.4.4 Isolate 4

Isolate 4 was used to test if the twin fluorogenic staining procedure had any effect on the subsequent ROT spectra. Examination of the oocyst sample at 2 weeks post egestion showed a high proportion of viable oocysts.

9.4.4.1   Viability determination

Viability by ROT was determined at 900kHz, by sense of rotation only. Non-rotating oocysts were checked to see that they were not stuck to the slide by observing Brownian motion of the particles. Using two counters, to check the sense of 100 oocysts took approximately 10 minutes. Very consistent indications of the high viability of the sample were found on both days.

Aliquot	Viable by ROT	Non-rotating	Non-viable by ROT	Total
1	93	9	3	105
2	91	6	5	102
3	88	5	2	95
4	93	8	1	102
5	115	6	3	124
6	100	4	4	108
7	135	3	2	140
Totals	715	41	20	776

(a) Day 1

Aliquot	Viable by ROT	Non-rotating	Non-viable by ROT	Total
1	79	2	2	83
2	111	2	4	117
3	99	8	3	110
4	151	8	4	163
5	101	9	4	114
6	110	5	3	118
7	104	6	4	114
8	130	6	3	139
Totals	885	46	27	958

(b) Day 2

Day	%Viable	%Non-rotating	%Non-viable
1	92.1	5.3	2.6
2	92.4	4.8	2.8

(c) Summary

Table 9.4 The viability determination of (n=1734) *C. parvum* oocysts checked for sense of rotation at 900 kHz on (a) day 1 and (b) day 2, summarised in (c).
Suspending medium conductivity 5 µS cm^{-1}.

9.4.4.2   Comparison of stained and unstained oocyst ROT spectra

From this sample with a high proportion of viable oocysts, two aliquots were simultaneously investigated. The first underwent the full staining procedure, the viability of the oocysts from the second aliquot were judged by morphological indicators at 400x magnification using phase contrast microscopy. A direct comparison of the spectra recorded is shown below in figure 9.8. No significant differences were observed in the frequency responses of the two aliquots.
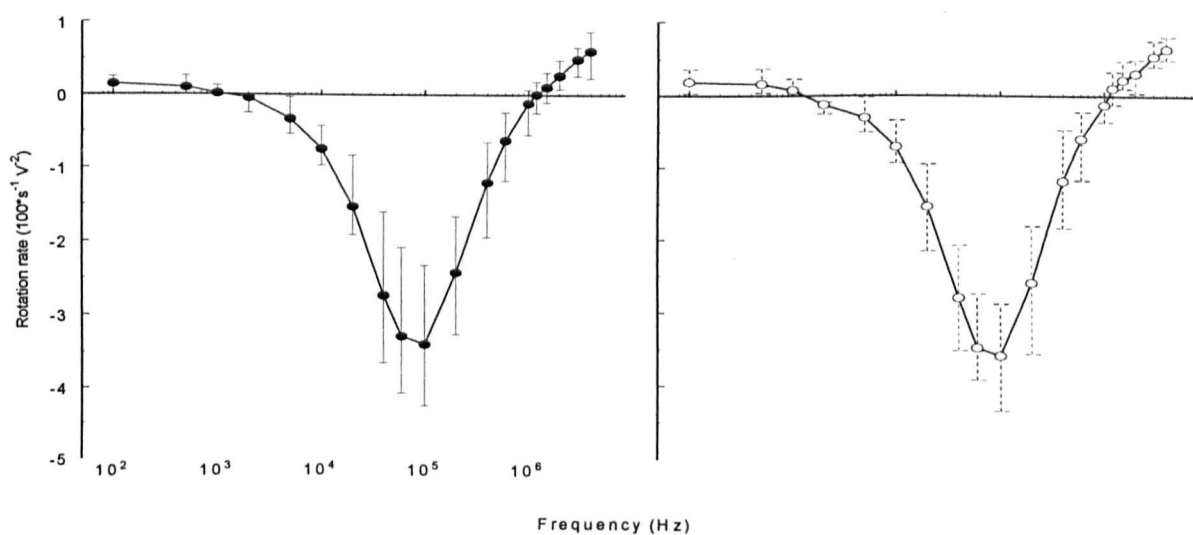
Figure 9.8 Comparison of mean rotation rates, and ranges observed for DAPI+/PI- viable (n=26) (-•-) and morphologically viable (n= 32) unstained (- o -) oocysts of isolate 4.

The stained oocysts of isolate 4 are shown below in figure 9.9. From this a frequency of 900 kHz can be seen to distinguish between the two groups. A problem is noted with this method, however, as the rotation rates at this point are comparatively small which leads to a small number of apparently non-rotating oocysts during a rapid survey of the sample as described above (approximately 5% of 1734 oocysts were recorded as non-rotating). A method that uses the rotation at more than one frequency would avoid this problem. For example, if the rotation rate was measured at 3MHz, oocysts with a rate of $> 0.7 \times 10^2$ rotations s^{-1} V^2 would be deemed non-viable.
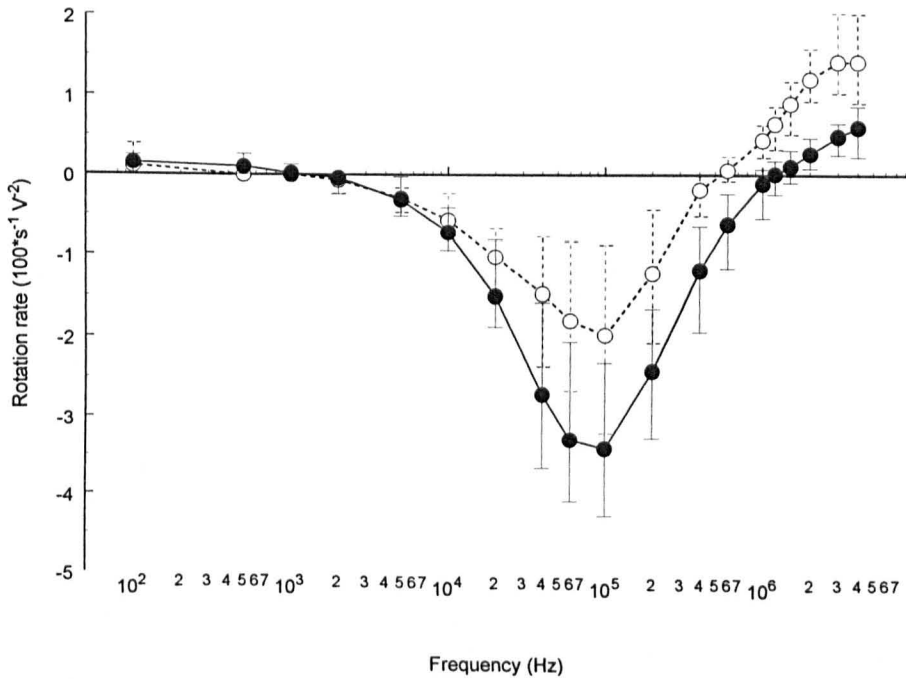
Figure 9.9 Summary of (n=26) viable DAPI+/PI- (•) and (n=9) non-viable DAPI+/PI+ (o) oocysts from isolate 4.
Data for oocyst shells are not shown for clarity.

9.4.5 Isolate 5

This isolate, of human origin, was problematic in that it contained many bacteria and other faecal debris.
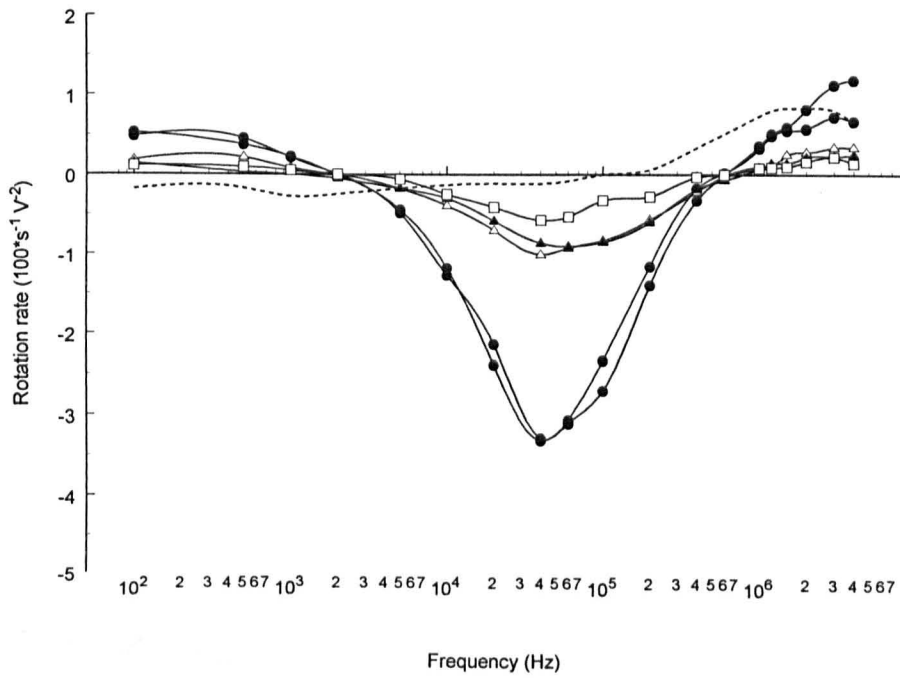
Figure 9.10 Examples of ROT spectra from isolate 5 oocysts with material attached.
Solid lines indicate viable DAPI+/PI- staining oocysts, with single (•), two (open triangle) and four (solid triangle) bacteria, and with debris (□). A DAPI+/PI+ staining oocyst is also shown with 2 bacteria attached (- -).

9.4.6 Isolate 6

Samples of age between 4 and 15 months were obtained from this isolate. Although recorded at a higher suspending medium conductivity ($35\mu S$ cm^{-1}) the fast rotation rate at 3MHz indicates the non-viability of these oocsts. Nothing morphologically unusual was observed about the non-staining oocyst with the exceptionally high ROT rate at 100Hz. Two other anomalous spectra were observed from this sample namely a shell with a large antifield peak magnitude, and a non-viable staining oocyst with an unusual antifield rotation at 100Hz.
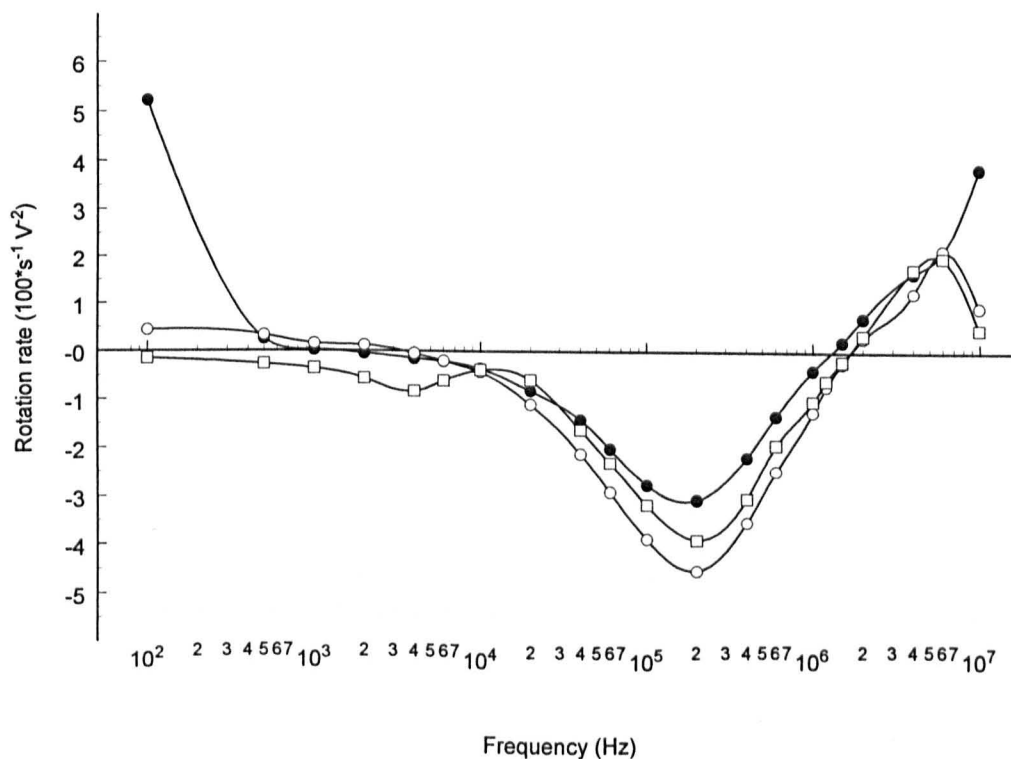
Figure 9.11 Anomalous ROT spectra from isolate 6.
Non-staining (•) 15 month old oocyst, (o) 15 month old shell, (□) 12 month old DAPI+/PI+ oocyst. All other (n=5) oocysts from this isolate were non-viable DAPI+/PI+ or were ghosts with high frequency crossovers of <400kHz, as seen for other isolates.

9.4.7 Isolate 7

This isolate had a high concentration of oocysts in the sample. It was therefore possible to compare two purification procedures, that of sucrose flotation and a simple sieving followed by repeated water washes. ROT spectra from oocysts purified by the sucrose flotation procedure are presented in figures 9.12 and 9.13 below.
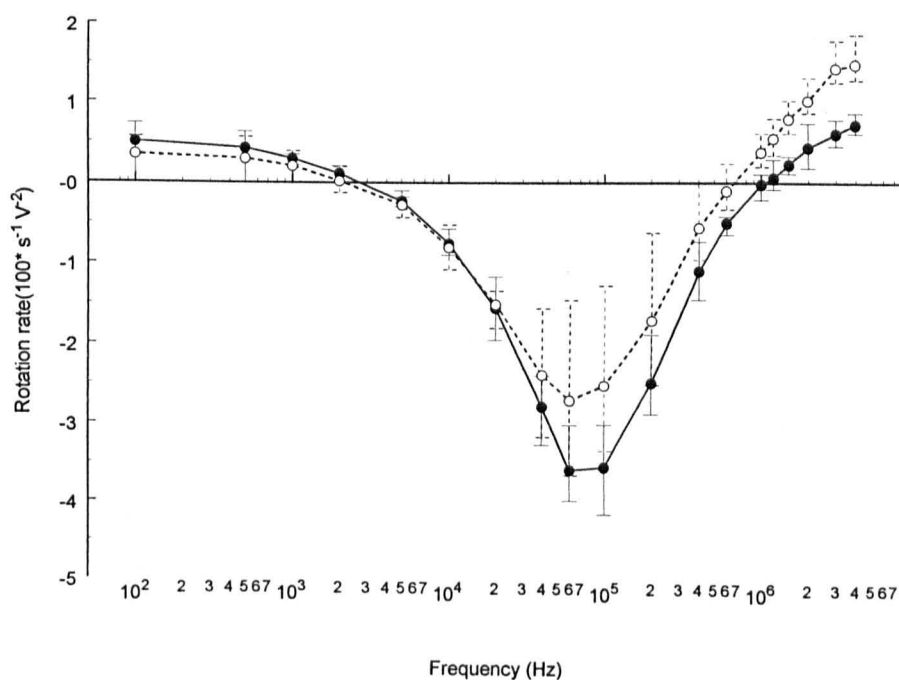
Figure 9.12 Mean and ranges for (n= 7) viable DAPI+/PI- (●) and (n= 7) non viable DAPI+/PI+ (o) isolate 7 oocysts purified by sucrose flotation.

The ghost oocysts were recorded at the same time as the other intact oocysts. No excystation conditions were used to induce ghost oocysts in the sample, those observed were therefore from excystation *in vitro* or natural deterioration.
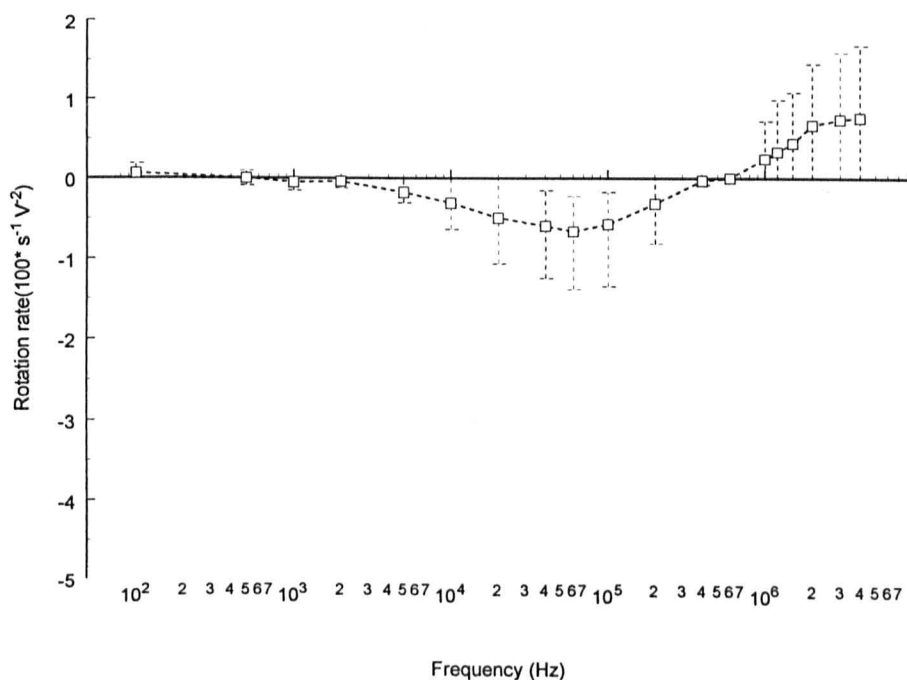
Figure 9.13 Mean and ranges for (n= 3) empty ghost oocysts (□) from isolate 7 purified by sucrose flotation.

All three ghosts lacked contents and possessed a gaping hole through which excystation may have occurred. Again this demonstrates the overlap between the ghosts and the viable oocysts, which may cause false positives in an automated system, that fails to also distinguish the ghosts.
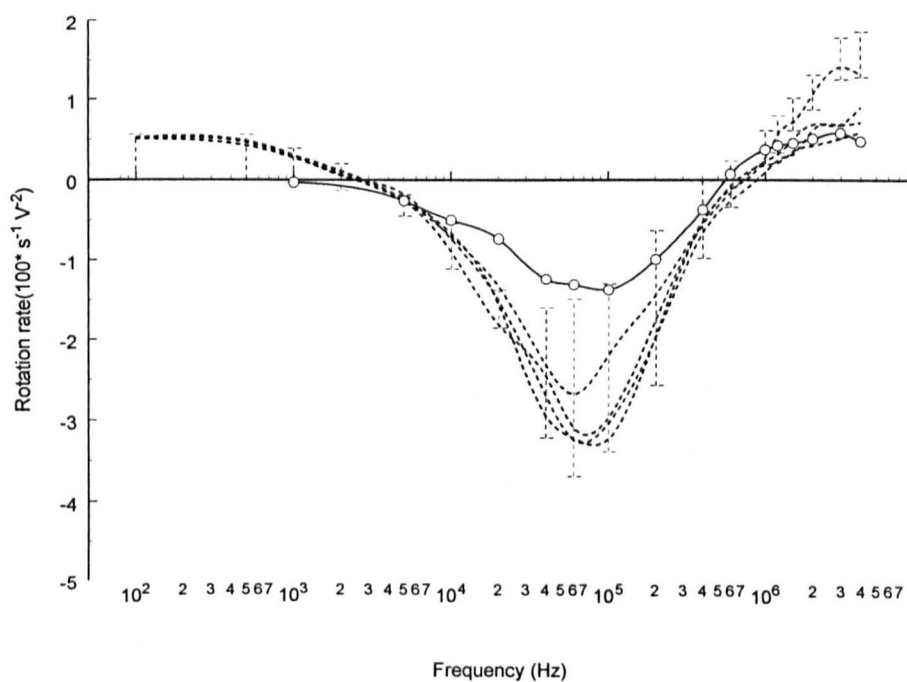
Figure 9.14 ROT spectra from isolate 7 oocysts purified by water washes, (n=4) DAPI+/PI+ non-viable oocyst spectra (- -) for comparison with the ranges of (n=7) non-viable DAPI+/PI- oocysts isolated by sucrose flotation (error bars showing range, no mean line).
Also shown is an example of an oocyst ghost isolated by water washes (-o-).

Only 1 of 4 of these non-viable oocysts purified by water washes overlap with those purified by sucrose at frequencies >2MHz. This suggests that an increase in the rate at these frequencies may be caused by purification with the sucrose flotation method. This increase is also apparent in the spectra presented below, figure 9.15, comparing viable spectra from the two purification procedures.
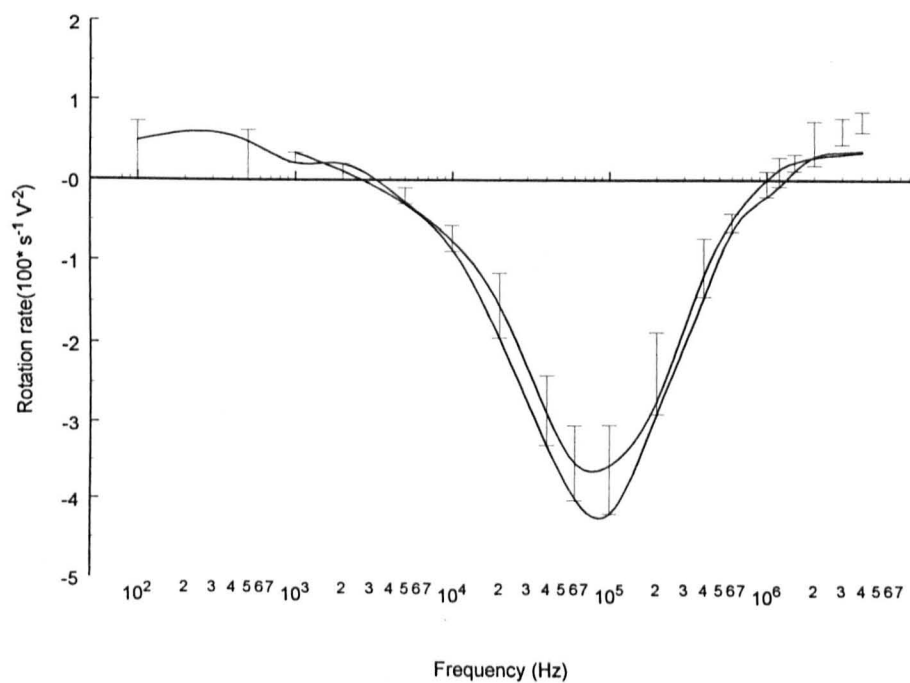
Figure 9.15 Comparison of viable ROT spectra from isolate 7 samples purified by two methods; (n=2) viable oocyst spectra isolated by water washes (-) and (n=7) viable oocysts isolated by sucrose flotation (error bars showing range, no mean line).

Interestingly the effect of purification procedure is being detected after 10 days storage in deionised water, suggesting that it may be irreversible.

9.4.8 Isolate 8

This 8 month old human isolate, possessed no viable oocysts by the vital stains or ROT. From a very low initial concentration, a total of 30 full spectra were recorded, figure 9.16 below.
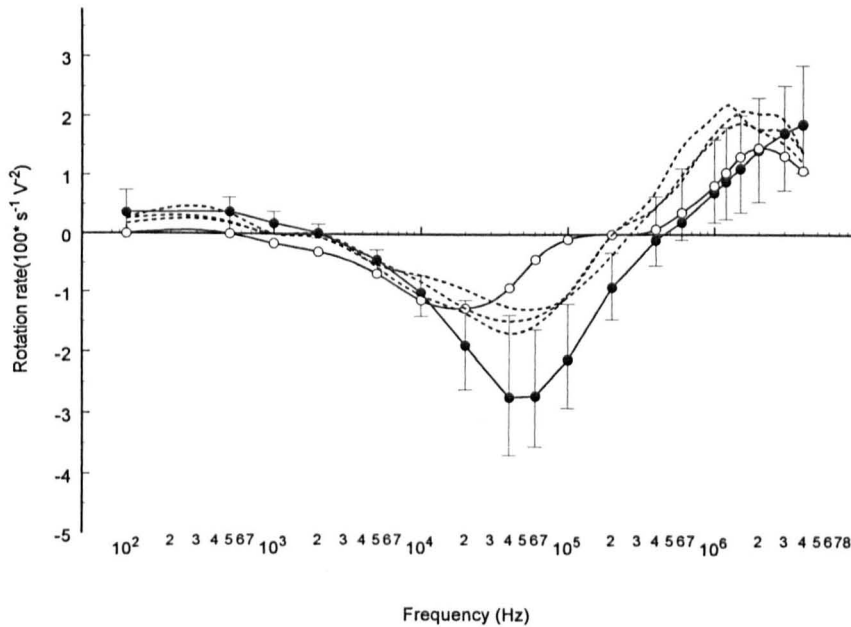
Figure 9.16 Summary of all ROT data collected for isolate 8.
Mean rotation rates with error bars showing ranges for (n=26) non-viable DAPI+/PI+ (•) oocysts, (n=3) ghosts (- -) and an example of a ghost with residual body(o).

9.4.9 Isolate 9

A 4 month old isolate of human origin, again with no detectable (DAPI+/PI-) viable oocysts.
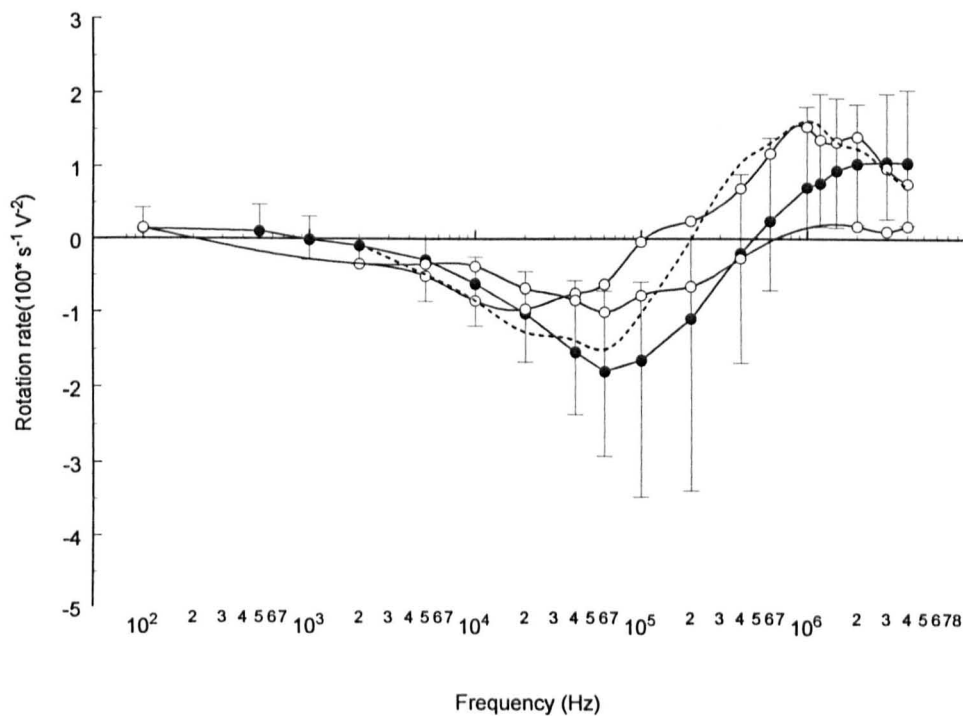
Figure 9.17 Summary of isolate 9.
Mean rotation rates with error bars showing ranges for (n=10) DAPI+/PI+ non-viable (•) oocysts, (n=1) empty ghost (-) and (n=2) ghosts with residual bodies (o).

9.4.10 Isolate 10

Although only 6 weeks old before purification no viable oocysts were found, indeed only two intact oocysts were observed, shown in figure 9.18.

Figure 9.18 ROT spectra of (n=2) non-viable isolate 10 oocysts.

Figure 9.19 Summary of ghost spectra for isolate 10.
Mean rotation rates with error bars showing ranges for (n=12) clean ghost oocysts (•) and a single ghost with bacterium on its surface (o).

Again this shows the effect of adherent bacteria-like bodies on the surface of the oocysts.

9.5   Conclusions

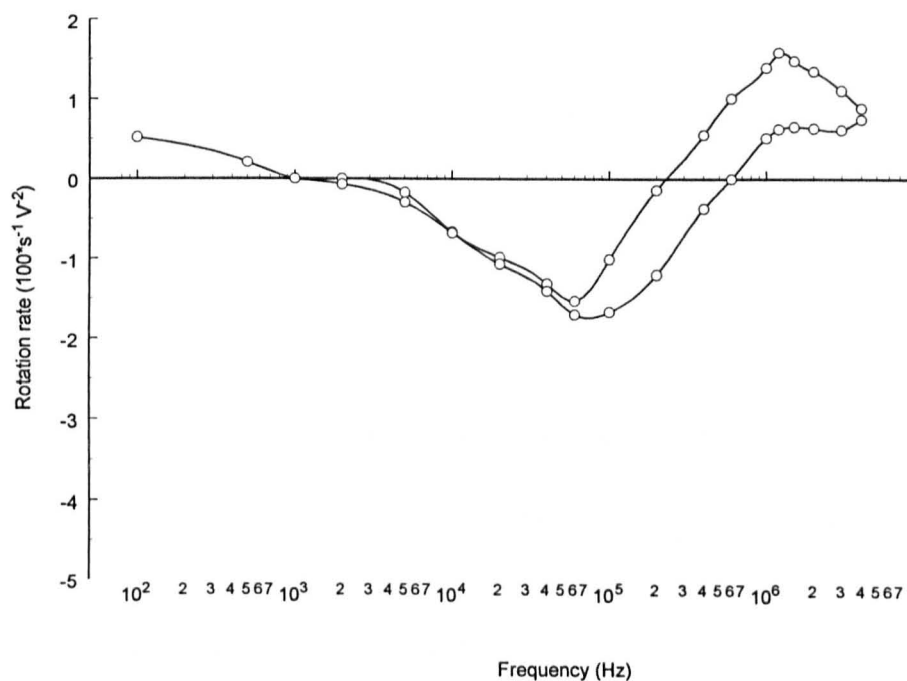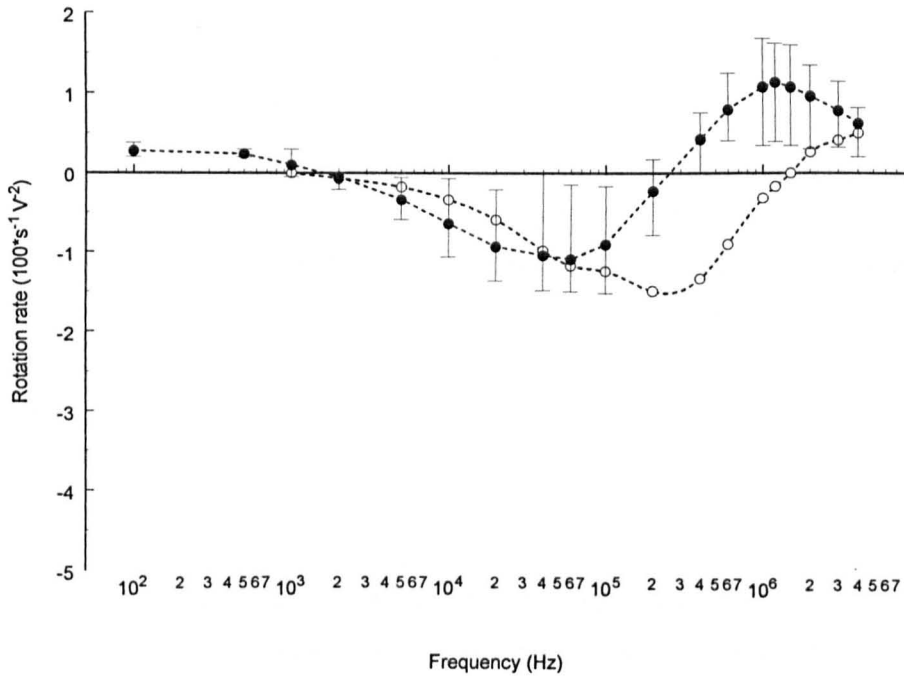Examination of 7 human, 2 bovine and 1 cervine-ovine isolates by electrorotation have been described. Non-viable oocyst spectra have been obtained for all isolates. Viable spectra were obtained from only 5 isolates, however, these were from samples under 2 months of age. With the exception of isolate 10, the samples that revealed no viable isolates were greater than 4 months old. These findings are consistent with a reduced survival rate in samples with increasing age.

Of the spectra recorded at $5\mu S\ cm^{-1}$, all the **clean** oocysts can be distinguished into either a viable or non-viable category by rotation sense at around 900kHz along with a measure of the rotation rate at around 3MHz, with viable oocysts having a rate of less than <0.8 units. Importantly with all of the isolates tested, the viability as given by the fluorogenic vital dyes agreed with the assessment using the ROT technique. It is worth noting that the ROT technique gave distinct responses for oocysts of isolate 3 that failed to take up either dye. These spectra had more 'viable' type qualities which is in agreement with the description of such oocysts by Campbell *et al.* (1992) as being 'viable upon a further trigger' determined by excystation.

It has been demonstrated to some extent that the purification procedure may increase the magnitude of the rate at 3MHz for both viable and non-viable oocysts, however, this comparison was only made for one isolate and so further work should be carried out on this.

With isolate 1, a clear demonstration of the effect of membrane integrity on the ROT spectra was described, with the fortunate occurrence of a viable oocyst excysting immediately after completion of a full spectrum recording. This almost instant (<1 s) emergence of the sporozoites, enabled another full spectrum to be recorded, this time of the gaping ghost with residual body. The change in high frequency crossover and the increase in magnitude at 3MHz was clearly shown.

The incorporation of vital dyes was not found to differ between isolates. From isolate 3, however, three examples of oocysts that failed to stain were described, figure 9.7. A clear shift of the spectra to higher frequencies was observed. From the literature (Campbell *et al.*, 1992) these oocysts have been described as being 'considered' viable and that this can be demonstrated with the dyes or by excystation following a further trigger, acidification. This further trigger was not incorporated into the twin staining procedure initially with the specific aim of recording spectra from this subgroup. The staining procedure itself was shown to have negligible effects on the spectra of viable oocysts, figure 9.8.

Several anomalous oocyst spectra were also described. These all had either bacteria or other material attached to the oocyst surface. Especially for isolate 5, this extra material was shown to either reduce the magnitude of the rotation rates, possibly through increased viscous drag, or importantly, in the case of at least one viable staining oocyst with debris attached, shift the high frequency crossover to frequencies associated with non-viable oocysts. This is a clear case of a potential false negative. It is suggested

therefore, as the twin dyes could still highlight the viability, that unless it is possible to clean up the oocysts, the stains should be used in conjunction with the ROT assay. Unsuccessful methods that were attempted in order to remove adherent particles included sonication and increased vortex times.

A comparison between the viable oocysts of the different isolates is interesting. Isolates 1 (CO) and 2 (Hu) exhibit very small or non-existent rotation rates at 100Hz at a suspending medium conductivity of $5\mu S$ cm^{-1}, whereas isolates 3 (Hu), 4 (Bo) and 7 (Hu) exhibit maxima of between 0.4 and 0.7 (rotations/s/V^2 x 10^2). The ranges of isolates 3, 4 and 7 do, however, extend to zero, and so this alone cannot be used to distinguish the two groups. No features at other frequencies are distinct enough to distinguish any of the isolates.

From a comparison of the non-viable oocysts between the isolates, isolate 6 (Bo) had a distinct oocyst (clean, D+/P+) with antifield rotation at 100Hz. This oocyst also had a definite secondary antifield peak at 4kHz, an observation that was rechecked during the experiment. An isolate 5 (Hu) oocyst, also exhibited this rare antifield rotation at 100Hz, although this individual had 2 adherent bacteria.

The antifield peak frequencies for the non-viable oocysts fall into two distinct categories. Isolate 4 (Bo) had peak frequencies at greater than 60kHz, whereas for isolates 3, 8 and 10 (all Hu) they were less than 60kHz. Recorded at identical conductivites, this difference may be attributed to either purification procedure (CsCl versus sucrose sedimentation) or the host species (Bo versus Hu).

Similarities in the ghost oocyst spectra for most isolates included a small rotation rate at 100Hz, a small antifield peak with a high frequency crossover at <400kHz, along with a typically large cofield peak at around 1MHz. An exception to this last feature was the ghost oocysts of isolate 7, for which no actual peak was observed for the cofield region for frequencies up to 4MHz. Apart from this one feature it was not expected that it would be possible to distinguish isolates as the spectra variation is so great.

9.6   References

Awad-El-Kariam, F.M., Robinson, H.A., Dyson, D.A., Evans, D., Wright, S., Fox, M.T. & McDonald, V. (1995) Differentiation between human and animal strains of *Cryptosporidium parvum* using isoenzyme typing. *Parasitology*. 110: 129-132.

Bonnin, A., Fourmaux, M., Dubremetz, J., Nelson, R., Gobet, P., Harly, G.B.M., Puygauthiertoubas, D., Gabrielpospisil, F. & Naciri, M.C.P. (1996) Genotyping Human and Bovine Isolates of *Cryptosporidium parvum* by Polymerase Chain-Reaction Restriction-Fragment-Length-Polymorphism Analysis of a Repetitive DNA-Sequence. *FEMS Microbiology Letters*. 137: 207-211.

Campbell, A.T., Robertson, L.J. & Smith, H.V. (1992) Viability of *Cryptosporidium parvum* oocysts: Correlation of *in vitro* excystation with inclusion or exclusion of fluorogenic vital dyes. *Applied and Environmental Microbiology*. 58: 3488- 3493.

Carraway, M., Tzipori, S. & Widmer, G. (1996) Identification of genetic-heterogeneity in the *Cryptosporidium parvum* ribosomal repeat. *Applied and Environmental Microbiology*. 62: 712-716.

Carraway, M., Tzipori, S., & Widmer, G. (1997) A new restriction fragment length polymorphism from *Cryptosporidium parvum* identifies genetically heterogeneous parasite populations and genotypic changes following transmission from bovine to human hosts. *Infection and Immunity*. 65: 3958-3960.

Ditrich, O., Palkovic, L., Sterba, J. Prokopic, J., Loudova, J. & Giboda, M. (1991) The first finding of *Cryptosporidium baileyi* in man. *Parasitology Research*. 77: 44-47.

Fayer, R., Speer, C.A. & Dubey, J.P. (1997) The general biology of *Cryptosporidium*. In: *Cryptosporidium and cryptosporidiosis*. (Ed. R. Fayer) CRC, Boca Raton.

Hill, B.D., Blewett, D.A., Dawson, A.M. & Wright, S. (1990) Analysis of the kinetics, isotype and specificity of serum and coproantibody in lambs infected with *Cryptosporidium parvum*. *Research in Veterinary Science*. 48: 76-81.

Jenkins, M.B., Ghiorse, W.C., Anguish, L.J., Bowman, D.D. & Walker, M.J. (1998) Viability of *Cryptosporidium parvum* oocysts: Assessment by the dye permeability assay. Letter to the Editor. *Applied and Environmental Microbiology*. 64: 3544-3545.

Lally, N.C., Baird, G.D., Mcquay, S.J., Wright, F. & Oliver, J.J. (1992) A 2359-Base Pair DNA Fragment from Cryptosporidium-Parvum Encoding a Repetitive Oocyst Protein. *Molecular and Biochemical Parasitology*. 56: 69-78.

Levine, N.D. (1984) Taxonomy and Review of the Coccidian Genus *Cryptosporidium* (Protozoa, Apicomplexa). *Journal of Protozoology*. 31: 94-98.

Mead, J.R., Humphreys. R.C., Sammons, D.W. & Sterling, C.R. (1990) Identification of isolate specific sporozoite proteins of *Cryptosporidium parvum* by 2 dimensional gel electrophoresis. *Infection and Immunity*. 58: 2071-2075.

Morgan, U., Sargent, K., Deplazes, P., Forbes, D., Spano, F., Hertzberg, H.E.A. & Thompson, R. (1998) Molecular characterisation of *Cryptosporidium* from various hosts. *Parasitology*, 117: 31-37.

Nichols G.L., McLauchlin, J., & Samuel, D.(1991) A Technique for typing *Cryptosporidium* isolates. *Journal of Protozoology*. 38: 237-240.

Nina, J.M.S., McDonald, V., Dyson, D.A., Catchpole, J., Uni, S., Iseki, M., Chiodini, P.L. & McAdam, K.P.W.L. (1992) Analysis of oocyst wall and sporozoite antigens from 3 *Cryptosporidium* species. *Infection and Immunity*. 60: 1509-1513.

O'Donoghue, P.J. (1995) Cryptosporidium and cryptosporidiosis in man and animals. *International Journal for Parasitology* 25: 139-195.

Ogunkolade, B.W., Robinson, H.A., McDonald, V. & Evans, D.A.F. (1993) Isoenzyme variation within the genus *Cryptosporidium. Parasitology Research.* 79: 385-388.

Ortega, Y.R., Sheehy, R.R., Cama, V.A., Oishi,K.K. & Sterling, C.R. (1991) Restriction-fragment-length-polymorphism analysis of *Cryptosporidium parvum* isolates of bovine and human-origin. *Journal of Protozoology.* 38: 40-41.

Peng, M., Xiao, L., Freeman, A., Arrowood, M., Escalante, A., Weltman, A.O., MacKenzie, W., Lal, A. & Beard, C. (1997) Genetic polymorphism among Cryptosporidium parvum isolates: Evidence of two distinct human transmission cycles. *Emerging Infectious Diseases.* 3: 567-573.

Pozio, E., Morales, M., Barbieri, F. & Larosa, G. (1992) *Cryptosporidium* - Different Behaviour in Calves of Isolates of Human Origin. *Transactions of the Royal Society of Tropical Medicine and Hygiene.* 86: 636-638.

Robertson, L.J., Campbell, A.T. & Smith, H. V. (1993) *In vitro* excystation of *Cryptosporidium parvum. Parasitology.* 106: 13-19.

Shirley, M.W. (1986) New methods for the identification of species and strains of *Eimeria.* In: *Research in Avian Coccidiosis* (Eds. L.R. McDougald, L.P. Joyner, & P.L. Long). Georgia : University of Georgia Press.

Smith, H.V., Patterson, W.J., Hardie, R., Greene, L.A., Benton, C., Tulloch, W.J., Gilmour, R.A., Girdwood, R.W.A., Sharp, J.C.M. & Forbes, G.I. (1989) An outbreak of waterborne cryptosporidiosis caused by post-treatment contamination. *Epidemiology & Infection.* 103: 703-715.

Wakelin, D. & Goyal, P.K. (1996) *Trichinella* isolates: parasite variability and host responses. *International journal for parasitology.* 26: 471-481.

Walliker, D. (1985) Characterisation of *Plasmodium falciparum* of different countries. *Annales de la Societe Belge de Medecine Tropicale.* 65: 69-77.

Conclusions and Recommendations for Future Work

This thesis contains the results of the first thorough investigation of two genera of protozoan parasites that infect man, namely *Cryptosporidium* and *Giardia*, using primarily the dielectric technique of electrorotation (ROT). Chapter two contains a review of ROT along with the related AC electrokinetic techniques of dielectrophoresis (DEP) and travelling wave dielectrophoresis (TWD) which have been used to a lesser degree in this study. The current status of these techniques was described, along with suggestions of potential applications in the field of Parasitology. It was identified that, with the exception of the malaria parasite *Plasmodium falciparum* which was indirectly studied through infected erythrocytes, the protozoa have been greatly ignored with few investigations to date of their dielectric properties.

Both the coccidian *Cryptosporidium* and the flagellate *Giardia* are of importance to human health as they can, for part of their life cycle, inhabit the intestine in a parasitic manner. It was the transmissive forms of each lifecycle that was identified as being appropriate to study by these techniques; namely the oocyst and cyst stages. Since the mid 1970's species of both these genera have been shown to be major causative agents of chronic diarrhoea in humans and other animals. Current techniques for the detection and viability determination of the transmissive stages of these parasites have their disadvantages, and so a sensitive detection method that could do both is seen, especially by the water industry, as a useful tool. The aim of the experimental work described in this thesis was to show whether the dielectric techniques described could be used as such a tool, in particular through ROT which lends itself to determining the physiological state of single particles. As well as distinguishing those that are potentially infective (revealed through measurement of their physiological state) it is also important to distinguish particles from different species of each genus as not all are infective to man. For example, viable cysts of *G. muris* are not infective to humans whereas viable cysts of the *G. duodenalis* type are. Particles from different species within the genera were therefore also investigated.

In Chapter 4 it was demonstrated that ROT does indeed give an indication of the viability of individual cysts of both *G. muris* and *G. duodenalis* type; this correlated well with a current method using a twin dye permeability assay. An important advantage of ROT was that of gaining information on the physiological state of a small number of cysts that fail to uptake any dye unless given a further trigger (listed in the full dye protocol). The disadvantage of this further trigger (acidification) in the dye assay was the extra time required of approximately 1 hour.

The description of the effect of an adherent bacterium on the ROT spectrum of a *Giardia* cyst was given in Chapter 4. It was concluded from the changes in the spectrum that both viscous drag effects and a change in dielectric properties was occurring. Although work has been done to show the effect of bacterium on artificial particles (Hodgson & Pethig, 1998) this is the first description of the effect of adherent bacteria on a biological particle. Further work to elucidate the precise cause of the observed

changes needs to be done, as well as work to remove bacteria from the particles of interest so that the ROT technique can be used without giving false-negative viability indications.

The first demonstration of isolate differences within a species detected by ROT was also described. Although observed in non-viable cysts, the rotations at certain frequencies were in opposite directions and so were distinct.

A suggestion for further work using the cysts of *Giardia* might include the ROT of cysts from *G. microti*, found in vole and muskrat faeces. In these cysts the trophozoites undergo cytokinesis prior to excystation, which should be distinguishable as more membranes would be present in the cyst. To distinguish these from other cysts would help for example in determining the source of environmental contamination of water.

ROT spectra from oocysts of *C. parvum* were described in Chapter 5 as a function of suspending medium conductivity to find the optimum conditions to determine viability. Overlap between the high frequency crossover points of the viable and non-viable oocysts at higher conductivities was observed, whereas at lower conductivities there was clearer distinction. Antifield peak magnitudes were found to be greater, and of greater separation at lower conductivities (ratio of the magnitudes 2.3:1 at $4\mu S$ cm^{-1} compared with 1.8:1 at $750\mu S$ cm^{-1}). This is a useful finding as the 'life-span' of the electrorotation electrodes is also greater at lower conductivities. Bacterial adhesion was shown to have an affect on the ROT spectra of *C. parvum* oocysts, over a range of medium conductivities.

A comparison of ROT with the fluorogenic dyes on 500 oocysts provided interesting data. An advantage of ROT over the dye assay was found in that it was possible to assess the physiological state of 8 oocysts that failed to stain. A modified version of the staining procedure was used in which a pre-acidification incubation at pH 2.7 for 1 hour was omitted, thus reducing the procedure time from ~1.5 hours to 30 minutes. That ROT could determine the viability of DAPI-/PI- oocysts without the need for this extra step is an important finding.

One limitation of the ROT technique that was identified was that, although it was sensitive enough to determine the physiological state of a single oocyst/cyst particle, the design of the electrodes and the pre-sample handling enabled only a fraction of the particles in any aliquot to be assayed. As these particles were obtained in relatively low concentrations this precluded the use of smaller electrode geometries such as polynomial type electrodes of < 0.5mm interelectrode gap, which have previously been demonstrated to assist positioning of particles prior to ROT analysis.

The experiments described in Chapter 6 assess the potential of TWD as a means for positioning the particles prior to ROT analysis. The appropriate conditions of applied field frequency, voltage and medium conductivity were found for the efficient translational motion of the oocysts both within a channel between electrode tips and over an array of electrodes.

The narrow window of conditions that TWD for these particles was observed can be both advantageous and disadvantageous. Such defined conditions may lead to differential travel of particles enabling separation, however, a frequency 'wall' above which conditions of positive DEP occur and prevent TWD was observed. Also the TWD velocity never reaches its theoretical maximum as the greatest torque is produced at a frequency (the antifield peak in the ROT spectrum) which coincides with positive DEP conditions. This limitation may become important for applications which require transport of particles over large distances.

Having demonstrated the successful translational motion of the oocysts the problem of the low particle concentration was then addressed. In Chapter 7, the development of a device, fabricated as a single layer electrode structure was described. Initial problems with corners in a square sided design culminated in a circular spiral design. Whereas previous examples of this type of electrode design have been demonstrated, the novel feature of this geometry was to incorporate a ROT chamber in the centre so that particles, once concentrated, could be assessed using the single frequency method used in Chapter 5 to compare ROT with the twin permeability dye assay. This was the first reported operation of a laboratory-on-a chip device that incorporates the combined electrokinetic effects of TWD and ROT. The generic design, as discussed, could readily be enlarged to increase the surface area and therefore the effective capture area.

Another problem encountered in such samples, especially from those purified from faeces, but also applicable to water concentrates, are the occurrence of debris which interfere with the ROT response. The controlled input of oocysts into the central chamber lends itself to the isolation of precise numbers of oocysts away from debris. Collection of these oocysts or indeed any such particles would be a useful tool, for example pre-sample handling for PCR or for precise dose studies for animal infectivity.

Collection of single oocysts through a hole manufactured by laser ablation into a polyimide substrate, onto a polycarbonate membrane was demonstrated six times. Although Chapter 7 demonstrates a successful sequence through the spiral device of; sample input, selective concentration, assay and subsequent collection, it requires skilled, patient operation. Future work in this area, especially addressing the challenges of sample input of many substrate types such as faecal samples, blood, urine, cerebrospinal fluid, and automation is seen as being of great importance.

Having addressed the problem of whether the ROT technique was sensitive to the target species of *Cryptosporidium parvum*, the problem of specificity was investigated, in particular whether ROT could distinguish *C. parvum* from *C. muris* and *C. baileyi*, species not infective to humans, but which may occur for example, in environmental water samples.

Studies of *C. baileyi* using ROT highlighted an effect of storage time, whereby the magnitude of low frequency rotation diminished over time (weeks). This is similar to, and may be due to, a reduction of surface charge over a similar storage time noted by Drozd & Schwartzbrod (1996). Clear distinctions

between viable and non-viable oocysts of *C. baileyi* were again observed. A total of five distinct morphological categories, representing different states of deterioration, were characterised by complete ROT spectra.

Similar work was undertaken with the oocysts of *C. muris*. Consistent differences between viable and non-viable oocysts were described. Interestingly no effect with storage time was found. However, differences between viable oocysts that did and did not include the dyes were found, again at the low frequency cofield part of the spectrum. Although the ability to assess physiological state was constant for the three species, no differences in the ROT spectra of sufficient size were found that would allow a simple test to distinguish the oocysts of *C. parvum, C. baileyi* and *C. muris*. It is therefore suggested that future work should address this issue, possibly through the use of dielectric labelling.

In Chapter 5 a correlation between the dye permeability assay and the ROT spectra for one isolate was described. The question of whether the ROT assay works with other isolates was addressed in Chapter 9. Oocysts obtained from isolates of human, bovine and cervine-ovine source were investigated. An important finding was that the physiological state of all **clean** oocysts from these isolates could be judged using ROT as described in Chapter 5, in full agreement with the twin dye permeability assay. The problem of adherent bacteria on the oocysts was reiterated here, as this interfered with the results. Non-staining oocysts from one isolate revealed a distinct shift in the whole spectrum to higher frequencies, but are considered viable by both techniques. The staining procedure itself was demonstrated not to have any significant effect on the ROT spectrum.

The clearest demonstration to date of the effect of membrane integrity on the ROT response was described for a single oocyst before and after excystation *in vitro*. From the two spectra it was concluded that three major changes to the spectrum occur; a decrease in the high frequency crossover, an increase in the magnitude of the high frequency cofield peak, and a shift in the region of the spectra from 20kHz to 200kHz to slightly higher frequencies. These observations consolidate the conclusions of the other work on determining the physiological state of these particles.

With regard to isolate differences detected by ROT, these should theoretically be concluded from viable oocyst spectra, as once the oocyst integrity is lost the effect of the storage media will have a significant effect as it is free to enter the oocyst. Even with viable oocysts the storage media, or history of the oocyst, must be considered to have some effect on the ROT response. Within the spectra obtained from the viable oocysts, differences between isolates were observed in the low frequency region. Of the five isolates from which viable oocysts were obtained a criterion of the spectrum was established which conveniently separated these isolates into two groups. Further work should be done to compare these groups with the two genotypes recently revealed by PCR analysis.

References

Hodgson, C.E. & Pethig, R. (1998) Determination of the viability of *Escherichia coli* at the single organism level by electrorotation. *Clinical Chemistry.* 44: 2049-2051.

Drozd, C & Schwartzbrod, J. (1996) Hydrophobic and electrostatic cell surface properties of *Cryptosporidium parvum. Applied and Environmental Microbiology.* 62: 1227-1232.

Publications arising from this work

Goater, A.D., Burt, J.P.H. & Pethig, R. (1997) A combined electrorotation and travelling wave device: applied to the concentration and viability of *Cryptosporidium. Journal of Physics D-Applied Physics.* 33: L65-L70.

Goater, A.D. & Pethig, R. (1999) Electrorotation and Dielectrophoresis. *Parasitology - Supplement.* 117: (in press). (Invited review).

Goater, A. D. & Pethig, R. (1999) Biophysical techniques for enhancing microbiological analysis, Future developments : Dielectrophoresis and Electrorotation. *Encyclopedia of Food Microbiology.* (Eds. R. Robinson, C. Batt & P. Patel) (in press) (Invited review).

Goater, A. D., Pethig, R., Paton, C. & Smith, H.,V. Single *Cryptosporidium* oocyst isolation and capture using a Travelling Wave Dielectrophoresis Device. *Institute of Physics Conference Series* (accepted for oral presentation at Electrostatics '99).